University of Nottingham

UK | CHINA | MALAYSIA

Novel orlistat LDL-like nanoparticles as potential anti-cancer medicines

By: George Bebawy BSc, MSc [a,b],

Supervisors: Dr Jonathan Burley[a], Prof. Philip M. Williams[a], and Prof. David Needham [a]

***[a] School of Pharmacy, University of Nottingham**

[b] Faculty of Pharmacy, Alexandria University.

Thesis submitted to the University of Nottingham for the degree of Doctor of Philosophy

School of Pharmacy

May 2022

Acknowledgment

First of all, I would like to thank all those at the University of Nottingham who have supported this work. Special thanks to my supervisors, Dr Jonathan Burley, Professor Phil Williams and Professor David Needham, who have given me the opportunity to work under their supervision. I gratefully acknowledge their continued encouragement over the past years, and the extensive support I have received in all my endeavours during my time at Nottingham. I wish to extend my thanks and appreciation to my internal assessor, Professor Snow Stolnik, for her expert advices and opinions on the project.

Deepest thanks and gratitude to Professor Anna Grabowska and Pamela Collier for their help in the cell work, to Denise Mclean, for her help and support while using the TEM, and to Carol Turrill, Julia Crouch, Amy Nairn and all technician team, for organizing numerous of meetings, conferences, ordering stuff and delivering trainings.

Special thanks are going to my colleagues in D19 and B09 for being great friends and support, thanks for your help, encouragement, and funny jokes. Additionally, I would like to acknowledge my home University, Alexandria University, and my sponsor, Newton-Mosharafa scholarships, for giving me the opportunity to have such a great experience.

A special debt of thanks is reserved for my family, especially my mother Mona Sakla and sister Marina Bebawy, whose love and support throughout my entire education has enabled me to reach this point, thank you, I could not have done it without you. Special thanks to my brother-in-law, Adel Aziz who was a real brother throughout my journey. Thanks to all my friends, in the UK and Egypt, who have always been there to talk through everything, and for being there whenever I need help and guidance, specially (Maxwell, Nada, Noha, Mona, Thata, Rebecca, Napoleon, Kate and Saif).

Finally, and most importantly, I would like to thank God, for helping me to finish this work and for providing me with such very encouraging opportunity to study at the prestigious

University of Nottingham. At the end, I would like to dedicate this thesis to the soul of Father, Hanna Fahmy Bebawy, may he rest in peace, hoping that he is, now and always, proud of his son.

“My grace is sufficient for you, for my power is made perfect in weaknesses”

(2 Corinthians 12:9)

Declaration

I hereby declare that the work contained in this thesis titled “Novel orlistat LDL-like nanoparticles as potential anti-cancer medicines” is the result of my own work conducted at the School of Pharmacy, University of Nottingham between March 2018, and March 2022, under the supervision of Dr Jonathan Burley, Professor Phil Williams, and Professor David Needham.

Abstract

Objectives: The field of Nano-therapeutics has gained vast attention over the past decades, described as the future cancer medicine. Controlling the particle size is highly crucial for many reasons including proper drug formulation, tumour targeting and enhancing bioavailability. Mostly, nanoparticles within the range of 100 to 200 nm are the most easily manufactured, yet they may not be the best option for optimum drug targeting and tissue accumulation which are in favour of smaller particles (< 50nm). Thus, preparing nanoparticles of small size (<50nm) in an easy way and with high concentrations of the required drug still requires work.

Additionally, fabrication of effective anticancer nanomedicine has taken a new pathway over the last decades, where new active pharmaceuticals ingredients (API) were introduced as novel therapeutics for cancer therapies. One of the recently studied drugs is orlistat, a weight loss medication that showed remarkable activity against many tumours through inhibiting cellular fatty acid synthesis and hindering cellular division and growth. However, orlistat is highly hydrophobic, and formulation of nanoparticles of small size to ensure cellular accumulation and yet having high drug content is still a hurdle. Therefore in this thesis, a straightforward solvent shift technique was adopted for preparation of phospholipids coated orlistat nanoparticles of controlled size, high stability, and immense drug content.

Various naturally existing organic and inorganic nanoparticles have been present before they were synthesized in labs. Among the naturally occurring nanoparticles is the low-density lipoprotein (LDL), a normal blood constituent, serving as a means of cholesterol delivery to tissues. Cholesterol is one of the main constituents of the cell membranes. Cells get their cholesterol requirement either through making it themselves, taking it up from LDL, or both. Distinctly, being of high proliferation rate, tumour cells need large amounts of cholesterol obtained chiefly from LDL to establish new membranes. Thus, LDL could be used as a vehicle to carry antitumor drugs, consequently acting as an excellent targeting modality.

Methods: The present thesis involved the preparation of nanoparticles of hydrophobic materials through rapid solvent exchange technique, including coating of the particles to control the size of the prepared nanoparticles. Investigating the effect of different concentrations of the materials used and the rate of nanoprecipitation on particle size and surface charge was conducted using dynamic light scattering and transmission electron microscopy. Afterwards, the results were compared to each other to find the inflection point in the particle size growth with the concentration of used material and effect of different coating on particle ripening.

This thesis as well involved the preparation of phospholipids coated orlistat nanoparticles through nanoprecipitation by solvent exchange technique, together with stabilising of the particles with surfactants to control the size of the prepared nanoparticles. Characterisation of the prepared nanoparticles was done using dynamic light scattering, transmission electron microscopy, differential scanning calorimetry (DSC) and polarised light microscopy (PLM). Prepared nanoparticles were further freeze dried to assess for shelf stability. Moreover, encapsulation efficiency and drug release patten were assayed.

Finally, preparation of novel LDL-like nanoparticles of the recent anti-cancer medication orlistat (ORL) was done through the simple straightforward solvent exchange technique, this includes coating of the particles with a mixture of phospholipids including POPC, DSPC, Cholesterol and DSPE PEG (5000) maleimide. An 11-mer peptide moiety, which resembles the active site of the apoprotein B of the natural LDL, is attached to the NPs through simple click chemistry. The prepared formulation was evaluated for its physico-chemical properties through size analysis and conjugation efficacy. Finally, the efficacy of the formulation was evaluated against breast cancer through cell studies on various breast cancer cell lines.

Key findings: Results showed that the prepared nanoparticles of different materials used (triolein, trihexanoin, tricaprin, and orlistat) shared a common pattern of particle size growth upon using high concentrations of the material. Yet, coating the nanoparticles during the solvent exchange resulted in controlling the size at high concentrations, near to the therapeutic doses, keeping it below 50nm. Moreover, the slow rate of nanoprecipitation (0.11ml/min), which is mostly adopted, enhanced the particles ripening, unlike the rapid solvent shift technique (1 ml/s). The prepared nanoparticles were of suitable zeta potential to ensure surface stability against further aggregation.

Moreover, the prepared coated orlistat nanoparticles showed a small controlled size (< ~50 nm) even at high drug loading concentrations, with a proper zeta potential of up to (-70 mV) which ensure stability against aggregation. Orlistat was completely coated with the phospholipid used according to DSC thermograms and PLM. Freeze drying the NPs did not affect its size upon storage for up to 6 months. The prepared formulation showed entrapment efficiency of 77% and a controlled release pattern over 1 week period.

Concerning the novel LDL-like ORL NPs, the prepared formulation was in size range of around 50 nm, and of spherical intact structure with a stable average zeta potential of -25 mV. The click chemistry employed for peptide attachment was successful with % free sulfhydryl groups in the conjugated peptide drop to 0.7%. The formulation showed enhanced cytotoxicity in all the employed breast cancer cell lines, resulting in significant decrease in the IC50 compared to other orlistat NPs formulation with no peptide conjugated. Moreover the rate of internalisation of the LDL-like ORL NPs was significantly enhanced in breast cancer cell lines, due to the combined effect of active and passive targeting.

Conclusions: In conclusion, coating of the particles and controlling the rate of solvent shift in our study resulted in a suitable and easy way of controlling particle size and avoiding undesired particle size growth. Although orlistat is highly hydrophobic, yet it could be formulated into

nanoparticles assemblies, using a simple method and with high stability, small controlled size and immense drug concentration. Finally, LDL-like ORL NPs is a promising formulation for combating breast cancer, with significant efficacy and targeting ability.

TABLE OF CONTENTS

Acknowledgment ..... *I*

Declaration ..... *III*

Abstract ..... *IV*

1 Chapter 1: General Introduction *1*

1.1 Cancer worldwide **1**

1.2 Breast cancer **2**

1.2.1 History and statistics 2

1.2.2 Types and pathology 3

1.2.3 Etiology and risk factors 5

1.2.4 Diagnosis 6

1.2.5 Treatment strategies 6

1.3 Nanotechnology for cancer therapy **10**

1.3.1 Targeting mechanisms 10

1.3.2 Nanoparticles delivery systems for breast cancer 15

1.4 Nanoparticles preparation techniques **17**

1.5 Theory of Nanoparticle formation using Nanoprecipitation technique **18**

1.5.1 Classical Nucleation Theory (CNT) 18

1.5.2 Ostwald ripening and particles condensation 21

1.5.3 DLVO theory 22

1.6 Rapid solvent shift technique (flash nanoprecipitation) **24**

1.6.1 Drugs properties 25

1.6.2 Solvent and anti-solvent nature 26

1.6.3 Stabilizers 27

1.6.4 Temperature 28
1.6.5 Drug concentration 28
1.7 LDL-like nanoparticles 29
1.8 Orlistat as promising anticancer 31
1.8.1 Fatty acid synthase enzyme (FASN) and breast cancer 31
1.8.2 Orlistat as FASN inhibitor 32
1.9 Research Design 32
1.9.1 Gap in Knowledge 34
1.9.2 Overriding Questions: 34
1.9.3 Overriding hypothesis 35
1.9.4 General Goals 35
2 Chapter 2 Materials and methods 36
2.1 EQUIPMENT AND TECHNIQUES 36
2.1.1 Dynamic light scattering (particle size) 36
2.1.2 Zeta potential 40
2.1.3 Transmission electron microscopy 43
2.2 MATERIALS 45
2.3 METHODS 46
2.3.1 Nanoparticles preparation 46
2.3.2 Coating of the NPs 48
2.3.3 Measuring the particle size and zeta potential: 48
2.3.4 TEM imaging of NPs 48
2.3.5 Freeze drying of the NPs 48
2.3.6 Drug incorporation assay 50
2.3.7 UV assay of orlistat 51

2.3.8 Encapsulation efficiency and drug loading 52
2.3.9 Drug release assay 53
2.3.10 Preparation of functionalised NPs 53
2.3.11 Cell studies on the prepared formulations 55
2.3.12 Statistical analysis 55
3 Chapter 3 Particle size control using solvent shift technique 56
3.1 INTRODUCTION 56
3.1.1 NPs' properties and its effect on efficacy of formulation 56
3.1.2 Parameters that Govern Nanoparticle Size Prepared through Rapid Solvent Shifting 58
3.1.3 Effect of concentration on the size of nanoparticles 60
3.2 AIMS AND OBJECTIVES 61
3.3 MATERIALS AND METHODS 61
3.3.1 Materials 61
3.3.2 Methods 63
3.4 RESULTS AND DISCUSSION 67
3.4.1 Measuring the mean particle size using DLS 67
3.4.2 Olive oil NPs: the effect of concentration over particle size 68
3.4.3 Effect of using different hydrophobic material on NPs properties. 76
3.4.4 Effect of coating the NPs over the particle size growth 79
3.4.5 Effect of the rate of nanoprecipitation on particle size 90
3.4.6 Orlistat nanoparticles 93
3.5 CONCLUSION 101
4 Chapter 4 Evaluation of orlistat nanoparticles as a candidate for LDL-like NPs 103
4.1 INTRODUCTION 103
4.1.1 Fatty acid synthase enzyme (FASN) and breast cancer 103

4.1.2 Orlistat as FASN inhibitors 104
4.1.3 Orlistat as a promising anti-cancer 104
4.1.4 Freeze-drying of nanoparticles 106
4.2 AIMS AND OBJECTIVES 109
4.3 MATERIALS AND METHODS 110
4.3.1 Materials 110
4.3.2 Methods 110
4.4 RESULTS AND DISCUSSION 115
4.4.1 Evaluation of stabilisers' effect on prepared NPs 115
4.4.2 Freeze drying and particles stability 122
4.4.3 Evaluation of drug incorporation 129
4.4.4 UV assay of orlistat 132
4.4.5 Drug loading and entrapment efficiency 133
4.4.6 Drug release assay 135
4.5 CONCLUSION 137
5 Chapter 5 Surface-functionalised LDL-like orlistat nanoparticles 139
5.1 INTRODUCTION 139
5.1.1 LDL-like nanoparticles 139
5.2 AIMS AND OBJECTIVES 142
5.3 MATERIALS AND METHODS 143
5.3.1 Materials 143
5.3.2 Methods 144
5.4 RESULTS AND DISCUSSION 152
5.4.1 Functionalised LDL-like Orlistat NPs 152

5.4.2 Effect of peptide coating on the NPs characteristics 155
5.4.3 Investigation the effect culture medium on POPC coated orlistat NPs 158
5.4.4 Investigation of orlistat binding to albumin 163
5.4.5 Investigation of the cytotoxicity of orlistat formulations 166
5.4.6 Investigation of cellular uptake 178
5.4.7 Cellular uptake mechanism 184
5.5 CONCLUSIONS 189
6 Chapter 6 Conclusions and future work 190
6.1 CONCLUSIONS 190
6.2 FUTURE WORK 195
7 Reference 196
8 Appendix 229
8.1 Calculations of number of particles, distance and amount of POPC for coating particles 229
8.2 Olive oil NPs 233
8.3 2D printer of tween 80 coated olive oil NPs particle size 235
8.4 Uncoated orlistat NPs 236
8.5 Slow Vs Fast injection 238
8.6 POPC coated orlistat NPs 239
8.7 Size analysis of POPC coated orlistat NPs in different stabilisers 241
8.8 TEM Orlistat NPs (coated vs uncoated) 245
8.9 Orlistat in Dimethyl acetamide DMA 246

8.10 Peptide coated NPs DLS 247

LIST OF FIGURES

Figure 1 Free energy diagram of Classical Nucleation Theory (CNT). 19

Figure 2 structure of Malvern zeta Sizer DLS, 1) Optical unit 2) Cells used, 3) Cell area, 4) MPT-2 tritrator which is an adjuvent added when required, 5) computer running the Zeta sizer software (160). 36

Figure 3 Measuring the Zeta potential of colloidal particles, showing the electric double layer and the boundary slipping plane (160).....41

Figure 4 Diagram representing a simplified structure of the transmission electron microscope TEM(165). 44

Figure 5 Automated syringe eVol™.....46

Figure 6 Diagram showing the steps of NPs preparation using rapid solvent shift technique.47

Figure 7 Malvern® zeta sizer nanorange ZS 47

Figure 8 Freeze dryer, Virtis benchtop lyophiliser® (SP scientific sentry 2.0).....49

Figure 9 Differential scanning calorimetry DSC Q2000 (TA® instruments, UK).....50

Figure 10 polarised light microscope PX023POL (Prior Scientific Inc® USA).....51

Figure 11 UV spectrophotometer (Agilent® Cary3500 UV-Vis spectrophotometer, USA)...51

Figure 12 Vivaspin® centrifugal concentrator, Sartorius Vivaspin® 20, mwco 5000 d, membrane PES.....52

Figure 13 slide-A- lyzer dialysis cassettes (thermos scientific™ mwco 3.5 Kd, UK) 53

Figure 14 Proposed structure of the LDL-like NPs functionalised with 11-mer peptide. 54

Figure 15 Jiang et al. results showing the effect of particle size of gold NPs on the endocytosis and uptake of the NPs in breast cancer cell lines.....57

Figure 16 Cabral et al. results showing the effect of particle size of polymeric micelles on the tumour volume and dose accumulation in prostate cancer cell lines.....57
Figure 17 chemical structure of employed excipients A) POPC, B) Tween80 and C) Lecithin 62
Figure 18 Particle size distribution by volume for olive oil NPs of 1 mM concentration, prepared by fast solvent injection technique.....68
Figure 19 Volume average PSD vs final olive oil concentration injected as 1:9 (v/v) into water for a range of final concentrations of 0.001 g/L to 3.5 g/L, expressed as mean of triplicates ± SD. 70
Figure 20 Comparison between olive oil and triolein NPs (Parsad et al.), in terms of volume PSD vs final oil concentration injected as 1: 9 ethanolic solution to water (v/v) for a range of initial concentrations of 0.01 mM to 10 mM, n=3 ±SD. 71
Figure 21 effect of final olive oil concentration on the estimated total number of the formed nanoparticles in dispersion prepared by direct ethanolic injection at a ratio 1:9 (v/v) in water, in a range of initial concentration of 0.01 mM to 10 mM.....73
Figure 22 effect of final olive oil concentration on the estimated average distance (nm) between nanoparticles in dispersion prepared by direct ethanolic injection at a ratio 1:9 (v/v) in water, in a range of initial concentration of 0.01 mM to 10 mM.....73
Figure 23 Comparison of Zeta potential between freshly prepared and aged (1 week after) olive oil nanoparticles, prepared by direct ethanolic injection at a ratio 1:9 (v/v) in water, in a range of initial concentration of 0.01 mM to 10 mM, n=3 ±SD.....75
Figure 24 Zeta potential of olive oil NPs compared to triolein NPs at 1 mM final concentration. The results are shown as average of triplicate ± SD.....75
Figure 25 Comparison of the effect of final lipid concentration on the particle size growth expressed as volume PSD, for olive oil, tricaprin and trihexanoin nanoparticles, prepared by

ethanolic injection in a ratio of 1:9 (v/v) in water, in an initial concentration range of lipids in ethanol of 0.01 mM to 10 mM, n=3 ±SD. 77
Figure 26 Comparison of the particle size growth of olive oil, tricaprin and trihexanoin nanoparticles, as normalised volume PSD.....78
Figure 27 Comparison of zeta potential of olive oil, tricaprin and trihexanoin nanoparticles prepared by injection ethanolic solutions into water in a ratio 1:9 (v/v), at different final concentrations (0.001 to 1 mM), n=3 ±SD. 78
Figure 28 Comparison of average volume particle size of olive oil NPs coated with either POPC, tween 80 in 10% ethanol and Lecithin coated triolein NPs in 10% DMSO in a molar ratio (1 core:1 coat), at different final olive oil concentration (0.0025 to 1 mM), n=3 ±SD...81
Figure 29 Comparison of average particle size by volume of olive oil NPs coated with either POPC, tween 80 in 10% ethanol and Lecithin coated triolein NPs in 10% DMSO in a molar ratio (2 core:1 coat), at different final olive oil concentration (0.0025 to 1 mM), n=3 ±SD...82
Figure 30 Comparison of average particle size by volume of olive oil NPs coated with either POPC, tween 80 in 10% ethanol and Lecithin coated triolein NPs in 10% DMSO in a molar ratio (4 core:1 coat), at different final olive oil concentration (0.0025 to 1 mM), n=3 ±SD...82
Figure 31 Comparison of average volume particle size of coated olive oil NPs with either POPC or tween 80 at different molar ratios (1:1, 2:1, and 4:1) to the uncoated olive oil nanoparticles, at different final olive oil concentration (0.0025 to 1 mM), n=3 ±SD.....83
Figure 32 Comparison of zeta potential of coated olive oil NPs with either POPC or tween 80 at different molar ratios (1:1, 2:1, and 4:1) to the uncoated olive oil nanoparticles, at different final olive oil concentration (0.0025 to 1 mM), n=3 ±SD. 84
Figure 33 Comparison of TEM between Lecithin, tween80, POPC coated NPs in a ratio (2oil:1coat), and 1 mM final core oil concentration. A) Lecithin coated triolein NPS, B) POPC coated olive oil NPs, and C) Tween 80 coated olive oil NPs. 86

Figure 34 Comparison of TEM between Lecithin, tween80, POPC coated NPS in a ratio (2oil:1coat), 0.1 mM final core oil concentration. A) Lecithin coated triolein NPS, B) POPC coated olive oil NPs, and C) Tween 80 coated olive oil NPs. 86
Figure 35 Comparison between average particle size (nm) of coated olive oil NPs at two different concentrations (0.1 and 1 mM) obtained by either DLS or TEM imaging for A) Tween 80 coating B) POPC coating and C) Lecithin coating, n=3 ±SD.....87
Figure 36 2D printed tween80 coated olive oil NPs in different molar ratios, printing was done through dispensing ethanolic solutions into anti solvent water at ratio 1:9, n=3 ±SD. 89
Figure 37 investigating the core: core ratio for POPC coated olive oil NPs at different olive oil concentrations prepared by rapid solvent shift technique from ethanolic solution in water (1:9), n=3 ±SD. 90
Figure 38 Effect of injection rate on particle size of uncoated olive oil NPs, using ethanolic injection into water in a ratio (1:9). 92
Figure 39 TEM imaging coated olive oil NPs prepared by either slow or rapid ethanolic injection (1:9) with core to coat ratio 2:1 and olive oil concentration of 1 mM final concentration, A) POPC coated NPs slow injection, B) POPC coated NPs rapid injection, C) Tween80 coated NPs slow injection and D) Tween80 coated NPs rapid injection. 92
Figure 40 Effect of increasing concentration on volume average particle size for orlistat NPs injected as 1:9 (v/v) into water for a range of initial concentrations of 0.025 mM to 40 mM, n=3 ±SD. 94
Figure 41 TEM images of uncoated orlistat NPs at different molar concentrations, A) 1mM, B) 0.1 mM, C) 2 mM, D) 3 mM, and E) 4 mM).....95
Figure 42 zeta potential of orlistat NPs injected as 1:9 (v/v) into water for a range of initial concentrations of 0.025 mM to 40 mM, shown as average of 3 readings ±SD. 95

Figure 43 effect of POPC coating of orlistat NPs on the average volume particle size in a molar ratio (2 core: 1 coat), injected as 1:9 (v/v) into water for a range of initial orlistat concentrations of 0.025 mM to 40 mM, n=3 ±SD. 96
Figure 44 TEM images of POPC coated orlistat NPs (2:1, core: coat) at different final orlistat concentrations, A) 0.1 mM, B) 1 mM, C) 2 mM, D) 3 mM, and E) 4 mM).....97
Figure 45 effect of final dispersion concentration on the total number of particles in dispersion for the uncoated orlistat NPs vs the POPC coated orlistat NPs (2:1, core: coat), prepared by direct ethanolic injection at a ratio 1:9 (v/v) in water, in a range of initial orlistat concentration of 0.025 mM to 40 mM.....98
Figure 46 effect of final dispersion concentration on the average distance (nm) between uncoated and POPC coated orlistat NPs in dispersion for the uncoated orlistat NPs vs the POPC coated orlistat NPs (2:1, core: coat), prepared by direct ethanolic injection at a ratio 1:9 (v/v) in water, in a range of initial orlistat concentration of 0.025 mM to 40 mM. 98
Figure 47 Comparison of volume particle size growth between orlistat and niclosamide stearate NPs prepared by direct ethanolic injection at a ratio 1:9 (v/v) in water, in a range of initial concentration of 0.025 mM to 10 mM, n=3 ±SD. 100
Figure 48 Comparison of average zeta potential between orlistat and niclosamide stearate NPs prepared by direct ethanolic injection at a ratio 1:9 (v/v) in water, in a range of initial concentration of 0.025 mM to 10 mM, n=3 ±SD. 100
Figure 49 chemical structure of orlistat 106
Figure 50 comparison of particle size of freshly prepared orlistat NPs (0.1, 1, 2 4 mM orlistat final concentration) after adding various stabilisers to the antisolvent during preparation, n=3 ±SD. 116

Figure 51 comparison of zeta potential of freshly prepared orlistat NPs (0.1, 1, 2 4 mM orlistat final concentration) after adding various stabilisers to the antisolvent during preparation, n=3 ±SD. 118
Figure 52 comparison of particle size of orlistat NPs (0.1, 1, 2 4 mM orlistat final concentration) after adding various stabilisers to the antisolvent during preparation and 2 weeks storage in fridge at 4º C, n=3 ±SD.....119
Figure 53 comparison of zeta potential of orlistat NPs (0.1, 1, 2 4 mM orlistat final concentration) after adding various stabilisers to the antisolvent during preparation and 2 weeks storage in fridge at 4º C, n=3 ±SD. 120
Figure 54 TEM images of POPC coated orlistat NPs (1 mM), A & B in MilliQ water, C) in 3 mM SDS, D) in 2% tween 80. 122
Figure 55 comparison of particle size of freshly prepared orlistat NPs (0.1, 1, 2 4 mM orlistat final concentration) before and after addition of cryoprotectant trehalose 10%, n=3 ±SD...123
Figure 56 Particle size (nm) map of different formulations of POPC coated orlistat NPs (2:1, with 2 mM orlistat final concentration) with addition of different cryoprotectants (Mannitol, Trehalose and Glucose) in different percent (5, 10 & 15 %).....125
Figure 57 Effect of Freeze drying on stability of NPs over long-term storage (6 months) compared to NPs left in fridge at 4ºC without freeze drying with respect to particle size, n=3 ±SD. 127
Figure 58 Size map showing effect of Freeze drying on stability of NPs over long-term storage (6 months) compared to NPs left in fridge at 4ºC without freeze drying. 127
Figure 59 Effect of Freeze drying on stability of NPs over long-term storage (6 months) compared to NPs left in fridge at 4ºC without freeze drying with respect to zeta potential, n=3 ±SD. 128

Figure 60 Images of POPC coated orlistat NPs after 6 months storage (2:1 and final concentration of orlistat 2 mM) from left to right of 1) freeze dried formulation before reconstitution 2) after constitution and 3) formulation stored without freeze drying. 128
Figure 61 DSC thermograms of a heat cool heat cycle for A) pure orlistat, B) Orlistat and POPC physical mixture, C) POPC coated orlistat NPs 130
Figure 62 PLM images to show birefringence for A) POPC lipid, B) Orlistat, C) POPC coated orlistat NPs D) uncoated orlistat NPs, 1) Dark field, 2) bright field. 131
Figure 63 Absorption spectrum of 1 mg / ml orlistat solution prepared in ethanol. 132
Figure 64 Calibration curve of orlistat solutions (10-150 μg/ml) in ethanol at λmax 205 nm. 133
Figure 65 drug release assay for POPC coated orlistat NPs, performed in 400 ml PBS (pH 7.4) at 37ºC and 350 rpm, n=3 ±SD. 136
Figure 66 Schematic presentation of the LDL- like nanoparticle compared to a cutaway schematic of the LDL(232) 140
Figure 67 Chemical structure of employed lipids A) DSPE PEG 5000 maleimide, B) DSPC and C) cholesterol. 144
Figure 68 Structure of LDL-like NPs 152
Figure 69 11-mer peptide analysis certificate, A) Mass spectroscopy showing molecular weight, B) HPLC assay showing purity. 153
Figure 70 Particle size analysis of LDL like orlistat NPs (containing either POPC or DSPC in the lipid layer) compared to the POPC coated orlistat NPs and the uncoated orlistat NPs in 3 different media (water, 3mM SDS and 2% tween 80), measured directly after preparation, n=3 ± SD. 156
Figure 71 TEM images of LDL-Like orlistat NPs with final orlistat concentration 2 mM... 156

Figure 72 surface charge LDL like orlistat NPs (containing either POPC or DSPC in the lipid layer) compared to the POPC coated orlistat NPs and the uncoated orlistat NPs in 3 different media (water, 3mM SDS and 2% tween 80), n=3 ±SD. 157
Figure 73 Z-average particle size distribution of POPC coated orlistat NPs (4 mM orlistat and 2:1 core to coat) prepared in water and DMEM, comparted to the particles size of POPC coated orlistat NPs prepared in water and diluted with DMEM at concentrations (1.4, 0.8, 0.4, 0.2, and 0.04 mM). A) XY scatter, B) Bar chart, n=3 ±SD. 159
Figure 74 Volume particle size distribution of POPC coated orlistat NPs (4 mM orlistat and 2:1 core to coat) prepared in water and DMEM, comparted to the particles size of POPC coated orlistat NPs prepared in water and diluted with DMEM at concentrations (1.40, 0.8, 0.4, 0.2, and 0.04 mM). A) XY scatter, B) Bar chart, n=3 ±SD. 160
Figure 75 Zeta potential (mV) of POPC coated orlistat NPs (4 mM orlistat and 2:1 core to coat) prepared in water and DMEM shown on secondary axis, comparted to the particles size of POPC coated orlistat NPs prepared in water and diluted with DMEM at concentrations (1.40, 0.8, 0.4, 0.2, and 0.04 mM) showed on primary axis. A) XY scatter, B) Bar chart, n=3 ±SD. 162
Figure 76 Fluorescence quenching assay of HSA, A) a diagram showing the concept of fluorescence quenching, B) Fluorescence spectra of HSA, measured at zero time, alone and in the presence of various concentrations of orlistat (ORL), at temperature T = 298 K, excitation wavelength = 280 nm, concentration of HSA 1.5×10^{-6} mol L^{-1} (1.5 µM), and at increasing concentration of orlistat (20, 40, 60 and 100 µM). 164
Figure 77 Stern–Volmer plots for the quenching of HSA by ORL at pH 7.4. 165
Figure 78 Double-log plots of ORL quenching effect on HSA fluorescence at pH 7.4. 166
Figure 79 cell survival curve for cytotoxicity assay (48 hrs) of 2 formulations, Peptide coated ORL NPs and POPC coated ORL NPs, in MCF-7 breast cancer cell line, n=6 ±SD. 168

Figure 80 cell survival curve for cytotoxicity assay of 2 formulations, Peptide coated ORL NPs and Peptide coated triolein TO NPs as a negative control, in MCF-7 breast cancer cell line, n=6 ±SD. 169
Figure 81 cell survival curve for cytotoxicity assay of ORL ethanolic solution as positive control compared to the vehicle Ethanol, in MCF-7 breast cancer cell line, n=6 ±SD. 170
Figure 82 cell survival curve for cytotoxicity assay of 2 formulations, Peptide coated ORL NPs and POPC coated ORL NPs, in BT-474 breast cancer cell line, n=6 ±SD. 171
Figure 83 cell survival curve for cytotoxicity assay of 2 formulations, Peptide coated ORL NPs and Peptide coated triolein TO NPs as a negative control, in BT-474 breast cancer cell line, n=6 ±SD. 172
Figure 84 cell survival curve for cytotoxicity assay of ORL ethanolic solution as positive control compared to the vehicle Ethanol, in BT-474 breast cancer cell line, n=6 ±SD.....173
Figure 85 cell survival curve for cytotoxicity assay of 2 formulations, Peptide coated ORL NPs and POPC coated ORL NPs, in MDA MB-453 breast cancer cell line, n=6 ±SD. 174
Figure 86 cell survival curve for cytotoxicity assay of 2 formulations, Peptide coated ORL NPs and Peptide coated triolein TO NPs as a negative control, in MDA MB-453 breast cancer cell line, n=6 ±SD. 175
Figure 87 cell survival curve for cytotoxicity assay of ORL ethanolic solution as positive control compared to the vehicle Ethanol, in MDA MB-453 breast cancer cell line, n=6 ±SD. 176
Figure 88 Comparison between the survival rate curves for the cytotoxicity assay of Peptide coated orlistat ORL NPs, in 3 different breast cancer cell lines, n=6 ±SD. 177
Figure 89 Comparison between the inhibitory concentrations (IC_{50}) of 2 different formulations, POPC coated ORL NPs and Peptide coated ORL NPs respectively, on the 3 utilised breast

cancer cell lines, BT-474, MCF-7 and MDA MB-453. **** Statistically significant difference at P value < 0.0001, n=6 ±SD. 178
Figure 90 Cellular uptake fluorescent imaging carried out on BT-474 breast cancer cell lines, captured at specific time intervals (1, 2, 4, 8 and 24 hours) following the treatment of the cells with one of the formulations (F1, F2) at two different concentrations each (100µM and 40µM). F1 is fluorescently labelled POPC coated orlistat NPs, F2 fluorescently labelled LDL-like orlistat NPs. A) Fluorescent microscopy images, B) Mean fluorescence intensity plot, n=3 ±SD. 181
Figure 91 Cellular uptake fluorescent imaging carried out on MCF-7 breast cancer cell lines, captured at specific time intervals (1, 2, 4, 8 and 24 hours) following the treatment of the cells with one of the formulations (F1, F2) at two different concentrations each (100µM and 40µM). F1 is fluorescently labelled POPC coated orlistat NPs, F2 fluorescently labelled LDL-like orlistat NPs. A) Fluorescent microscopy images, B) Mean fluorescence intensity plot, n=3 ±SD. 182
Figure 92 Cellular uptake fluorescent imaging carried out on MDA MB 453 breast cancer cell lines, captured at specific time intervals (1, 2, 4, 8 and 24 hours) following the treatment of the cells with one of the formulations (F1, F2) at two different concentrations each (100µM and 40µM). F1 is fluorescently labelled POPC coated orlistat NPs, F2 fluorescently labelled LDL-like orlistat NPs. A) Fluorescent microscopy images, B) Mean fluorescence intensity plot, n=3 ±SD. 183
Figure 93 Cellular uptake rate using fluorescence microscopy for LDL-like ORL NPs in 3 different breast cancer cell lines, BT-474, MCF-7 and MDA MB 453 respectively, plotted as mean fluorescence intensity at concentration of 100 µM orlistat. **** Statistically significance between the three cell lines at P<0.0001 for each time point, n=3 ±SD. 184

Figure 94 Cellular uptake fluorescent imaging carried out on BT 474 breast cancer cell lines, captured at specific time intervals (30,60 and 120 minutes) following the treatment of the cells with one of the formulations (F1, F2) in presence or absence of Suramin. F1 is fluorescently labelled POPC coated orlistat NPs, F2 fluorescently labelled LDL-like orlistat NPs. A) Fluorescent microscopy images, B) Mean fluorescence intensity plot. **** Statistically significance between the three cell lines at P<0.0001 for each time point, n=3 ±SD. 186
Figure 95 Cellular uptake fluorescent imaging carried out on MCF-7 breast cancer cell lines, captured at specific time intervals (30,60 and 120 minutes) following the treatment of the cells with one of the formulations (F1, F2) in presence or absence of Suramin. F1 is fluorescently labelled POPC coated orlistat NPs, F2 fluorescently labelled LDL-like orlistat NPs. A) Fluorescent microscopy images, B) Mean fluorescence intensity plot. **** Statistically significance between the three cell lines at P<0.0001 for each time point, n=3 ±SD. 187
Figure 96 Cellular uptake fluorescent imaging carried out on MDA MB 453 breast cancer cell lines, captured at specific time intervals (30,60 and 120 minutes) following the treatment of the cells with one of the formulations (F1, F2) in presence or absence of Suramin. F1 is fluorescently labelled POPC coated orlistat NPs, F2 fluorescently labelled LDL-like orlistat NPs. A) Fluorescent microscopy images, B) Mean fluorescence intensity plot. **** Statistically significance between the three cell lines at P<0.0001 for each time point, n=3 ±SD. 188

LIST OF TABLES

Table 1 Chemotherapy combination regimens for breast cancer control 8
Table 2 Nanocarrier delivery systems for targeting breast cancer A) already available product in market, B) under clinical trials. 12
Table 3 Nanocarrier approaches for chemotherapeutic targeting of breast cancer.....15

Table 4 Validation parameters for UV spectroscopic assay of orlistat in ethanol. 133

Table 5 Encapsulation efficiency and drug loading percent for the prepared POPC coated orlistat NPs, n=3 ±SD. 134

Table 6 Composition of various surface functionalised LDL NPs formulations..... 146

Table 7 percentage free sulfhydryl groups determined by Ellman's assay 154

Table 8 Stern–Volmer quenching constants for the interaction of ORL with HSA at pH 7.4 and room temperature. 165

Table 9 Stern–Volmer binding constants for the interaction of ORL with HSA at pH 7.4 and room temperature. 166

LIST OF EQUATIONS

Equation 1 $\mathbf{\Delta Ghomo = 4\,\pi r2\gamma + 43\,\pi\, r3\Delta Gv}$ 19

Equation 2 $\Delta G_v = -\boldsymbol{KB\,T}\ln(\boldsymbol{S})\boldsymbol{Vm}$ 20

Equation 3 $\Delta G_{\mathrm{Crit}} = \mathbf{43\pi\ rcrit2}$ 20

Equation 4 $R_{\mathrm{Crit}} = -\mathbf{2\gamma\Delta Gv}$ 20

Equation 5 $R_{\mathrm{Crit}} = \mathbf{2\gamma Vm\ KB\ T}\ln(\boldsymbol{S})$ 20

Equation 6 $\mathbf{J = A\ eEa\ KBT}.(-\Delta\mathbf{GKBT})$ 21

Equation 7 $\boldsymbol{R3 = 8\,\gamma\, C\infty Vm\, D9\, RgT\, t = KORt}$ 22

Equation 8 $\boldsymbol{Evdw = -AR12\ D\ KBT}$ 23

Equation 9 $\boldsymbol{EEDL = 2\,\pi\,\varepsilon\,\varepsilon o\,R\ \psi o\,2}\ln(\mathbf{1} + \boldsymbol{e} - \boldsymbol{Dk} - \mathbf{1})\boldsymbol{KBT}$ 23

Equation 10 $E_{\mathrm{Total}} = E_{\mathrm{vdW}} + E_{\mathrm{EDL}}$. 24

$\boldsymbol{dH = k\,T3\pi\eta D}$ Equation 11 Stokes Einstein equation 37

$\boldsymbol{UE = 2}\varepsilon\,\mathrm{z}\,\boldsymbol{f(ka)3}\,\eta$ Equation 12 Henry's equation 41

Equation 13 $\boldsymbol{R = 34\pi n1/3}$ 60

Equation 14 $\mathbf{Volume\ of\ partcles\ (V) = 43\pi r3}$, $\mathbf{Mass\ of\ particle\ (m) = \rho \times V}$ 72

Equation 15 $\mathbf{Number\ of\ particlesml = Concentrationmass\ of\ one\ particle}$ 72

Equation 16 $\mathbf{Distance\ cm = (1number\ of\ particles/ml)13}$ 72

LOD = $\mathbf{3}\ \boldsymbol{sm}$ Equation 17 Limit of detection.....113

LOQ = $\mathbf{10}\ \boldsymbol{sm}$ Equation 18 Limit of quantification 113

Equation 19 Entrapment Efficiency.....134

Equation 20 Drug loading percent 134

$\boldsymbol{F0F = 1 + Kq\tau 0Q = 1 + KSVQ}$ Equation 21 Stern-Volmer equation.....148

$\mathbf{log}(\boldsymbol{F0 - FF}) = \mathbf{log}\boldsymbol{Kb} + \boldsymbol{n}\mathbf{log}[\boldsymbol{Q}]$ Equation 22 binding constant equation.....165

LIST OF ABBREVIATIONS

A.D.	Anno domini
AML	Acute myeloid leukaemia
ANOVA	Analysis of variance
B.C.	Before Christ
BRCA	Breast cancer gene
BSA	Bovine serum albumin
C3a	complement component 3a
ca.	Circa
Sodium CMC	Carboxy methyl cellulose
CML	Chronic myeloid leukaemia
CNT	Classical nucleation theory
CT	Chemotherapy
CTACl	Cetyl trimethylammonium chloride
DCIS	Ductal carcinoma in situ
DL	Drug loading

DLS	Dynamic light scattering
DLVO	Derjaguin, Landau, Verwey and Overbeek
DMA	Dimethyl acetamide
DMEM	Dulbecco's Modified Eagle Medium
DMF	Dimethyl formamide
DMSO	Dimethyl sulfoxide
DNA	Deoxyribonucleic acid
DSC	Differential scanning calorimetry
DSPC	Distearoyl phosphatidylcholine
DSPE PEG 5000	Distearoly phosphatidyl ethanolamine polyethylene glycol 5000
ECM	Extracellular matrix
EE	Entrapment efficiency
EGF	Epidermal growth factor
EGFR	Epidermal growth factor receptor
EPR	Enhanced permeation and retention
ER	Estrogen
ET	Endocrine therapy
FASN	Fatty acid synthase enzyme
FDA	Food and drug administration
GIT	Gastrointestinal tract
GRAS	Generally recognised as safe

HDL	High density lipoprotein
HER-2	Human epidermal growth factor
HPMC	Hydroxyl propyl methyl cellulose
HSA	Human Serum albumin
HSP27	Heat shock protein 27
IDS	Infiltrating ductal carcinoma
IGF-IR	Insulin like growth factor-insulin receptor
ILS	Infiltrating lobular carcinoma
KNO_3	Potassium nitrate
LCIS	Lobular carcinoma in situ
LDL	Low density lipoprotein
LDLR	Low density lipoprotein receptor
LDV	Laser Doppler velocimetry
LOD	Limit of detection
LOQ	Limit of quantification
MBI	Molecular breast imaging
MRI	Magnetic resonance imaging
25-NBD	Nitrobenzoxadiazole
NPs	Nanoparticles
OLO	1,2-dioleoyl-3-linoleoyl-sn-glycerol
OOO	Triolein
ORL	Orlistat

PBS	Phosphate buffer saline
PCL	poly-ε-caprolactone
PDI	Polydispersity index
PLA	Polylactide
PLGA	Polylactic co glycolic acid
PLM	Polarised light microscopy
PM	Personalised medicine
PMM	poly (methylidene malonate 2.1.2)
POO	Glycerol dioleate palmitate
POPC	1-palmitoyl-2-oleoyl phosphatidyl choline
PR	Progesterone
PSD	Particle size distribution/diameter
PVA	Polyvinyl acetate
PVP	Polyvinyl pyrollidone
Re	Reynauld's number
RES	Reticuloendothelial system
RT	Radiotherapy
SA	Specific aim
SDS	Sodium dodecyl sulfate
SEM	Scanning electron microscopy
SPIO	Super paramagnetic iron oxides
TEM	Transmission electron microscopy

Tg	Glass transition temperature
THF	Tetrahydro furan
TO	Triolein
UV-Vis	Ultraviolet-visible
VEGF	Vascular endothelial growth factor
VLDL	Very low density lipoprotein
ZS	Zeta sizer

1 Chapter 1: General Introduction

1.1 Cancer worldwide

Cancer is considered one of the most hazardous clinical conditions being associated with high mortality rates. The reason behind this is the abnormal and uncontrolled cell division that may affect the normal body functions. Worldwide, cancer is considered one of the leading causes of mortality(1,2), accounting for over 160,000 deaths in the UK and 90,000 deaths in Egypt based on the most recent statistics(3,4). Over 200 types of cancers are identified now and many attempts to treat them with either radiation, chemotherapy or surgery have been done, however; an effective regimen to control cancer is still unavailable. Recently, targeted drug delivery has emerged as a way to improve the therapeutic outcome of anticancer treatments achieving a selective effect on tumour cells; hence protecting other tissues from their toxic side effects and improving their therapeutic index.(5) Nanotechnology was applied in oncology to provide alternative ways for drug delivery through targeting the tumour and reducing its resistance(6). The simplest and most widely used type of nanomedicine is liposomal formulations. It has been used since the approval of liposomal doxorubicin and daunorubicin for treatment of Kaposi's sarcoma in 1995, which then have been used in breast and ovarian cancer (7).

Most targeted nanomedicines focus mainly on the passive way of delivery, also known as enhanced permeability and retention effect (EPR), as a way to enhance the pharmacokinetic profiles, permeability, and distribution of anticancer therapy to the cancer tissue. This is attributed to the fact that most of solid tumours are characterized by enormous network of fenestrated blood vessels (8).

Considering the relatively poor efficacy of the available traditional therapies for cancer, especially with aggressive tumours, the recent approaches to cancer treatment should focus on the identification of 'cancer-specific markers' to enable the effective targeted delivery of anticancer agents to tumours.

1.2 Breast cancer

1.2.1 History and statistics

Throughout all cancer types, breast cancer is the most abundant type of cancer in women worldwide. For instance, approximately 1.7 million new cases were diagnosed with breast cancer in 2012 (9), this counts for about 12% of all new cancer cases and 25% of all cancers in women. The history of breast cancer dates back to around 1,500 years B.C, many civilizations described breast cancer and tried to find approaches to its management. This includes the ancient Egyptian civilization (10,11), where the condition was mentioned in various papyri such as Edwin Smith (12) and George Ebers papyri (13). Later on, the Ancient Greeks also described the disease (14).

Nonetheless, breast cancer is not restricted to females, male breast cancer is also possible to occur, representing around 0.8%–1% of all breast cancer cases (15–17) .

Survival rates vary widely every year, positively those rates increased tremendously in the recent years (up to 90%)(18). This striking improvement could be related to the development of the screening methods, early diagnosis, and the new treatment strategies (19).

Aiming towards a new era of breast cancer eradication, the new field of proteomics has identified several blood-based biomarkers, including HSP27, transcriptional regulator 14-3-3σ, C3a, and fibrinogen-α4. Those biomarkers can help in effective tumour targeting. Moreover, many proteomic studies of breast cancer have been carried out aiming to aid the development of personalized medicines (PM), this in turn may help improve early detection and treatment of the tumour (20–22). Yet, resistant, and metastatic breast cancer remains a great hurdle for clinical eradication (23–25).

1.2.2 Types and pathology

Breast cancer can be simply defined as any anomalistic overgrowing cancerous tissue that affects any of the breast tissues. Normally the breast is formed of two main tissues, the glandular and the stromal tissues, in addition to the lymphatic tissue that is responsible for the immune function and the clearance of pathogens and waste(26).

Despite the fact that most of the tumorous growths affecting human breast are considered non-cancerous, or in other words benign, including cysts and fibrosis, yet those benign tumours could still develop into cancerous tumours, especially with the lack of proper diagnosis and with increasing the risk factors that will be discussed later(27).

Breast cancer could be classified in various ways, i.e., according to the degree of invasion, depending on the type of tissue affected, the stage of development, and finally on molecular levels depending on the expression of specific receptors on the cancerous cells.

In the following section we will discuss in brief most of the used classifications for breast cancer.

1.2.2.1 Degree of Invasion

1.2.2.1.1 Non-Invasive Breast Cancer

It is considered when the cancerous cells are confined to their specific tissue of origin and do not spread into the surrounding connective or lymphatic tissues(28).

1.2.2.1.2 Invasive Breast Cancer

In this case cancerous tissue will break through its tissue of origin into the surrounding tissues. One should note that it is different from metastasis, where the cancer cell travels to other body organs. Cancer can be invasive without being metastatic(29).

1.2.2.2 Type of tissue

1.2.2.2.1 Lobular carcinoma in situ (LCIS)

It refers to cancerous tumours confined in the lobules (milk glands) of the breast.

1.2.2.2.2 Ductal carcinoma in situ (DCIS):

Cancerous tumour growth affecting the milk ducts of the breast, and considered the most common non-invasive breast cancer.

1.2.2.2.3 Infiltrating lobular carcinoma (ILC)

It is considered the metastatic type of the lobular breast cancer.

1.2.2.2.4 Infiltrating ductal carcinoma (IDC)

It is the invasive type of ductal carcinoma, invading the surrounding breast tissues.

1.2.2.3 Stage of development

Breast cancer could be classified into 4 stages depending on how advanced the tumour is, and its invasion to the surrounding tissues. Stages are assigned roman numbers from I to IV, starting from stage I describing small tumour mass confined to a single tissue, Stage II with bigger tumours invading 1 to 3 lymph nodes, Stage III with bigger tumour mass invading more than 3 lymph nodes and finally Stage IV describing metastatic breast cancer that travels and invades other body organs(28).

1.2.2.4 Molecular subtype

Due to the nature of the breast cancer, being very heterogeneous, it could be classified based on the hormonal receptor. Three main hormonal receptors are used for this molecular classification, oestrogen (ER), progesterone (PR) and human epidermal growth factor 2 receptor (HER 2) (30).

Accordingly, breast cancer could be divided into 3 main molecular subtypes, the double positive (ER, PR +) that is subdivided into Luminal A and B depending on the abundance of

the biomarker protein Ki 67(31), the HER-2 positive (i.e., the triple positive breast cancer, and double negative breast cancer), and the triple negative (2).

1.2.3 Etiology and risk factors

The exact cause of cancer remains mysterious, with great scientific efforts are continuously made to study the development of cancerous cell, and relating this to the causes of developing cancer. However, many risk factors are well know that may increase the rate of developing breast cancer, mainly in women, are well known, which will be discussed in brief in the following section.

1.2.3.1 Aging

According to several studies, the risk of developing breast cancer increases significantly with aging, with around 77% of breast cancer patients aged 50 and over. This is due to the hormonal disturbances that increase with aging and menopause(32).

1.2.3.2 Genetic risk factors

Several studies have linked many types of cancers to some genetic mutations that result in abnormal cell growth and development of the cancerous tissues. Among those studies, breast cancer was found to be linked to mutations affecting 2 genes, BRCA1 and BRCA2(33). Inheritance of those mutated genes results in increasing the risk of developing breast cancer by a chance of up to 80%(34).

1.2.3.3 History of breast cancer

Chances of developing breast cancer increases in women whose first-degree relatives developed breast cancer. Additionally, women with cured breast cancer have a higher chance of developing breast cancer again, known as recurrence.

1.2.3.4 Other personal habits

This may include the use of hormonal replacement therapies or oral contraceptives, that results in change in the normal hormonal balance. The overconsumption of alcohol, smoking, obesity, and physical inactivity are considered as well among the factors that increases the chances of developing breast cancer (35).

1.2.4 Diagnosis

Early and proper diagnosis of breast cancer could improve the outcomes of treatment strategy. Poor prognosis and staging of breast cancer could result in a decrease in survival rate, and increases the chances of metastasis(36). Many methods have been developed for the breast cancer diagnosis. The most important is mammography, which indicates X-ray imaging of the breast. Considered as one of the conventional diagnosis methods, yet one of the most commonly used(37). Another adjunct diagnosis tool together with mammography is magnetic resonance imaging (MRI). MRI is a highly sensitive diagnosis tool, that can help in staging breast cancer, with no radiation used(38). Recently, a novel diagnosis tool known as molecular breast imaging (MBI) is developed, depending on the use of radioactive tracer that specifically marks cancerous tissues, and can be visualised by a nuclear scanner(39). However, breast biopsy remains the only definitive tool for breast cancer diagnosis, identifying the cancerous tissues, classifying it and determining its stage(40).

1.2.5 Treatment strategies

Many approaches are available for the control of breast cancer, this includes the conventional strategies such as surgery, radiotherapy (RT), endocrine (hormonal) therapy (ET), and chemotherapy (CT), or the novel targeted therapies including the use of monoclonal antibodies and through the use of nanotechnology. The choice of an effective algorism for the best treatment outcomes depends mainly on the stage of breast cancer, usually starts with surgery followed by other adjuvant therapies(41).

1.2.5.1 Surgical management of breast

Surgical management of breast cancer includes either surgical removal of the tumour with the surrounding tissues, which is known as the breast conservation surgery, or the complete removal of the affected breast known as mastectomy.

1.2.5.2 Radiotherapy

Radiotherapy (RT) refers to the use of radiations such as X-rays or gamma rays to eradicate cancerous cells. It is usually employed following breast conservation surgery to attempt complete removal of any remaining cancerous cells that may cause tumour recurrence. RT is typically given over a period of five to seven weeks following the employed surgery(42).

1.2.5.3 Endocrine therapy

Hormonal therapy of breast cancer depends on the molecular subtype of the cancer expressed. The Endocrine therapy (ET) helps supressing tumour growth through blockage the action of hormones. Endocrine therapies are usually employed for patients with cancerous tissues that are overexpressing the oestrogen receptors (ER). ET includes the use of oestrogen blockers such as Tamoxifen, or Aromatase enzyme inhibitors, which blocks the enzyme responsible for production of oestrogen, such as Anastrazole. Oestrogen blockers only are recommended for premenopausal patients, while both ER blockers and aromatase enzyme inhibitors can be used in postmenopausal patients(43).

1.2.5.4 Targeted therapy (monoclonal antibodies)

HER-2 targeted monoclonal antibodies are introduced for breast cancer, those expressing HER-2 receptors and are not sensitive to hormonal therapies. The first approved monoclonal antibody used is Trastuzumab, which is usually used in combination with chemotherapies for the control of HER-2 positive tumours(44). Nowadays, Pertuzumab in conjunction with Trastuzumab and docetaxel is the first line treatment regimen for patients with HER-2 positive metastatic breast cancer(45).

1.2.5.5 Chemotherapy

It involves the use of chemical anti-cancer medications, those medications either kill or stop the growth of the fast-growing cancerous cells. Chemotherapy is widely used for management of breast cancer, given either before surgery to shrink tumour, or after surgery to prevent recurrence. Typically, chemotherapies are given in cycles, followed by recovery periods. Many combination chemotherapy cycles can be used as regimens for breast cancer, the most important are described in **Table 1**.

Table 1 Chemotherapy combination regimens for breast cancer control

Strategy Abbreviations	Component
AC	Adriamycin (Doxorubicin), and Cyclophosphamide.
CAF	Cyclophosphamide, Adriamycin (Doxorubicin), and 5-Fluorouracil,
CMF	Cyclophosphamide, 5-Fluorouracil, and Mitoxantrone.
MMF	Methotrexate, 5- Fluorouracil and Mitoxantrone.
MFL	Mitoxantrone, 5-Fluorouracil and leucovorin.
VATH	Vinblastine, Doxorubicin, Thiotepa, and Halotestin.
Single-Agent Regimens	Paclitaxel Vinorelbine

Although most of the CT are administered through the intravenous IV route of administration, few are suitable for oral administration including methotrexate and cyclophosphamide. Recently great efforts are done towards development of more orally suitable chemotherapeutics to enhance patient's acceptance and compliance (46,47). Several chemotherapeutics formulations that can be suitable for oral administration are under investigation for breast cancer. Idarubicin, etoposide, taxane, gimatecan and vinorelbine are among those chemotherapeutics investigated in novel formulations for oral use(48–50).

However, the use of chemotherapy remains troublesome, due to the expected side effects occurring from its use, as it lacks selectivity.

1.2.5.5.1 Side effects of chemotherapy

As the chemotherapy travels through the body, it can affect other non-cancerous tissues of the body such as hair follicles, bone marrow and digestive system, resulting in undesirable side effects. Although most of those side effects are reversible, meaning that they end once the treatment is finished, however, some may be long term or even irreversible(51).

Among the short term and most common side effects of the vast majority of chemotherapeutics are hair loss, GIT disorders (nausea, vomiting, loss of appetite constipation and diarrhoea), immunosuppression with increased risk of infections, and nerve damage.

On the other hand, certain chemotherapeutics employed for breast cancer can cause long term permanent side effects including infertility, bone thinning, heart damage and leukaemia. Additionally, the chemotherapy regimen always has a negative impact on the patient mental health, usually impacted as feeling of fear, sadness, isolation, and depression.

All of those side effects resulted in the increased interest in developing more selective and targeted formulation for breast cancer chemotherapeutics to enhance the patient's quality of life(52).

1.3 Nanotechnology for cancer therapy

The inadequate selectivity of the available chemotherapeutics, that results in the wide range of side effects, have led to the increased urge for formulations with higher selectivity and targeting to the cancerous cells(41). Among the approaches for enhancing chemotherapeutic selectivity is the use of nanotechnology for medicinal formulations that could help targeting tumours. Nano-therapeutics refers to an area of drug formulation that employs nanotechnology in preparation of drug particles in the range between 1 to 100 nm(53).

Recently, various nano-therapeutics for breast cancer control are either in market or under investigation, with increased interest in the research of development of novel nano sized drug carriers for chemotherapeutics. Those nanoparticles could enhance the selectivity towards the tumour either through their physico-chemical properties (passive targeting), and/or through the utilisation of specific targeting moieties that could be attached to the prepared nanoparticles (active targeting).

1.3.1 Targeting mechanisms

1.3.1.1 Passive targeting

Inflammation and hypoxia are well known conditions that increase the permeability of the endothelium of blood capillaries to increase the blood flow to the affected area. Since this is the normal case for most tumour, causing inflammation and hypoxia at the affected site, most of tumours are characterised by leaky blood vessels. Additionally, the rapidly growing tumours result in development of abnormally fenestrated blood vessels(54). All of those factors result in enhancing the permeation of macromolecules and nano-sized particles into the tumour tissues. Moreover, the absence of normal lymphatic drainage in tumours leads to increasing the retention of the nanosystems within the tumour, in a way better than for small drug molecules which are easily washed out by the circulation(55). This effect is known as enhanced

permeation and retention (EPR), in this case the encapsulation of drugs in nano-sized systems enhances their pharmacokinetics and provide some tumour selectivity(56).

Since the establishment of EPR concept, extensive research was done to make use of this passive targeting mechanism in development of drug formulations for cancer therapy(57). Some of those formulations are already in the market such as Doxil© and Caelyx©, that are nanoparticle formulations of anti-cancer drugs that depends on passive tumour targeting(58). However, the EPR effect is still of low selectivity to tumours, as it depends mainly on the intrinsic tumour characteristics including the degree of angiogenesis, the intratumour pressure and degree of tumour growth(59).

Thus, in order to make full use of the EPR effect, several approaches were proposed to enhance the accumulation of nanoparticles in tumours. Those approaches are either through the use of permeation enhancers, which are chemicals that increase tumours perfusion such as bradykinin, or through modulating the physico-chemical characteristics of the nanocarriers(60).

Particle size and surface charge have a direct effect on the efficiency of the nanocarrier, affecting its adhesion to tumours, cellular uptake, circulation time, and retention in tumours(61). For instance, large nanoparticles (>200 nm) could be easily cleared by the reticuloendothelial system (RES), while tiny particles have high renal clearance. Thus, the optimal size range for the best pharmacokinetic profile lies in the range between 20- 200 nm(57). Another example are too hydrophobic nanosystems that could be easily opsonised and cleared; hence it is preferred to make nanoparticle surface more hydrophilic(62). This could be achieved through the use of hydrophilic polymers, generally polyethylene glycol (PEG), in a way that covers the nanoparticle surface from the immune system. PEGylation is a well-established mechanism for surface modification of nanocarriers to produce what is known as stealth nanoparticles, they are usually incorporated at loading of 5-9 mol%(62).

1.3.1.2 Active targeting

Active targeting refers to the attachment of specific ligand to the surface of nanocarriers. Following the accumulation of the nanocarriers in tumour tissue, those ligands bind to specific receptors overexpressed on tumour cell, which in turns enhance the uptake and penetration of the nanocarriers.

The concept of active targeting was proposed in the 1980s, through the investigation of antibody grafted liposomal formulation(63). Since then, many other ligands were identified such as peptides, aptamers, and nucleic acids and. Several ligands are discovered and utilised nowadays, thanks to the identification of biomarkers and receptors overexpressed in each tumour type(64). One of the most common ligands used in literature and in clinical trials is folic acid, which binds to folate receptors overexpressed in many tumour tissues including breast cancer(65).

Advances in nanotechnology field resulted in better outcomes in the field of breast cancer eradication, some rely on passive tareting while others rely on active tareting. Various types of nanocarrier systems are extensively studied for targeting breast cancer, some are already in the market, and other are still in clinical trials (66). **Table 2** shows the most common advances in targeting breast cancer using nanocarrier systems, either available in the market (Table 2A), or still under clinical trials (Table 2B).

Table 2 Nanocarrier delivery systems for targeting breast cancer A) already available product in market, B) under clinical trials.

Product name	**Nanocarrier system**	**Chemotherapeutic**	**Cancer target**	**Date approved**
Doxil/Caelyx (Janssen)	PEGylated liposome	Doxorubicin	Ovarian, breast cancer, leukaemia	FDA, 1995

DaunoXome (Galen)	Non-PEGylated liposome	Daunorubicin	HIV-related Kaposi sarcoma	FDA, 1996
DepoCyt (Pacira)	Non-PEGylated liposome	Cytarabine	AML, non-Hodgkin lymphoma	FDA, 1999
Myocet (Teva UK)	Non-PEGylated liposome	Doxorubicin	Metastatic breast cancer	FDA, 2000
Marqibo (Spectrum)	Non-PEGylated liposome	Vincristine	Non-Hodgkin's lymphoma	FDA, 2012
Onivyde (Merrimack)	PEGylated liposome	Irinotecan	Breast, pancreatic, sarcomas, or brain	FDA, 2015

Table 2B

Passive targeting	**Name**	**Nanocarrier system**	**Chemotherapeutic**	**Target tumour**	**Phase of clinical trial**
	NK 105	Micellar nanoparticle	Paclitaxel	Metastatic or Recurrent	Phase III

				Breast Cancer	
	EndoTAG-1	Cationic liposomes	Paclitaxel	HER2-negative Breast Cancer Liver Cancer and Neoplasm Metastasis	Phase II
	Nab-rapamycin (ABI-009)	Albumin-bound nanoparticles	Rapamycin	Solid Tumours	Phase I
	CRLX-101 (IT-101)	Cyclodextrin-based polymer	Camptothecin	Solid Tumour, and Ovarian Cancer	Phase II
	NC-6300	PEGylated polymer	Epirubicin	Solid Tumour	Phase I/II
	IT-141	PEGylated polymer	SN-38 (metabolite of irinotecan)	Cancer, and Recurrent Solid Tumours	Phase I
Active targeting	**BIND-014**	PSMA-targeting polymer (prostate-specific membrane antigen)	Docetaxel	Prostate Cancer Metastatic Cancer and Solid Tumor	Phase I/II

	MBP-426	TfR-targeting liposome(transferrin receptor)	Oxaliplatin	Cancerous tissues	Phase I
	Anti-EGFR-IL-dox	EGFR-targeting liposome	Doxorubicin	Breast Cancer	Phase II
	ThermoDox	Therapeutic directed (thermally sensitive liposome)	Doxorubicin	Breast Cancer	Phase I/II

1.3.2 Nanoparticles delivery systems for breast cancer

After the great advances in the nanotechnology field as a way of targeted delivery of chemotherapeutics, many nanosystems were developed for managing breast cancer. **Table 3** illustrates the classification of most of the used approaches for nanosystems available for breast cancer, either in market or still under investigation. Some of those nanosystems approaches will be discussed briefly in the following section.

Table 3 Nanocarrier approaches for chemotherapeutic targeting of breast cancer.

Organic drug delivery	**Inorganic drug delivery**	**Localised drug delivery**	**Receptor based**
Micelles (67) Liposomes (68) Polymers(69) Dendrimers(70)	Gold NPs(71) SPIO NPS(72) Quantum dots(73)	Nanofibers(74) Hydrogels(75) Intraductal(76)	HER 2(77) EGFR(78) IGF-IR(79) VEGF(80)

1.3.2.1 Organic drug delivery approaches

This type of nanocarriers utilises organic substances in their formulation, including lipids, polymers, or surfactants. Micelles, liposomes, polymeric nanoparticles, solid lipid nanoparticles and dendrimers are among the examples for this approach.

Micelles refers to colloidal particles prepared from conjugates of water-soluble polymers or surfactants, hence suitable for delivery of hydrophilic chemotherapeutics. This type of nanocarriers have been studied extensively since they were first proposed (81), and for instance have been studied for the delivery of doxorubicin and paclitaxel to breast cancer cell lines(67,69).

Another example is liposomes, which are spherical particles with a membrane like structure formed of single or multiple layers of phospholipids(82). Their size ranges from 50 to 200 nm and have shown great advantage being biocompatible and biodegradable(83).

Recently, polymeric nanoparticles have gained great attention, due to the wide ranges of polymers available or could be synthesised, which in return could help manipulate the physico-chemical properties of the prepared nanocarriers. Polymers range from the natural such as chitosan and cellulose to synthetic such as poly-ε-caprolactone (PCL), poly-(lactic-co-glycolide), and polylactide (PLA). Clinical investigation of polymeric nanosystems of chemotherapeutic drugs like paclitaxel, doxorubicin, camptothecins, and platinates is currently carried out (84). Moreover, polymeric NPs were proven to have a higher loading capacity for poorly water-soluble drugs, and better physicochemical properties (solubility, stability) compared to liposomes(85).

1.3.2.2 Inorganic drug delivery approaches

This includes nanosystems prepared from inorganic materials, particularly metallic particles. The most commonly known is gold nanoparticles which are used as a chemotherapy by themselves or could be conjugated to chemotherapeutics or ligands for better targeting of

tumour tissues(86). Gold nanoparticles showed great sensitivity and specificity and can be used as a diagnostic marker for breast cancer(87).

Another interesting metallic nanoparticles are those prepared from superparamagnetic iron oxides (SPIO-NPs), which are referred to as magnetic nanoparticles (88). Besides their use as a magnetic resonance contrast agent, they can be further used for targeting tumours using magnetic fields, among which is breast cancer(89,90).

1.3.2.3 Localized drug delivery approaches

One of the approaches to overcome the side effects of systemic chemotherapies is to apply the anti-cancer medication locally to the tumour. This could be useful for early-stage tumours and those that are near to body surfaces. Nonetheless, the medication should be manipulated in specific formulation to enhance its localisation in tumour tissues for prolonged time. Among those specific formulations that have been studied for breast cancer management are hydrogels, nanofibers, and the use of intraductal catheters(91).

1.4 Nanoparticles preparation techniques

Many techniques have been proposed for the preparation of nanoparticles, this could be classified into the top-down techniques (miniaturisation) and the bottom-up techniques(92). The top-down techniques involve the breakdown of larger drug particles into small nanometre sized drug particles by applying either shear, friction, pressure, or combination of those forces(93). Nanoparticles preparation methods using the top-down method include high pressure homogenisation, sonication, and media milling. Although this method is considered reproducible and easy for scale-up, yet they only produce large particles in the size range of few hundred nanometres to 2 μm(94,95). Production of smaller nanoparticles, i.e., <100 nm, using the miniaturisation technique is still a hurdle(92).

On the contrary the bottom-up method involves the assembly of smaller molecules into a nanometre sized particles, among the bottom-up techniques are the nanoprecipitation(96),

emulsification, solvent evaporation(97), and supercritical fluid techniques(98). The bottom-up method is more extensively used in research to produce small sized nanoparticles. However, most of the bottom-up techniques are complex and difficult to scale up for industrial production. Thus, great efforts are continuously made to develop techniques that are easy to scale up, together with production of stable small nanoparticles(99). In our work we studied the use of a specific nanoprecipitation technique, known as rapid solvent shift or flash nanoprecipitation(100), to produce small sized nanoparticles (<50 nm), while keeping the method easy enough for scale-up.

1.5 Theory of Nanoparticle formation using Nanoprecipitation technique

1.5.1 Classical Nucleation Theory (CNT)

The process of precipitation of particles using the solvent shifting method involves a concept known as 'nucleation.', the nucleation process is described based on classical nucleation theory(101). However, the process may include some 'non-classical' ways of nucleation.

'Nucleation' is a process that takes place when a system is brought into a non-equilibrium metastable state. This metastable state is described as a supersaturated condition that represents a local minimum of the free energy. Due to this local minimum free energy, the system is stable towards small fluctuations (102). However, with an increase in microscopic fluctuations, the random collisions of the dissolved molecules of the solute in the solution lead to the formation of the clusters of a new phase which are calle 'Nuclei'. These nuclei represent the new state that represents the new minimum of the free energy possessed by the bulk system, and the transformation of the phase (from clusters to nuclei) takes place through the energy barrier which represents the local maximum free energy state(103,104).

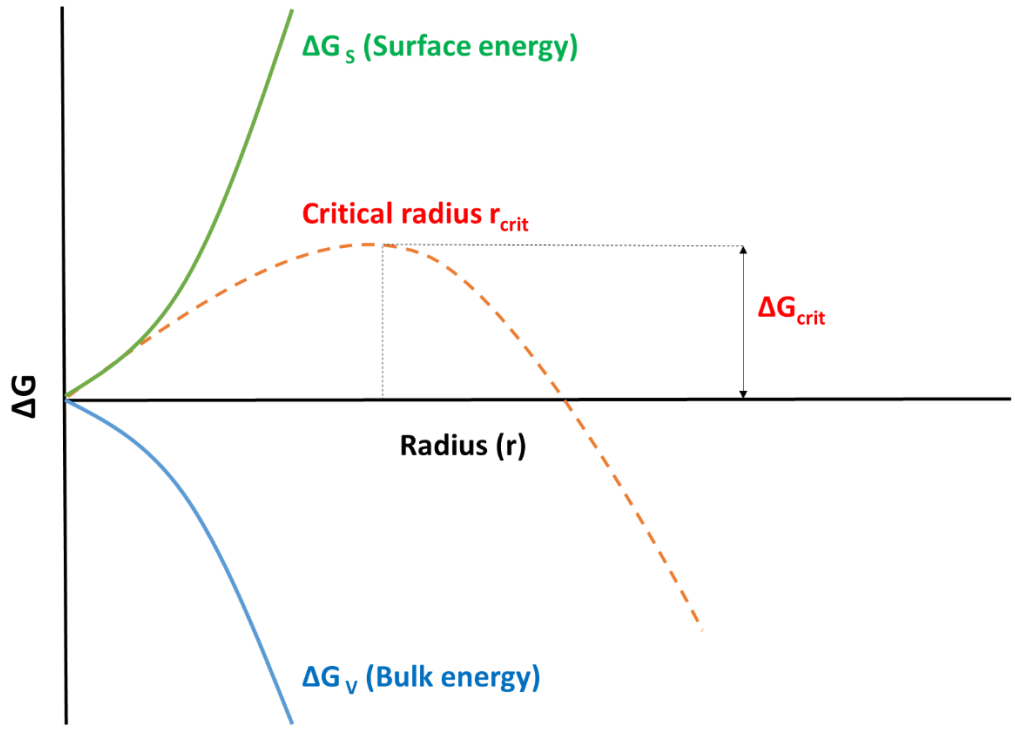

Figure 1 Free energy diagram of Classical Nucleation Theory (CNT).

The process of nuclei formation in a supersaturated solution consisting of homogeneously distributed molecules can be explained through random collisions that lead to the aggregation of these molecules towards the formation of clusters or 'embryos'. As the cluster or embryo reaches a particular size known as 'critical' size, it can be regarded as the 'critical nucleus.' Assuming it to be spherical, the radius of this critical nucleus can be predicted on the basis of CNT (**Figure 1**). It is important to note that, according to CNT assumptions, the collisions between any two pre-existing clusters, the break-off of pre-existing clusters into two or more smaller clusters or the collisions between two particles are ignored (105,106).

By considering the nature of nucleus as 'spherical,' the CNT assumes that the interior of the nucleus is in the bulk new-phase state, and the interfacial tension ($\boldsymbol{\gamma}$) is the same as for a planar interface of the coexisting new and mother phases. With these assumptions, the free energy of homogeneous nucleation ($\Delta \boldsymbol{G}_{\text{homo}}$) for a spherical particle with radius $\boldsymbol{r}$, the surface energy $\boldsymbol{\gamma}$ and the bulk free energy of volume ΔG_v, is quantitatively represented as

Equation 1 $$\mathbf{\Delta G_{homo}} = \mathbf{4}\,\boldsymbol{\pi r^2 \gamma} + \frac{\mathbf{4}}{\mathbf{3}}\,\boldsymbol{\pi}\,\boldsymbol{r^3}\mathbf{\Delta G_v}$$

The free energy of the bulk nucleus is expressed as the difference between the free energy of the bulk particle and the solution as

Equation 2 $\Delta G_v = -\frac{K_B T \ln(S)}{V_m}$

Where k_B is Boltzmann's constant, T is temperature (K), S is the degree of supersaturation and Vm is the molecular volume

In the **Equation 3,** as the surface term is always positive while the bulk free energy is always negative, the maximum free energy through which a cluster will pass to form a stable nucleus can be obtained by differentiating ΔG with respect to r and setting it to zero ($d\Delta G/dr = 0$). This gives critical free energy ΔG_{crit}:

Equation 3 $\Delta G_{Crit} = \frac{4}{3}\pi r_{crit}^2$

The critical radius of the nucleus is given by:

Equation 4 $R_{Crit} = -\frac{2\gamma}{\Delta Gv}$

Combining **Equation 3** and **Equation 5** then give:

Equation 5 $R_{Crit} = \frac{2\gamma V_m}{K_B T \ln(S)}$

Thermodynamically, the critical size reflects a metastable state as any radii smaller than r_{crit} will be unstable and dissolve back in the solution while any radii larger than r_{crit} will lead to the unlimited growth, this is explained in **Figure 1**.

The green curve represents surface free energy, and blue curve represents the bulk free energy. Combining these two terms allows the prediction of the critical radius at which a cluster of molecules become stable and start growing as a stable nucleate (red curve at r_{crit}).

From the **Figure 1,** it can be said that the positive surface term offers a barrier to form the critical nucleus. Once it is formed, the negative volume term then allows the nucleus to grow into a particle and attain the bulk properties.

Considering the kinetic barriers, the rate of nucleation (J) can be expressed as;

Equation 6 $\mathbf{J = A\, e^{\left(\frac{E_a}{K_B T}\right).\left(\frac{-\Delta G}{K_B T}\right)}}$

Where the first exponent ($\frac{E_a}{K_B T}$) represents the kinetic barriers with an overall activation energy E_a, while the second exponent ($\frac{-\Delta G}{K_B T}$) represents the thermodynamic barrier. The parameter A is a pre-exponential factor which is determined by the properties of the nucleating solute. The theoretical value of the pre-exponential factor has been reported to be ~1030 $cm^{-3}\ s^{-1}$; however, it is very difficult to measure in practice.

The kinetic barriers are generally neglected due to difficulty in their quantification. On the other hand, the thermodynamic barrier can be calculated based on the assumptions of CNT, which mainly involve consideration of the similar behaviour of the nanoscopic nuclei, and macroscopic phase, i.e., the nuclei possess same structure and corresponding interfacial energies as the bulk. This is the background for nucleation based on CNT.

However, there have been discussions about the assumptions of the CNT and their lack of applicability to the extremely small clusters of few (~ 10) molecules, where the radius of curvature is so high that the centre of the curve is not in the thermodynamic limit and the interface is sharply curved, thus changing its free energy. Erdemir et al.(107) have discussed such shortcomings of CNT in detail, thus taking the discussion towards the other non-classical theories too.

1.5.2 Ostwald ripening and particles condensation

Ostwald ripening is considered one of the mechanisms of particle growth, where the growth of particles is caused due to change in their apparent solubility depending on the size of the particle. Due to the high surface area available for dissolution and the surface energy of smaller particles within the solution, these smaller particles redissolve and then molecularly diffuse onto the larger particles allowing their further growth. This diffusion controlled growth can be

expressed by following equation obtained from the mathematical treatment by Lifshitz and Slyozov (108).

Equation 7 $$R^3 = \frac{8\,\gamma\,C_\infty V_m\,D}{9\,R_g T}\,t = K_{OR}t$$

where R is the average radius of all particles (nm), γ is the particle surface tension (mN/m), C_∞ is the solubility of the particle material in the medium (μM), V_m is the molar volume of the material (cm^3/mol), D is diffusion coefficient of the particle material (cm^2/s), R_g is universal gas constant (8.314 J / mol. K.), T is absolute temperature (K), t is the time (s) and k_{OR} is the rate constant for the Ostwald ripening (nm^3/s).

For most hydrophobic materials, the growth of particles due to Ostwald ripening is expected to be absent. However, if the rate of injection is slow, then during the solvent shifting from the maximum organic solvent to the organic solvent-aqueous mixture, the particle can grow due to condensation ripening, in a process similar to Ostwald ripening, in the regions of higher organic solvent content. In this case the smaller nuclei coalescence over the larger particles resulting in particle size increase.

1.5.3 DLVO theory

The DLVO stands for Derjaguin, Landau, Verwey and Overbeek, the scientists behind this theory which works on the explanation of the stability of colloids in suspension. The theory has an in-depth sight into the balance between two opposing forces, the electrostatic repulsion due to surface charge and oppositely Van der Waals attraction forces, this balance could explain why some colloidal systems may suffer instability as aggregation while others do not.

To understand the theory, two forces should be put in consideration, the first is the electrostatic repulsion which occurs when two particles approach each other and their likely charged double layers (layer formed from the surface charge of the particles covered with counter ions) begin to interfere. The electrostatic repulsion could be defined as the energy that must be overcome to force and bring the particles together. The maximum energy is related to the zeta potential.

On the other hand, the second force is Van der Waals attractions, which is the result of forces between the mass of individual particles. The effect is additive; that is, one particle of the colloid has a Van der Waals attraction to each other particle. This is repeated for each particle in the colloid to get the total force.

Combing both force, DLVO theory explains the stability of colloids against agglomeration. At each distance, if the attractive force is greater than the repulsive one, the formed colloid will be unstable, and vice versa.

Surface forces at the interface of the particle and the dispersant are quite important. Colloidal particles carry the same electrical charge which produces a force of mutual repulsion between them, where if this charge is high, the particles will remain dispersed and vice versa. This charge could be predicted from the surface forces known as zeta potential (109,110).

The way in which these two energies mentioned above (electrostatic repulsion and Vander Waals attraction) are calculated is given as follows

For two spheres of radii R_1 and R_2 separated by a distance D, the Van der Waals interaction energy is given by the following equation in K_BT (K_B is Boltzmann constant and T is absolute temperature in Kelvin) units:

Equation 8 $$E_{vdw} = \frac{-AR}{12\,D\,K_BT}$$

In the equation, A is Hamaker constant which is defined as ($A=\pi^2 C\rho 1\ \rho 2$) where $\rho 1$ and $\rho 2$ are the number of atoms per unit volume in the two bodies and C is the coefficient in the atom-atom pair potential. The unit of Hamaker constant is J.

Similarly, for two spheres of same radii, i.e., $R_1=R_2=R$, separated by a distance D, the electric double layer interaction energy in K_BT units can be given by the following equation:

Equation 9 $$E_{EDL} = \frac{2\,\pi\,\varepsilon\,\varepsilon_o\,R\,\psi_o^2\,\ln\left(1+e^{-\left(\frac{D}{k^{-1}}\right)}\right)}{K_BT}$$

Where k is the Debye length, ε is the dielectric constant of the medium, ε_0 is the permittivity of free space, ψ_0 is the surface potential, and e is the charge of the electron. The surface potential can be approximated to the zeta potential (ζ) for calculations.

Equation 8 and Equation 9 were used for the calculation of total interaction energy in case of nanoparticles, where

Equation 10 $E_{Total} = E_{vdW} + E_{EDL}$.

1.6 Rapid solvent shift technique (flash nanoprecipitation)

Rapid solvent shift technique (also known as flash nanoprecipitation) is considered one of the newly introduced bottom-up techniques for nanoparticles formulation. The process relies on a rapid mixing, kinetically controlled form of nanoprecipitation, particularly for water insoluble (hydrophobic) drugs. Solvent shift refers to mixing an organic solvent drug mixture miscible with aqueous anti-solvent, at relatively high speed. The technique is simple, efficient and can be easily scaled up for industrial production. Additionally, flash nanoprecipitation is suitable to prepare stable nanoparticles of hydrophobic drugs (i.e., nano-suspensions or nano-emulations), through stabilising the surface of NPs by stabilisers including lipids, polymers, and surfactants. This stabilisation can pave the way to production of nanoparticles of tailored size and high stability(111).

Since this proposed technique is considered a subtype of nanoprecipitation, it follows the stages of the classical nucleation process mentioned before. The process starts with nucleation, followed by growth of the formed nuclei by capturing more of the dissolved molecules. Yet, the flash nanoprecipitation involves rapid mixing of organic miscible phase with aqueous phase, which creates a high supersaturation state that favours the rapid formation of plentiful nuclei(106). Then growth occur by condensation and/or coagulation, simultaneously with precipitation of the stabiliser layer of lipids, polymers, and/or surfactants, and hence controlling

the particle size. This coating process encapsulate the drug into a hydrophobic core, preventing further growth or aggregation of the nanoparticles(93).

Besides the principle that size controlled and stable nanoparticles requires rapid nucleation rate and slower growth rate, many other factors could govern the physicochemical properties of the prepared NPs. Drug properties, the solvents nature, stabilisers, temperature, and drug concentration are the most important parameters that could have further effect on the particle size, zeta potential, morphology, and stability of the NPs(100).

1.6.1 Drugs properties

Since the technique is used for hydrophobic drugs, the whole process of nucleation and growth is expected to occur during mixing of the solvent/anti-solvent phases. Thus, the drug molecule should be sufficiently hydrophobic with minimum solubility in the aqueous anti-solvent phase. The n-octanol partition coefficient, log P or calculated Clog P, is the key indicator of the drug hydrophobicity. It is the ratio between the partitions of drug dissolved between n-octanol (organic hydrophobic phase) and water. Higher log P values indicate more hydrophobic nature with higher partitioning in the hydrophobic phase and low aqueous solubility. It is reported that the technique of rapid solvent shift is suitable for drugs with log P > 6. Unstable and large sized nanoparticles were the outcome of flash nanoprecipitation of drugs with log P <6 due to the rapid condensation and Ostwald ripening as suggested by Pustulka et al(112). Another study by Zhu et al. showed that flash nanoprecipitation of drugs with log P <2 are unable to form nanoparticles by flash nanoprecipitation due to high solubility, while those drugs with 2>log P <9 formed nanoparticles that can grow through condensation and Ostwald ripening, yet the drugs with log P > 12 formed high stable nanoparticles(113). Consequently, hydrophobic materials and drugs were frequently used for the rapid solvent shift technique, for example β-carotene, curcumin, cyclosporine A, and itraconazole. In order to manipulate more hydrophilic

drug in this process, production of prodrug of higher hydrophobicity has been employed (114–118).

1.6.2 Solvent and anti-solvent nature

Flash nanoprecipitation involves mixing organic and aqueous phase (water or aqueous solution or aqueous buffers), they should be miscible for the drug molecules to precipitate in the aqueous phase. Polar organic solvents that are miscible with water can be used, for instance ethanol, methanol, acetone, dimethyl sulfoxide (DMSO), dimethyl formamide (DMF), and tetrahydrofuran (THF). The choice of the organic solvent to be used will be related to which will dissolve more of the drug and other stabilisers, in order to reach a higher supersaturation condition upon mixing with anti-solvent(102).

The volume ratio of mixing the solvent and the anti-solvent phases greatly affects the supersaturation state and in return affects the properties of the formed nanoparticles. Low volume of solvent to anti-solvent, increases the supersaturation at the interface between the organic and the aqueous phase; resulting in rapid nucleation rate and smaller nanoparticles, and vice versa(119).

Another important factor is the rate of mixing the two phases, which have a direct influence on the rate of nucleation and growth of nanoparticles. Mixing of dispersion after the nanoprecipitation process can trigger growth of particles, either through condensation or Ostwald ripening. The organic solvent in the mixture enhances the Ostwald ripening by solubilising the drug particles, which are then redispose over other particles. Additionally mixing could enhance mechanical condensation between adjacent particles(120). Hence the best case scenario is to remove the organic solvent after the nanoprecipitation technique. Solvents of high boiling point, i.e., DMSO and DMF, can be removed by dialysis, whilst those solvents of low boiling point, i.e., ethanol and acetone, are eradicated by evaporation. Another approach is to follow the nanoprecipitation technique with freeze drying or spray drying, this

will not only remove the organic solvent, but will enhance the stability of the nanoparticles for long term storage(115).

1.6.3 Stabilizers

For various reasons the use of stabilisers such as phospholipids, surfactants and polymers are highly encouraged during the process of rapid solvent shift nanoprecipitation. Primarily, stabilisers encapsulate the precipitated drug, and protect the formed nanoparticles from further growth and agglomeration(121). Hence, stabilisers are used to control particle size growth, by lowering the interfacial energy and increasing the nucleation rate, as well as preventing further aggregation of the particles by Ostwald ripening, condensation, or aggregation(122).

Both the type and the concentration of the selected stabiliser greatly affect the nanoparticles physicochemical properties. Various stabilisers were proposed for the process of flash nanoprecipitation, they can be polymers such as hydroxylpropylmethyl cellulose (HPMC), sodium carboxymethyl cellulose (CMC), polylactic co-glycolic acid (PLGA), polyvinyl acetate (PVA) or poloxamers. Besides polymers, other stabilisers are used including surfactants such as Tween 80, sodium dodecyl sulfate (SDS), cetyltrimethylammonium chloride (CTACl), and phospholipids. The affinity of the stabiliser to the drug surface will influence the particle size formed. The higher this affinity, the faster is the adsorption of the stabiliser to the drug surface and hence the smaller the particle size formed, and vice versa(123). Another factor is the steric configuration and charge of the stabiliser, which governs the stability of the formed nanoparticles against aggregation. Stabilisers either charged or conferring steric hindrance, will prevent further aggregation of the particles. For electrostatic stabilisation, charged stabilisers increase the repulsion forces between the formed nanoparticles and prevent agglomeration, thus increasing the stability of the formed nanoparticles(124). Usually a mixture of different types of stabilisers are used to enhance the nanoparticles stability through synergistic effect, some could be added to the organic phase including polymers, non-ionic surfactants and/or

phospholipids, or even to the anti-solvent phase including the ionic polymers and surfactants(125).

Concerning the concentration of the stabilisers, it is related to its molecular structure and aqueous solubility. The concentration of the used stabilisers should be adjusted to avoid particle size increase. Insufficient stabiliser could result in poor drug encapsulation, while excessive amount could increase particle size through increasing viscosity of the final dispersion and enhancing drug diffusion. For instance, in a study by Guhagarkar et al.(126) they showed that the particle size of PVA coated nanoparticles decreased from 1000 to 300 nm with increasing PVA content from 0.1 % to 0.5%., however excessive use of PVA, i.e., 4%, resulted in significant particle size increase.

1.6.4 Temperature

It is well known that temperature plays an important role in kinetics governed process such as nanoprecipitation, affecting the drug solubility, degree of supersaturation and the rate of nucleation and growth. Typically, flash nanoprecipitation technique is carried out at room temperature to control the effect of temperature on the overall process. Nevertheless, Kim et al.(127) studied the effect of temperature on the particle size of nanoparticles prepared by rapid solvent shift technique. The results showed a direct relationship between increasing temperature and particle size growth. Lowering the temperature decreases the drug solubility, while enhancing the degree of supersaturation, resulting in increasing the rate of nucleation, yet reducing the rate of growth by reduction of the Brownian motion(127). Thus, for further control of nanoparticle size for some drug moieties, scientists can perform the process of flash nanoprecipitation at low temperatures, i.e., 4 ^{o}C or even ice bath(128).

1.6.5 Drug concentration

Among the factors affecting the particle size of the formed nanoparticles by flash nanoprecipitation is the used drug concentration. Drug concentration has a complex effect on

the final particle size. Usually increasing the drug concentration increases the degree of supersaturation, which in returns increases the rate of nucleation resulting in small particle size. For instance, Zhang et al. showed that increasing concentration of atorvastatin calcium from 20 to 60 mg/ml resulted in a decrease in particle size from 400 to 250 nm, yet increasing the concentration to 80 mg/ml resulted in particle size increase due to aggregation(129).

The effect of drug concentration is complex, and depends on many factors such as the drug hydrophobicity, the stabilisers used, and the solubility of the drug in organic phase. Although increasing drug concentration is expected to increase the supersaturation and decrease the particle size as described above, however, the increased nucleation rate could increase the particle aggregations, especially in the absence of stabilisers and in case of more hydrophobic molecules. Zhang et al. as well investigated this for cefuroxime axetil nanoparticles prepared by flash nanoprecipitation with no stabilisers, and results showed that the particle size of the prepared nanoparticles increased significantly from 300 to 800 nm with increasing the drug concentration from 60 to 120 mg/ml(130). Therefore, screening the drug concentration influence on the particle size is crucial to obtain ultrafine nanoparticles by rapid solvent shift technique(131).

1.7 LDL-like nanoparticles

Lipoproteins are normal constituent of human blood that are responsible for transport of lipids and cholesterol into the body cells. They are considered natural nanoparticles ranging in the size between 8 to 1200 nm, and classified according to their lipid content into high density lipoprotein (HDL), low density lipoprotein (LDL), and very low density lipoprotein (VLDL). The use of those lipoproteins as a carrier for drug entities has been extensively studied, being biodegradable and not recognised by human immune system. As a result, they are able to provide a solution for the biocompatibility issues associated with most of the synthetic nanoparticles (132).

Recently over expression of specific receptors for hormones, growth factors or other metabolites in tumour cells resulted in increasing interest in the field of targeted therapeutics. It was found that low density lipoprotein receptors LDLR are specifically overexpressed in most tumour tissues. This is attributed to the high metabolic requirements of cancerous cells for cholesterol for cellular proliferation. Therefore, encapsulation of anti-tumour drugs into the LDL matrix was studied as a targeting mechanism for tumours (133). LDL nanoparticles are internalised through receptor mediated uptake involving the Apo-lipoprotein B-100 found as a part of the structure of the LDL(134). Other cellular uptake mechanisms are as well included in the uptake of LDL such as clathrin-mediated endocytosis, caveolae mediated transport, and macro-pinocytotic uptake known as cell drinking (135). Additionally, the properties of the nanoparticles including the surface charge and structure could influence the uptake of the particles through electrostatic, Van der Waals or steric interactions (135).

Nonetheless, the use of LDL as a natural nanocarriers has several drawbacks. LDLs isolated from human blood are usually difficult to handle and microbiologically unstable, where they can be easily contaminated with pathogens, thus commercial sources of LDL that provides sterile LDLs are available. Another drawback is that it is very difficult process to isolate homogenous LDLs with homogenous structure and size and in usable quantities from human blood (136). Additionally, native LDL vehicles lack selectivity, as LDL receptors are expressed in most healthy tissues, this could be manipulated by surface modification such as PEG or adjusting the particle dimensions.

Hence synthetic preparation of LDL-like nanoparticles has been highly urged, in order to combine the advantages of the: LDL, while avoiding the drawbacks through preparation of reproducible, large amounts, targeted nanoparticles with homogenous properties and in an easy way(137).

1.8 Orlistat as promising anticancer

1.8.1 Fatty acid synthase enzyme (FASN) and breast cancer

In 1950s, Medes et al., showed that tumours could utilise glucose to produce acetate through a de novo lipogenesis similar to that found in liver tissues, since then, many studies were carried out on various tumours to have a more understanding of this phenomenon(138). On the mid 1980s it was found that rapidly growing tumours can generate a portion of their fatty acids requirements through a de novo synthesis(139). In 1994, Kuhajda et al. discovered a prognostic molecule in patients with worsened breast cancer tumours, it was the rate determining enzyme for de novo fatty acid biogenesis, namely fatty acid synthase (FASN)(140).

Nowadays, FASN upregulation is shown in most of human cancer and precursor lesions, which is highly attributed to worsened patient survival rates. FASN catalyses the endogenous synthesis of fatty acids in cancerous tissues and thus enhances cancer cells survival and growth(141). It was found that FASN signalling regulates the progression and aggressiveness of cancerous tissues, through affecting and controlling cell proliferation, cell survival, cell adhesion, extracellular matrix (ECM) organization, migration, invasion, and even the malignant transformation (142).Since then, FASN was suggested to be a prominent oncogene like factor (143).

FASN has received a great attention as a therapeutic target for cancer treatment. Several inhibitors of FASN have been developed and studied over the past decades, which are characterised for their molecular properties and cellular activity and even some are in preclinical or clinical investigation such as Cerulenin, C75 and orlistat(144).

Due to the pharmaceutical liabilities of FASN inhibitors, extensive research is targeted towards manipulating those drugs in better formulations for the optimum therapeutic output (145).

1.8.2 Orlistat as FASN inhibitor

Orlistat is a potent irreversible inhibitor of FASN, acting through bonding covalently with the thioesterase domain of the enzyme(146). Orlistat as an anticancer agent has been studied in several tumours including prostate cancer, however its efficacy in breast cancer requires more investigation(147).

Due to various pharmaceutical liabilities of orlistat including hydrophobicity and poor solubility, in addition to pharmacological limitations including poor bioavailability and selectivity, all of this resulted in many attempts to develop optimised formulations of orlistat(148). Nanotechnology was employed to prepare advanced and optimised formulations of orlistat. Nano-ORL, an amphiphilic hyaluronic acid conjugate of orlistat, was developed by Hill et al.(149) and showed enhanced oral bioavailability of orlistat, with an increase in the cytotoxic effect in breast cancer cell lines. Bhargava-Shah et al.(150), prepared a conjugated PLGA-PEG nanoparticles as a nanocarrier for orlistat, which improved cytotoxicity in triple negative breast cancer cell lines.

However, formulations that can combine several advantages such as biocompatibility, better tumour accumulation and enhanced therapeutic effect, while circumventing the poor physicochemical properties of orlistat are still unavailable.

1.9 Research Design

LDL nanoparticle preparation using the rapid solvent shift technique requires a highly hydrophobic material ($2 < \text{Log P} < 9$), with an extremely low water solubility, and still soluble enough in other water-miscible organic solvents such as ethanol. Zhigaltsev et al.(151) had used Triolein as their test material for NPs preparation using the solvent shift method, this may provide an expectation that hydrophobic materials would form similar nanoparticles (of size range 20-50 nm) and may also provide a literature reference to make initial comparisons.

In our research we screened a variety of hydrophobic materials, including lipids (i.e., olive oil, trihexanoin, tricaprin, and triolein) and APIs (i.e., orlistat and niclosamide stearate). Olive oil was selected as our preliminary hydrophobic test material for several reasons, among which that triolein is its main component(152), it has very low water solubility in the nanomolar range (6.9 nM), and its solubility in other water-miscible solvents such as ethanol (~35 mM in ethanol)(153). Moreover, due to its liquid nature at room temperature (MP = - 6°C), no additional complexities associated with crystallization, solidification or supercooling of the compound are anticipated. It is also a relatively abundant, inexpensive material, and with great safety profile as well as a common foodstuff. These all reasons supported the selection of olive oil as an initial model test material for testing the properties of NPs prepared by the proposed rapid solvent shift technique. The preliminary studies on olive oil will give an idea about the properties of the prepared NPs by the proposed method that could be applied on other drugs of choice later on.

Olive oil consists mainly of triglycerides (Triolein OOO, Glycerol dioleate palmitate POO, 1,2-dioleoyl-3-linoleoyl-sn-glycerol OLO, with the value of Triolein (OOO), surpasses 70% of concentration of Olive oil. Moreover, free fatty acids are considered a part of the natural constituents of the olive oil, this includes Oleic acid which is the most abundant among all other fatty acids, while margaric, margaroleic and lignoceric acids have the least percentage(152).

Results regarding triolein nanoparticles prepared by Prasad et al (154) using the ethanolic injection technique showed a concentration dependent change in particle size, whilst coating of triolein nanoparticles with phospholipids resulted in a control over the particle size growth. These results are expected to be relevant to nanoparticles prepared from other hydrophobic moieties, in terms of particle size, zeta potential, and size growth, where a controlled size range

is expected for coated particles compared to their uncoated nanoparticles counterpart, especially at higher material loading.

The whole studied process will be further investigated on the novel anti-cancer drug orlistat (ORL) for preparation of size stable nanoparticles, which will be further modified into a novel LDL-like NPs formulation for breast cancer targeting.

1.9.1 Gap in Knowledge

Controlling the particle size of nanomedicines is highly crucial for many reasons including proper drug formulation, tumour targeting and enhancing bioavailability(155). Unfortunately, most of the available nanoparticles formulations either marketed or under investigation lie within the range of 100 to 200 nm, however, they may not be the best option for optimum drug targeting and tissue accumulation which is in favour of smaller particles (<50nm)(156–158). Therefore, preparing nanoparticles of small size (<50nm) in an effortless way and with high concentrations of the required drug still requires work.

On the other hand, orlistat is highly hydrophobic; with poor bioavailability and metabolic stability(147,159) which hinder the process of formulating the drug into nanomedicine with effectively small size and high drug concentration, therefore, there is an urge for an easy and remarkably beneficial nano-formulation of orlistat using solvent shift technique that may ensure a small, controlled particle size and high drug loading together with stability for extended period of time.

1.9.2 Overriding Questions:

Do different hydrophobic materials give comparable properties as Triolein when prepared as nanoparticles using rapid ethanolic injection, in terms of particle size?

Does coating of those nanoparticles with single layer of phospholipids cause a control over particle size growth?

Does adhering a peptide to prepare functionalised LDL-like NPs result in controlled size and stable particles?

Does the LDL-like orlistat NP formulation show targeting and efficacy against breast cancer?

1.9.3 Overriding hypothesis

The overriding hypothesis of this work is coating the hydrophobic NPs with phospholipids cause a shield surrounding the formed nuclei and hence preventing further particle growth.

Additionally, the presence of stabilisers (such as surfactants) in the anti-solvent phase could help in a better surface stability against aggregation.

1.9.4 General Goals

To determine the particle size distribution and zeta potential of wide range of hydrophobic material nanoparticles prepared by rapid ethanolic injection both before and after coating, and in presence of stabilisers such as surfactants.

Testing this on preparing functionalised LDL-like NPs of our drug of choice orlistat, and testing its efficacy against breast cancer cell line.

2 Chapter 2 Materials and methods

2.1 EQUIPMENT AND TECHNIQUES

2.1.1 Dynamic light scattering (particle size)

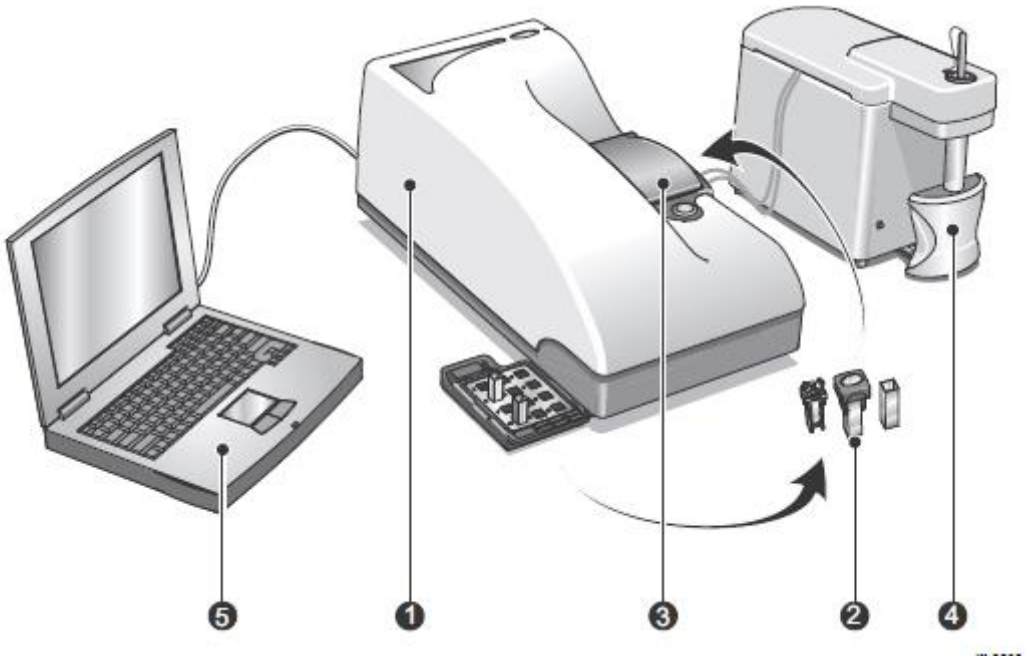

Figure 2 structure of Malvern zeta Sizer DLS, 1) Optical unit 2) Cells used, 3) Cell area, 4) MPT-2 tritrator which is an adjuvent added when required, 5) computer running the Zeta sizer software (160).

Dynamic light scattering (DLS) is the most widely used technique for measuring the size of particles suspended in liquid, in the sub-micron range using the Malvern® Zeta Sizer (ZS) (**Figure 2**). It depends mainly on sensing the Brownian motion of the particles and correlating this to their size. Brownian motion is the random movement of the particles in the solvent, typically the bigger the particles the slower will be their movement and vice versa. Many factors that affect this type of motion should be controlled to get accurate size results, the most important are temperature and the viscosity of the solvent. Hence the device is supplied with a thermostat, however most of the readings are done at room temperature, additionally the solvent viscosity and refractive index are considered.

To sum up, the Brownian motion and its correlation to the particle size could be elucidated from the Stokes-Einstein equation as follows,

$$d(H) = \frac{k\,T}{3\pi\eta D}$$ **Equation 11 Stokes Einstein equation**

where: -

d(H) = hydrodynamic diameter

D = translational diffusion coefficient

k = Boltzmann's constant

T = absolute temperature

η = viscosity

Since the Brownian motion in our case is related to movement and diffusion of our suspended particles in a solvent of choice, thus the obtained diameter is called a hydrodynamic diameter and is irrelevant to the shape of the particles, as the device gives the hydrodynamic diameter of the sphere that has the same diffusion coefficient as the tested particles. This hydrodynamic diameter is affected by several factors that will be discussed in the following section.

2.1.1.1 Factors affecting the hydrodynamic diameter of particles

2.1.1.1.1 Ionic strength

The presence of ions in the medium and their concentration highly affects the movement of the particles suspended, as the particles are usually surrounded by a double layer of ions called the Debye length (K_D). At low conductivity of the medium, this double layer is extended around the suspended particles and resulting in apparently large hydrodynamic diameter. On the other hand, this double layer could be supressed by enhancing the solvent electric conductivity through addition of ions and salts to get an approximate measurement of the actual particle size.

Typically, the DLS is usually calibrated using standard polystyrene latex particles, this standard is supplied in a range of particle sizes including 30, 60 and 100 nm. The standard polystyrene

latex particles should be diluted in 10 mM sodium chloride to supress the electric double layer and ensure that the reported measurement is the same as the expected diameter of the standard.

2.1.1.1.2 Surface Structure

The structure of the suspended particles highly influences their diffusion speed, for example the presence of some polymers projecting out into the medium such as polyethylene glycol (PEG) will reduce the diffusion speed (larger particle size measurement) more than in case that the polymer is flat.

2.1.1.1.3 Non-Spherical Particles

As mentioned before, DLS depends on measuring the diameter of the sphere that has the same diffusion speed as the tested particles. Hence, if the particles are not spherical, the changes in their size could be hard to detect.

Thus, it is particularly important to study the morphology of the prepared particles using other techniques such as the transmission or scanning electron microscopy.

2.1.1.2 Light Scattering Theories

As mentioned before, the zeta sizer measures the diffusion speed of the suspended particles through using the light scattering. The particles are subjected to a beam of laser of certain wavelength, then the intensity of the scattered light is measured. This intensity is expected to increase in case of particles moving at low speed (larger particles) than in case of those with high speed (of smaller particle size).

2.1.1.2.1 Rayleigh scattering

The Rayleigh theory is imposing a direct relationship between the intensity of the scattered light and the particle diameter, specifically $I \propto d^6$, where I = intensity of light scattered, d = particle diameter.

The d^6 term in the above relationship indicates that as particle size increase by a factor of 10, the intensity of scattered light will increase by a factor of 10^6 or one million times. Hence the imposed disadvantage will be the overestimation of larger particles compared to smaller ones. Thus, the d^6 factor also means it is difficult to use the DLS to measure a mixture of particles with a great variation in particle size, for instance 1000 and 10 nm, as the light scattered from the smaller particles will be of minute contribution to the total light scattered.

2.1.1.2.2 Mie Theory

Mie theory is more widely applied for those particles of a size close enough to the wavelength of the employed Laser light, which is the most common scenario. Mie theory is used in the zeta sizer software for conversion of the intensity distribution into volume.

In dynamic light scattering, the diffusion speed of particles due to Brownian motion is elucidated by measuring the fluctuation rate of the scattered light intensity. Simply, the smaller the particle size the greater will be those fluctuations due to the increased speed of the particles. The best way to convert those fluctuations due to Brownian motion into particles size is to use a device called a digital auto correlator.

2.1.1.3 Size distribution

As we measure the intensity of scattered light, the size of the particles obtained from the auto correlator is relative to the scattered light intensity and hence it will be known as intensity size distribution.

Subsequently, the sample input parameters (either reported in literature or obtained by experiment), including refractive index and viscosity, can be used to elucidate the volume size distribution through the help of Mie theory. The importance of volume distribution lies in its ability to give more understanding for the importance of any tail or secondary peaks present in the distribution. Generally, the d(intensity) > d(volume) > d(number)

For more understanding of the differences between the intensity, volume, and number distributions, consider a sample formed of 2 population of particles that are equal in number, one with size of 5 nm and the other is 50 nm. Plotting the number distribution of this sample will result in 2 peaks of 1:1 ratio (positioned at 5 and 50nm). Converting the number distribution into volume distribution will result in 2 peaks of ratio 1:1000 (because the volume of a sphere is equal to $\frac{4}{3}\pi$ $(d/2)^3$. Finally, the intensity distribution will show 2 peaks with a ratio of 1:1000000 (because the intensity of scattering is proportional to d^6 from Rayleigh's approximation).

2.1.2 Zeta potential

Zeta potential, known as surface charge, could be estimated using the Zeta sizer as well. This is obtained through measuring the electrophoretic mobility of the particles using Laser Doppler Velocimetry (LDV), which determines the laser scattering due to particle motion.

To understand more, surface charge is developed on colloidal particles surface due to the electrical double layer effect. The net charge on the particle surface results in distribution of ions from the medium around it, with higher concentrations of counter ions (opposite in charge) close to its surface. Consequently, a double layer is formed, the first bound firmly to the particles is called the Stern layer and the other is called the diffuse layer of counter ions.

During the motion of particles, ions attached to it will move as well, while ions outside this boundary, which is called the slipping plane **Figure 3**, are not expected to move. The potential at this slipping plan is defined as zeta potential.

Zeta potential give an indication of the stability of the colloidal system, where the higher the charge on the particles the greater will be the repulsion between them, hence more stability against aggregation. The range of Zeta potential indicating good stability should be either >+30 mV or < -30 mV(161).

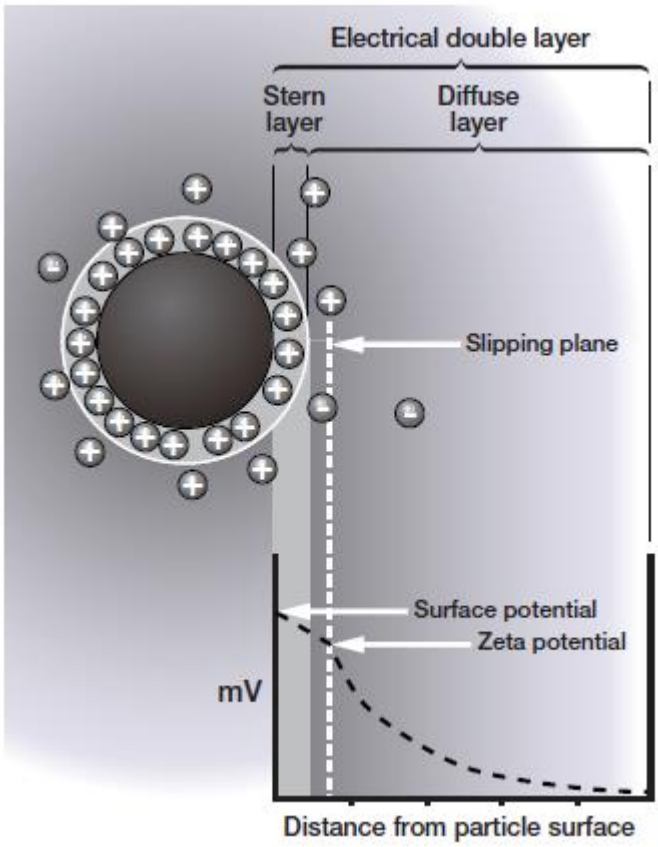

Figure 3 Measuring the Zeta potential of colloidal particles, showing the electric double layer and the boundary slipping plane (160).

As mentioned before, the Zeta potential is measured using the electrophoretic mobility of the particles, this could be estimated by Henry equation as follows,

$$\boldsymbol{U_E = \frac{2\varepsilon\, z\, f(ka)}{3\,\eta}}$$ **Equation 12 Henry's equation**

Where: ʒ: Zeta potential.

U_E: Electrophoretic mobility.

ε: Dielectric constant.

ɳ: Viscosity.

f(Ka): Henry's function (162).

The samples are loaded in a micro-electrophoresis cell with electrodes to which a potential is applied. The charged particles will start to move to the electrode of the opposite charge(163). The velocity of the particles is measured using Laser Doppler Velocimetry.

2.1.3 Transmission electron microscopy

Transmission electron microscopy (TEM) is a widely used technique for characterisation of nanomaterials, as high-quality images could be obtained at extremely high magnification power. The TEM can provide images at spatial resolution at the order of atomic dimension of the sample.

The TEM device, shown in **Figure 4,** consists of an electron gun which acts a source of electron beam, this beam will pass through a series of lenses into the specimen, which will finally be viewed over a fluorescent screen. The device is equipped with a camera to take images and a computer to store the captured images.

The incident electron beam is transmitted through the specimen, will be transformed into scattered electrons as they interact with the sample, then those scattered electrons are magnified through the objective lens and collected via the imaging lens which is then viewed over fluorescent plan to give images for the sample components, which is captured by camera generating high-resolution images. The distance between the objective lens and the imaging lens will indicate the magnification power employed.

For colloidal nanomaterials, TEM can provide information on the size, morphology, and aggregation of particles within the dispersion. Compared to the scanning electron microscopy SEM, TEM is more sensitive in getting high resolution images for small particle sizes with high spatial resolution. The reason mainly is because the SEM acts through interaction of the electron beam with the surface of the sample only, resulting in releasing of secondary photons to be detected, while in case of TEM the electron beam is transmitted through the thin layer of the sample and then detected on the other side.

One can simply compare the TEM to the simple light optical microscopy, but with higher magnification power and optical resolution. Where the light beam in the optical microscopy is

replaced by electron beam in TEM, the glass lens is replaced with electromagnetic lenses and images are viewed on fluorescence plan instead of the eye piece.

Despite of the various advantages of TEM, which include powerful magnification and the provision of information regarding compound and element structures, however TEM requires special maintenance, particularly because of its ultra-high vacuum system (164).

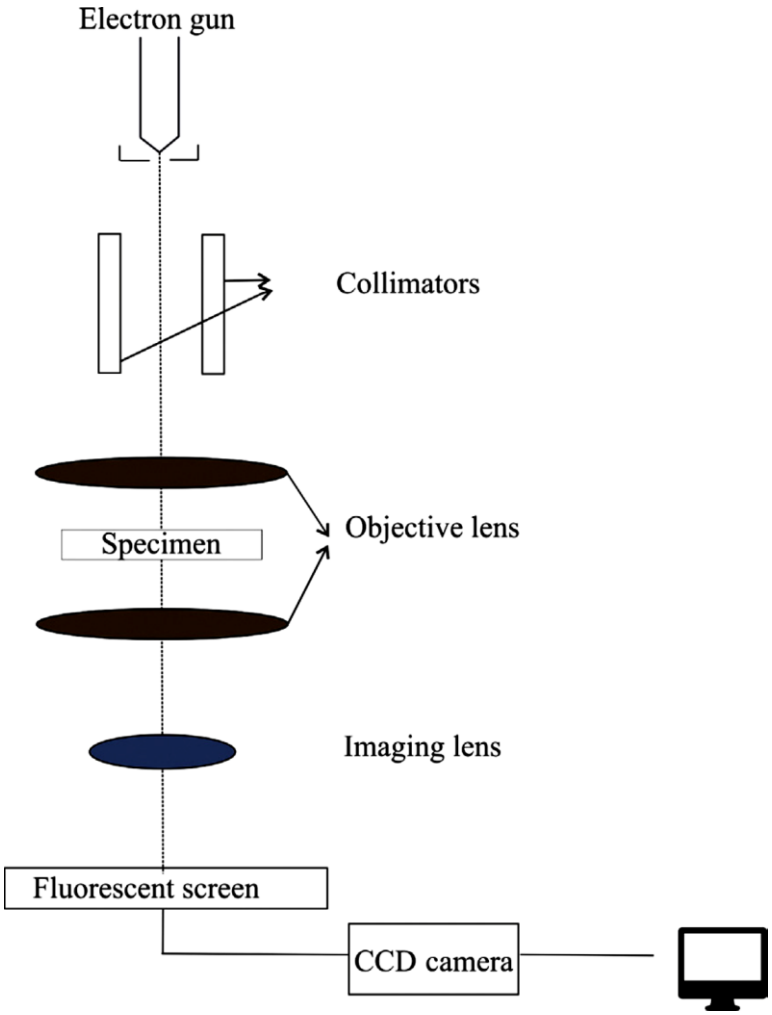

Figure 4 Diagram representing a simplified structure of the transmission electron microscope TEM(165).

2.2 MATERIALS

Extra virgin olive oil, Triolein (Merck life science, >=99% purity), Tricaprin (Alfa Aesar, >98% purity), Trihexanoin (Alfa Aesar, > 99% purity), Tridecanoate (Merck life science, 99% purity), Orlistat (Merck life science, >98% purity), Niclosamide stearate, 1-palmitoyl-2-oleoyl phosphatidyl choline (POPC) (Merck life science, TLC >99% purity), DSPC (Di stearoyl phosphatidylcholine) (Stratech scientific ltd., Avanti polar lipids > 99% purity), DSPE PEG 5000 maleimide (Stratech scientific ltd., Avanti polar lipids > 99% purity), Cholesterol (Stratech scientific ltd.,> 99% purity), Soybean Lecithin (Fisher scientific UK ltd., Purity >98%), Tween80 (ThermoFisher scientific, >97% purity), Sodium dodecyl sulfate (SDS) (Sigma Aldrich, ACS reagent 99% purity), potassium nitrate KNO_3 (Sigma Aldrich, ACS reagent 99% purity) , Ellman's reagent powder 5,5'-dithio-*bis*-(2-nitrobenzoic acid) (DTNB) (Fisher scientific ltd, at least 99% pure), pure ethanol (Sigma Aldrich, anhydrous pure >99.5%), dimethyl sulfoxide (DMSO) (VWR international ltd.,>98% purity), Trehalose dihydrate (Sigma Aldrich, >99% purity) , D-Mannitol (Sigma Aldrich, >99% purity), Glucose (Sigma Aldrich, >99% purity), 1-mercapto undecanol (Sigma Aldrich, 97% purity), Phosphate buffer saline tablets (Sigma Aldrich), culture medium Dulbecco's Modified Eagle Medium DMEM (VWR scientific ltd. Sterile filtered), phenol red free RPMI medium (ThermoFisher scientific, sterile filtered), Human serum albumin HAS (Merck life science, lyophilized powder, 97% purity agarose gel electrophoresis), 25-NBD cholesterol (Scientific laboratory supplies ltd, Avanti polar lipids, <99% purity), breast cancer cell lines MCF-7, BT474 and MDA MB 453 (all supplied by ATCC, and stored in liquid nitrogen until used) and MilliQ® water, all materials not specified were of analytical grade, unless otherwise mentioned.

2.3 METHODS

2.3.1 Nanoparticles preparation

In our work, nanoparticles were prepared by rapid solvent exchange method through direct injection of ethanolic solution of hydrophobic materials into deionised water using automated syringe eVol™ **Figure 5**.

Figure 5 Automated syringe eVol™

First of all, the materials employed (which will be discussed in detail in Chapter 3 and 4) are dissolved in ethanol at room temperature. Afterwards, nanoparticles were prepared by directly injecting ethanolic solution into MilliQ® water in a volume ratio of 1:9, under stirring using magnetic stirrer at 500 rpm. The process is done using the eVol™ automated syringe at a rate of 1 ml/s, a detailed diagram for the process is shown in **Figure 6**.

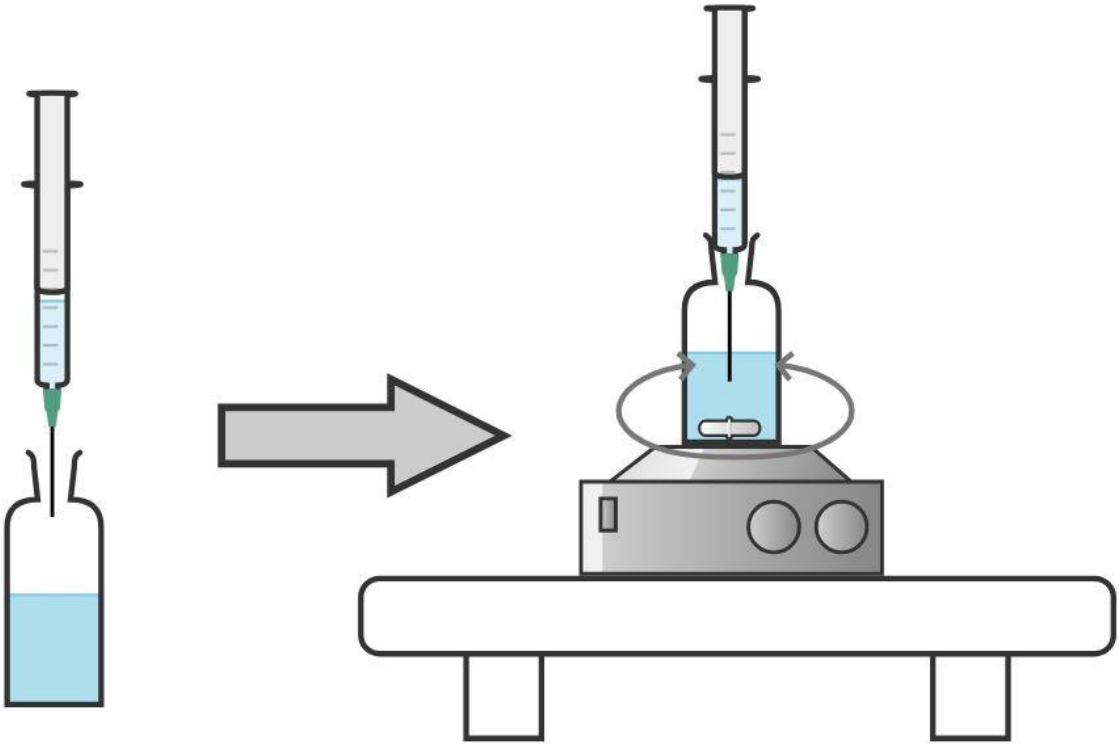

Figure 6 Diagram showing the steps of NPs preparation using rapid solvent shift technique.

Following injection, the nanoparticle dispersion is removed immediately from the magnetic stirrer and characterized using Malvern® zeta sizer nanorange (ZS) (**Figure 7**).

Figure 7 Malvern® zeta sizer nanorange ZS

2.3.2 Coating of the NPs

Coating was done through the same nanoprecipitation technique, briefly the coating together with the core material were dissolved in ethanol at specific molar ratio. Then NPs were prepared through injecting ethanolic solution into antisolvent water at ratio of 1:9 using eVol™ syringe injector as outlined above.

2.3.3 Measuring the particle size and zeta potential:

Freshly prepared nanoparticle dispersions are subjected immediately to particle size and zeta potential analysis, this can be done through pipetting 1 ml of each dispersion of different concentration into either cuvette (for particle size) or zeta cell (for zeta potential), followed by running the analysis at 25ºC, auto-attenuator and wavelength 600 nm.

2.3.4 TEM imaging of NPs

TEM images of NPs were captured using negative staining. Samples were prepared, stained using 2% uranyl acetate (provide by NMRC lab, university of Nottingham), and fixed over carbon coated copper mesh grids (TEM Grids C200Cu100, Generon Ltd, Dublin, Ireland). Samples are left over the mesh grids for at least 1 minute to allow sedimentation of the particles over the mesh, then the samples were dried using a piece of filter paper to suck the liquids. TEM imaging was done using FEI® Tecnai Biotwin transmission electron microscope (Eindhoven, The Netherlands) at 100 KV, equipped with a camera Eagle 4K CCD (Eindhoven, The Netherlands), and TIA software (FEI®) (Eindhoven, The Netherlands). Images were processed using ImageJ, Fiji® package for counting the particles.

2.3.5 Freeze drying of the NPs

Some of the chosen formulations were freeze dried using Virtis benchtop lyophiliser® (SP scientific sentry 2.0) to enhance stability of the prepared formulations over storage (**Figure 8**).

First of all, NPs were prepared with specific cryoprotectant at specific ratio (will be discussed in detail in Chapter 4). Then, the prepared NPs dispersions were flash frozen using liquid

nitrogen, followed by placing them in the lyophiliser. The pressure was then reduced to 100 mTorr and the temperature was set to −50 C and held for 24 h to allow drying. The dried samples were then stored in freezer at -20 °C in sealed bags with silica beads until further used.

Figure 8 Freeze dryer, Virtis benchtop lyophiliser® (SP scientific sentry 2.0)

2.3.6 Drug incorporation assay

Incorporation studies were done using both DSC and polarised light microscopy techniques.

2.3.6.1 Differential scanning calorimetry (DSC)

DSC was done using DSC Q2000 (TA® instruments, UK) (**Figure 9**). Samples (10mg) were weighed separately in aluminium DSC pans, which were then compressed to be hermetically sealed. The prepared pans were placed in DSC, and a heat cool heat run was done for each sample under nitrogen gas, starting at 20°C to 350°C at a rate of 5°C/min. Afterwards, DSC thermograms were collected and analysed.

Figure 9 Differential scanning calorimetry DSC Q2000 (TA® instruments, UK)

2.3.6.2 Polarised light microscopy

Microscopic images were captured using polarised light microscope PX023POL (Prior Scientific Inc® USA) (**Figure 10**). A suitable mass of each sample (~ 20 mg) was added on a clean microscopic slide. The samples were viewed under both bright and dark fields to check for the birefringence, colour absorption and optical similarities.

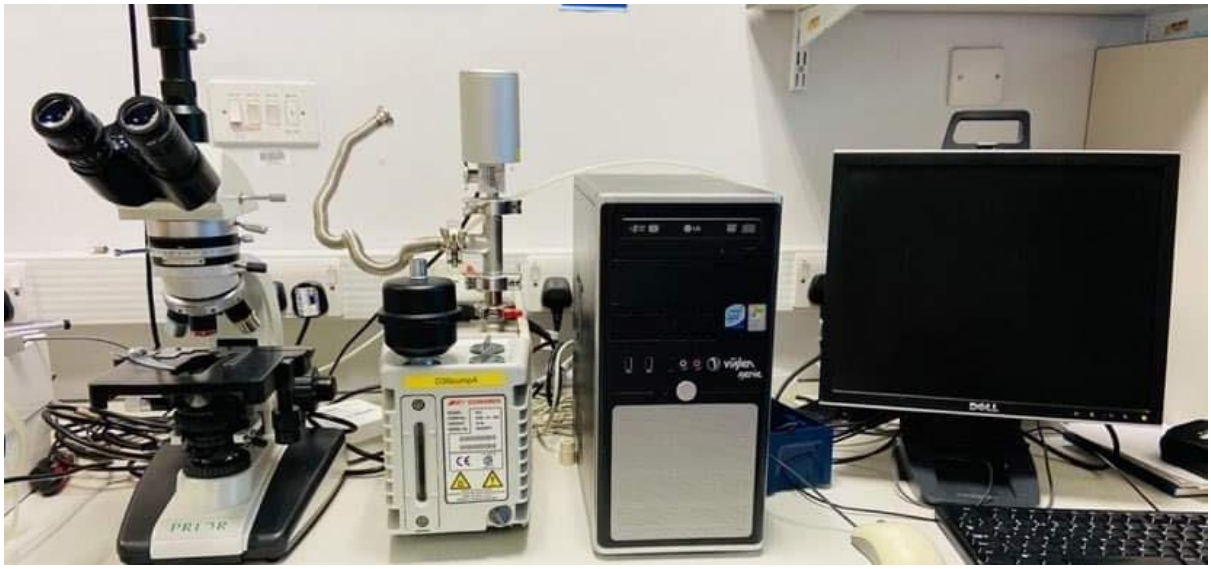

Figure 10 polarised light microscope PX023POL (Prior Scientific Inc® USA)

2.3.7 UV assay of orlistat

Orlistat (1 mg/ml) in ethanol solution was scanned over the range of (200 – 700) nm using UV spectrophotometer (Agilent® Cary3500 UV-Vis spectrophotometer, USA) (**Figure 11**), and the wavelength of maximum absorbance (λ_{max}) was determined (166).

Serial dilutions (10 - 150 µg / ml) were prepared and the absorbance of the prepared solutions was measured at the predetermined (λ_{max}). The measured absorbance values were plotted against the corresponding concentrations to obtain a calibration curve.

Figure 11 UV spectrophotometer (Agilent® Cary3500 UV-Vis spectrophotometer, USA)

2.3.8 Encapsulation efficiency and drug loading

The percent of drug encapsulated into the nanoparticles was measured using two approaches. The first one through centrifugation ultrafiltration technique, simply nanoparticle formulations were loaded in Vivaspin® centrifugal concentrator(167) (Sartorius Vivaspin® 20, mwco 5000 d, membrane PES) (**Figure 12**), and were centrifuged at 6000 rpm for 5 min in 5 cycles using a cooling centrifuge (Eppendorf® cooling centrifuge, Eppendorf® AG, Germany). Afterwards, the filtrate containing the free drug was separated, freeze dried and reconstituted and assayed. The other method is through dialysis(168), using slide-A- lyzer dialysis cassettes (thermos scientific™ mwco 3.5 Kd, UK) **(Figure 13**), where 3 ml of each NP formulation was loaded to the cassette and then suspended in 200 ml of phosphate buffer saline PBS (pH 7.8) and kept in the fridge for 24 hours, then 40 ml sample were taken, freeze dried, and analysed for content of free drug.

Figure 12 Vivaspin® centrifugal concentrator, Sartorius Vivaspin® 20, mwco 5000 d, membrane PES.

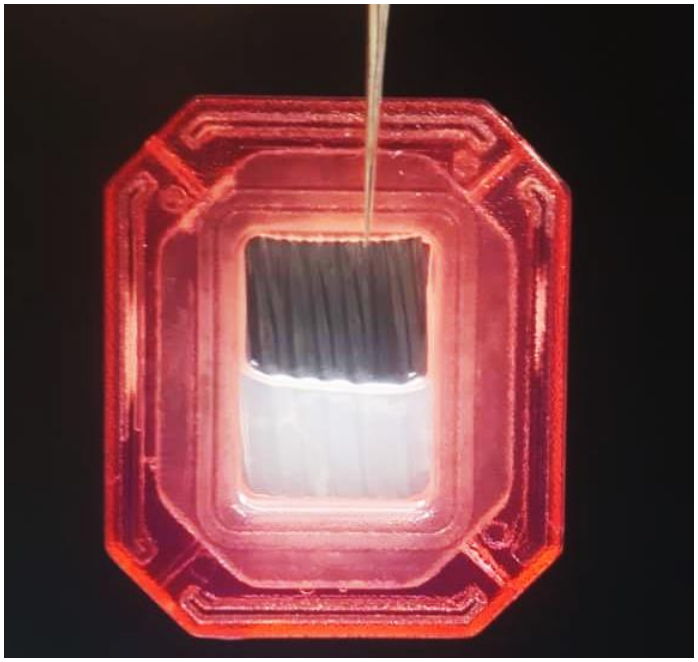

Figure 13 slide-A- lyzer dialysis cassettes (thermos scientific™ mwco 3.5 Kd, UK)

2.3.9 Drug release assay

Drug release assay was carried out in PBS (pH 7.4) containing 0.2% tween 80 to challenge the drug release pattern. 3 ml sample of the nanoparticle formulation was loaded into slide-A- lyzer dialysis cassettes (thermos scientific™ mwco 3.5 Kd, UK). Then the cassette was allowed to suspend into 400 ml of release medium and kept at 37ºC and 350 rpm for 1 week. At predetermined time intervals, 40 ml samples were withdrawn and were compensated by fresh release buffer. Samples were freeze dried and assayed spectrophotometrically.

2.3.10 Preparation of functionalised NPs

Orlistat NPs were functionalised to resemble the structure of the LDL, using a mixture of phospholipids and cholesterol, together with 11-mer peptide that mimics the active site of the apoprotein B in structure (**Figure 14**). NPs were prepared using the straightforward solvent shift technique. Simply, ethanolic solution of the drug together with a mixture of the phospholipids (POPC or DSPC), Cholesterol and DSPE PEG 5000 maleimide peptide

conjugate in a ratio 45:50:5 respectively (with a coat to core molar ratio 1: 1.6) were directly injected into water under stirring as mentioned before.

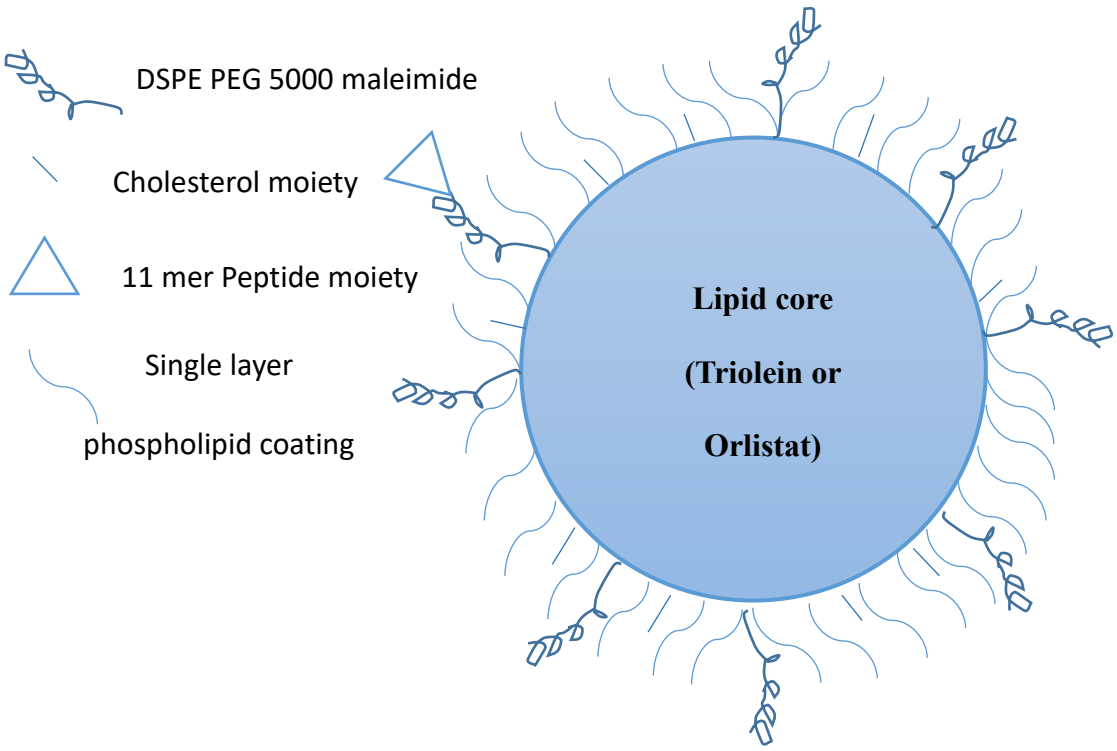

Figure 14 Proposed structure of the LDL-like NPs functionalised with 11-mer peptide.

Concerning DSPE PEG 500 maleimide peptide conjugate, it was prepared by simple click chemistry. This is done through incubation of the peptide with the prepared NPs having the DSPE PEG maleimide 5000 already incorporated in the NPs coat for 24 hours.

2.3.10.1 Ellman's test for free sulfhydryl groups

The efficiency of the peptide conjugation to the lipid moiety was confirmed using Ellman's test for the free sulfhydryl groups(169). To prepare Ellman's reagent, 1 mL of reaction buffer (0.1 M sodium phosphate with 1 mM EDTA, pH 8.0) was added to 4 mg Ellman's powder followed by vortexing for 1 minute at RT. Afterwards, 2.5 uL of 4 mg/mL Ellman's reagent was added to 100 uL of sample of interest or buffer only as blank, the absorbance of the samples was measured using UV/Vis spectrophotometer at λ_{max} 412 nm(169). The concentration of the free sulfhydryls was calculated using the extinction coefficient of E = 14150 $M^{-1}cm^{-1}$. The test

was carried out for 11-mercapto undecanol as a reference, the 11-mer peptide solution, DSPE PEG 5000 maleimide peptide conjugate, and the peptide functionalized orlistat NPs.

2.3.10.2 Investigation of orlistat binding to albumin

Orlistat binding assay was carried out through a fluorescent quenching technique using Fluorescence spectrophotometer, (Agilent® Cary eclipse fluorescence spectrophotometer, USA). First of all the fluorescence spectrum of human serum albumin (HSA) was scanned (170). Afterwards 20 μL of stock orlistat ethanolic solution were added to the HSA solution. The fluorescence emission spectra of HSA in the presence of increasing amounts of the drug under study were recorded. The data were analysed afterwards by the Stern–Volmer equation(171).

2.3.11 Cell studies on the prepared formulations

Three different breast cancer cell lines were used for cell work, BT-474, MDA MB453 and MCF-7. For the cell growth MCF-7 cell line was grown in phenol red free RPMI medium, while for the other 2 cell lines (BT-474 and MDA MB 453), they were grown in DMEM culture media.

After proliferation, cells of each cell line separately were seeded in separate well plates, at 1000 cells per well in their cells regular medium. Afterwards, cells were incubated at 37ºC, and 5% CO_2.

Cell lines where then used for cytotoxicity study using Presto Blue cytotoxicity assay, and for cellular uptake study using Fluorescence microscopy.

2.3.12 Statistical analysis

Statistical analysis for the results was done to determine the significance differences between samples. Two-way ANOVA test was utilised using GraphPad Prism® software.

3 Chapter 3 Particle size control using solvent shift technique

3.1 INTRODUCTION

3.1.1 NPs' properties and its effect on efficacy of formulation

Achieving high accumulation inside the tumour and thus an enhanced efficacy of the formulation is highly attributed to the physico-chemical properties of the prepared nanoparticles, this includes particle size, charge, and shape.

3.1.1.1 Particle size

Concerning the particle size, small particle size (below ~50 nm) has been reported to result in both better retention in the tumours, and better cellular uptake into the cancerous tissues (through endocytosis) compared to the larger particles. Jiang et al.(156) studied the effect of antibody-coated gold and silver nanoparticles within the size range of 2–100 nm on the cellular response. They found that all the tested particles could alter the signalling processes of the cell functions (including cell death), but the 40 and 50 nm nanoparticles were found to be most efficient in inducing receptor-mediated endocytosis (**Figure 15**).

Cabral et al.(158) used drug-loaded polymeric micelles of size 30, 50, 70 and 100 nm to compare their accumulation and effectiveness in both highly and poorly permeable tumours. They found that all the micelles penetrated the highly permeable tumours in mice, but in case of poorly permeable tumours, only 30 nm micelles were able to penetrate and achieve the desired antitumor effect (**Figure 16**).

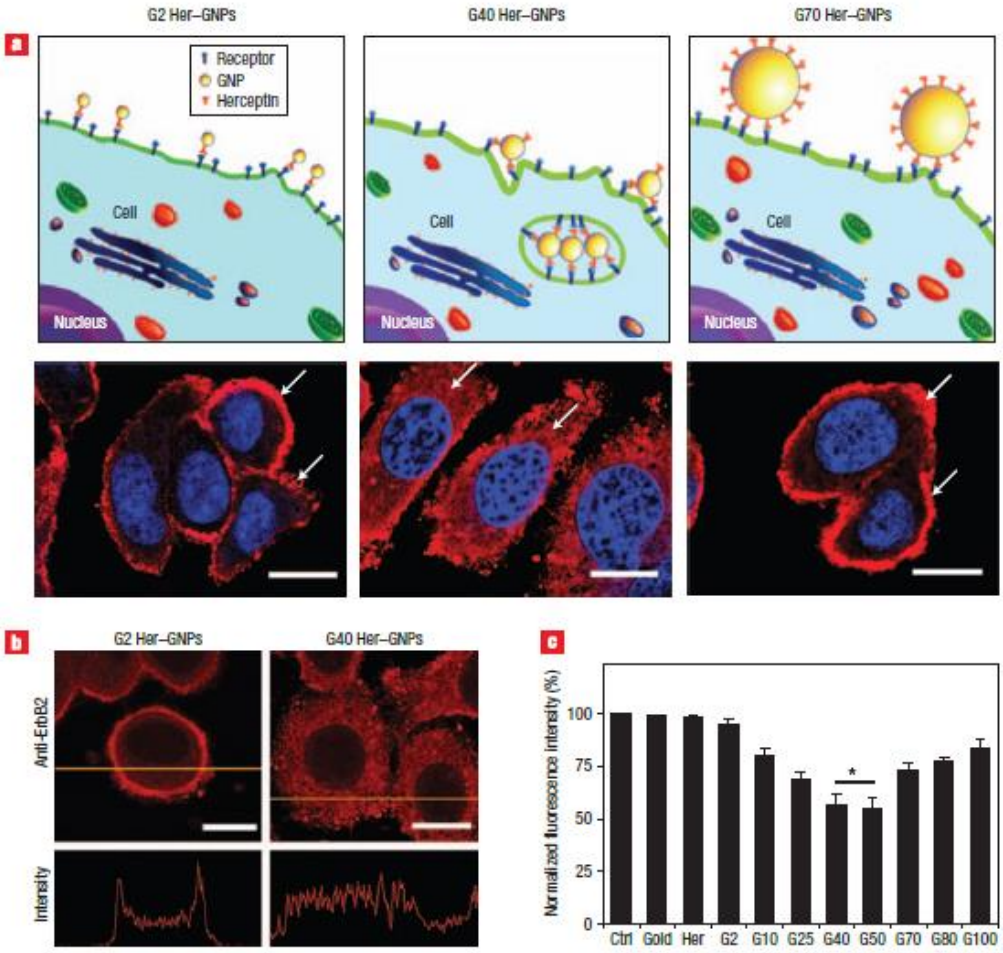

Figure 15 Jiang et al. results showing the effect of particle size of gold NPs on the endocytosis and uptake of the NPs in breast cancer cell lines.

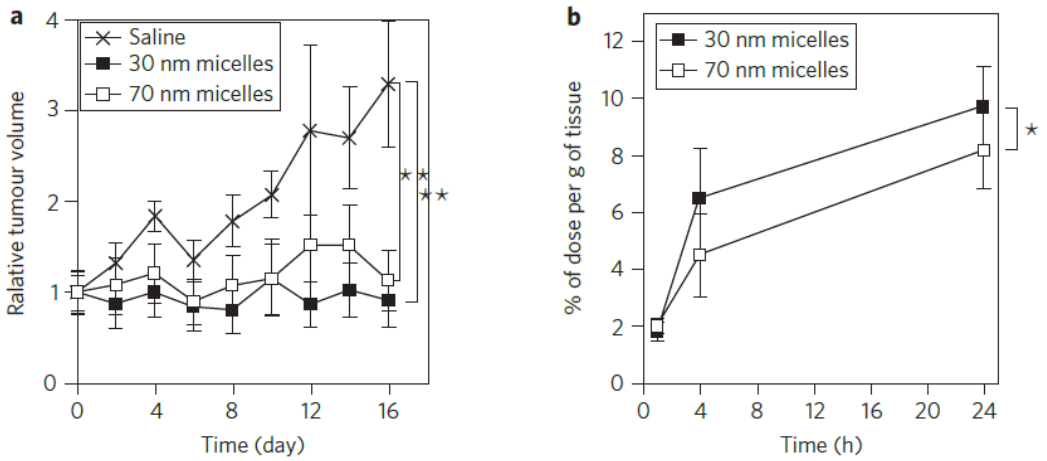

Figure 16 Cabral et al. results showing the effect of particle size of polymeric micelles on the tumour volume and dose accumulation in prostate cancer cell lines

3.1.1.2 Surface charge

Regarding the surface charge on particle, positively charged particles could decrease blood circulation time, due to opsonisation and clearance by reticuloendothelial system (RES), compared to the negatively charged and uncharged particles. Interestingly, it has also been reported that, the positively charged particles possess better accumulation in tumour tissues due to the favourable interaction between the positively charged NPs and the tumour blood vessels, hence preventing their redistribution in the systemic circulation (172).

3.1.1.3 Nanoparticle shape

Meanwhile, the shape of the nanoparticle could have an influence on the behaviour of the nanoformulation. Chauhan et al.(173) compared the tumour distribution kinetics of nanorods with a length of 44 nm and nanospheres of 35 nm in mammary tumours in mice. Their hydrodynamic diameters were found to be same. As compared to the nanospheres, they found that the nanorods were transported across vessel walls 4.1-times faster. The penetration inside the tumour was also 1.7-times higher for nanorods as compared to the volume to which the nanospheres were distributed.

Accordingly, developing LDL-like nanoparticles with a controlled size in the range of <50 nm is still a hurdle. This size range is required not only to mimic the real LDL in their size and properties (20-25 nm), but also to ensure the best accumulation and penetration to the tumours and consequently reaching the best therapeutic outcome.(174) Therefore, rapid solvent shift technique was studied as a simple and straightforward method for NPs preparation with particle size control.

3.1.2 Parameters that Govern Nanoparticle Size Prepared through Rapid Solvent Shifting

Rapid solvent shifting technique is a simple technique that depends on the fact that when a solute dissolved in a specific solvent and then swiftly exposed to an excess of anti-solvent(175),

it precipitates out of solution due to change in the solubility. However, this entire process of precipitation driven by solvent shifting, can be subdivided into discrete events in time, characterized by the solute physico-chemical properties. Assessing these parameters from the basic principles of solution, fluid-flow, mixing, nucleation, growth, and colloid stabilization can thereby provide the necessary understanding of the nanoparticle fabrication by rapid solvent shifting process. These parameters include:

1. Organic Solvent: the used organic solvent influences the nature of the organic solution of test materials, drugs and/or lipids, governing the amount of the materials used and hence the degree of supersaturation.

2. Fluid Flow: The nature of the fluid flow and the dependence of turbulence on the Reynaud's number. The nature of the fluid flow is determined by parameters such as the geometry of the flow channel, pipe's cross-sectional area, volumetric flow rate, the viscosity of the flowing liquid. These parameters can be normalized through one dimensionless number called Reynolds number (Re). Re is the ratio of inertial forces and the viscous forces for organic and aqueous streams of flow(176).

3. Mixing: The extent of mixing of organic and aqueous phase under either diffusion limited or turbulent flow greatly affect the growth and condensation of the formed nuclei.

4. Solubility and Supersaturation in Anti-Solvent: The solubility of the test material in the anti-solvent and its degree of supersaturation governs the stability of the formed nuclei and controls the rate of particles growth.

5. Nucleation: Nanoparticle nucleation and its initial critical radius of the employed material will determine the final particle size

6. Post nucleation events: Collection of the nanoparticles and their colloid stability, and any further aggregation, coalescence, or ripening, especially against time and ionic strength, will affect the properties of the formed NPs.

7. Surface Properties*:* The presence of a surface monolayer and/or coating of the NPs will have a direct influence on the initial precipitation and subsequent colloid stability

8. Phase separation: Any phase separation for solute mixtures.

With the help of first six parameters, the mechanism of nanoparticle formation through rapid solvent shifting was understood. Last two parameters may help in controlling the nanoparticle size and designing the nanoparticle Formulation.

3.1.3 Effect of concentration on the size of nanoparticles

For the sake of understanding the effect of the concentration of the hydrophobic materials added in organic solvent on the size of nanoparticles, it is reported that an increase in the size of nanoparticles due to increased supply of solute monomers is expected.

Moreover, the interparticle distance could be studied by utilizing Wigner-Seitz radius (spherical). This 'Wigner-Seitz radius' is often used in atomic physics and is defined as the radius occupied by one atom, and is also reported as a measure of interparticle distance. For instance, in a 10 ml volume, the density of molecules could be calculated for a range of concentrations using following equation (177).

Equation 13 $\boldsymbol{R = \left(\frac{3}{4\pi n}\right)^{1/3}}$

Where R is Wigner Seitz radius and n is the particle density.

Though this is considered an approximation, it is expected that with increasing the molar concentration of the solute in the solution, the time averaged intermolecular distance decreases, thus leading to more encounters of the solute molecules resulting into increase in size.

Therefore, for a given set of parameters (such as the geometry used for rapid solvent shifting, at lab temperature 20 °C), an increase in the measured size of the nanoparticle with increase in concentration of solute is expected, in absence of any coating or stabilisers.

3.2 AIMS AND OBJECTIVES

The main objective of the work is to investigate the rapid solvent shift technique (flash nanoprecipitation), as a method for nanoprecipitation and for preparation of NPs of controlled particle size (<50 nm).

The method was investigated on several model hydrophobic materials and drugs to be then applied on our drug of choice orlistat (chapter 4).

SA1: Investigating the effect of changing concentration on the properties of the prepared NPs, in terms of particle size and surface charge.

SA 2: Investigating the effect of applying rapid solvent shift technique using different materials and drugs on the properties of the prepared NPs.

SA 3: Comparison between the preparation of NPs by the proposed rapid solvent shift technique and the slow dripping method.

SA 4: Investigating the effect of coating of the NPs on the particle size growth, and evaluating the optimum ratio for coating the NPs.

3.3 MATERIALS AND METHODS

3.3.1 Materials

Extra virgin olive oil, Triolein (Merck life science, >=99% purity), Tricaprin (Alfa Aesar, >98% purity), Trihexanoin (Alfa Aesar, > 99% purity), Tridecanoate (Merck life science, 99% purity), Orlistat (Merck life science, >98% purity), Niclosamide stearate, 1-palmitoyl-2-oleoyl phosphatidyl choline (POPC) (Merck life science, TLC >99% purity, **Figure17 A**), Soybean Lecithin (Fisher scientific UK ltd., Purity >98%, **Figure 17 C**), Tween80 (ThermoFisher scientific, >97% purity, **Figure 17 B**), pure ethanol (Sigma Aldrich, anhydrous pure >99.5%), dimethyl sulfoxide (DMSO) (VWR international ltd.,>98% purity), and MilliQ® water, all materials were of analytical grade and used as supplied, unless otherwise mentioned.

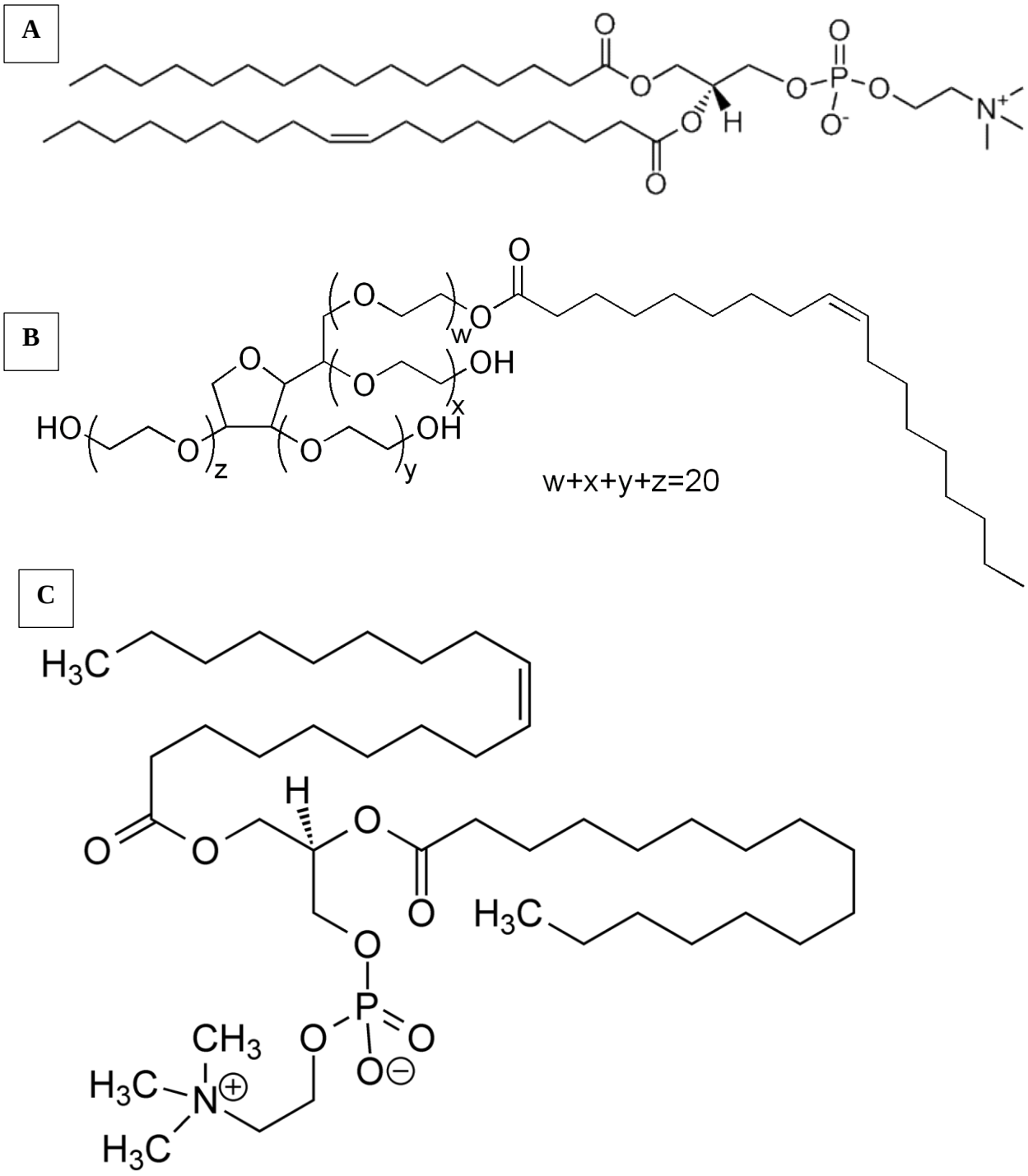

Figure 17 chemical structure of employed excipients A) POPC, B) Tween80 and C) Lecithin

3.3.2 Methods

3.3.2.1 Nanoparticles preparation using rapid solvent shift technique

Olive oil nanoparticles were prepared by solvent exchange method through direct injection of ethanolic solution into water. Briefly, olive oil (aqueous solubility 6.14 e^{-06}mg/ml) was dissolved in ethanol to obtain different concentration (35 to 0.01 g/L).

A solubility study was carried out at room temperature, by dissolving olive oil in ethanol in the order of increasing concentration, till reaching the saturated solubility; above which no more olive oil could be dissolved, the saturated solubility of olive oil in ethanol at room temperature (25ºC) was found to be around 35 g/L

Glyceryl tridecanoate (also known as tricaprin) Glyceryl trihexanoate (also known as Trihexanoin), Orlistat and Niclosamide stearate nanoparticles were prepared through direct injection of ethanolic solution into water as well. Briefly, each compound was dissolved in ethanol to obtain different concentration (10 to 0.01 mM). As tricaprin is solid at room temperature (melting point=32ºC, supplied in amber 20 ml glass vials), it was heated by rubbing the glass vial till melting, before it could be mixed with the ethanol.

Afterwards, nanoparticles were prepared by directly injecting 0.5 ml of each ethanolic solution into 4.5 ml of MilliQ® water kept over a magnetic stirrer at 500 rpm, using eVol™ automated syringe, at injection rate of 1 ml/s, ensuring the needle to be under the antisolvent surface. Following injection, the nanoparticle dispersion is removed immediately from the magnetic stirrer and characterized using Malvern zeta sizer nanorange (ZS).

3.3.2.2 Coating of the NPs

Three coating materials were utilised for this process, distinctively Lecithin, Tween 80 and POPC. The coating material was employed for olive oil core material as model material. The effect of coating will further be studied later on the drug of choice orlistat.

Coating was done through nanoprecipitation technique, briefly the coating together with the core material were dissolved in organic solvent (ethanol for POPC and tween 80, DMSO for lecithin due to poor solubility in ethanol) at different molar ratio, (1:1), (2:1), (4:1) (core : coat). Then NPs were prepared through injecting 0.5 ml of each ethanolic solution into 4.5 ml of water using eVol™syringe injector as mentioned before.

For the model drug orlistat, the effect of coating was done after choosing the optimum coating material as well as the optimum core to coat ratio following the experiments on olive oil. The preparation of coated orlistat NPs was done using the same previously mentioned technique and will be discussed in details later.

3.3.2.3 Measuring the particle size and zeta potential:

Freshly prepared nanoparticle dispersions were subjected immediately to particle size and zeta potential analysis, this can be done through pipetting 1 ml of each dispersion of different concentration into either cuvette (for particle size) or zeta cell (for zeta potential), followed by running the analysis at 25ºC, auto-attenuator and wavelength 600 nm. All results are expressed as mean of triplicates (n=3) ± SD.

3.3.2.4 TEM imaging of NPs

TEM images of NPs were captured using negative staining. Samples were prepared, stained using 2% uranyl acetate, and fixed over carbon coated copper mesh grids. TEM imaging was done using FEI® Tecnai Biotwin transmission electron microscope (Eindhoven, The Netherlands) at 100 KV, equipped with a camera Eagle 4K CCD (Eindhoven, The Netherlands), and TIA software (FEI®) (Eindhoven, The Netherlands). Images were processed using ImageJ, Fiji® package for counting the particle size.

3.3.2.5 Effect of coat to core ratio on particle size.

2D inkjet printing was employed to inspect the effect of the amount of coating on protecting the precipitated NPs against further growth (178). 2D printing could produce several samples via a single printing that enhance overall experimental efficiency with time.

Simply, Tween 80 coated olive oil NPs of different coat to core ratios were prepared using the 2D printer (piezoelectric sciflexarayer). Specifically, Tween 80 and olive oil ethanolic mixtures were dispensed using the device in different molar ratios (coat :core 1:9, 1:4, 3:7, 2:3, 1:1, 3:2, 7:3, 4:1) into 96 well plate (Garnier® bio-one 96 well plate) containing MilliQ® water in a ratio of (1 ethanolic solution volume 6 µl : 9 water volume 54 µl) with total volume of 60 µl formulation. Particle size analysis was done using DLS plate reader (Wyatt Dynapro® Plate reader).

3.3.2.6 Effect of injection rate on particle size growth

To investigate the effect of the rate of ethanolic injection on the size of the formed NPs, Tween 80 or POPC coated olive oil NPs were prepared either through rapid or slow injection. For the rapid injection technique (1 ml/s) 0.5 ml of ethanolic solution of olive oil together with either POPC or tween 80 in a ratio (core: coat 2:1) was injected into 4.5 ml of MilliQ® water under magnetic stirring (500 rpm) at a rate of 1 ml/s using eVol™ syringe system. On the other hand, for slow injection technique (0.1 ml/min) the ethanolic solution was injected into water at a rate of 0.1 ml/min (0.00167 ml/s) using a 1 ml syringe. The ethanolic solutions were prepared at olive oil concentrations 10 and 1 mM respectively, in order to compare between a high and a low concentration of the material and the effect of injection rate on particle size.

3.3.2.7 Preparation and coating of orlistat NPs

Orlistat nanoparticles were prepared by solvent exchange method as mentioned previously through direct injection of ethanolic solution into water. Briefly, orlistat was dissolved in ethanol to obtain different concentration (40 to 0.01 mM).

Afterwards, nanoparticles where prepared by directly injecting 0.5 ml of each ethanolic solution into 4.5 ml of MilliQ® water kept over a magnetic stirrer at 500 rpm. Following injection, the nanoparticle dispersion is removed immediately from the magnetic stirrer, and characterized using Malvern zeta sizer nano range ZS.

Coating of orlistat with POPC was done through nanoprecipitation technique, briefly POPC together with orlistat was dissolved in ethanol at core to coat molar ratio, of (2:1). Then NPs were prepared through injecting 0.5 ml of each ethanolic solution into 4.5 ml of water using eVol™ syringe injector.

Similarly, nanoparticles of niclosamide stearate were prepared for comparison reasons.

3.4 RESULTS AND DISCUSSION

3.4.1 Measuring the mean particle size using DLS

Figure 18 represents the particle size distribution obtained from DLS measurement of olive oil NPs, prepared using fast solvent injection of ethanolic solution into antisolvent water at concentration of 1 mM final concentration, measured in triplicates. The data shows that the size was distributed around a mean, with no visible variation between the triplicates, with a unimodal peak.

The mean particle size was 140 nm with a standard deviation of the 3 sample of ± 0.6. The size distribution has a median of 124 nm representing around 15% of the distribution, the mean of the distribution of the particle size on the other hand was 140 nm with standard deviation ± 50 nm from the mean, and polydispersity index (PDI) of 0.098. (PDI <0.3) indicating uniformity of size distribution (179). The three traces appear visually very similar, all forming a single clear peak centred around 140 nm. There is no evidence of multiple peaks, therefore the size distribution is unimodal, and it is reasonable to characterise the data using a single measured mean value(180).

The nanoprecipitation technique resulted mostly in fine size distribution in particle size, where there is no striking difference between the mean and the median of size distribution. The results here was representable for all the measurements carried out in the study, with unimodal distribution and a low PDI values (Found in Appendix). The DLS data was always compared in terms of volume, as the particle size is small (<300 nm), and the data obtained were reliable according to the guidelines of Malvern® zetasizer(160).

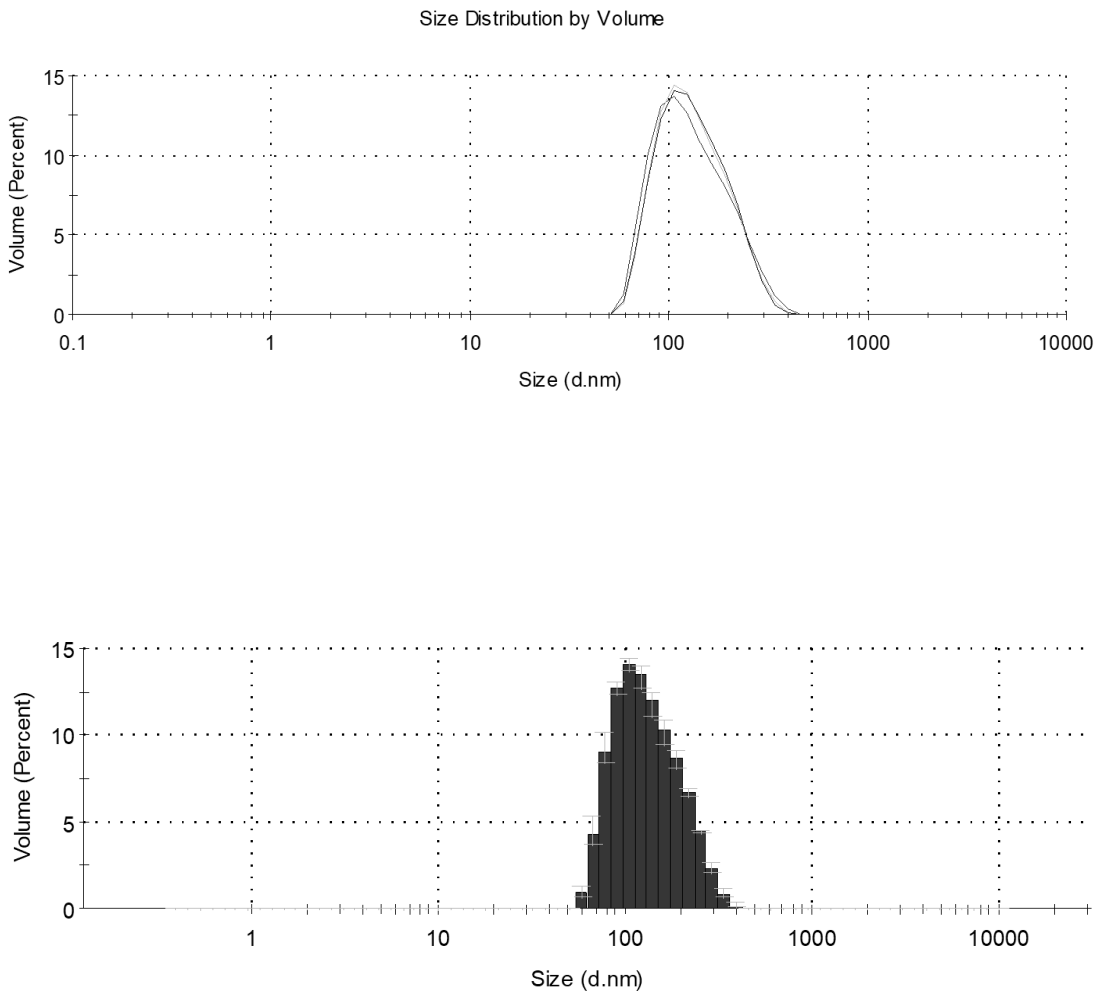

Figure 18 Particle size distribution by volume for olive oil NPs of 1 mM concentration, prepared by fast solvent injection technique.

3.4.2 Olive oil NPs: the effect of concentration over particle size

3.4.2.1 Particle size data

The effect of concentration of olive oil over particle size distribution is shown in **Figure 19**, where this plot shows the effect of concentration of olive oil in the final dispersion on volume particle size diameter measured (PSD), using a Malvern zeta sizer nanorange ZS DLS (600 nm wavelength).

The plot shows the mean particle size diameter in nanometres (y-axis), versus the concentration of the olive oil as its final dispersion concentration. The initial concentration of olive oil in

ethanolic solution is 10 times higher than the final concentration, as the particles are prepared by solvent shifting technique at a ratio of 1:9.

What the data shows is that at the lowest concentrations, the size of the nanoparticles is approximately around 20 nm. This is actually the value calculated by Critical Nucleation Theory (154).

At higher concentrations, the particles diameter starts to increase as concentration increases. The significance of this is that concentration-dependent increase in the size of the nanoparticles was due to the increase in the nucleation and growth rate as mentioned in the introduction before.

Theoretically, the predicted diameters should be decreasing at higher concentrations due to the decrease in the interfacial tension between the organic and the aqueous phase upon mixing(181), while the degree of supersaturation was expected to remain constant. However, the experimental data emphasized the increase of particle size which indicated the presence of Ostwald ripening, where small nuclei formed will redissolve and deposit on the larger ones leading to increase in particle size.

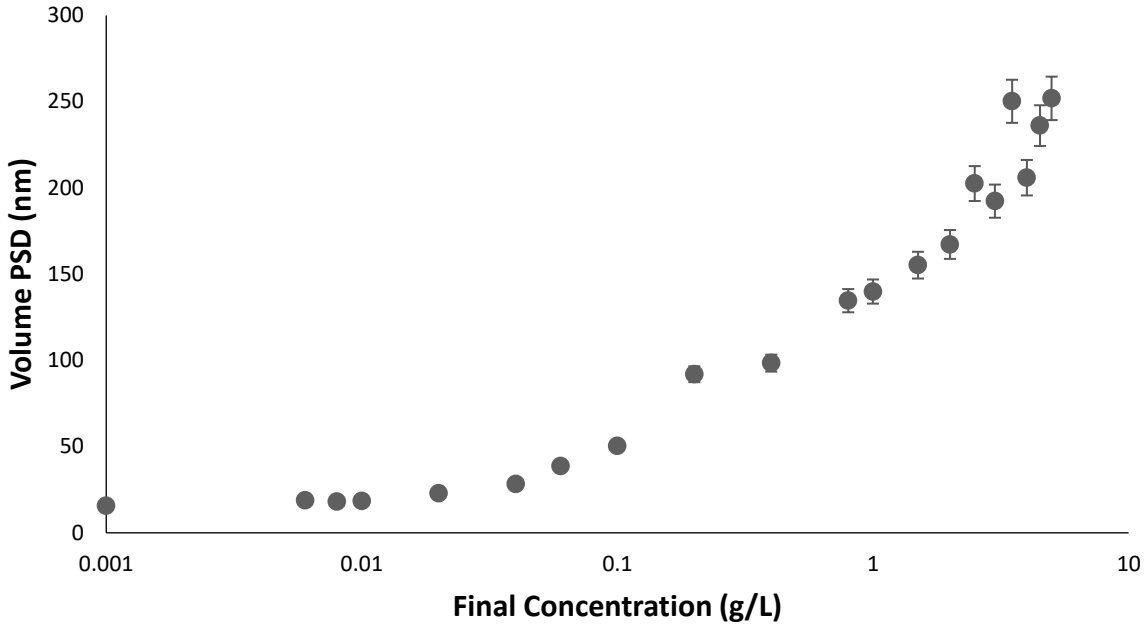

Figure 19 Volume average PSD vs final olive oil concentration injected as 1:9 (v/v) into water for a range of final concentrations of 0.001 g/L to 3.5 g/L, expressed as mean of triplicates ± SD.

3.4.2.2 Comparison to Triolein data.

Figure 20 shows a comparison of the particle size of olive oil NPs prepared by rapid solvent shift technique to that of triolein NPs measured by Prasad et al.(154).

The triolein NPs showed particle size similar to our measured data for olive oil, because olive oil is mainly composed of triolein (~70%). What these results show, is that at very low concentrations the limit size of such nanoparticles (~20 nm) is reached (**Figure 20)**. Both olive oil and Triolein nanoparticles shared a size inflection point at a concentration of around 0.2 mM, below which the particles maintained an average particle size of 20 ±5 nm. However, by increasing the concentration the particle size increases tremendously (up to 120 nm).

The reason for this trend is suggested to be that at higher concentrations, the formed nuclei during the nanoprecipitation tend to redissolve and condenses on each other resulting in particle

size growth as mentioned before. Moreover, at higher concentration, more nuclei are formed, increasing the collision between them, and leading to more particles condensation.

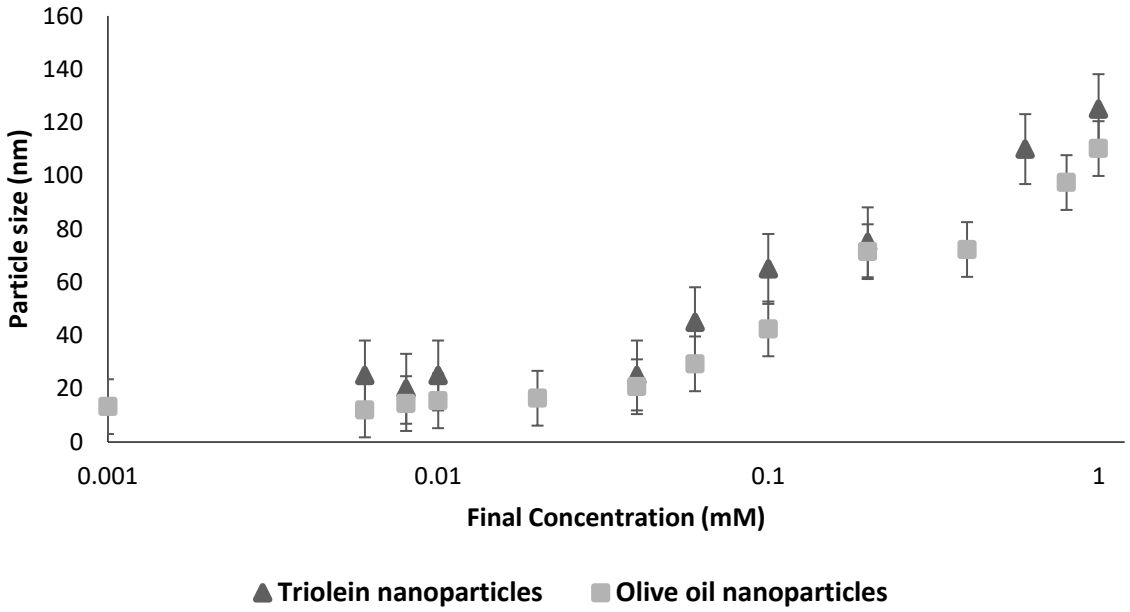

Figure 20 Comparison between olive oil and triolein NPs (Parsad et al.), in terms of volume PSD vs final oil concentration injected as 1: 9 ethanolic solution to water (v/v) for a range of initial concentrations of 0.01 mM to 10 mM, n=3 ±SD.

3.4.2.3 Effect of concentration on the number of particles

Interestingly, the number of the nanoparticles as well as the distance between them were found to be strongly dependent on the concentration of material used. The number of NPs and the distance between them could be roughly estimated calculated using the following as suggestd by David Needham research group Equation 14-Equation 16

Equation 14 $\mathbf{Volume\ of\ partcles\ (V) = \frac{4}{3}\pi r^3,\ Mass\ of\ particle\ (m) = \rho \times V}$

Equation 15 $\frac{\text{Number of particles}}{\text{ml}} = \frac{\text{Concentration}}{\text{mass of one particle}}$

Equation 16 $\mathbf{Distance\ (cm) = \left(\frac{1}{number\ of\ particles/ml}\right)^{\frac{1}{3}}}$

The actual distance between particles could futhere be determined by Nanoparticles tracking analysis, unfortunately this was not available in our study.

Figure 21 and Figure 22 show the effect of final olive oil concentration on the number of particles and distance between them respectively, prepared by the rapid solvent shift technique at different olive oil concentrations.

There is an inverse relationship between the number of particles and the distance of separation, which is logical, as when the number of particles formed increases the distance between them will decrease. But what is interesting is the trend between the concentration and the number of particles which was not linear. It was expected that increasing the concentration will definitely increase the number of NPs formed. However, it was found that at the higher olive oil concentrations there is an observed decrease in the number of particles. This could be a further indication for particle condensation mentioned, where at the higher concentration any small particles formed will redissolve and deposit on the larger nuclei, which in turns decrease the overall number of particles.This trend was observed as well for the distance between particles, where at the higher olive oil concentrations, there was an unexpected increase in the distance between the particles.

The main objective thereby is to control this particle growth and stabilising the number of formed nuclei while keeping the particle size small.

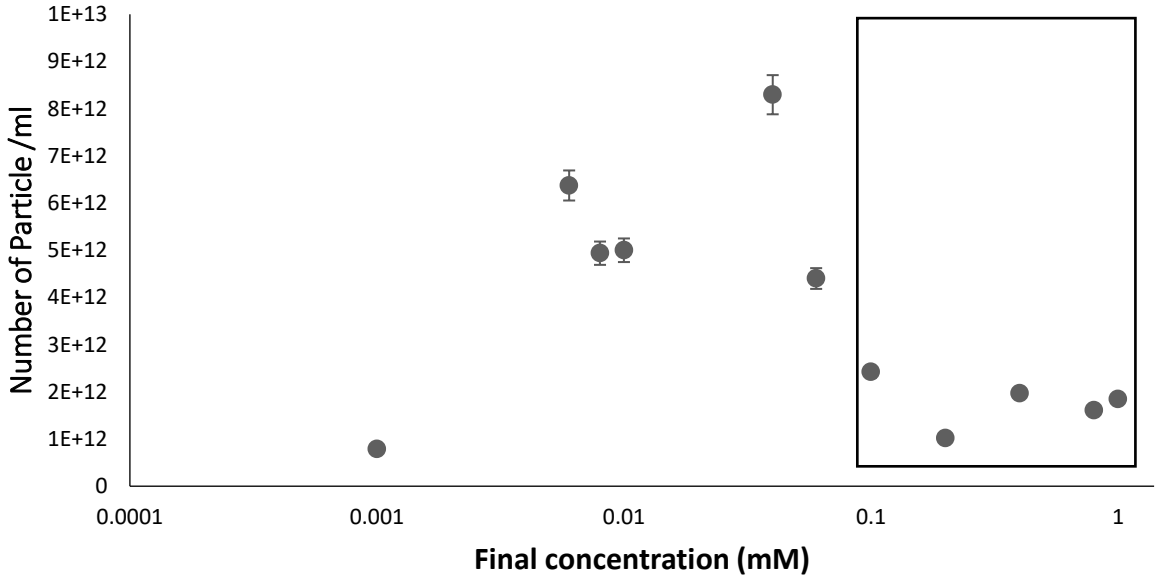

Figure 21 effect of final olive oil concentration on the estimated total number of the formed nanoparticles in dispersion prepared by direct ethanolic injection at a ratio 1:9 (v/v) in water, in a range of initial concentration of 0.01 mM to 10 mM.

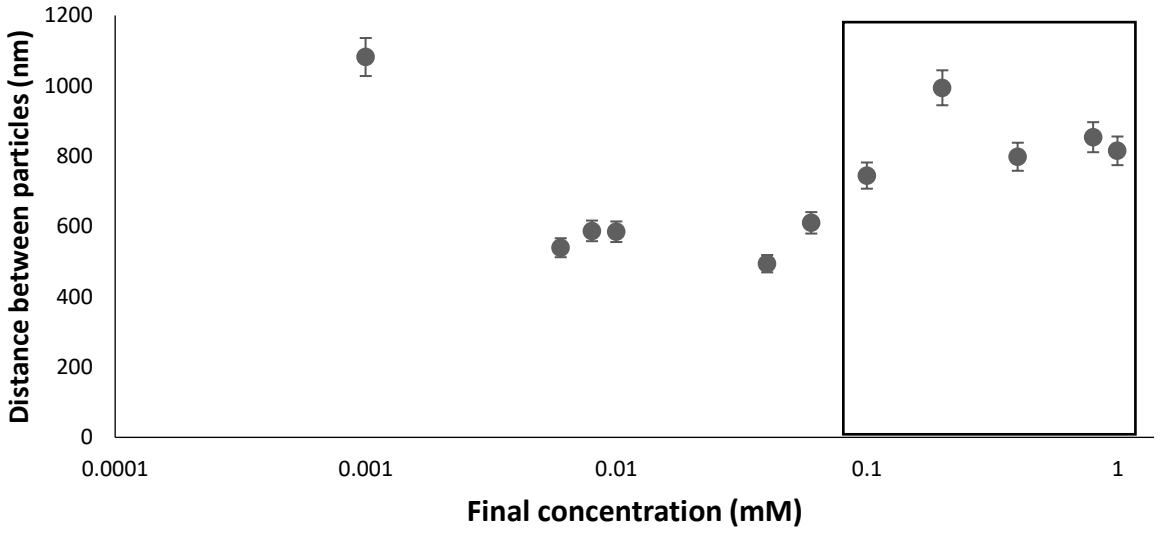

Figure 22 effect of final olive oil concentration on the estimated average distance (nm) between nanoparticles in dispersion prepared by direct ethanolic injection at a ratio 1:9 (v/v) in water, in a range of initial concentration of 0.01 mM to 10 mM.

3.4.2.4 Effect of concentration on surface charge

The results of Zeta potential measurement for both freshly prepared and aged olive oil (1 week after preparation) nanoparticles as a function of the final concentration of olive oil in dispersion are shown in **Figure 23**. Zeta potential is particularly useful to understand the surface stability of the formed NPs, where a highly negative or highly positive zeta potential will increase the repulsion between the particles and hence prevent particles aggregation during storage.

The results show an average zeta potential in the range between -80 to -30 mV with an average Zeta potential of -55 ±25 mV for all formulations, either fresh or aged. The negative zeta potential is mainly related to the content of free fatty acids found in olive oil, which are negatively charged due to the carboxylic acid groups in their structure.

On the other hand, aged nanoparticles showed a greater fluctuation in zeta potential (between -95 to -15 mV average -55 ± 35 mV) compared to the freshly prepared ones. This may be attributed to the variation in the levels of the free fatty acids that are leached from the triglycerides present in olive oil.

The zeta potential of the prepared olive oil nanoparticles showed an interestingly higher values compared to the triolein nanoparticles (**Figure 24**). For triolein nanoparticles, the reported zeta potential measurements in literature for the highest concentration (1 mM) sample in water was around -14 mV (± 2 mV), while for olive oil nanoparticles the zeta potential was -53.3 ± 12. Assuming the same value in 10% ethanol-water, the absence of any salts (providing infinite Debye length), Olive oil nanoparticles show better electrostatic stability due to higher negative charge, which could be explained by the presence of free fatty acids in the oil that act as stabilizer. This could increase the repulsion forces between the formed particles and hence avoiding the unfavourable aggregation.

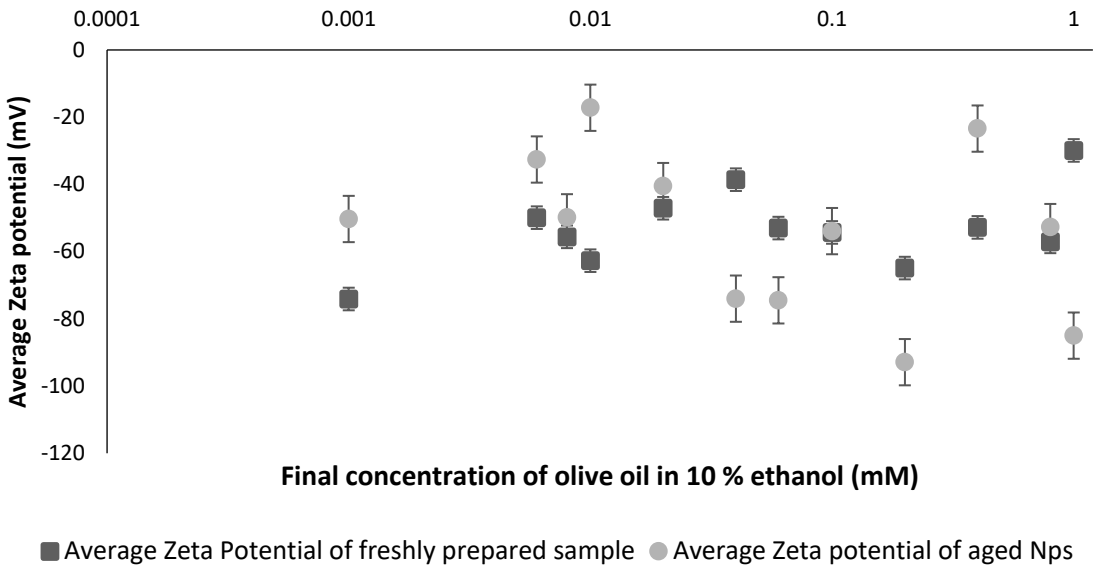

Figure 23 Comparison of Zeta potential between freshly prepared and aged (1 week after) olive oil nanoparticles, prepared by direct ethanolic injection at a ratio 1:9 (v/v) in water, in a range of initial concentration of 0.01 mM to 10 mM, n=3 ±SD.

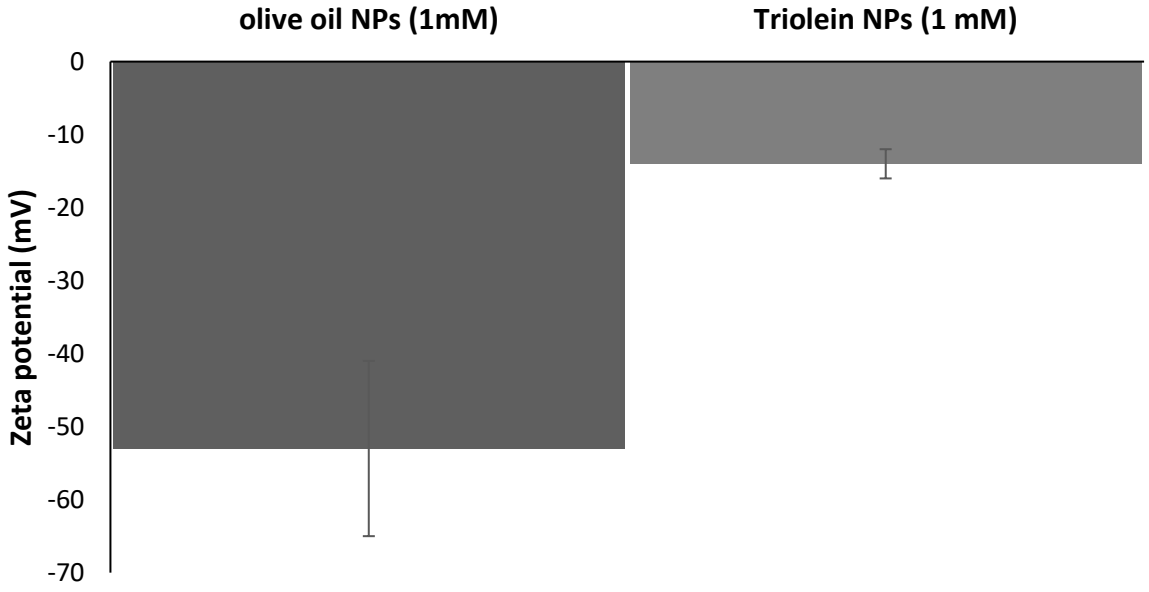

Figure 24 Zeta potential of olive oil NPs compared to triolein NPs at 1 mM final concentration. The results are shown as average of triplicate ± SD.

3.4.3 Effect of using different hydrophobic material on NPs properties.

The effect of different materials used on the particle size of the prepared NPs by solvent exchange technique was depicted in **Figure 25**. Volume PSD data of three different lipids, distinctively olive oil, tricaprin (Glyceryl tridecanoate) and trihexanoin (Glyceryl trihexanoate), prepared by solvent exchange method at different molar concentrations was compared to each other, at various molar concentrations. The aim was to find the trend of particle size growth related to different lipids, which have different fatty acid chain length (olive oil C12, Tricaprin C10 and trihexanoin C6).

All the prepared NPs showed the same trend of particle size growth with increasing concentration as previously mentioned for olive oil. The particle size was kept minimal at lower concentration till a point after which the particle size increased with increasing concentration, this concentration point is defined as the inflection point. To find the inflection point of particle growth, the data was studied using hinge function as shown in **Figure 26**. Tricaprin nanoparticles has an inflection point at slightly higher concentration (~0.06 mM) compared to that of olive oil counterparts (~0.02 mM) while Trihexanoin showed an inflection point at very low concentration limit (~0.008 mM). This could be attributed to the solubility of different lipids in the organic solvent, for instance Tricaprin has better solubility in ethanol compared to triolein(182), hence showing higher saturated solubility in ethanol. This may lead to the formation of more stable smaller nuclei with increasing concentrations during the solvent exchange, hence decreasing the chance for particle growth later. On the other hand, Trihexanoin have the shortest fatty acid chain length (C6), thus it has better aqueous solubility (0.00045 mg/ml) compared to olive oil (6.14 e^{-6} mg /ml) which may lead to solubilisation of the formed nuclei in the bulk phase resulting in particle growth by Ostwald ripening(183,184).

Figure 27 shows a comparison of average zeta potential of NPs of different lipids (olive oil, tricaprin, and trihexanoin) prepared by solvent exchange method at different final lipid

concentrations. As shown in the figure, Ticaprin and Trihexanoin nanoparticles have a less negative average zeta potential (-30 mV and -39 mV respectively) compared to that of olive oil nanoparticles (-53 mV) due to the free fatty acids content of olive oil. This negative zeta potential increases the surface stability (electrostatic stability) of the formed nanoparticles against aggregation.

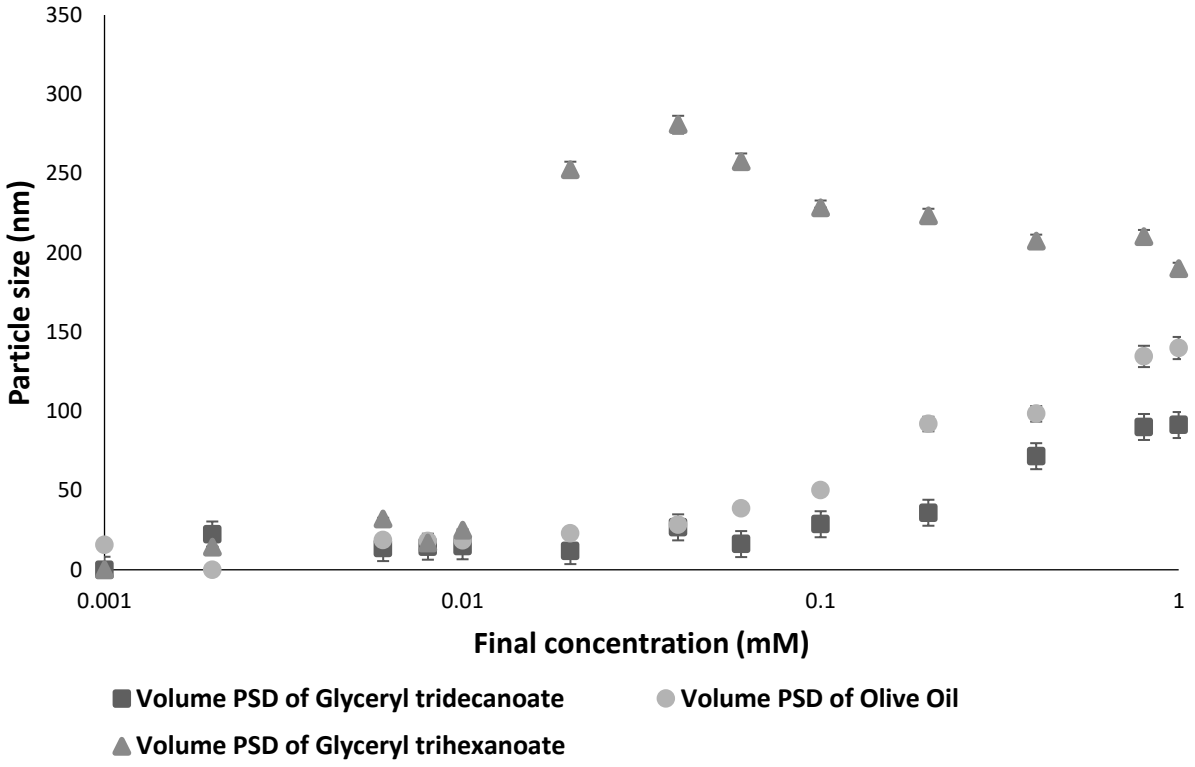

Figure 25 Comparison of the effect of final lipid concentration on the particle size growth expressed as volume PSD, for olive oil, tricaprin and trihexanoin nanoparticles, prepared by ethanolic injection in a ratio of 1:9 (v/v) in water, in an initial concentration range of lipids in ethanol of 0.01 mM to 10 mM, n=3 ±SD.

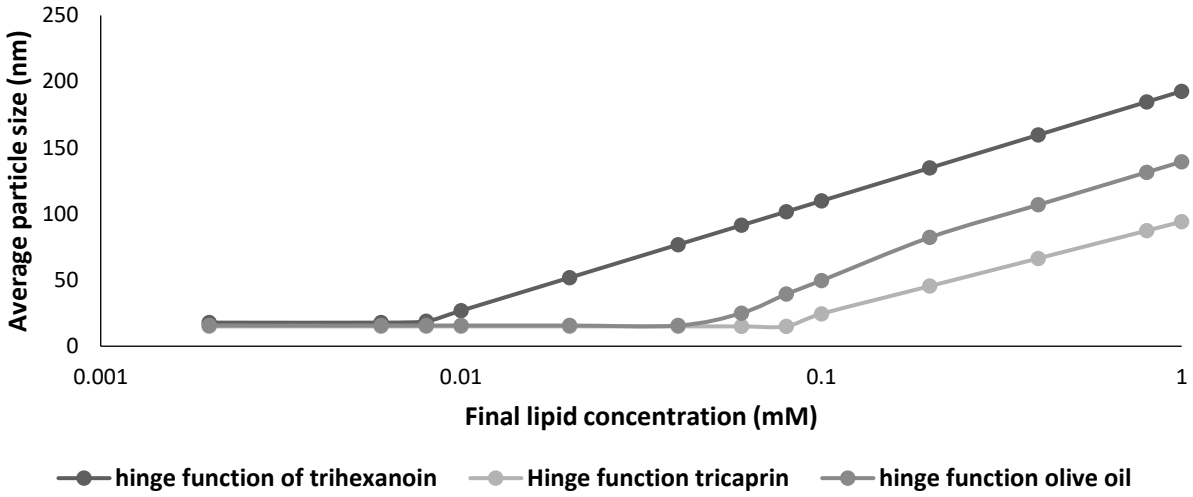

Figure 26 Comparison of the particle size growth of olive oil, tricaprin and trihexanoin nanoparticles, as normalised volume PSD.

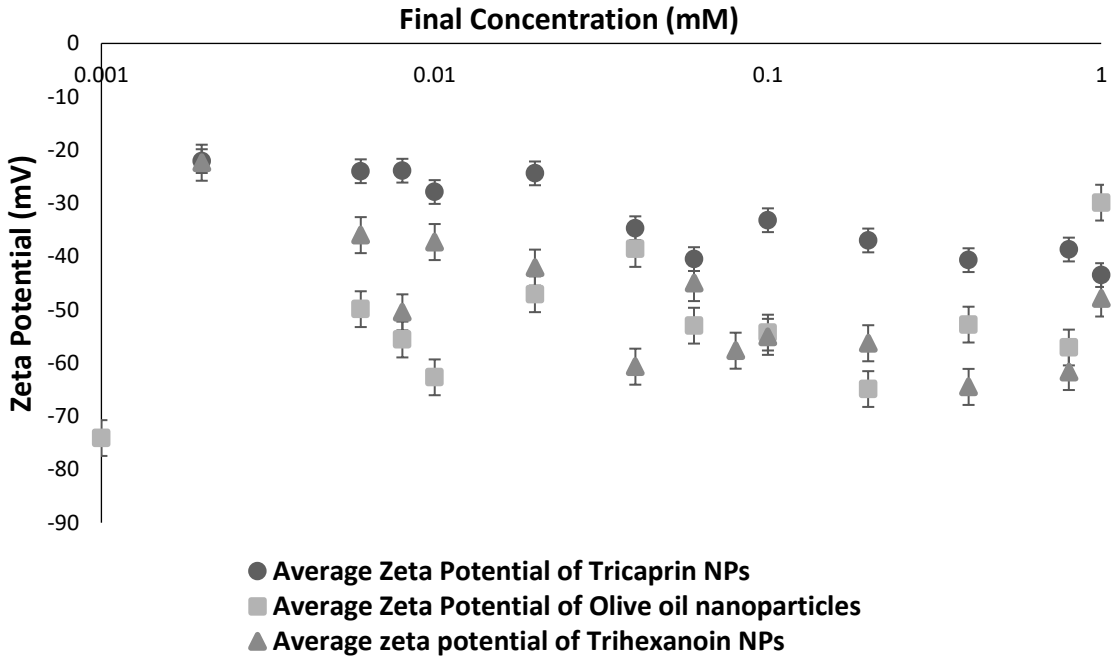

Figure 27 Comparison of zeta potential of olive oil, tricaprin and trihexanoin nanoparticles prepared by injection ethanolic solutions into water in a ratio 1:9 (v/v), at different final concentrations (0.001 to 1 mM), n=3 ±SD.

3.4.4 Effect of coating the NPs over the particle size growth

3.4.4.1 Effect of the coating material: tween 80, POPC, Lecithin.

Screening of various coating materials in various ratios was done to investigate the effect of coating of NPs on preventing the unfavourable particle size growth due to condensation of particles (**Figure 28** to **Figure 30** discussed in this section). Moreover, further investigation was done to find out the optimum concentration ratio for the best control over particle size and to ensure single coating of all the formed nanoparticles (shown in **Figure 36**, will be discussed later).

Figure 28 to **Figure 30** show the effect of coating of olive oil NPs with two different coating materials (namely POPC, Tween80), and Triolein with lecithin (due to the incompatibility between olive oil and lecithin), at three different core to coat molar ratios, 1:1, 2:1, and 4:1 respectively in the three figures. The results were expressed as a mean of three readings ± SD.

Concerning lecithin, it was utilised with triolein and was prepared in DMSO. The reason behind this is attributed to the reported incompatibility of Lecithin with the vegetable oils (185), where the solubility of lecithin is highly reduced in presence of other oils. Moreover, it is reported that Lecithin has low ethanolic solubility(186) thus was prepared in DMSO, which is considered a toxic solvent compared to ethanol(187). Although lecithin was able to help prevent particle size growth for the prepared triolein NPs, but it will not be our material of choice being problematic in mixing and dissolving.

On the other hand, tween 80 and POPC showed an enhanced control over the particle size growth of the prepared NPs, however this control was highly relatable to the employed molar core to coat ratio. As shown in the **Figure 28 to Figure 30**, it was found that the best molar ratio (core: coat) is (2:1), which was able to control the size of olive oil NPs (<~ 50 nm) even at the highest employed concentration. The proper amount of the coating material will completely coat all the formed nuclei during the nanoprecipitation and subsequently act as a

barrier for further growth. This was further emphasized in **Figure 31**, where a particle size around 50 nm was maintained even at high olive oil concentrations when coated with either POPC or tween 80 at ratio 2:1.

On the contrary, the overuse of coating material (1:1) **Figure 28** will result in formation of micelles, which appears as double peaks in DLS specially in number distribution. While using insufficient amounts of the coating material **Figure 30** (4:1) will not be enough to adequately coat all the particles and hence resulting in the undesirable particle size growth. Hence, a proper molar ratio for coating the NPs should be employed for the process; in order to maintain a good control over particle size growth.

As mentioned before (chapter 1), the choice of coating for the nanoparticles depends on its properties; essentially, it should be compatible with the materials in the core of the nanoparticles. As the materials used in this study are highly lipophilic, hence the proper coating materials should possess more lipophilic domains at their surface to interact adequately with the lipophilic core material in the NPs and ensure complete coating of the system.(188), accordingly POPC (being a phospholipid) is more preferred.

Concerning electrostatic stability, the average Zeta potential of the various coated olive oil nanoparticles (with either POPC, tween 80 or Lecithin) prepared at different molar core to coat ratios, was studied at different olive oil final concentration in dispersion, as shown in **Figure 32**. It was obvious that coated NPs at any molar ratio showed a negative zeta potential between -30 to -50 mV with an average zeta potential of -40 mV. This negative zeta potential can imply an electrostatic barrier against aggregation between the formed nanoparticles.

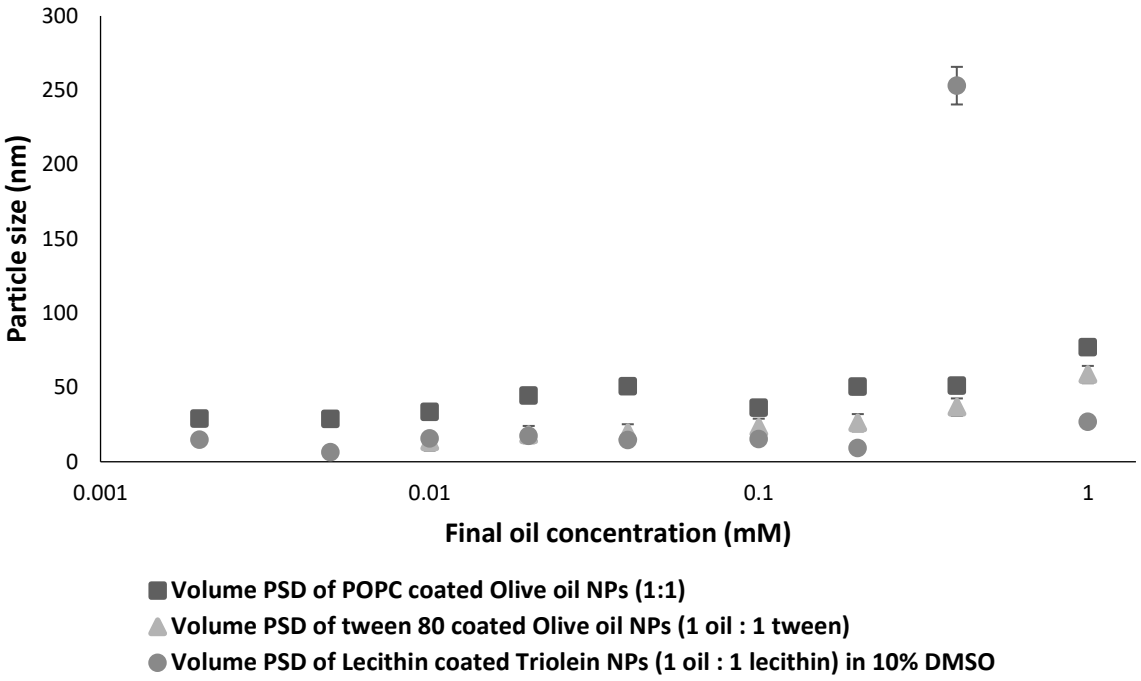

Figure 28 Comparison of average volume particle size of olive oil NPs coated with either POPC, tween 80 in 10% ethanol and Lecithin coated triolein NPs in 10% DMSO in a molar ratio (1 core:1 coat), at different final olive oil concentration (0.0025 to 1 mM), n=3 ±SD.

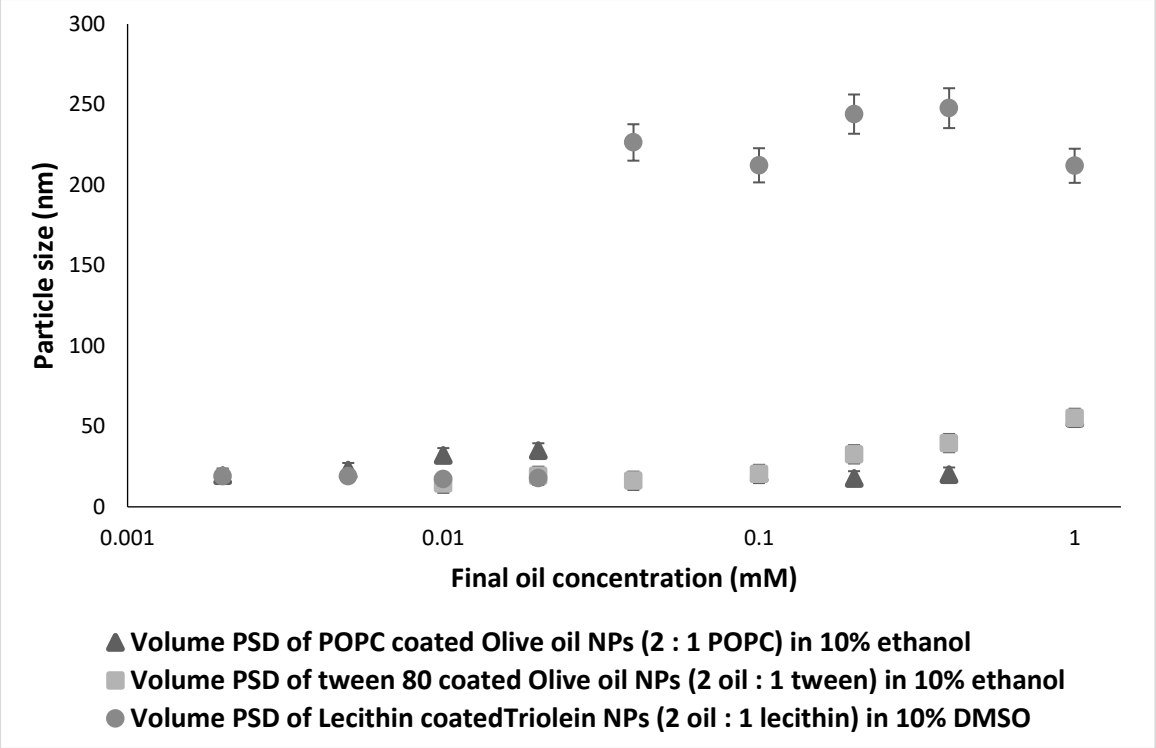

Figure 29 Comparison of average particle size by volume of olive oil NPs coated with either POPC, tween 80 in 10% ethanol and Lecithin coated triolein NPs in 10% DMSO in a molar ratio (2 core:1 coat), at different final olive oil concentration (0.0025 to 1 mM), n=3 ±SD.

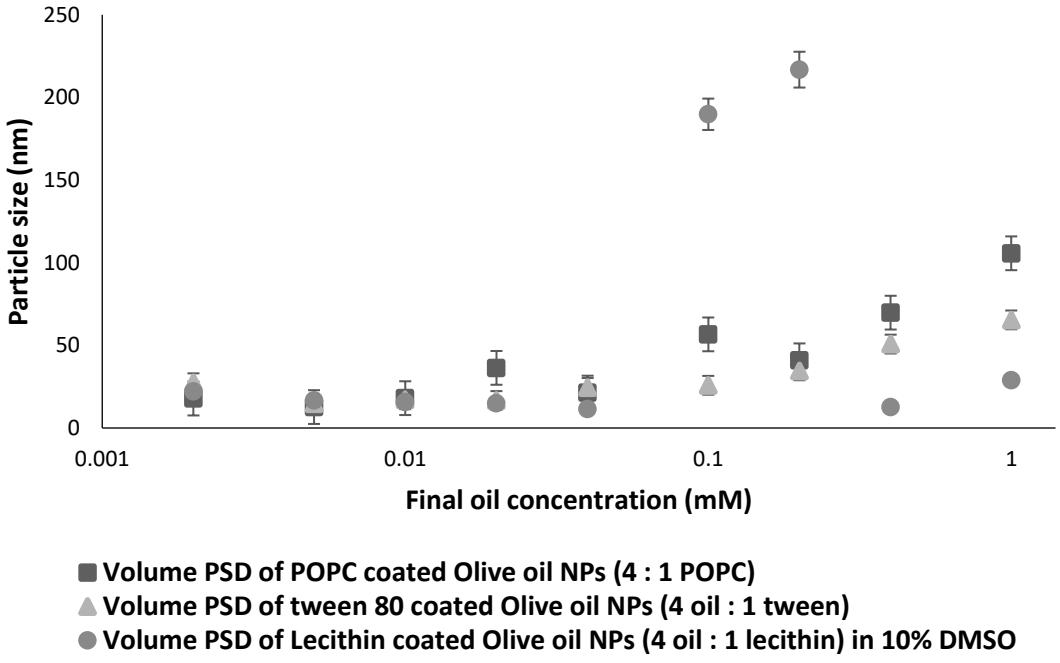

Figure 30 Comparison of average particle size by volume of olive oil NPs coated with either POPC, tween 80 in 10% ethanol and Lecithin coated triolein NPs in 10% DMSO in a molar ratio (4 core:1 coat), at different final olive oil concentration (0.0025 to 1 mM), n=3 ±SD.

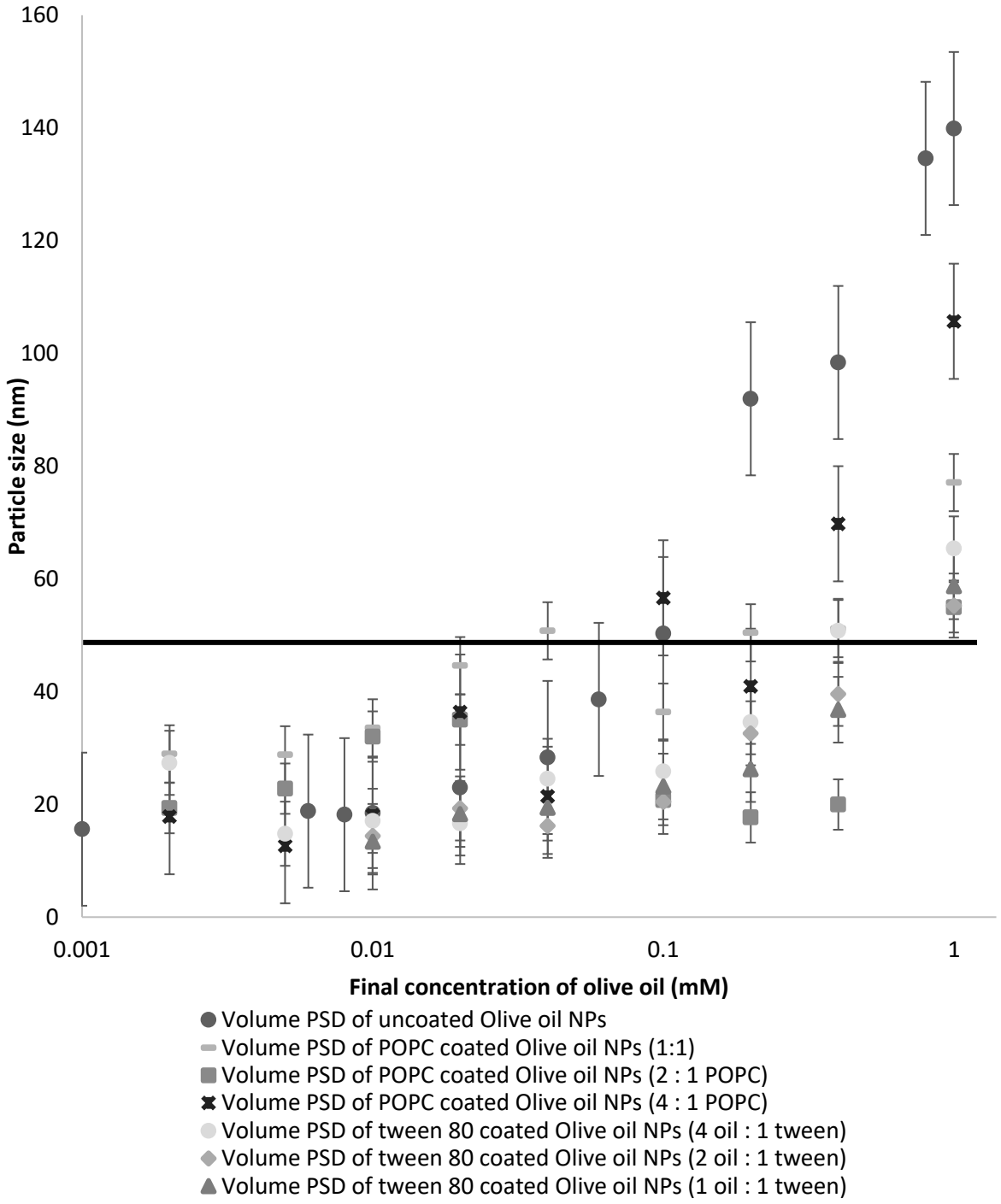

Figure 31 Comparison of average volume particle size of coated olive oil NPs with either POPC or tween 80 at different molar ratios (1:1, 2:1, and 4:1) to the uncoated olive oil nanoparticles, at different final olive oil concentration (0.0025 to 1 mM), n=3 ±SD.

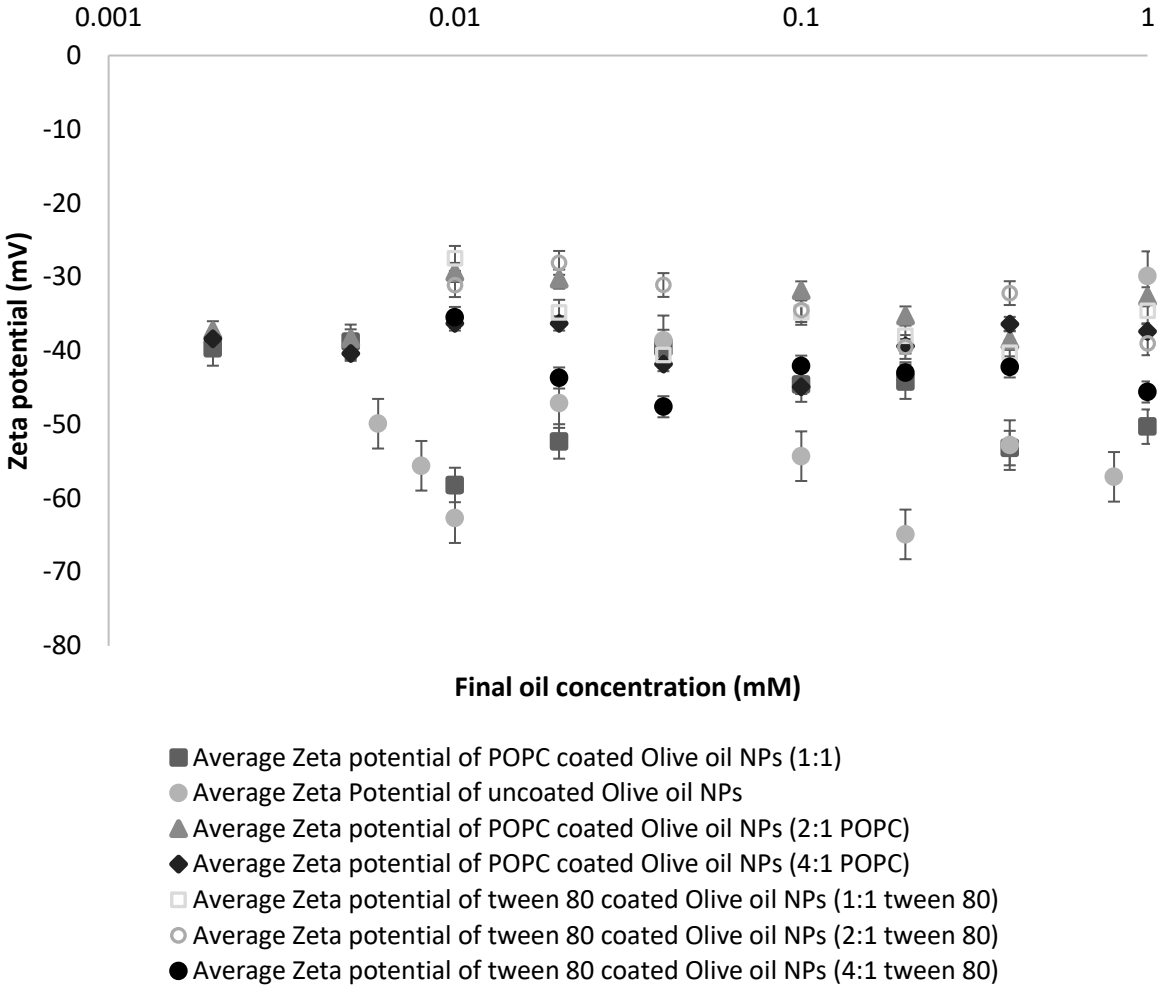

Figure 32 Comparison of zeta potential of coated olive oil NPs with either POPC or tween 80 at different molar ratios (1:1, 2:1, and 4:1) to the uncoated olive oil nanoparticles, at different final olive oil concentration (0.0025 to 1 mM), n=3 ±SD.

3.4.4.2 Evaluation of NPs using TEM

Figure 33 and Figure 34 represent the TEM images for the coated olive oil NPs with the three coating materials under investigation, namely Lecithin POPC and tween 80, in a core to coat ratio of 2:1 and in two different olive oil final dispersion concentrations, 1 and 0.1 mM respectively.

All the prepared NPs showed roughly a spherical structure. Concerning the particle size and its distribution, counting of the particles in each image was done using ImageJ® program. The particle size count asserts the results found by the DLS, with an average particle size of (~ 50,

60, 100 nm) for tween80, POPC and lecithin respectively at core concentration of 1 mM, and (~30, 35, 50 nm) at core concentration of 0.1 mM, which are similar to the results obtained by DLS as shown in **Figure 35**.

A comparison between the results obtained from the DLS to the particle size calculated from the TEM, for either POPC coated, Tween 80 coated or Lecithic coated NPs olive oil NPs in the two chosen olive oil concentrations (1 & 0.1 mM), is shown in **Figure 35**. There is no significant difference in the average particle size between the two methods for the three prepared coated NPs at any concentration. This indicate the consistency and stability of the particles, resulting in accurate measurments by the DLS that is comparable to the actual sizes seen under the microscope.

Despite this similarity, the TEM images showed some variation in the diameters of the particles, specially in case of Lecithin coated NPs. As shown in the images there are many small particles and some large particles, which could emphasise our theory of particle size condensation of the smaller particles into larger ones. This happens mainly due to the failure of the coating material to completely coat the prepared NPs, resulting in particle size growth and inconsistant size range.

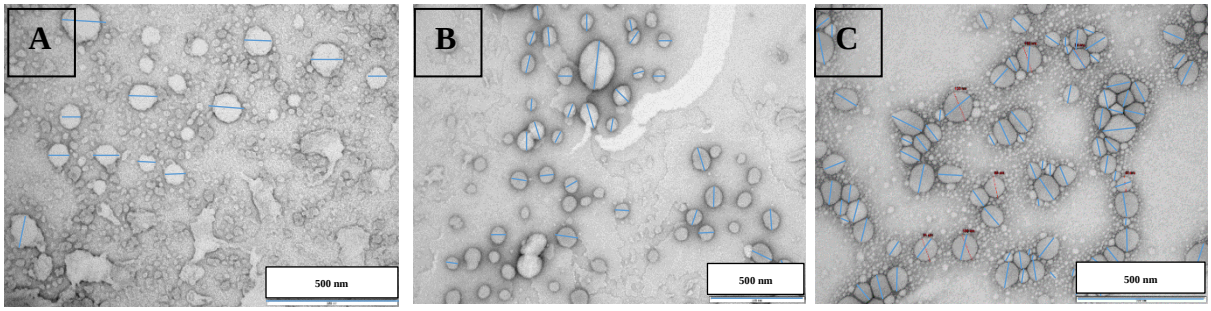

Figure 33 Comparison of TEM between Lecithin, tween80, POPC coated NPs in a ratio (2oil:1coat), and 1 mM final core oil concentration. A) Lecithin coated triolein NPS, B) POPC coated olive oil NPs, and C) Tween 80 coated olive oil NPs.

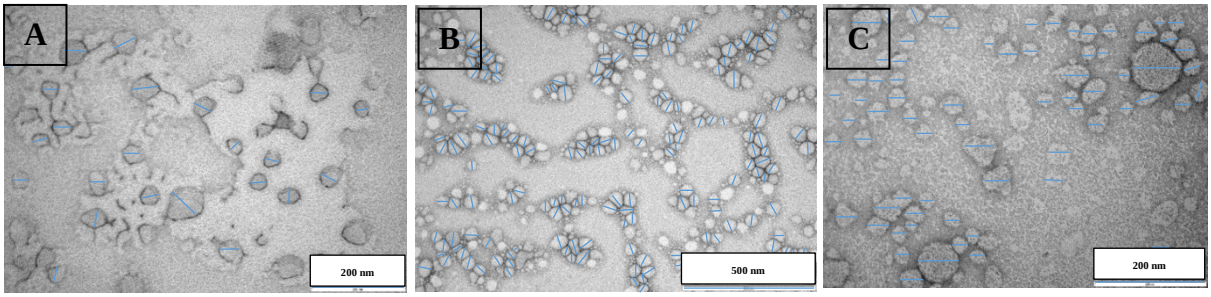

Figure 34 Comparison of TEM between Lecithin, tween80, POPC coated NPS in a ratio (2oil:1coat), 0.1 mM final core oil concentration. A) Lecithin coated triolein NPS, B) POPC coated olive oil NPs, and C) Tween 80 coated olive oil NPs.

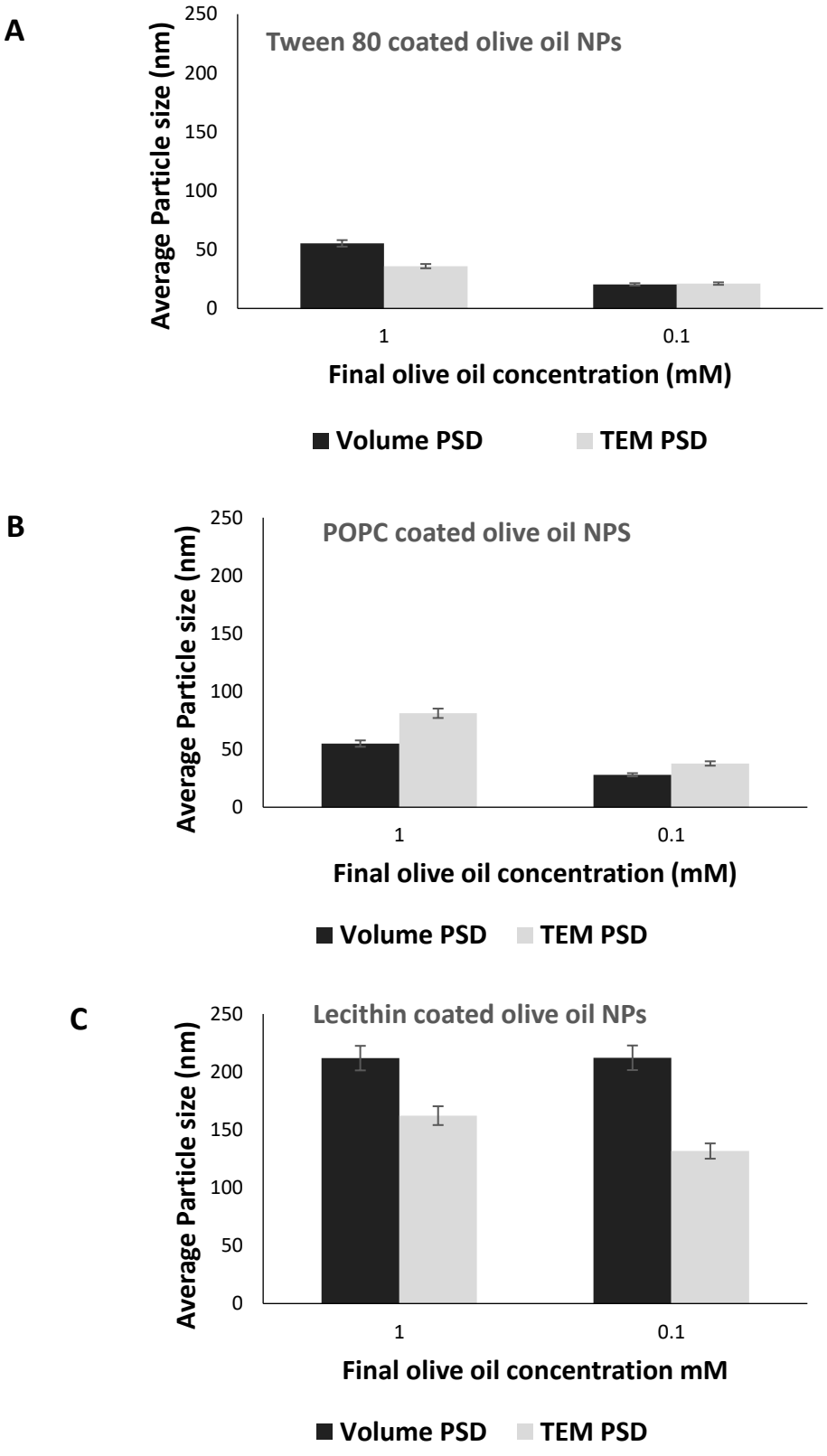

Figure 35 Comparison between average particle size (nm) of coated olive oil NPs at two different concentrations (0.1 and 1 mM) obtained by either DLS or TEM imaging for A) Tween 80 coating B) POPC coating and C) Lecithin coating, n=3 ±SD.

3.4.4.3 Effect of core to coat ratio on particle size

Figure 36 demonstrates the effect of coating olive oil NPs at various molar ratios of olive oil to tween 80 on the particle size growth (nm) prepared by rapid solvent shift technique using the piezo electric 2D printer. The experiment was done in order to precisely determine the best core to coat molar ratio to prepare NPs of controlled particle size (< 50 nm). The preparation of the NPs through rapid solvent shift technique was employed using 2D printing to save time and materials, where all the required ratios could be printed at once in less than an hour and using few nanograms of materials.

Results show the effect of different molar ratios (core: coat) over the size of the formed nanoparticles at 4 different concentrations of olive oil (0.01, 0.1, 1 and 10 mM initial concentrations, equivalent to 0.001, 0.01, 0.1 and 1 mM final concentrations respectively) after ethanolic injection in water at ratio 1:9. All data was shown as a mean of triplicate ± SD.

The screening showed that the best molar ratio to control particle size growth lies between the molar ratios of (2:3) and (3:7) (coat: core), which is equivalent to (1.5:1) and (2.3:1) (core: coat) respectively, if we take an average it will be 2:1 as previously mentioned. As shown, those ratios ensured controlled size of the formed particles (~<50 nm) at all olive oil concentrations. The reason for this is the complete coating of olive oil during the nanoprecipitation with no excess micelles formation.

Additionally, different core to coat ratios for POPC coated olive oil NPS were investigated to emphasize the previous results. **Figure 37** illustrates the effect of three olive oil to POPC ratios (1:1, 2:1 and 4:1) at range of olive oil concentrations (from 0.001 to 1 mM), and the effect on particle size of the prepared NPs by rapid solvent shift technique.

As shown in **Figure 37**, both 1:1 and 4:1 ratios resulted in poor control over particle size growth compared to the 2:1 ratio, especially at higher olive oil concentrations.

The excess use of coating material (1:1) will result in formation of micelles of larger particle size, while using insufficient amounts of the coating material (4:1) will not be enough to adequately coat all the particles as mentioned before.

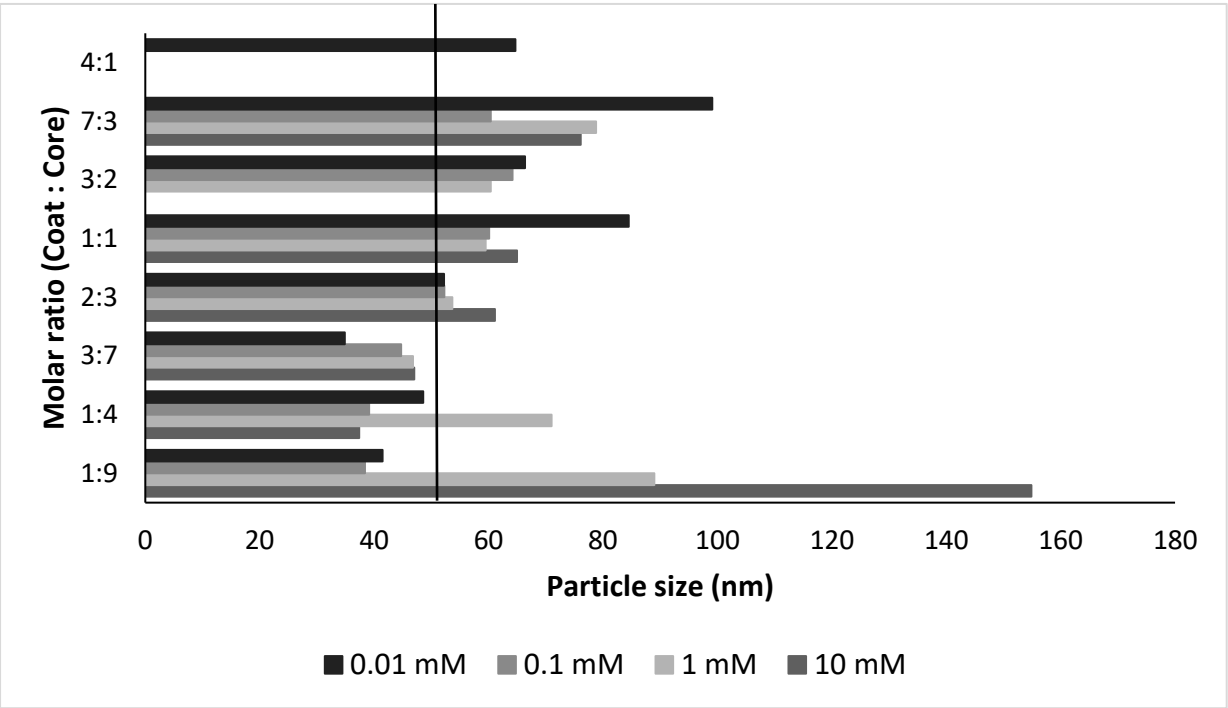

Figure 36 2D printed tween80 coated olive oil NPs in different molar ratios, printing was done through dispensing ethanolic solutions into anti solvent water at ratio 1:9, n=3 ±SD.

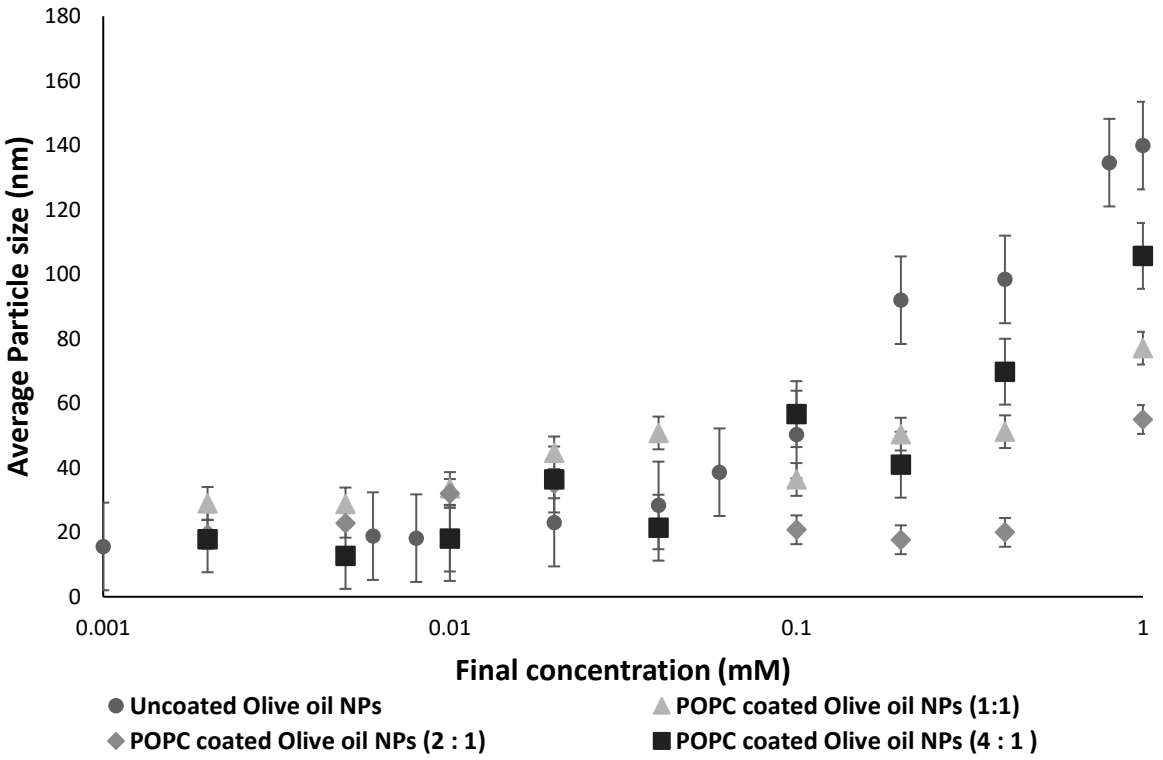

Figure 37 investigating the core: core ratio for POPC coated olive oil NPs at different olive oil concentrations prepared by rapid solvent shift technique from ethanolic solution in water (1:9), n=3 ±SD.

3.4.5 Effect of the rate of nanoprecipitation on particle size

Figure 38 presents the mean NPs diameter from DLS measurements for the "fast" and "slow" injections of the ethanolic olive oil solution into water (the anti-solvent) for the two chosen final concentrations of olive oil (0.1 and 1 mM). Comparing injection rates, the measured mean diameter of the olive oil NPs produced is visibly larger when "slow" injection is employed compared to "fast" injection. For the 0.1 mM final concentration the difference is approximately three-fold (ca. 150 vs 50 nm) and for the 1 mM final concentration the difference is almost two-fold (ca. 240 vs 140 nm, both slow vs fast respectively). The lower concentration of 0.1 mM produces smaller NPs than the higher concentration of 1 mM for equal injection rates (e.g., 150 vs 240 nm for "slow"; and 50 vs 140 nm for "fast" respectively).

"Fast" injection producing smaller particles compared to "slow" injection in anti-solvent precipitation has been reported before multiple times in the literature, particularly for poorly

soluble drug molecules(189). This effect has been ascribed to “fast injection” , and result in reducing the time available for solvent/anti-solvent mixing compared to slow injection, thereby reducing the time available for particle growth, and consequently smaller particles are produced for “fast” injection compared to “slow”(190). While much of the literature focusses on poorly soluble drugs whereas the present study investigates olive oil (which is a liquid at room temperature and therefore forms nano-droplets rather than solid particles), however the underlying processes during anti-solvent injection are expected to be essentially the same.

The differences in final particle size which arise from the two different final concentrations of olive oil (higher concentration producing larger particles) is however contrary to a body of relevant literature(190). It has been reported that higher concentrations tend to produce higher super-saturations than lower concentrations which leads to a higher nucleation rate, more nuclei being formed, and the resulting particles formed immediately upon injection being smaller(190). However, with olive oil the higher concentrations clearly lead to larger rather than smaller droplets being produced. This phenomenon has been observed before with artemisin and was ascribed to condensation of particles (which is also favored by high concentrations) dominating over the initial nucleation events. It seems reasonable that this also happens with olive oil being injected into water, olive oil droplets are likely to coalesce very readily, and the formation of large droplets at high concentrations is therefore suggested to be due to a strong coalescence of small droplets into larger subsequent to the initial nucleation of the olive oil droplets in the anti-solvent.

TEM imaging as shown in **Figure 39** emphasised the results of DLS (Appendix) showing smaller spherical particles for either POPC or tween 80 coated NPs (average size 55 nm and .35 nm respectively) prepared by the fast injection compared to the slow injection technique (average size 210nm and 150 nm respectively) as counted by ImageJ®.

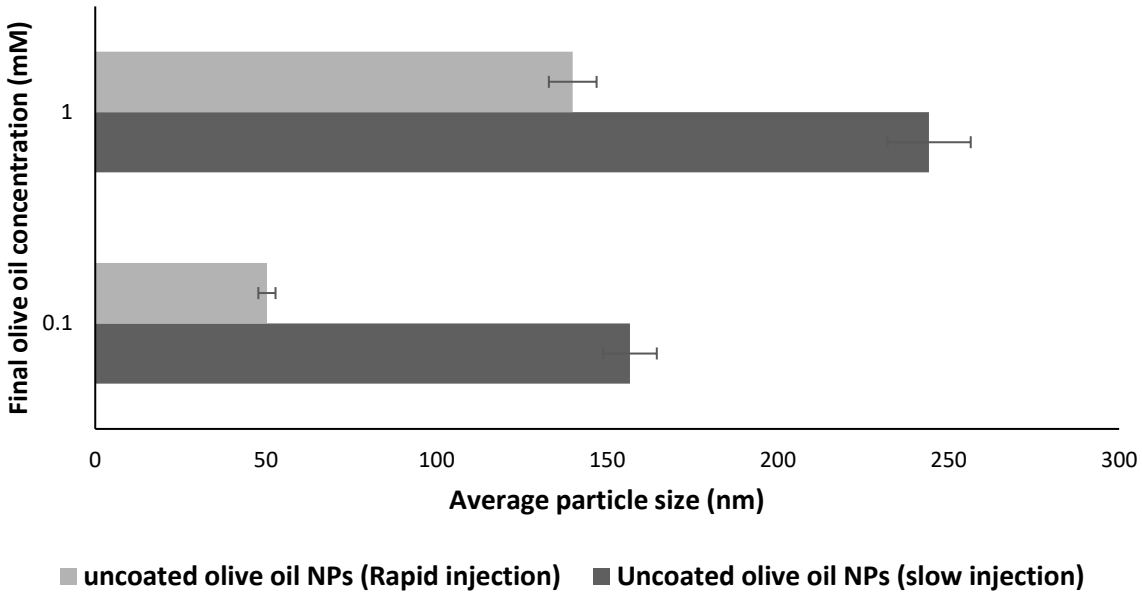

Figure 38 Effect of injection rate on particle size of uncoated olive oil NPs, using ethanolic injection into water in a ratio (1:9).

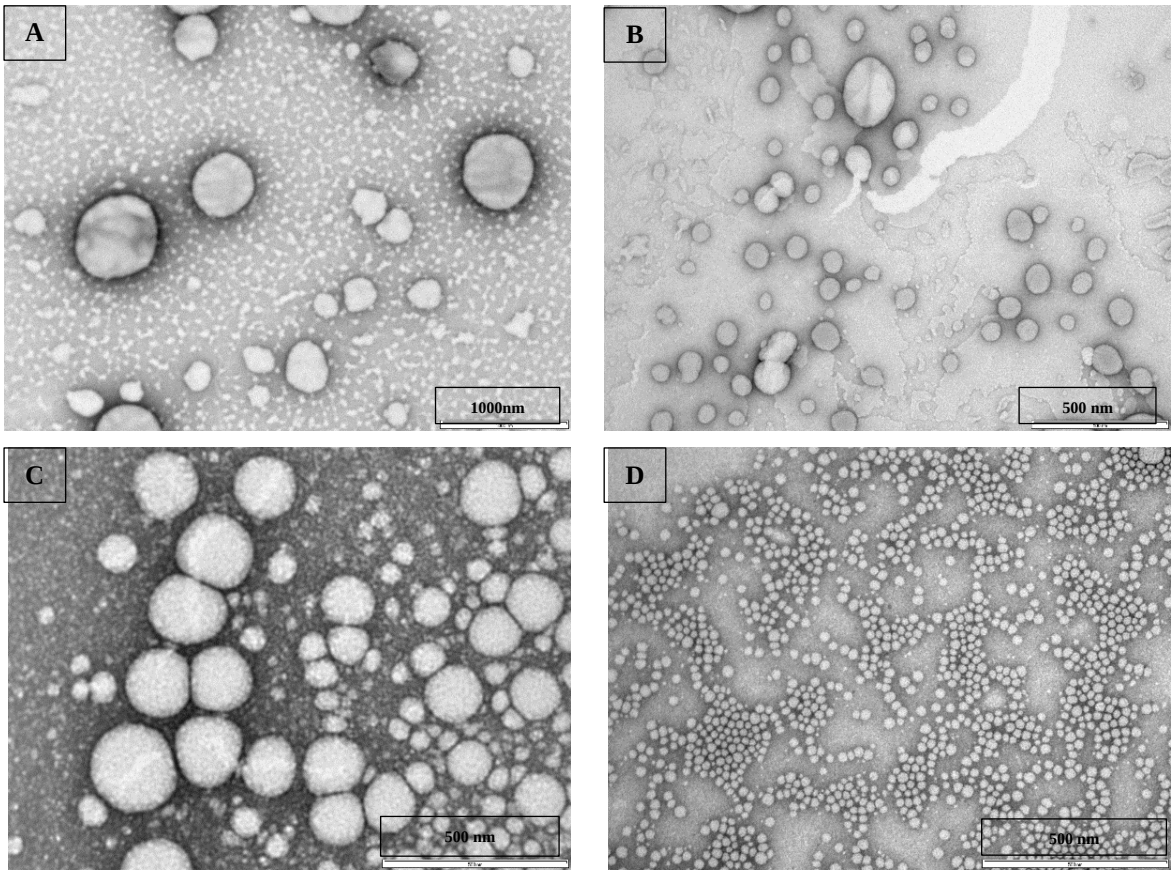

Figure 39 TEM imaging coated olive oil NPs prepared by either slow or rapid ethanolic injection (1:9) with core to coat ratio 2:1 and olive oil concentration of 1 mM final concentration, A) POPC coated NPs slow injection, B) POPC coated NPs rapid injection, C) Tween80 coated NPs slow injection and D) Tween80 coated NPs rapid injection.

3.4.6 Orlistat nanoparticles

3.4.6.1 Concentration vs particle size analysis and surface charge

Orlistat, a highly hydrophobic drug (Log P= 8.11) with an incredibly low water solubility ($9.19e^{-05}$ mg/mL), is expected to be a suitable candidate drug for rapid solvent technique, sharing an extremely low water solubility like olive oil ($6.14\ e^{-06}$mg/ml). Hence, we expect orlistat to share a similar overall behaviour of particle size growth to that of olive oil NPs during the rapid solvent shift with increasing concentration. Furthermore, orlistat is expected to form nucleates in the form of size limited nanoparticles, as it was observed in case of olive oil. These nucleates can get kinetically trapped to form lipid-coated nanoparticles(104). However, unlike olive oil, orlistat being solid at room temperature, there was a possibility of the relatively higher tendency of orlistat nanoparticle growth(151). In such scenario, it was interesting first to study the uncoated nanoparticles and then fabricate lipid-coated nanoparticles.

Figure 40 illustrates the effect of orlistat final concentration over the particle size distribution following rapid solvent shift technique. This plot shows the effect of concentration of orlistat in the final dispersion on volume particle size diameter measured (PSD), using a Malvern zeta sizer nanorange ZS DLS (600 nm wavelength).

As expected, Orlistat shares the same particle size growth behaviour described before for all the hydrophobic materials, where the particle size was stable at lower concentrations till an inflection point, after which the size increases with increasing concentrations. The inflection point for Orlistat NPs was found to be around 0.1 mM. However, results show that orlistat forms NPs of average large particle size even with the smaller concentrations employed (>50nm). The solid nature of orlistat is considered the main factor here that favours the growth of particles during the nanoprecipitation.

Figure 41 shows the TEM of uncoated orlistat NPs at 4 different concentrations, prepared by rapid solvent technique. The prepared NPs were spherical in shape and consistent in size at all

employed concentrations. Moreover, particle size measurement from TEM images agrees with that obtained from DLS. It was found that larger particles are formed (with average particle size of ~70 to 80 nm) for the higher concentrations (4, 3 and 2 mM), compared to relatively smaller particles (average particle size ~ 40 to 50 nm) for (1, 0.1 mM) concentrations respectively.

Concerning surface charge, **Figure 42** shows the average zeta potential (mV) for uncoated orlistat NPs at various orlistat final concentration in dispersion, prepared by rapid solvent shift technique. Uncoated orlistat NPs showed an average Zeta potential of (-40 mV) with a Zeta Potential range between (-17 to -51 mV). The negative Zeta potential for the formed orlistat NPs suggests a high surface stability against aggregation.

As mentioned before, this particle size growth should be controlled to prepare NPs of optimised properties (<50nm). Thus, further investigation of the coating effect on the particle size growth of orlistat NPs is required.

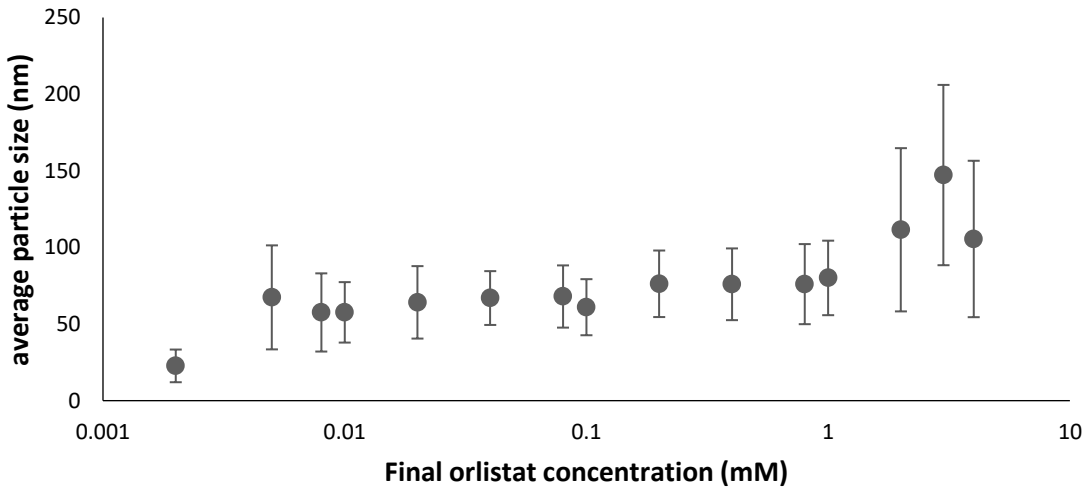

Figure 40 Effect of increasing concentration on volume average particle size for orlistat NPs injected as 1:9 (v/v) into water for a range of initial concentrations of 0.025 mM to 40 mM, n=3 ±SD.

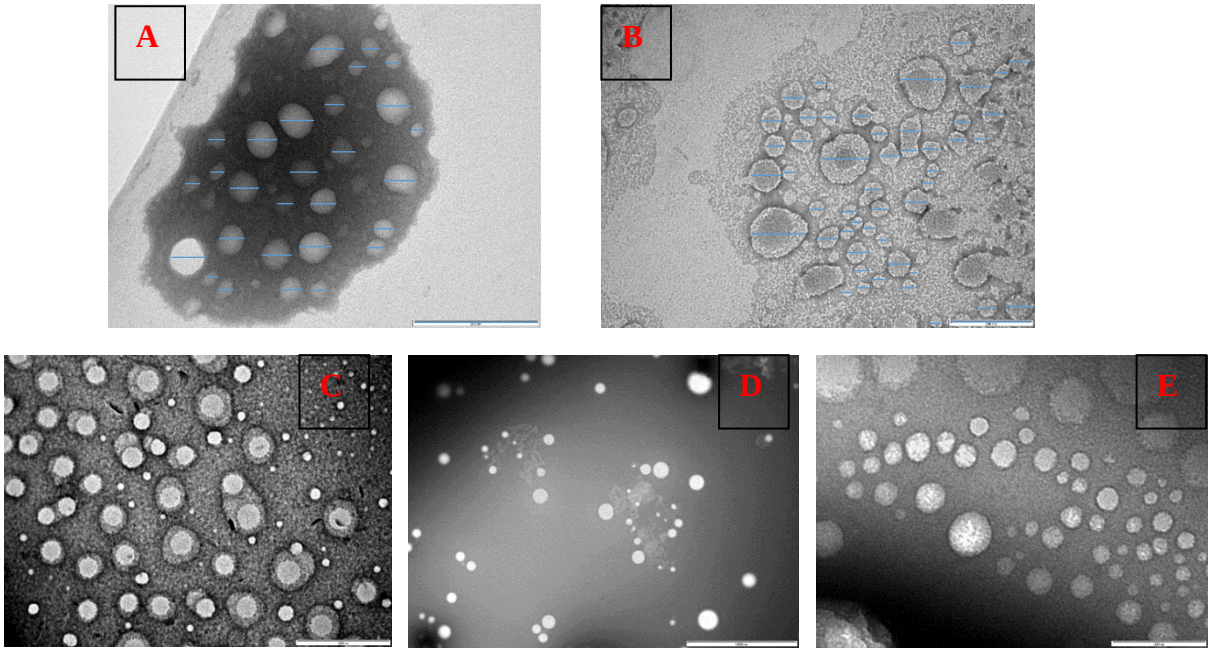

Figure 41 TEM images of uncoated orlistat NPs at different molar concentrations, A) 1mM, B) 0.1 mM, C) 2 mM, D) 3 mM, and E) 4 mM)

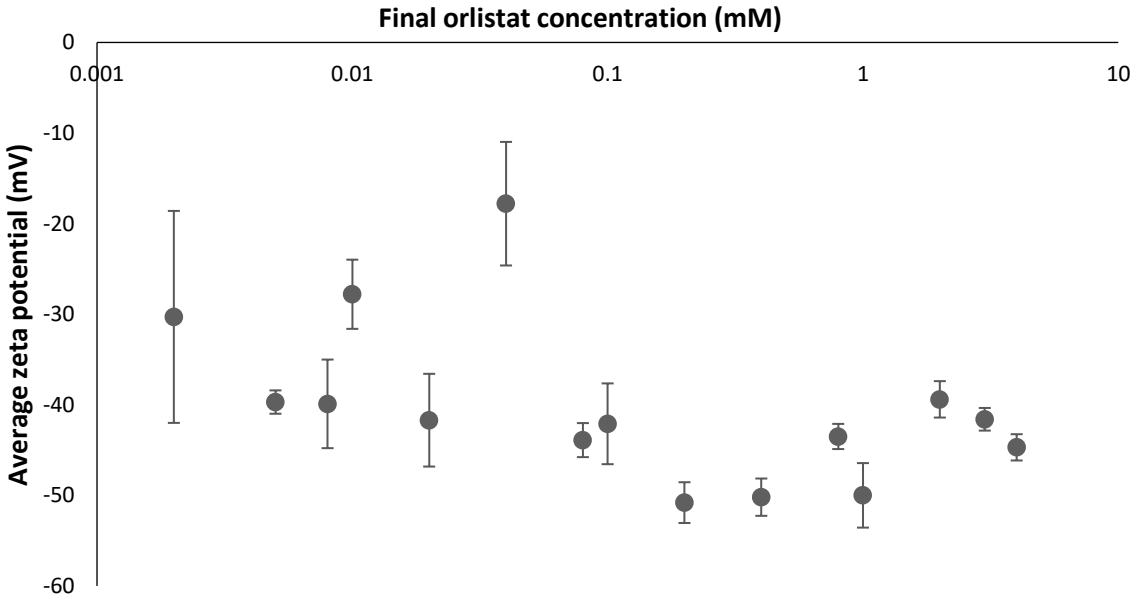

Figure 42 zeta potential of orlistat NPs injected as 1:9 (v/v) into water for a range of initial concentrations of 0.025 mM to 40 mM, shown as average of 3 readings ±SD.

3.4.6.2 Coating of Orlistat NPs

Coating of orlistat NPs with POPC to counteract growth and control particle size was investigated. **Figure 43** shows the particle size of POPC coated orlistat NPs (at core to coat

ratio 2:1) compared to that of uncoated orlistat NPs, at various orlistat final concentration, prepared by rapid solvent shift technique.

As mentioned before, coating the particles is expected to provide a protective shield that prevents ripening of the formed nuclei, and controls the particle size. For POPC coated orlistat NPs at a ratio of (2:1) (core: coat), the particle size was kept at a controlled stable range of an average (~ 30 nm) even at the highest employed orlistat concentration, unlike the larger particles of uncoated orlistat (~70 nm).

TEM imaging was carried out to have a better insight on the structure of the POPC coated orlistat NPs. **Figure 44** shows the TEM images of POPC coated orlistat NPs at 5 different concentrations (4, 3, 2, 1, and 0.1 mM). Results of TEM imaging showed that even at the highest orlistat concentration (4 mM), the average counted particle size was approximately ~ 30 nm, which is comparable to that of lower orlistat concentration (0.1 mM, ~25nm), indicating the efficacy of coating the orlistat NPs in controlling the particle size against undesirable growth.

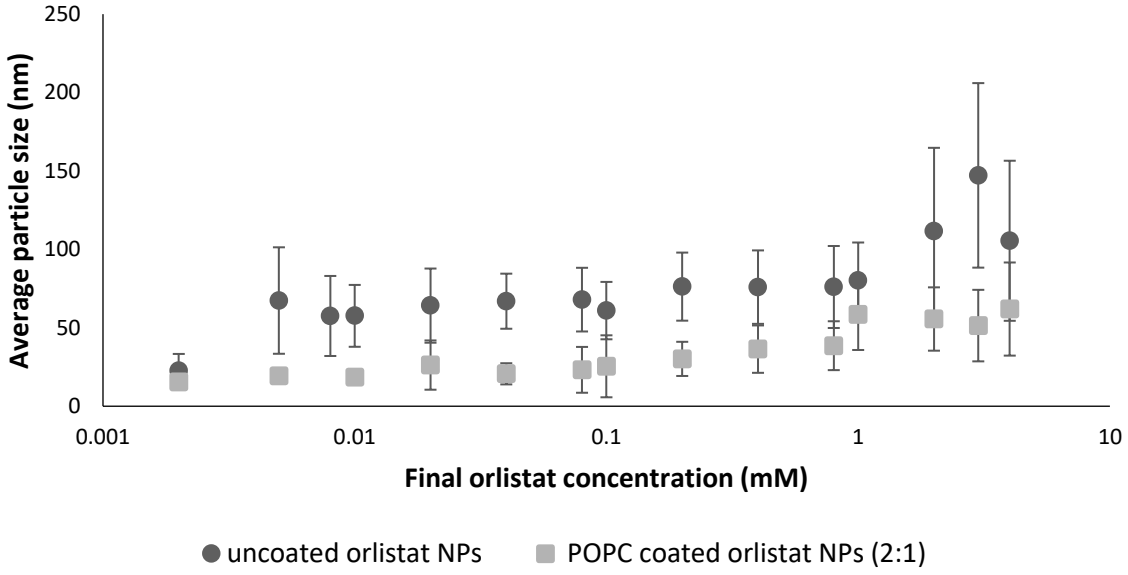

Figure 43 effect of POPC coating of orlistat NPs on the average volume particle size in a molar ratio (2 core: 1 coat), injected as 1:9 (v/v) into water for a range of initial orlistat concentrations of 0.025 mM to 40 mM, n=3 ±SD.

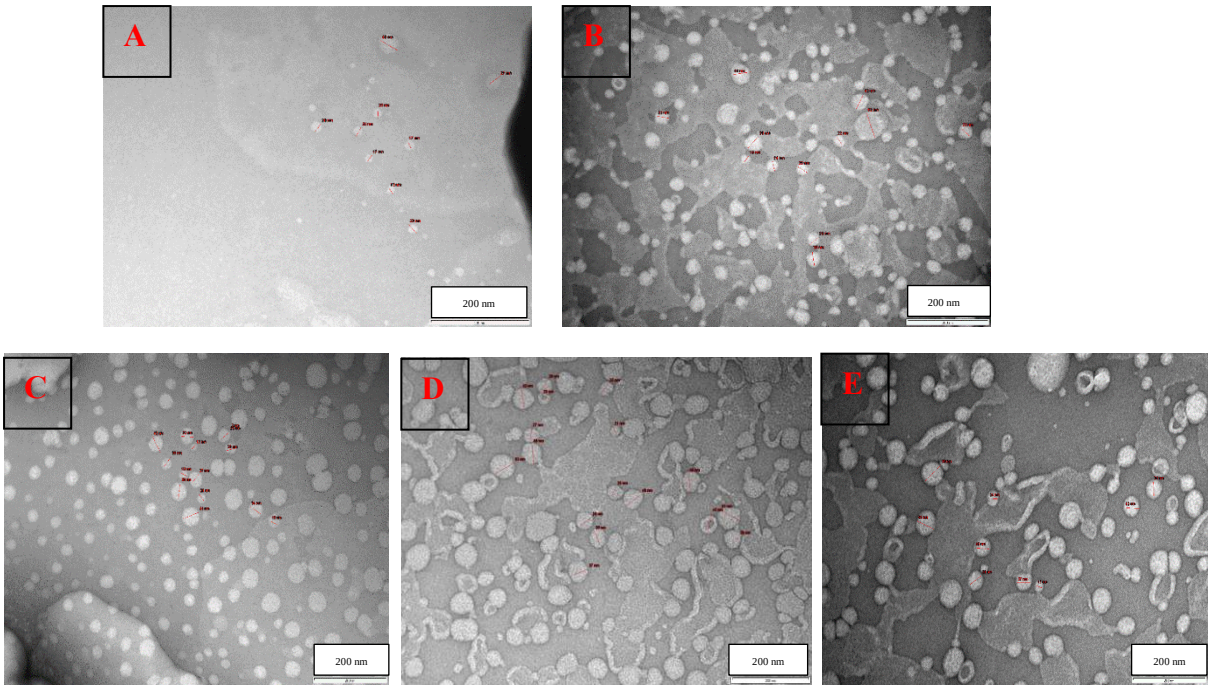

Figure 44 TEM images of POPC coated orlistat NPs (2:1, core: coat) at different final orlistat concentrations, A) 0.1 mM, B) 1 mM, C) 2 mM, D) 3 mM, and E) 4 mM)

3.4.6.3 Number of particles

The variation in the number of particle and distance between them (calculated as mentioned before for olive oil NPs) for both uncoated and POPC coated orlistat nanoparticles against the final orlistat concentration in dispersion is shown in **Figure 45 and Figure 46** respectively. As mentioned before there is an inverse relation between the number of particles in dispersion and the distance between them. Interestingly, POPC coated NPs (2:1, core: coat) showed an increase in the number of particles compared to the uncoated particles. This could be attributed to the larger number of stable nuclei formed during the nanoprecipitation, which are kept at smaller size. The reason behind this is the presence of the protective single layered coat of POPC that act as a shield, preventing the particles condensation and size growth. This increase in the number of particles would decrease the distance between the formed NPs, this could increase the chance of aggregation of particles with time. However, thanks to the negative zeta potential, surface repulsion is expected to prevent any further aggregation and size growth.

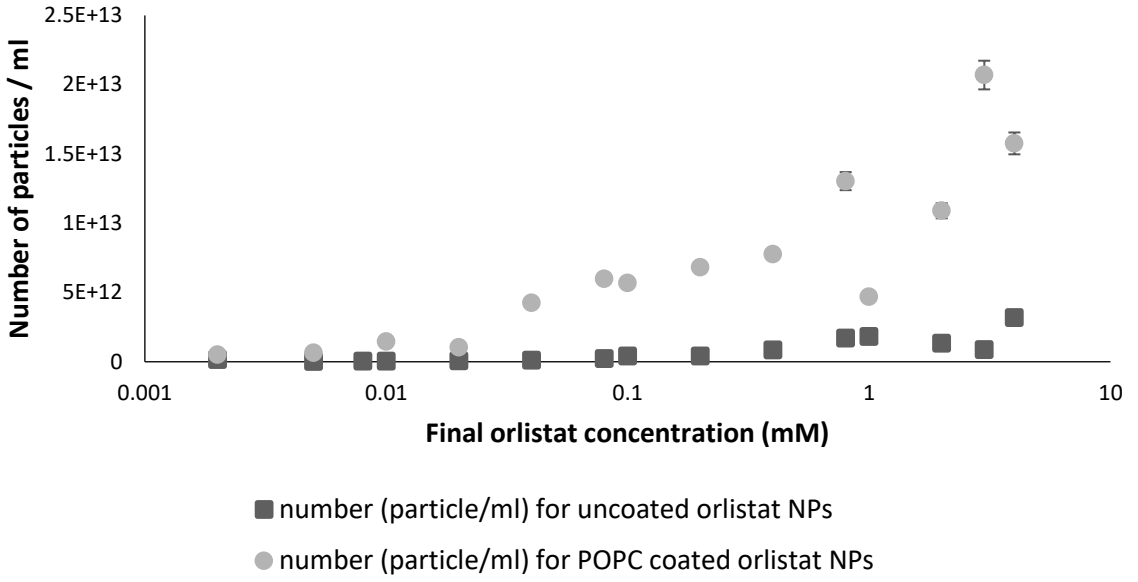

Figure 45 effect of final dispersion concentration on the total number of particles in dispersion for the uncoated orlistat NPs vs the POPC coated orlistat NPs (2:1, core: coat), prepared by direct ethanolic injection at a ratio 1:9 (v/v) in water, in a range of initial orlistat concentration of 0.025 mM to 40 mM.

.

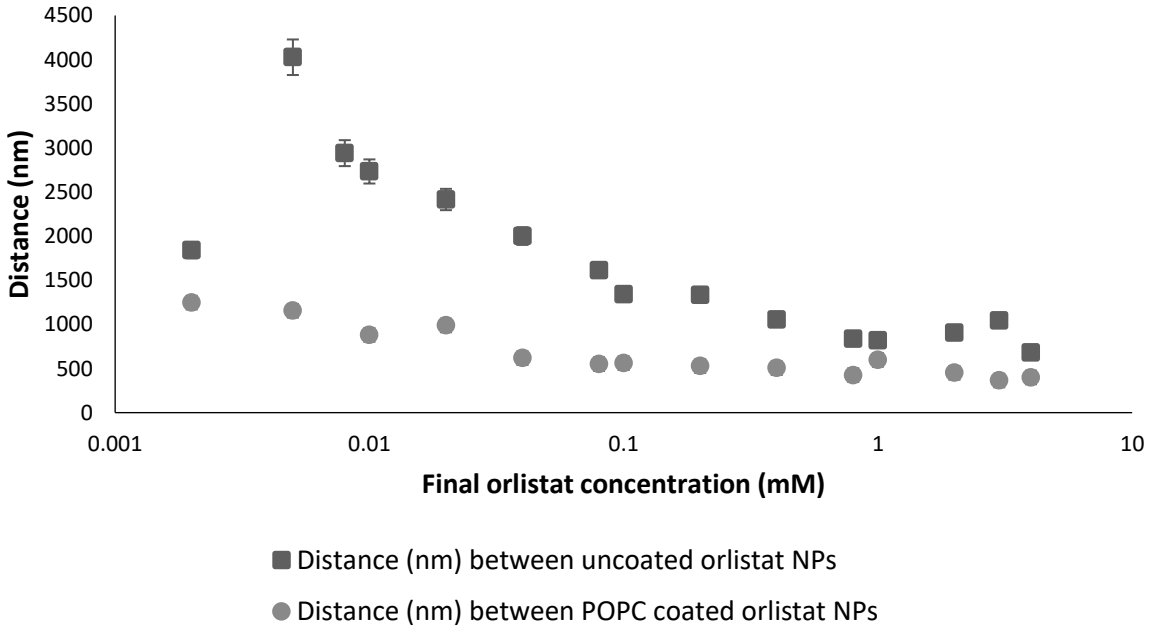

Figure 46 effect of final dispersion concentration on the average distance (nm) between uncoated and POPC coated orlistat NPs in dispersion for the uncoated orlistat NPs vs the POPC coated orlistat NPs (2:1, core: coat), prepared by direct ethanolic injection at a ratio 1:9 (v/v) in water, in a range of initial orlistat concentration of 0.025 mM to 40 mM.

3.4.6.4 Comparison of orlistat NPs to other drugs (niclosamide stearate NPs)

Niclosamide is an anti-parasitic drug that is widely used for treatment of various GIT worm infection. Recently, it was found that it has an effective anticancer activity against many types of tumours(191). This could be due to its mechanism of action, where it can result in uncoupling of oxidative phosphorylation in cancerous cells resulting in cell cycle arrest and cell death. Niclosamide stearate prodrug was extensively studied by Needham et.al (192), as a successful candidate for LDL-like nanoparticles through nanoprecipitation. Niclosamide stearate is a solid hydrophobic prodrug with extremely low aqueous solubility (8.3 nM, 5 e^{-06} mg/ml) (193), similar to that of orlistat. Hence, comparing the properties of the prepared NPs of both drugs could help us understand more the process of NPs formation and size growth.

Orlistat NPs were compared to freshly prepared Niclosamide stearate NPs in terms of particle size and surface charge, both were prepared under the same conditions, using rapid solvent shift technique of ethanolic injection into water in a ratio of 1:9. Different concentrations of both drugs were employed to study the similarities and differences between the two candidates.

Figure 47 demonstrates the particle size of the prepared orlistat and niclosamide stearate NPs. As shown in the figure, particles size growth of orlistat was higher compared to their niclosamide stearate counterparts, this may be attributed to the higher solubility of orlistat in ethanol (~20 mg/ml) compared to niclosamide stearate (~ 6 mg/ml). The formed larger particles, in case of orlistat, makes it more challenging for developing a stable small size NPs of orlistat. On the other hand, both drugs shared the same inflection point of 0.1 mM.

Figure 48 shows the zeta potential of both orlistat and niclosamide stearate NPs prepared by solvent shift technique. Both NPs formulations showed a negative zeta potential of ~ -40 and -50 mV for orlistat and Niclosamide stearate respectively, which may confer a high surface stability against aggregation.

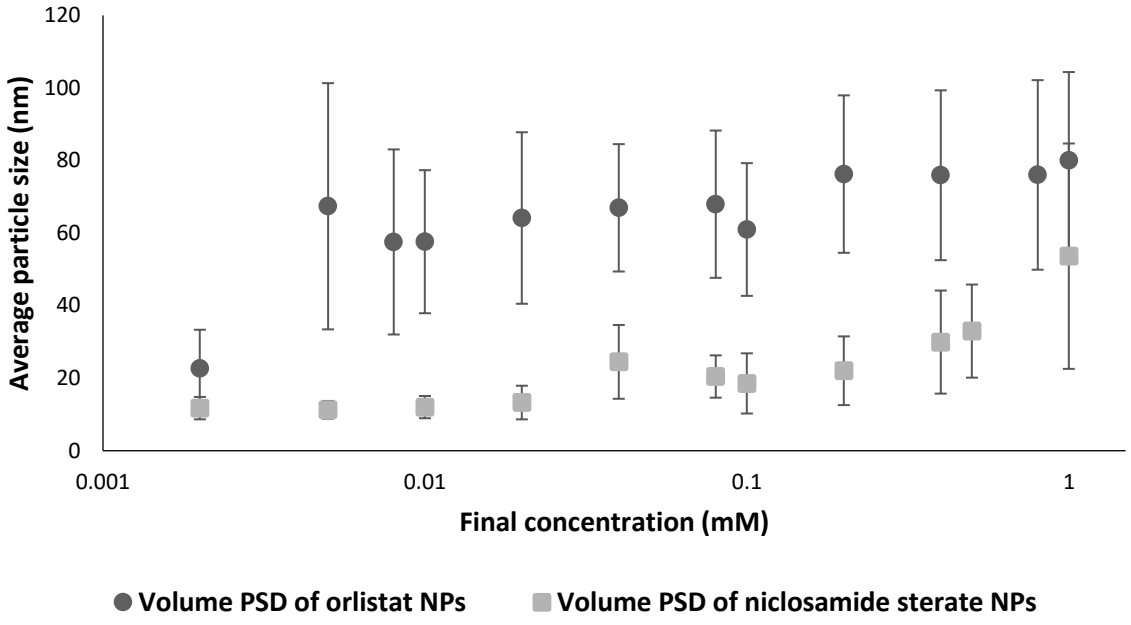

Figure 47 Comparison of volume particle size growth between orlistat and niclosamide stearate NPs prepared by direct ethanolic injection at a ratio 1:9 (v/v) in water, in a range of initial concentration of 0.025 mM to 10 mM, n=3 ±SD.

.

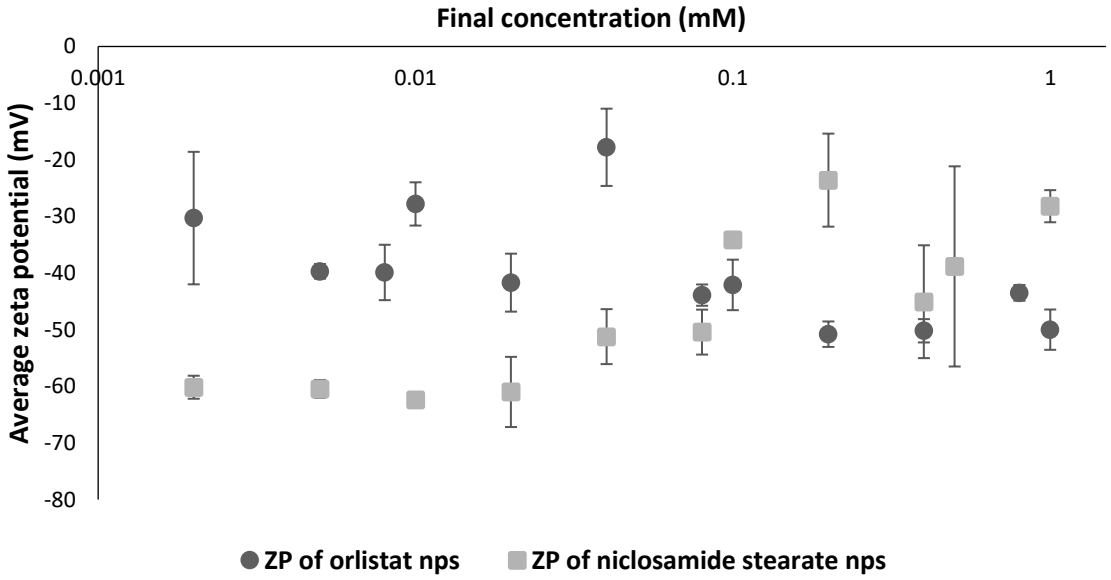

Figure 48 Comparison of average zeta potential between orlistat and niclosamide stearate NPs prepared by direct ethanolic injection at a ratio 1:9 (v/v) in water, in a range of initial concentration of 0.025 mM to 10 mM, n=3 ±SD.

3.5 CONCLUSION

- Solvent shift technique is a nanoprecipitation technique for hydrophobic materials, in which the particle size of the formed particles is dependent on the concentration (SA1).
- Controlling of particle size growth as a function of concentration could be achieved by coating of the NPs with a single layer of phospholipids or surfactants (SA4).
- Hydrophobic lipids including olive oil, tricaprin, and trihexanoin shared similar trend of particle size growth at higher concentrations when prepared by rapid solvent shift technique. The inflection point depends on the lipid structure (SA2).
- Olive oil NPs showed a negative zeta potential, mainly due to the free fatty acids present in the composition of the oil. This may help stabilising the formed NPs against any further aggregation (SA1)
- Coating of olive oil NPs with POPC, tween 80 and lecithin was useful in controlling particle size growth. However, POPC and tween 80 coated NPs were more stable in terms of size, of which POPC will be more interesting in developing LDL-like NPs (SA4).
- The core to coat molar ratio greatly affects the control of particle size. Utilising insufficient coating material may result in incomplete coating of the formed NPs and hence particle size growth. On the other hand, higher amount of coating materials is undesirable leading to formation of unfavourable micelles and decreasing the drug loading (SA4).
- Screening various core to coat ratios showed that the optimum ratio should be around 2:1, or to be in the range between 1.5: and 2.3 :1 (SA4).
- Rapid solvent shift technique was better than the slow dripping method for preparing smaller NPs in size, especially for hydrophobic materials (SA3).
- Orlistat NPs, a hydrophobic drug candidate, was successfully prepared by rapid solvent shift technique. The prepared NPs showed similar behaviour to other hydrophobic

materials, showing a particle size growth with increasing concentrations, despite being solid material (SA2).

- Comparing orlistat to drugs, such as niclosamide stearate, showed similarity in behaviours in terms of particle size and surface stability (SA2).
- Coating of orlistat with POPC in molar ratio 2:1 (core: coat) was effective in preventing particle size growth (SA4).
- Negative surface charge of the prepared orlistat NPs would be a useful tool to protect against any further aggregation (SA2).

4 Chapter 4 Evaluation of orlistat nanoparticles as a candidate for LDL-like NPs

4.1 INTRODUCTION

4.1.1 Fatty acid synthase enzyme (FASN) and breast cancer

After 3 decades of intensive research in the field of tumour fat metabolism, particularly in the glycolytic carbon flux pathway, it was found that most tumours have the ability of de novo synthesis of lipids from acetate or glucose found in the cells, in a pathway similar to that found in most lipogenic tissues such as liver (138). Later in 1980s it was found that the rapid growing cancerous cells could produce their requirements of fatty acids through a de novo biogenesis. Kuhajda et al. found that fatty acid synthase enzyme (FASN) was a key biomarker for patients with late-stage breast cancer(140).

Since then, FASN enzyme upregulation was observed in most of human cancers, including breast carcinomas, and was preserved as an important hallmark of most tumours and their precursor lesions(141,194,195). Fatty acid synthesis in cancerous cells through the FASN pathway should imply great advantages not only for the tumour growth and proliferation, but also in cell adhesion, migration and invasion, the case that may cause metastasis and worsen the patient survival(196–198).

Hence, FASN has received a great attention as a therapeutic target, through development of several inhibitors and characterisation of several formulations targeting FASN activity in tumour cells(144,199,200). However, development of therapeutic targeted formulations of FASN inhibitors makes it difficult to translate their effect in clinical field, thus intensive research is done in optimising formulations of FASN inhibitors(201). Moreover, the first generation of FASN inhibitors with low in vivo bioavailability resulted in emerging of the new second generation FASN inhibitors, of which orlistat (ORL) is one of the best candidates(202).

4.1.2 Orlistat as FASN inhibitors

Among the most prominent second generation FASN inhibitors discovered is orlistat, an FDA approved inhibitor for pancreatic lipase enzyme that was developed as a treatment for obesity. Lately, orlistat was preserved as a potent irreversible inhibitor of FASN. The mechanism of inhibition is suggested to be through its ability to form a covalent bond with the serine amino acid moiety found in the thioesterase domain of FASN enzyme(146,203).

Nevertheless, orlistat antitumor action on breast cancer is limited to reduction of proliferation of HER-2 overexpressing breast cancer cell lines(204). This is mainly due to the pharmacological limitation of orlistat related to its poor bioavailability and lack of selectivity. Therefore, recently many attempts have been made to develop successful formulations of orlistat with improved potency against breast cancer cell lines and enhancing its bioavailability, selectivity, and solubility. Hill et. al, developed a self-assembled NPs formulation of hyaluronic acid bio conjugated orlistat to circumvent its hydrophobicity, the formulation showed a significant improvement in cytotoxicity against triple negative breast cancer cell lines(149). Additionally, Bhargava-Shah et. al, used PEG- conjugated poly(lactic-co-glycolic acid) nanoparticles (PLGA-PEG-NPs) NPs of orlistat (size range 130-300 nm) as a module to enhance cytotoxicity against breast cancer(150). Furthermore, folate receptor targeted orlistat NPs showed enhanced bioavailability and activity in breast cancer tumours xenografts compared to the free orlistat (205). Thus, one could say that the vehicle of orlistat delivery to tumour cell will greatly affects the behaviour in the tumour, and this will lead to urge of developing new orlistat targeted formulation for better therapeutic actions(206).

4.1.3 Orlistat as a promising anti-cancer

Orlistat (ORL) is an FDA approved weight reduction medication, which when taken orally, restrains gastric and pancreatic lipases. Notwithstanding lipase action, ORL has been demonstrated to be a strong inhibitor of fatty acid synthase FASN, where ORL ties to the

thioesterase domain of the enzyme, prompting the hydrolysis of the β-lactone group inside orlistat (146,207).

Almost all malignant growths show expanded endogenous unsaturated fats synthesis, disregarding the degree of circulating dietary unsaturated fats. The key catalyst culpable for this procedure is homodimeric and multifunctional FASN, which consistently utilizes malonyl-CoA, acetyl-CoA, and NADPH for this process(208). The essential product of FASN is the 16-carbon unsaturated fatty acid palmitate. Basically, palmitate is created to store excess energy as triglycerides in healthy lipogenic tissues (i.e., liver) and is directed by dietary intake. Yet, the action of FASN and the destiny of palmitate are very extraordinary in malignant tissues, where palmitate is principally incorporated into phospholipid synthesis, the main class of lipids found in cell membranes. Additionally, there is much evidence that FASN presents a survival advantage to malignancies and their antecedent lesions(209). FASN has been perceived as a potential target for cancer treatment due to its extensive expression in nearly most types of cancers. Hence, many molecules that target FASN have been examined for cancer therapy, including cerulenin, C75, epigallocatechin-3-gallate, and triclosan, yet these showed many undesirable side effects(210). In this way, new molecules with less side effects are required.

Orlistat showed great advantage in cellular assays as it adequately hinders FASN, diminishes malignant cell growth, endothelial cell expansion, and angiogenesis. The mechanism behind these effects is related with cell cycle blockage, ER stress, and apoptosis. Furthermore, in vivo tumour models have demonstrated that orlistat lessens tumour development, metastasis, and angiogenesis at high concentrations(211). Nevertheless, orlistat is incredibly hydrophobic; its anticipated log P is 8.1 with poor bioavailability and metabolic stability, hence, a method for improving conveyance of orlistat to tumours is needed.

Nanoparticles preparation through solvent shift technique best fits hydrophobic materials with incredibly low water solubility in the nanomolar range, meanwhile still soluble enough in other

water-miscible solvents such as ethanol. As Zhigaltsev et al.(151) used triolein as their successful test material, accordingly it is expected that other hydrophobic material could form nanoparticles, comparable to triolein NPs, upon coacervation process. Consequently, preparation of size-tailored nanoparticles of orlistat could be achieved, which may be useful for further modification to reinforce breast cancer targeting.

Orlistat (**Figure 49**) is (S)-2-formylamino-4-methyl-pentanoic acid (S)-1-[[(2S, 3S)-3-hexyl-4-oxo-2-oxetanyl] methyl]-dodecyl ester with a molecular weight of 495.7 g/mol. Orlistat is a white to off-white crystalline powder, which is highly hydrophobic, with extremely low water solubility of $9.19e^{-05}$ mg/ml. On the other hand, it is highly soluble in wide range of organic solvent including chloroform, methanol, and ethanol (solubility in ethanol~ 20mg/mL). Orlistat has no pK_a within the physiological pH range(159).

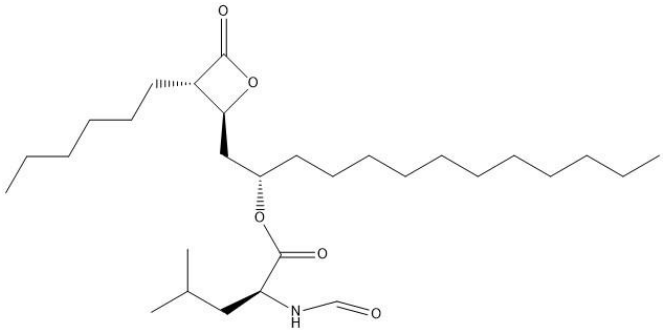

Figure 49 chemical structure of orlistat

4.1.4 Freeze-drying of nanoparticles

Stability of NPs formulation was a great hurdle for long period of time, especially during storage(212). One method of improving long term stability of NPs is through drying processes, among which freeze drying is the most favourable. It is well known that the solid dosage form has higher stability compared to the liquid suspensions, hence converting the NPs colloidal suspension into solid powder might prevent any undesirable aggregation or condensation that may occur over time. Additionally, solid powdered formulations help in keeping the structure of the NPs and prevent drug leakage or degradation. Abdelwahed et. al, showed that freeze

dried nanocapsules of the unstable drug poly(ε-caprolactone) were stable after 6 months of storage under harsh conditions of temperature and humidity(213). Another study carried out by Roy et. al, showed that the lyophilised NPs of poly (methylidene malonate 2.1.2) (PMM 212) maintained its properties, in terms of in vitro cytotoxicity and drug content, after 12 months of storage at room temperature, compared to the NPs suspension kept at -40 °C (214). Dehydroemetine NPs for treatment of leishmaniosis developed by Fouarge et. al were freeze dried using 5% glucose as cryoprotectants, the size and structure of the NPs were conserved after storage for up to 24 months(215). Heiati et. al, freeze dried solid lipid nanoparticles of azidothymidine, which kept the size and drug content over long term storage(216).

Another importance for solid dosage form is the ease of administration and handling, where the powdered drug dosage forms are easily administered as such or after reconstitution through various routes of administration, i.e., parenteral, pulmonary, oral, or nasal.

4.1.4.1 Freeze drying and cryoprotectants

Developing of freeze-dried formulation of NPs is a complex process, since the formulation should preserve some important characteristics in the final product, among which is preserving the initial physico-chemical characteristics of the NPs, this includes acceptable particle size distribution, ease of reconstitution, unchanged activity of the encapsulated drug and elegant suspension appearance. Furthermore, the formulation must ensure long term stability with minimal effect on the previously mentioned characteristics with time. In order to achieve a high-quality product, the right excipients in optimal quantities should be used during the formulation process, the most important of such excipients is the cryoprotectants.

The successful formulation should guarantee the resistance of NPs structure to the stresses of the freeze-drying process, this is attributed to the components of the formulation, including the type and the amount of cryoprotectant used, the nature of used surfactants in formulation and the chemical nature of the NPs structure. Accordingly, wide attention should be given to

studying the effect of different components and selecting the optimum formulation for the best outcome of freeze-drying process(212).

4.1.4.2 Choosing the cryoprotectant

During the process of freeze drying, colloidal suspension may suffer of great destabilisation stress due to freezing and dehydration, for example, phase separation during freezing may occur into ice, and a cryo-concentrated solution of NPs is formed, which may enhance the irreversible aggregation of NPs(217). Additionally, crystallization of ice is another destabilising stress factor resulting into more fusion of the NPs. Consequently, special excipients are added to protect the system from freezing and drying stress, those excipients are known as cryoprotectants and lyoprotectants respectively(213).

Cryoprotectants are generally a material that can vitrify at a specific glass transition temperature (Tg) (218), this glass transformation results in immobilization of the NPs and thereby avoiding their aggregation. Among the most commonly used cryoprotectants are sugars including sucrose, trehalose, glucose, and mannitol. It is worth mentioning that the freezing process should be carried out below the Tg of the frozen amorphous sample in order to ensure complete drying of the sample(219). Particle isolation hypothesis is the main suggested theory for how the cryoprotectant stabilise the NPs dispersions. Simply it proposes that the used cryoprotectants, especially sugars, isolates the individual nanoparticles in the unfrozen state, mainly through formation of hydrogen bonds with the particles, which in return prevent aggregation of the NPs during freezing(220).

The type of cryoprotectant is critical in the overall properties of the freeze-dried formulation. The most advantageous cryoprotectant for most biomolecules was found to be trehalose, thanks to its low hygroscopicity, low chemical reactivity, high Tg and lack of internal hydrogen bonding that increase the chance for better bonding to the NPs during freeze drying(221).

Consequently, pilot studies should be done to select the best cryoprotectant that can preserve the properties of the NPs formulation used. The properties of the chosen cryoprotectant greatly affect the stability of NPs during the freeze-drying process, for example mannitol, a commonly used cryoprotectant, usually crystallizes and forms eutectic mixtures resulting in phase separation and increasing the chance for NPs aggregation and size growth upon reconstitution(217).

Besides the importance of choosing the type of cryoprotectant used in freeze drying process, the amount of this material is crucial in stabilisation of the formulation following the freezing process. The low amounts of cryoprotectants will be insufficient for stabilizing the colloidal suspension(222), while the excessive amounts will destabilise the NPs during reconstitution resulting in aggregation and particle size growth due to the increase affinity towards the cryoprotectant that prevent the reconstitution of the NPs(223).

4.2 AIMS AND OBJECTIVES

The main objective of the work is to prepare orlistat NPs with controlled size (<50 nm), in order to be further studied for surface functionalisation and preparation of LDL-like NPs.

POPC coated Orlistat NPs prepared by rapid solvent shift technique were further stabilised through the use of surfactants, as well as freeze drying, ensuring stable physical properties of the prepared formulation.

SA1: Investigating the effect of adding stabilisers, such as salts and surfactants, on the stability of particle size of the prepared formulations, in addition to its effect on surface charge.

SA 2: Investigating the effect of freeze drying on the size and surface stability of the NPs formulation over long storage periods, in terms of particle size and surface charge.

SA 3: comparison between the effect of different cryoprotectants on the physicochemical properties of the freeze-dried orlistat NPs formulation.

SA 4: Investigating the structure and incorporation of orlistat within the coating material (POPC lipid with other surfactants as stabilisers), and the overall physical properties of the prepared POPC coated orlistat NPs.

SA 5: Evaluation of the POPC coated orlistat NPs in terms of drug loading, encapsulation efficiency and drug release.

4.3 MATERIALS AND METHODS

4.3.1 Materials

Orlistat (Sigma Aldrich, 97% purity), 1-palmitoyl-2-oleoyl phosphatidyl choline (POPC) (Merck life science, TLC >99% purity), Tween80 (ThermoFisher scientific, >97% purity), Sodium dodecyl sulfate (SDS) (Sigma Aldrich, ACS reagent 99% purity), potassium nitrate KNO_3 (Sigma Aldrich, ACS reagent 99% purity), pure ethanol (Sigma Aldrich, anhydrous pure >99.5%), Trehalose dihydrate (Sigma Aldrich, >99% purity) , D-Mannitol (Sigma Aldrich, >99% purity), Glucose (Sigma Aldrich, >99% purity) Phosphate buffer saline tablets (Sigma Aldrich), and MilliQ® water, all materials were of analytical grade and used as supplied, unless otherwise mentioned.

4.3.2 Methods

4.3.2.1 Orlistat NPs

Orlistat nanoparticles were prepared by solvent exchange method as mentioned previously (Chapter 3 Methodology) through direct injection of ethanolic solutions at various concentrations into water using eVol™ syringe injector. Following injection, the nanoparticle dispersion is removed immediately from the magnetic stirrer, and characterized using Malvern zeta sizer nano range ZS.

Coating of orlistat with POPC was done through the same nanoprecipitation technique.

4.3.2.2 Measuring the particle size and zeta potential:

Freshly prepared nanoparticle dispersions are subjected immediately to particle size and zeta potential analysis using Malvern® Zeta sizer as mentioned before.

4.3.2.3 TEM imaging of NPs

TEM images of NPs were captured using negative staining as previously described. TEM imaging was done using FEI® Tecnai Biotwin transmission electron microscope Images were processed by using ImageJ, Fiji® package for counting the particle size.

4.3.2.4 Addition of stabilisers to NPs formulations

The POPC coated orlistat NPs (in a ratio 2 core: 1 coat as molar ratio) were further stabilised through addition of surfactants and/or salts to the antisolvent during the nanoprecipitation process. Three different stabilisers were investigated, specifically 10mM KNO_3, 3mM SDS with 10 mM KNO_3, and 2% tween 80. The effect of addition of stabilisers to the NPs formulation was investigated in terms of particle size and surface charge.

4.3.2.5 Freeze drying of the NPs

The prepared orlistat NPs (2 mM final concentration of orlistat either uncoated or POPC coated in a ratio 1:1.6, coat to core) were freeze dried using Virtis benchtop lyophiliser® (SP scientific sentry 2.0) to enhance stability of the prepared particles over storage.

Initially, NPs were prepared with different cryoprotectants, namely Trehalose, Mannitol and Glucose in three different concentrations of each (5, 10 and 15% w/v). The prepared NPs were flash frozen using liquid nitrogen, followed by placing them in the lyophiliser. The pressure was then reduced to 100 mTorr and the temperature was set to −50 °C and held for 24 h to allow drying. The dried samples were then stored in freezer at -20 °C in sealed bags with silica beads until further used. The freeze-dried NPs were reconstituted 6 months, and tested for stability regarding particle size growth and zeta potential.

4.3.2.6 Drug incorporation assay

Incorporation of orlistat into the prepared NPs was assayed to ensure complete coating of the prepared NP formulations. The loading efficacy of the prepared NPs were estimated at 60% of the total formulation mass. Incorporation studies were done using both DSC and polarised light microscopy techniques.

4.3.2.6.1 Differential scanning calorimetry (DSC)

DSC was done for pure orlistat drug, orlistat/ POPC physical mixture and the POPC coated orlistat NPs Using DSC Q2000 (TA® instruments, UK). Samples (10 mg) were weighed separately in aluminium DSC pans, which were then compressed to be hermetically sealed. The prepared pans were placed in DSC, and a heat cool heat run was done for each sample in the range between 0 ºC to 350 ºC, at a rate of 5ºC/min and under nitrogen gas flow. Afterwards, DSC thermograms were collected and analysed.

4.3.2.6.2 Polarised light microscopy (PLM)

Microscopic images for pure orlistat, POPC, Uncoated orlistat NPs, and POPC coated NPs were captured using polarised light microscope PX023POL (Prior Scientific Inc® USA). A suitable mass of each sample (~ 20 mg) was added on a clean microscopic slide. The samples were viewed under both bright and cross polarised fields (dark fields) to check for the birefringence, colour absorption and optical path similarities.

4.3.2.7 UV assay of orlistat

Orlistat (1 mg/ml) in ethanol solution was scanned over the range of (200 – 700) nm using UV/Vis spectrophotometer (166), and the wavelength of maximum absorbance (λ_{max}) was determined.

Serial dilutions (10 - 150 µg / ml) were prepared and the absorbance of the prepared solutions was measured at the predetermined (λ_{max}). The measured absorbance values were plotted against the corresponding concentrations to obtain a calibration curve. Validation parameters

of the spectrophotometric assay were limited to linearity, limit of detection (LOD), Limit of quantification (LOQ), inter-day precision. LOD and LOQ are described in the following equations.

$$\mathbf{LOD} = \frac{\mathbf{3}\,\boldsymbol{s}}{\boldsymbol{m}} \qquad \textbf{Equation 17 Limit of detection}$$

$$\mathbf{LOQ} = \frac{\mathbf{10}\,\boldsymbol{s}}{\boldsymbol{m}} \qquad \textbf{Equation 18 Limit of quantification}$$

Where (s) is standard deviation and (m) is the slope of the related calibration curve.

4.3.2.8 Encapsulation efficiency and drug loading

The percent of drug encapsulated into the nanoparticles was measured using two approaches. The first one through centrifugation ultrafiltration technique, simply nanoparticle formulation (2 mM orlistat final concentration) was loaded in Vivaspin® centrifugal concentrator (Sartorius Vivaspin® 20, mwco 5000 d, membrane PES), and were centrifuged at 6000 rpm for 5 min in 5 cycles using a cooling centrifuge (Eppendorf® cooling centrifuge, Eppendorf® AG, Germany). Afterwards, the filtrate containing the free drug was separated, freeze dried and reconstituted in ethanol and assayed using UV spectrophotometer (Fischer scientific ™ UK) at λ_{max} 205 nm. The other method is through dialysis, using slide-A- lyzer dialysis cassettes (thermos scientific™ mwco 3.5 Kd, UK), where 3 mls of NP formulation were loaded to the cassette and then suspended in 200 ml of phosphate buffer saline PBS (pH 7.8) and kept in the fridge for 24 hours, then 40 ml sample were taken, freeze dried, and analysed for content of free orlistat using same spectrophotometric method.

4.3.2.9 Drug release assay

Drug release assay was carried out in PBS (pH 7.4) containing 0.2% tween 80 to challenge the drug release pattern. In brief, 3 ml sample of the nanoparticle formulation was loaded into slide-A-lyzer dialysis cassettes (thermos scientific™ mwco 3.5 Kd, UK). Then the cassette was allowed to suspend into 400 ml of release medium and kept at 37 ºC and 350 rpm for 1 week.

At predetermined time intervals (1, 2, 3, 4, 7 days), 40 ml samples were withdrawn and were compensated by fresh release buffer. Samples were freeze dried and assayed spectrophotometrically as before, release pattern was studied as cumulative percent release versus the time.

4.4 RESULTS AND DISCUSSION

4.4.1 Evaluation of stabilisers' effect on prepared NPs

4.4.1.1 Freshly prepared NPs

As mentioned before, coating orlistat NPs with a single layer of phospholipids is expected to provide a protective shield that prevents ripening and controls the particle size. For POPC coated orlistat NPs at a ratio of (2:1) (core: coat), the particle size was kept at controlled range of (~ 50 nm) even at higher drug concentrations. However, ensuring the stability of the particles over time is still hard to control, thus we investigated the addition of stabilisers including salts and surfactants to the formulation. This could help us as well understand the behaviour of NPs prepared by rapid solvent shift technique.

Further stabilisation of the formulation was done using surfactants to control the size of particles at the higher drug concentration (1 to 4 mM). Three different stabilisers were employed, either 3 mM sodium dodecyl sulfate (SDS) with 10 mM potassium nitrate, 10 mM potassium nitrate, or 2% tween 80. The stabilisers were added to the antisolvent aqueous phase to stabilise the formed particles following the nanoprecipitation. Following the preparation, the particle size and the surface charge were evaluated.

Figure 50 represents a comparison between the mean particle size (nm) measured by DLS of either the uncoated orlistat NPs, POPC coated orlistat NPs in water, or POPC coated orlistat NPs in each of the previously mentioned stabilisers. All the formulations were prepared by rapid solvent shift technique and at 4 different orlistat concentrations (4, 2, 1 and 0.1 mM).

As shown in the figure, the addition of surfactants to the counter phase such as 3 mM SDS or 2% tween 80 resulted in significant decrease of the size of the freshly prepared NPs, at all the employed concentrations of orlistat, compared to either the uncoated particles or the POPC coated orlistat NPs prepared in water. This size control is attributed to the presence of

surfactants in the aqueous phase that results in prevention of any further condensation between the formed nuclei during the nanoprecipitation.

In our study we utilised two different surfactants, an anionic surfactant SDS and a non-ionic surfactant tween 80, each of them has a unique way of stabilising the formed NPS. SDS will act mainly through its negative charge that confers an electrostatic repulsion force between the precipitated NPs and hence will prevent the condensation of the nuclei at the time of nanoprecipitation. On the other hand, Tween 80 is a non-ionic surfactant, it will mainly act through addition of steric stability of the prepared NPs, which will prevent further condensation. Addition of salts (10 mM potassium nitrate) as shown, did not protect the particles from the event of growth, they will act to sequester the ionic double layer around the nanoparticles, however, are not expected to affect the particle size.

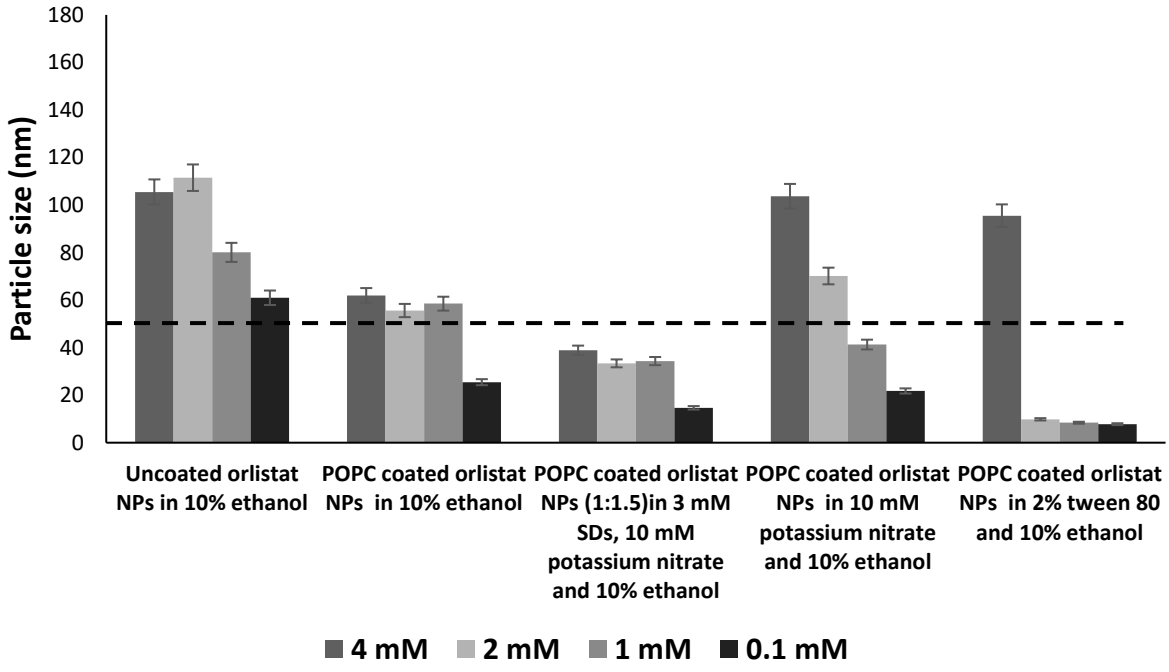

Figure 50 comparison of particle size of freshly prepared orlistat NPs (0.1, 1, 2 4 mM orlistat final concentration) after adding various stabilisers to the antisolvent during preparation, n=3 ±SD.

Concerning the surface charge, **Figure 51** illustrates a comparison between the average zeta potential (mV) measured by zetasizer, of either the uncoated orlistat NPs, or POPC coated orlistat NPs in each of the previously mentioned stabilisers. All the formulations were prepared by rapid solvent shift technique and at 4 different orlistat concentrations (4, 2, 1 and 0.1 mM).

As shown in the figure, the surface charge was significantly reduced in presence of the 10 mM potassium nitrate and the 2% tween 80 as stabilisers, with an average zeta potential of -15 mV. On the contrary, addition of 3 mM SDS highly increased the negative surface charge up to an average of – 70 mV compared to the uncoated orlistat NPs with an average of -50 mV.

The zeta potential of the prepared orlistat nanoparticles showed a significant negative zeta potential in the absence of any salts, this is because of the effect of the electric double layer that provides infinite Debye length. Yet, addition of salts, in this case potassium nitrate, resulted in sequestering the double layer, hence reducing the surface charge. In presence of salts we could see the actual surface charge of the orlistat NPs being around the average of – 15 mV.

Addition of surfactant sodium dodecyl sulfate interestingly implied a significant negative zeta potential of around -70 mV. This surface charge is expected due to the negative charge of the anionic surfactant. Yet, this negative charge was implied even in the presence of salts that sequester the double layer (10 mM potassium nitrate). This significant negative surface charge could be extremely useful in enhancing NPs stability by increasing the repulsion forces between the formed particles and avoiding any further aggregation. Hence, it is noticeably clear that the SDS is expected to confer the maximum stability over the particle size growth, compared to the non-ionic surfactant.

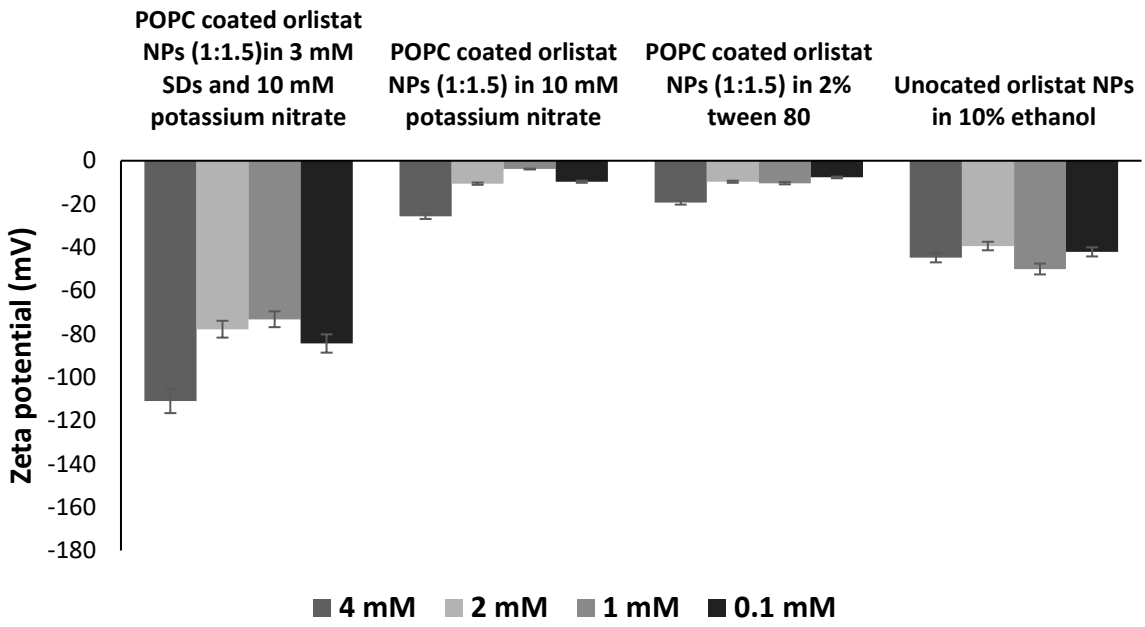

Figure 51 comparison of zeta potential of freshly prepared orlistat NPs (0.1, 1, 2 4 mM orlistat final concentration) after adding various stabilisers to the antisolvent during preparation, n=3 ±SD.

4.4.1.2 After 2 weeks of storage

The stability of the prepared NPs was investigated after storage in fridge (4ºC) for two weeks, in terms of particle size and surface charge. **Figure 52** shows a comparison of the average particle size of POPC coated orlistat NPs (2:1 core to coat) prepared in different stabilisers after 2 weeks of storage in fridge to that of the freshly prepared, all at 4 different final orlistat concentrations (4,2 ,1 and 0.1 mM). As shown in the **Figure 52,** addition of surfactants such as SDS and Tween80 stabilised the prepared nanoparticles over the period of storage, with no significant change in particle size, at any of the employed concentrations of orlistat.

Results of particle size stability shown in **Figure 52** indicate that the prepared NPs showed stability over 2-weeks storage in presence of surfactants, which may be attributed to the stabilization of the surface of the prepared NPs, either through surface charge of steric

hindrance, which prevents further condensation of the NPs with time and prevent further growth as mentioned before.

Figure 53 shows comparison of the average zeta potential (mV) of POPC coated orlistat NPs (2:1 core to coat) prepared in different stabilisers after 2 weeks of storage in fridge to that of the freshly prepared, all at 4 different final orlistat concentrations (4,2 ,1 and 0.1 mM).

Concerning the Zeta potential there was no significant difference (at $p<0.05$, two-way ANOVA) before or after 2 weeks of storage for all the prepared NPs as in **Figure 53**.

However, Tween 80 stabilised NPs showed minimal negative zeta potential compared to SDS, the high negative zeta potential will confer stability on the formulation upon long term storage. Hence SDS was chosen as a model stabiliser for the upcoming studies.

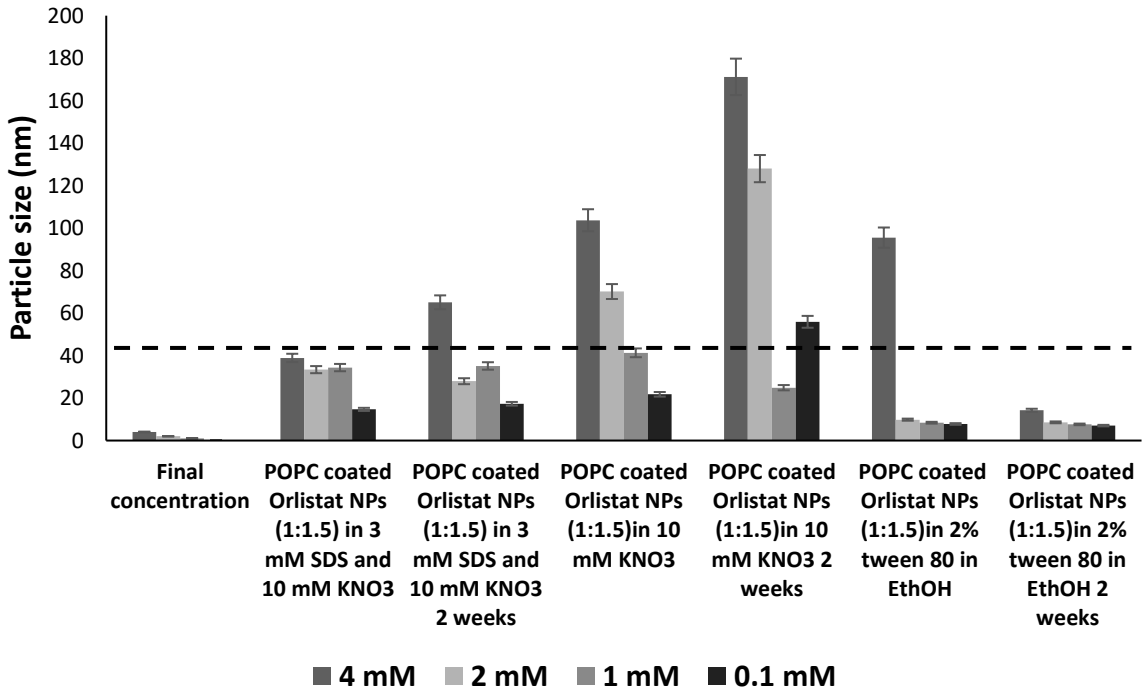

Figure 52 comparison of particle size of orlistat NPs (0.1, 1, 2 4 mM orlistat final concentration) after adding various stabilisers to the antisolvent during preparation and 2 weeks storage in fridge at 4º C, n=3 ±SD.

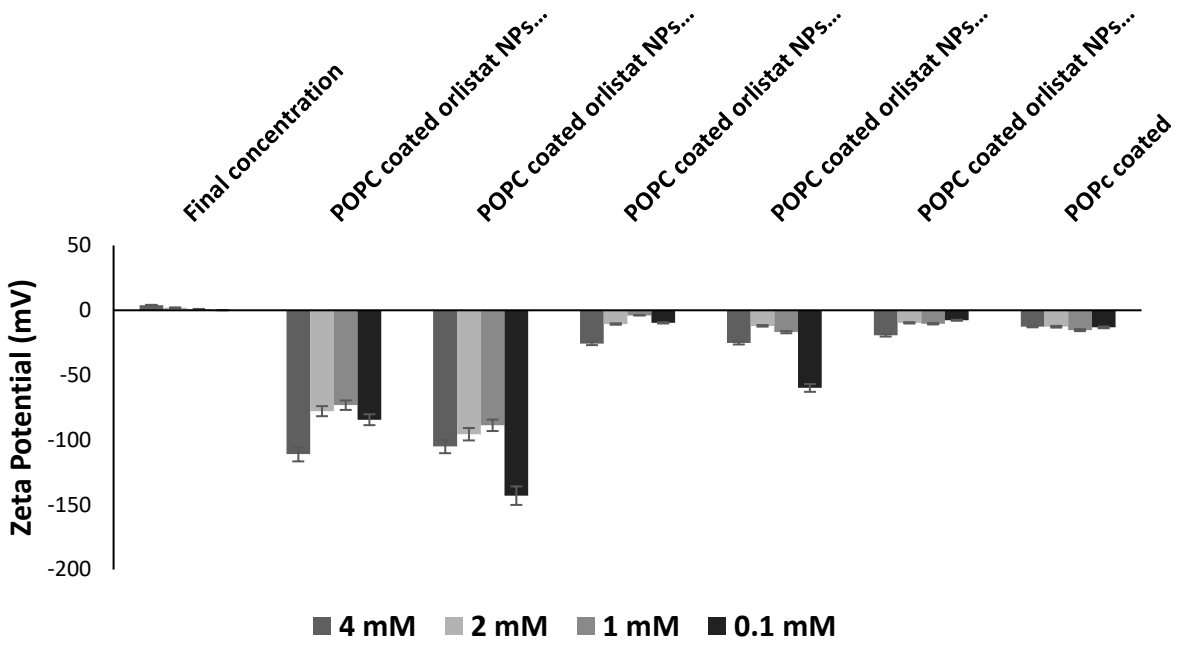

Figure 53 comparison of zeta potential of orlistat NPs (0.1, 1, 2 4 mM orlistat final concentration) after adding various stabilisers to the antisolvent during preparation and 2 weeks storage in fridge at 4º C, n=3 ±SD.

4.4.1.3 TEM of Stabilised orlistat NPs

Further investigation of the characteristics of the prepared NPs and the effect of addition of stabilisers was done using TEM, in order to get real images of the prepared formulations.

Figure 54 demonstrates the TEM images for POPC coated orlistat NPs at molar concentration of 1 mM, images A and B are for formulations prepared in water, while image C and D are for formulations prepared in 3 mM SDS and 2% tween 80 respectively, all the NPs formulations were assayed after 2 weeks of storage in fridge at 4ºC.

TEM images of the prepared POPC coated orlistat NPs in **Figure 54** showed the process of condensation of the particles in the absence of the stabilisers during storage, where smaller particles condense together into larger particles (**Figure 54 A & B**). This could be observed clearly by the presence of large particle in the middle surrounded by many small particles aggregated on the surface. This aggregation is not preferred as it will increase the overall particle size, as well as will give a chance for condensation between the small particles into

one bigger particle. The average particle size calculated form TEM images in absence of stabilisers was around 60 nm.

On the contrary addition of surfactants as stabilising agents (**Figure 54 C & D**) decreases the probability of condensation of the particles with time. As shown form the images, the presence of surfactants enhanced the formulation stability, through prevention of the condensation or the aggregation of the POPC coated orlistat particles. This will in return resulted in a consistent spherical NPs of small average diameter (~ 40 nm) as counted by Image J®. It was clear as well that SDS resulted in increasing the distance between the particles compared to tween 80, thanks to the negative charge that enhances the repulsion between the particles and prevent their aggregation.

However, in order to further stabilise the particles against any aggregation over long-term storage, and in order to prepare solid dosage form for the ease of handling and administration, freeze drying of the prepared formulation was investigated.

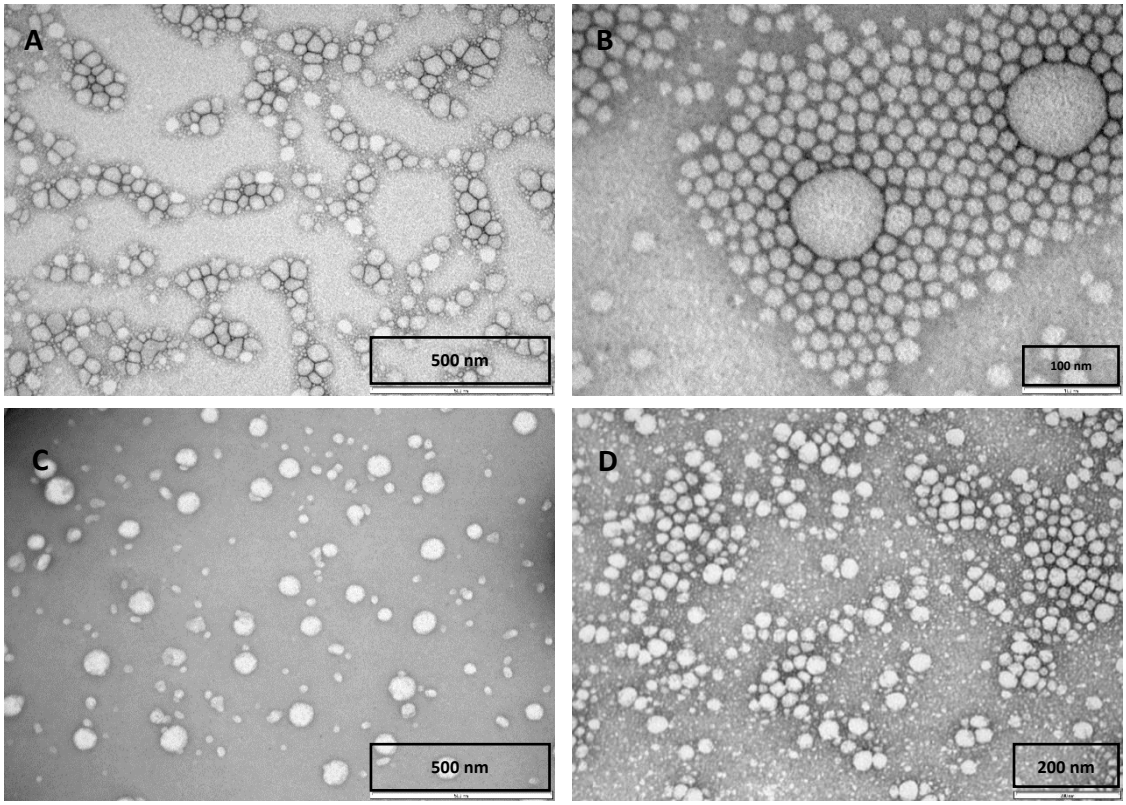

Figure 54 TEM images of POPC coated orlistat NPs (1 mM), A & B in MilliQ water, C) in 3 mM SDS, D) in 2% tween 80.

4.4.2 Freeze drying and particles stability

4.4.2.1 Pilot experiment using 10% trehalose and different orlistat concentrations

A pilot experiment was carried out to investigate the effect of addition of the cryoprotectants on the particle size of the prepared NPs. In this aspect we investigated the use of 10% trehalose as a cryoprotectant in different NP formulations.

Figure 55 shows a comparison of the average particle size of POPC coated orlistat NPs in either 10 mM potassium nitrate alone or with 3 mM SDS, with or without addition of 10 % trehalose to the aqueous phase, compared to the particle size of the POPC coated orlistat NPs and the uncoated orlistat NPs. All the formulations were prepared at four different

concentrations (4, 2, 1, and 0.1 mM), and results are expressed as the average of 3 measurements ± SD.

As shown in **Figure 55**, addition of cryoprotectant to the formulation with SDS as stabiliser, has minimal effect on the particles size of the NPs at the various employed concentration, compared to the other formulations with no SDS. This may be due to the negative zeta potential of the formulation that would prevent condensation of the formed NPs and particle size growth. This minimal effect on particle size moved us towards investigating the effect of using various cryoprotectants at various concentration on the particle size of the prepared NPs before and after freeze drying, in order to choose the optimum type and concentration of the cryoprotectant for our designed formulation.

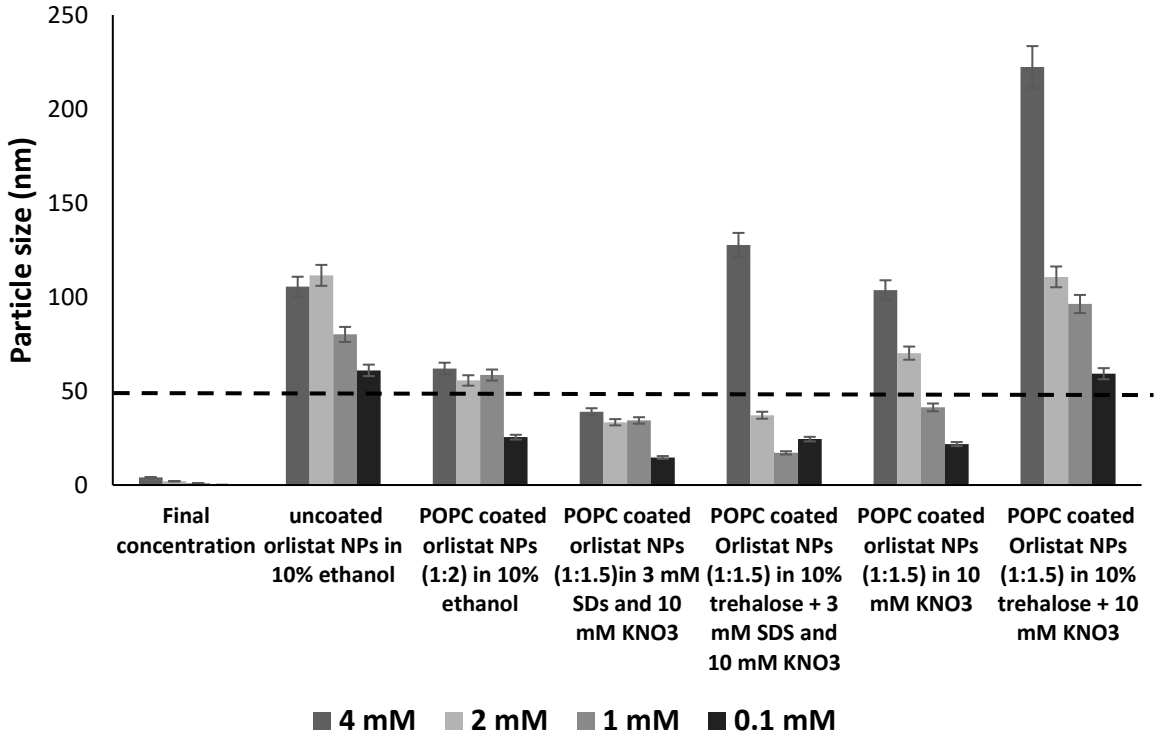

Figure 55 comparison of particle size of freshly prepared orlistat NPs (0.1, 1, 2 4 mM orlistat final concentration) before and after addition of cryoprotectant trehalose 10%, n=3 ±SD.

4.4.2.2 Investigating different cryoprotectants in different amounts

Investigation of using different cryoprotectants, namely Glucose, Mannitol and Trehalose, in three different concentrations, 5, 10 and 15%, on the physico-chemical properties of the prepared NPs, was carried out. POPC coated orlistat NPs (2:1) formulation at final concentration of 2 mM was chosen as a model, in the presence of 3 mM SDS and 10 mM KNO_3 as stabilisers. The study was done to show the effect of using the cryoprotectants on the particle size and surface charge of the prepared NPs before freeze drying, to ensure that the choice of the best cryoprotectant in an optimum concentration for preserving our NPs formulation. This is followed by examining the same parameters after freeze drying, storage over a period of 6 months, and reconstitution. The results were finally compared to the same samples stored in the fridge for the same period of time without freeze drying, to interrogate the influence of freeze drying over the stability of the NPs formulation.

4.4.2.2.1 Before freeze drying

As mentioned before in the pilot experiment using 10% trehalose, addition of cryoprotectants has a minimal effect on the particle size of our POPC coated orlistat NPs. This was further inspected through using of three different cryoprotectants, particularly mannitol, trehalose, and glucose at 3 different concentrations (5, 10 &15%). **Figure 56** illustrates a size map (nm) for the POPC coated orlistat NPs (2:1 at a concentration 2 mM) prepared in 3 mM SDS and 10 mM KNO_3, compared to the same formulation after addition of the 3 cryoprotectants, at 3 different concentrations separately.

It is obvious that all the prepared formulations with different cryoprotectants lies in the preferred zone below 50 nm in size, with minimal effect on the particle size compared to the formulation with no cryoprotectants. To have a deep insight on the difference between those utilised cryoprotectants, all the prepared formulation were freeze dried to investigate the particle size after reconstitution.

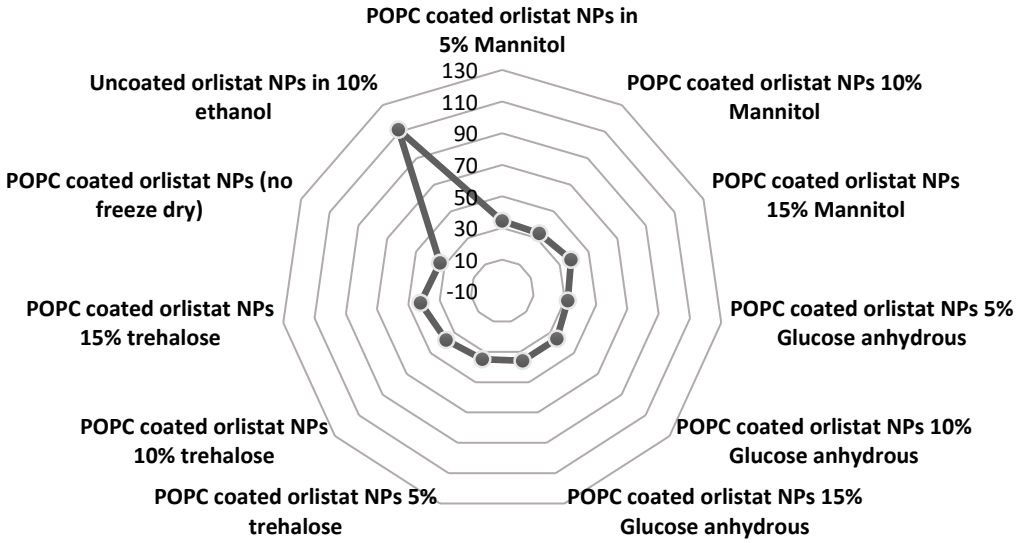

Figure 56 Particle size (nm) map of different formulations of POPC coated orlistat NPs (2:1, with 2 mM orlistat final concentration) with addition of different cryoprotectants (Mannitol, Trehalose and Glucose) in different percent (5, 10 & 15 %).

4.4.2.2.2 After 6 months storage

For proper storage and use of the prepared NPs while keeping its characteristic size for long period of time, lyophilisation was employed for the prepared NPs. Freeze drying could prevent any undesirable condensation of the particles, which may occur due to the continuous Brownian motion of the particles in dispersions. However, direct freeze drying of NPs formulation could result in aggregation and difficulty of reconstitution, hence cryoprotectants are added before freeze drying to remove excess moisture from the formulation, and protect size stability over long storage time(224).we investigated the effect of freeze drying using several cryoprotectants on the size and surface charge stability as shown in **Figure 57 to Figure 60**.

Figure 57 describes a comparison of the average particle size of the prepared POPC coated orlistat NPs, with or without cryoprotectants. The comparison is between the freeze-dried formulations stored over a period of 6 month, the stored formulation without freeze drying

(stored in fridge for 6 months at 4ºC), and that of the freshly prepared samples before freeze drying. The same results were presented in the form of a size map shown in **Figure 58**.

It is clearly demonstrated that freeze drying helped the NPs formulation to retain its size stability over six months storage period, compared to that stored without freeze drying. The average particle size of the formulations stored without freeze drying increase dramatically to a range between ~ 150 to 1200 nm, which is due to condensation occurring over lengthy periods of storage. On the other hand, freeze dried samples retrained its particle size and elegant colloidal appearance over the period of storage, as demonstrated in the size map **Figure 58** and real images in **Figure 60.** Images in **Figure 60** show a clear disaggregated dispersion after reconstitution of the freeze-dried formulation compared to the aggregated formulation stored without freeze drying.

The type and percentage of cryoprotectant play a vital role in the effectiveness of the freeze drying on the size and charge protection. From the results shown, Mannitol was not suitable for conserving the size after reconstitutions, as explained before, this is mostly due to the crystallization of mannitol during freezing steps especially at higher concentrations(217), that my result in phase separation into a NPs rich layer, hence increasing the chance of condensation of the NPs and increasing the particle size. In that context our compatible cryoprotectant for the optimum size control during nanoprecipitation technique was found to be either trehalose or glucose (5-15%).

Regarding the surface charge, the effect freeze drying in presence of various cryoprotectants on the surface charge expressed as the average zeta potential (mV), was depicted in **Figure 59**. The addition of cryoprotectants did not affect the negative surface charge of the prepared formulations, with all the formulations have an average zeta potential in the range between -120 to -20 mV. However, the freeze-dried samples showed a decrease in surface charge compared to those stored without freeze drying, this is related to the surface of the NPs being

masked by the hydrogen bonds formed with the utilised cryoprotectants during the freeze-drying process(225).

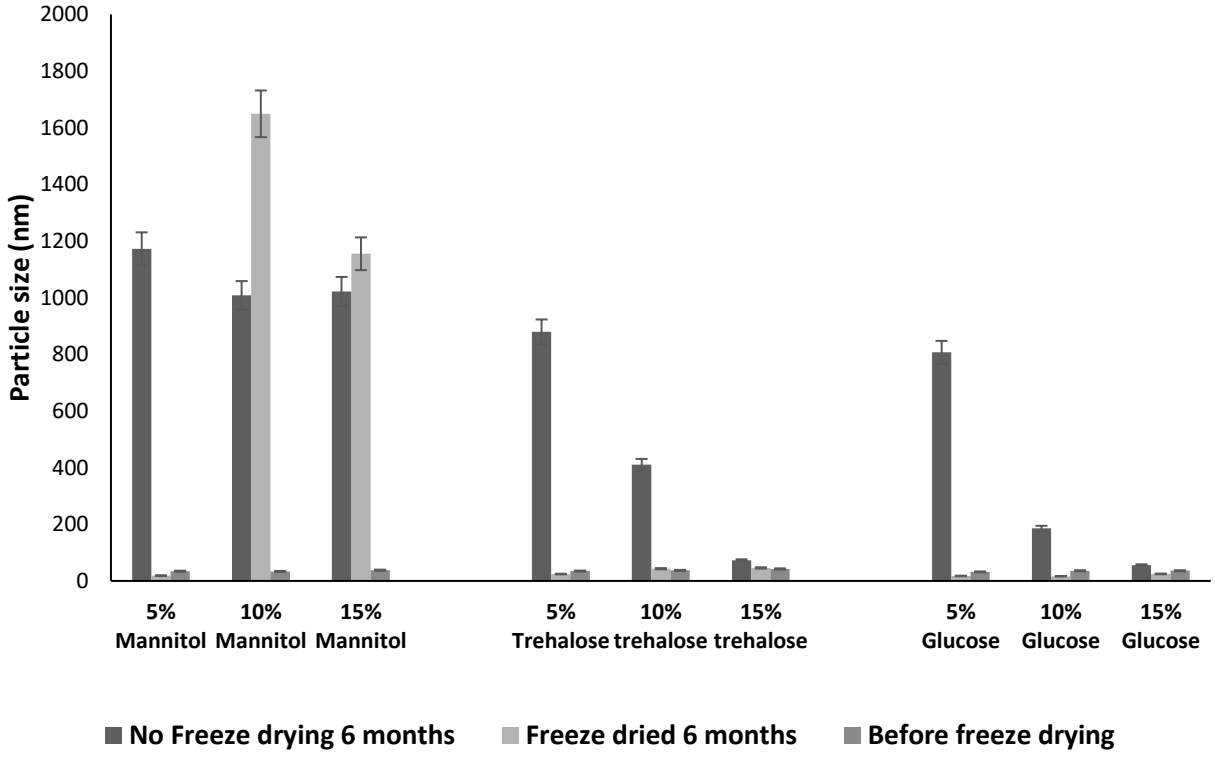

Figure 57 Effect of Freeze drying on stability of NPs over long-term storage (6 months) compared to NPs left in fridge at 4ºC without freeze drying with respect to particle size, n=3 ±SD.

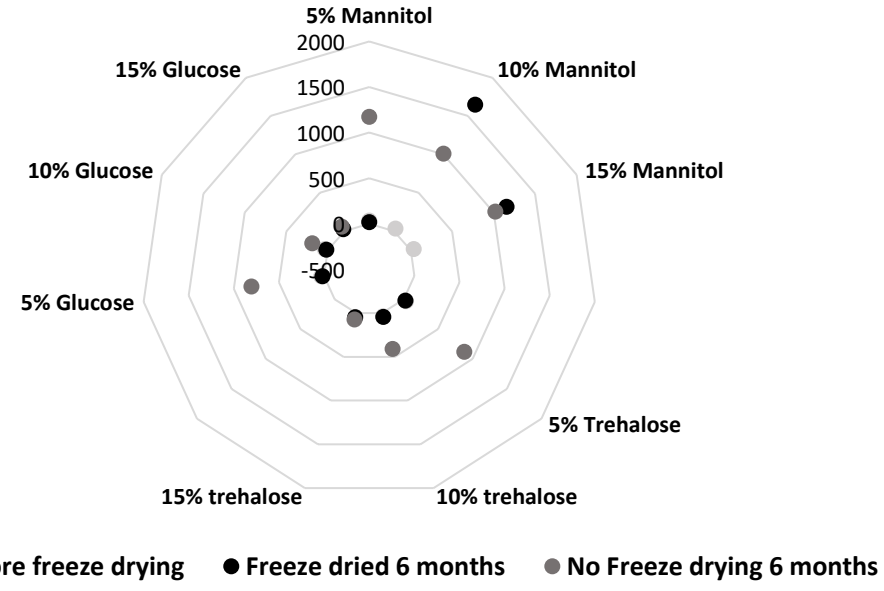

Figure 58 Size map showing effect of Freeze drying on stability of NPs over long-term storage (6 months) compared to NPs left in fridge at 4ºC without freeze drying.

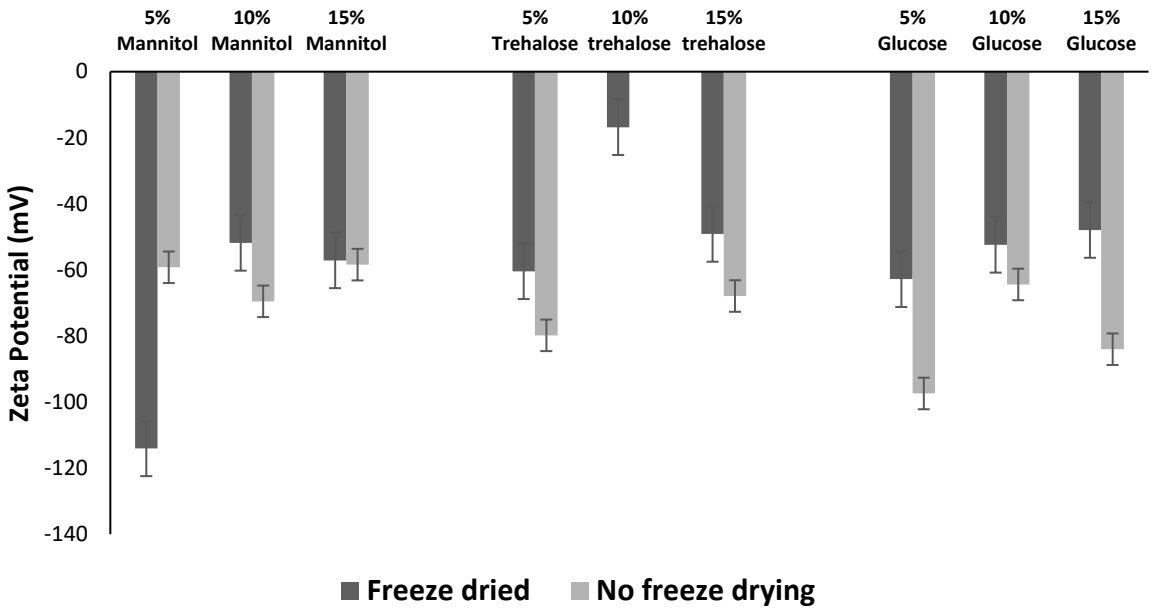

Figure 59 Effect of Freeze drying on stability of NPs over long-term storage (6 months) compared to NPs left in fridge at 4°C without freeze drying with respect to zeta potential, n=3 ±SD.

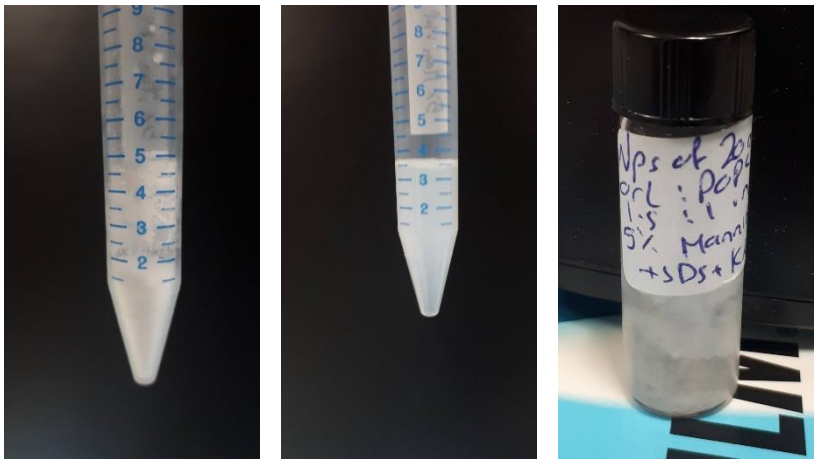

Figure 60 Images of POPC coated orlistat NPs after 6 months storage (2:1 and final concentration of orlistat 2 mM) from left to right of 1) freeze dried formulation before reconstitution 2) after constitution and 3) formulation stored without freeze drying.

4.4.3 Evaluation of drug incorporation

4.4.3.1 Differential scanning calorimetry

Orlistat incorporation into the POPC coated nanoparticles was investigated using differential scanning calorimetry. **Figure 61** shows the DSC thermograms of pure orlistat drug, orlistat/ POPC physical mixture, and freeze dried POPC coated orlistat NPs. The DSC thermograms of orlistat shown in **Figure 61** showed an endothermic peak at 45º C indicating that orlistat recovered its crystallinity following melting(226). Concerning the physical mixture with POPC, the same endothermic peak at 45ºC was observed. However, in case of the POPC coated orlistat NPs, the endothermic peak completely disappeared, indicating complete incorporation of orlistat into the matrix of the POPC in NPs through melting in an amorphous form, unlike the physical mixture(227).

4.4.3.2 Polarised light microscopy (PLM)

Figure 62 shows polarised light microscope (PLM) images of POPC lipid, orlistat, POPC coated orlistat NPs and uncoated orlistat NPs (from A to D), on both bright and dark field (1 and 2). The experiment was done to indicate the coating of orlistat with POPC through comparing the optical path and birefringence of the prepared coated NPs to that of POPC.

Polarised light imaging confirmed the results of DSC, where images of the prepared POPC coated NPs shared remarkable similarity to that of POPC in terms of optical path and colour absorbance, indicating the coating of orlistat with an outer layer of POPC.

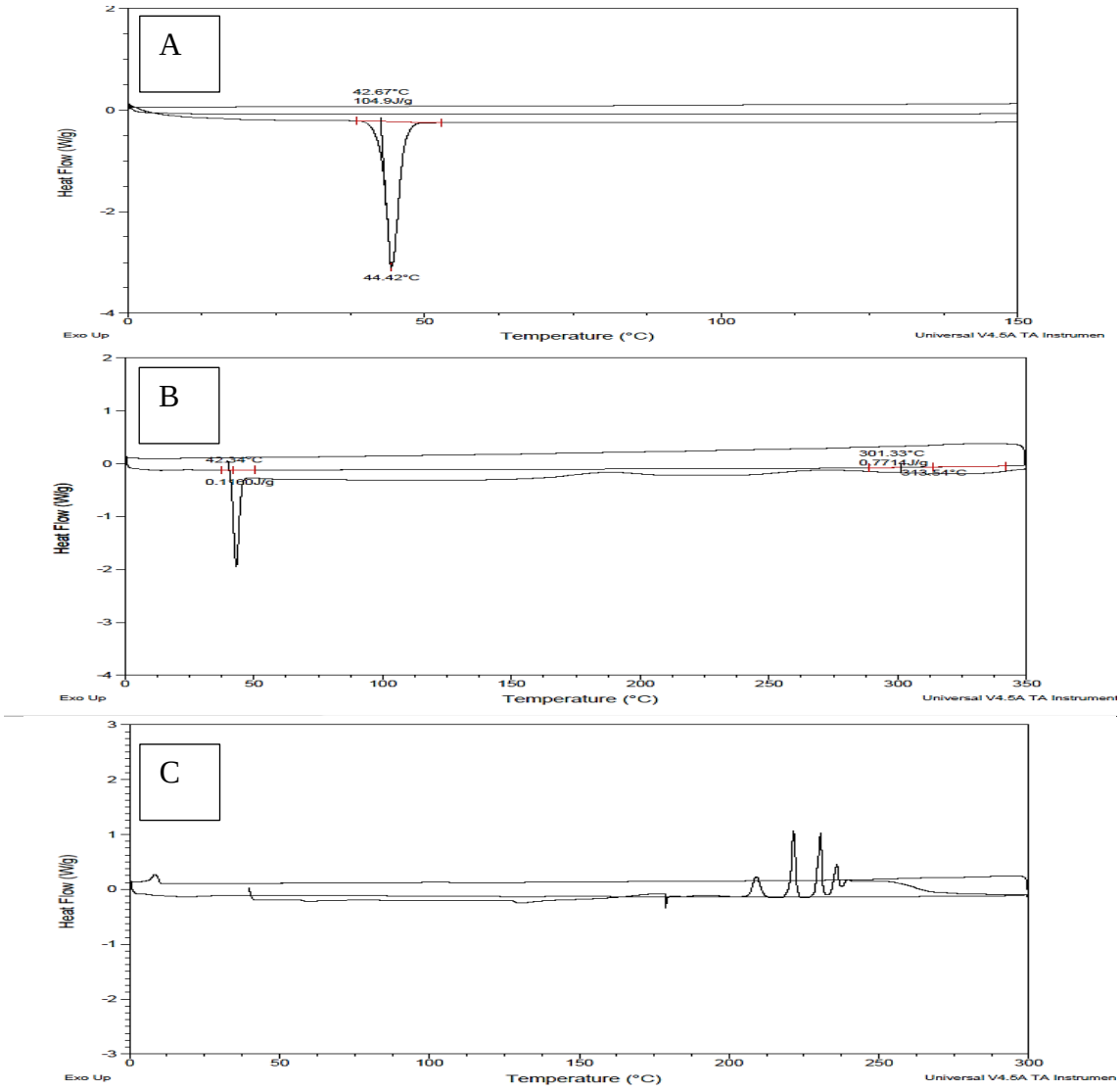

Figure 61 DSC thermograms of a heat cool heat cycle for A) pure orlistat, B) Orlistat and POPC physical mixture, C) POPC coated orlistat NPs.

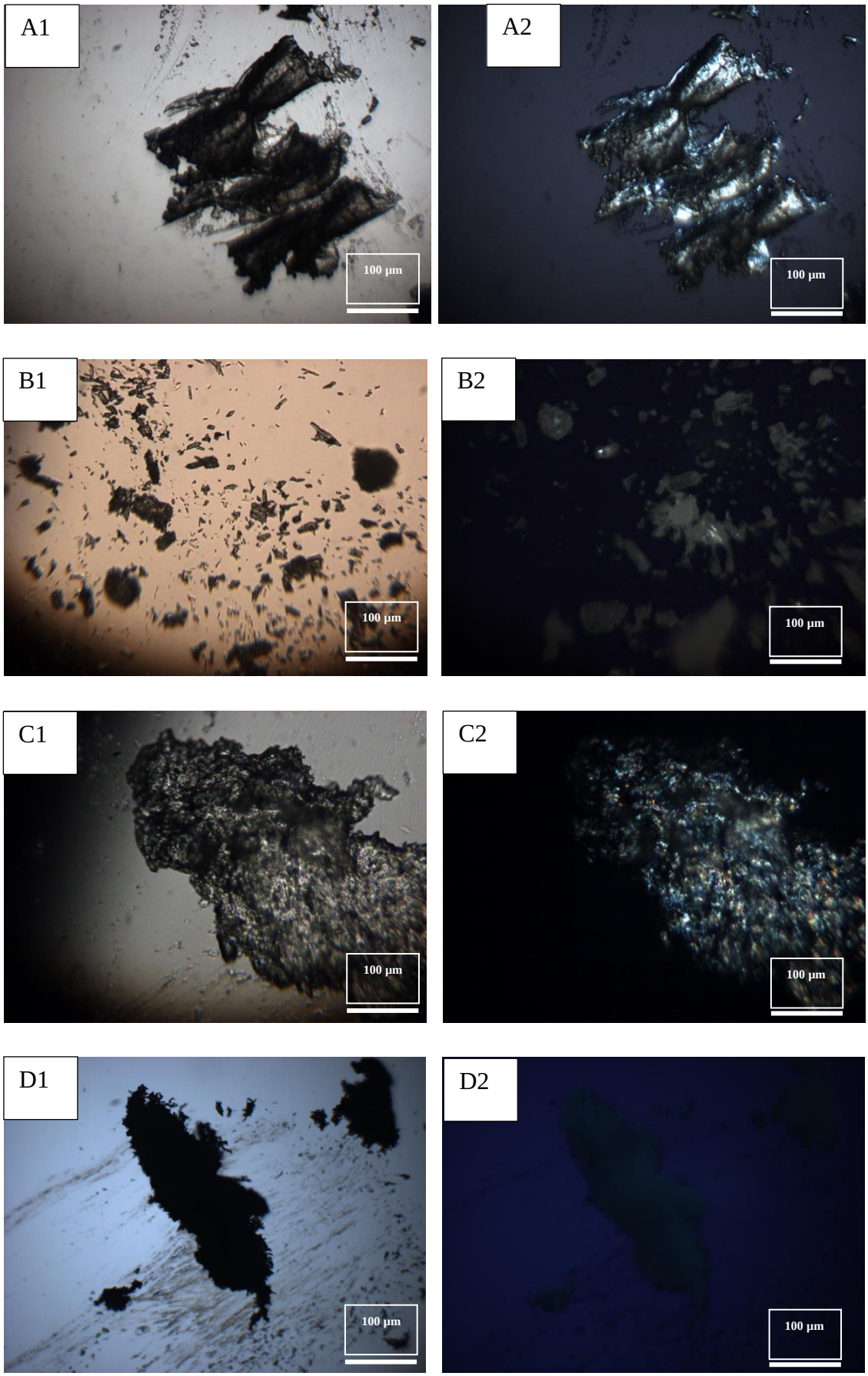

Figure 62 PLM images to show birefringence for A) POPC lipid, B) Orlistat, C) POPC coated orlistat NPs D) uncoated orlistat NPs, 1) Dark field, 2) bright field.

4.4.4 UV assay of orlistat

Scanning of orlistat solution (1 mg / ml) in ethanol showed a maximum wavelength of absorbance (λ_{max}) at 205 nm as shown in **Figure 63**. Calibration curve of orlistat (10- 150 µg / ml) in ethanol at 205 nm was plotted as shown in **Figure 64**, with a coefficient of correlation R^2 0.98. The method was further validated to ensure the accuracy of the results, with validation parameters for this method of assay were limited to linearity, inter-day precision, limit of detection (LOD) and limit of quantification (LOQ) data shown in **Table 4**. Results showed that the used method in this study was simple, and specific, with limit of detection (LOD) and limit of quantification (LOQ) 20 and 60 µg/ml respectively. The method will be further be used for determination of the drug concentrations in release study, drug loading, and entrapment efficiency experiments.

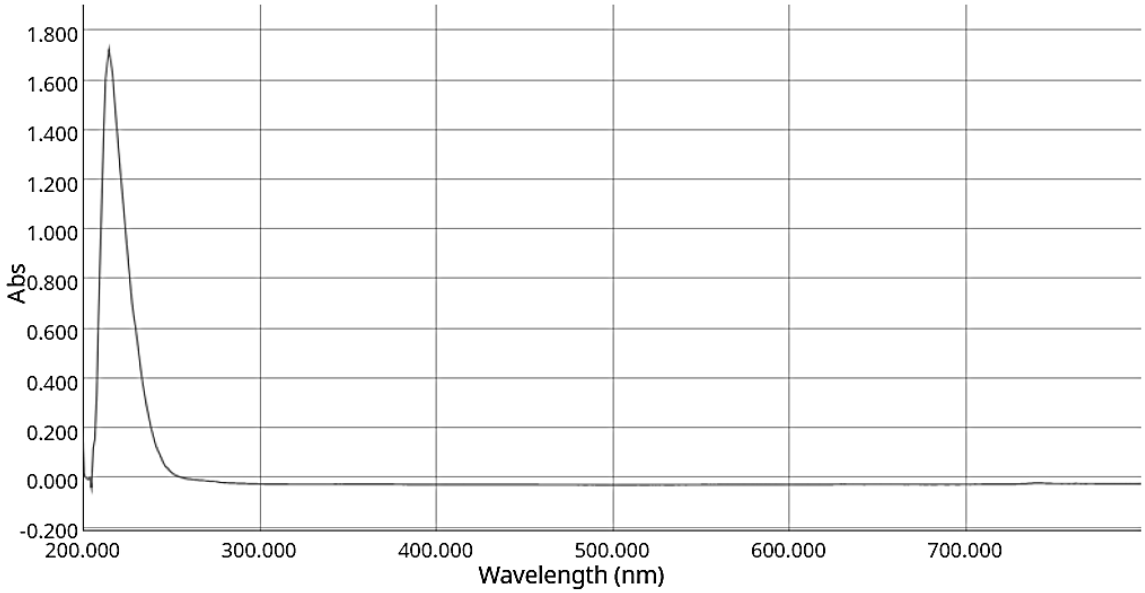

Figure 63 Absorption spectrum of 1 mg / ml orlistat solution prepared in ethanol.

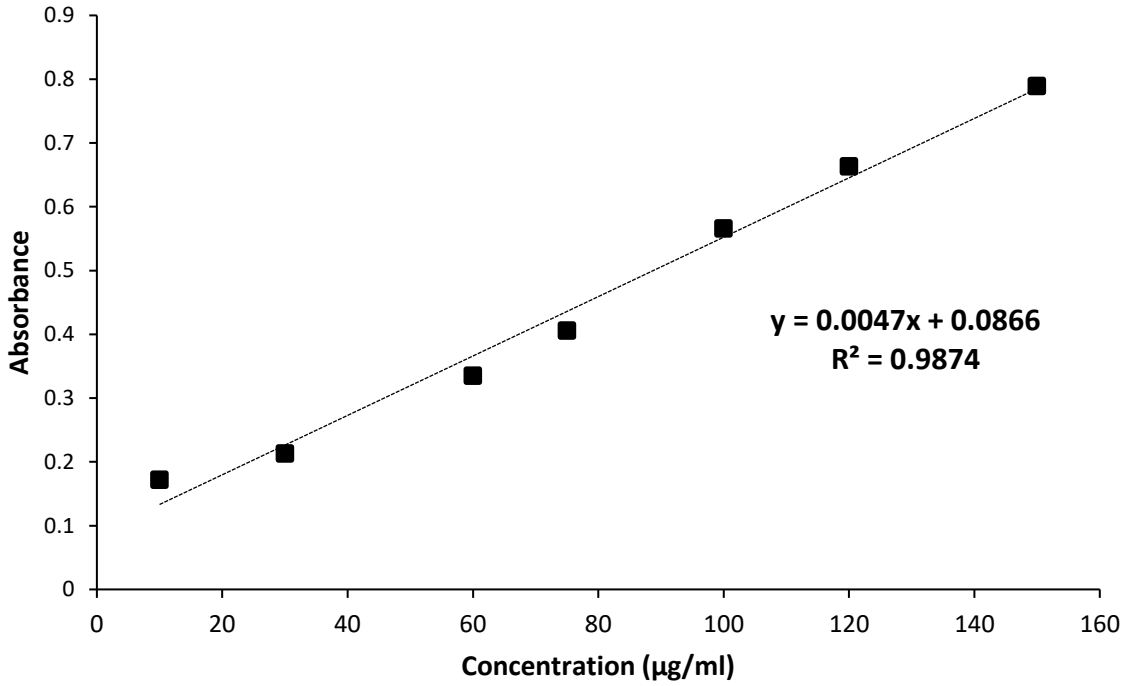

Figure 64 Calibration curve of orlistat solutions (10-150 µg/ml) in ethanol at λmax 205 nm.

Table 4 Validation parameters for UV spectroscopic assay of orlistat in ethanol.

Standard error of regression (STEYX)	0.028551833
Slope of regression	0.0047
Limit of detection (LOD)	20.04703182
Limit of quantification (LOQ)	60.74858126
Precision	R value 0.9874
Intraday variation	CV% is always < 2%

4.4.5 Drug loading and entrapment efficiency

Drug loading and entrapment efficiency (EE %) results are depicted in **Table 5**. To understand this, simply the entrapment efficiency (EE %) **(Equation 19)** is a ratio of the drug incorporated into the NPs to the total amount of the drug used; hence it reflects the efficiency of drug

incorporation in our system. The prepared POPC coated NPs showed EE% of an average between 73 & 79% measured using 2 different methods measured on two different days for different samples, the centrifugation ultrafiltration and dialysis respectively, data were measured as a mean of 3 samples ± SD, indicating the accuracy and repreducability of the results. This means that most of the drug is entrapped within the structure of the NPs and coated with the employed lipid, which in turns gives an indication on the efficiency of the rapid solvent shift technique as a simple method for coating hydrophobic drug moieties with lipids. On the other hand, drug loading percent known as loading efficiency (DL %) (**Equation 20**) is a ratio between the encapsulated drugs to the total weigh of the NPs, thus reflects the content of the drug in the total formulation, which is important for determination of the drug dose in the formulation. Interestingly, our orlistat NPs showed significantly high loading percent of 69% compared to the other NPs formulation in literature(149,228) due to the limited amount of used excipients in the formulation of the NPs structure.

Table 5 Encapsulation efficiency and drug loading percent for the prepared POPC coated orlistat NPs, n=3 ±SD.

Amount of drug in NPs (mg/3ml formulation)	Amount free drug (mg)	%EE CUF	%EE Dialysis	Loading efficiency
~ 6 mg	~ 1.2 – 1.3	73% ± 1.3	79% ± 1.3	69%

Equation 19 Entrapment Efficiency

$$\boldsymbol{Entrapment\ Efficiency}\ \% = \frac{(\boldsymbol{Total\ mass\ of\ drug\ in\ formulation\ -\ Free\ drug})}{\boldsymbol{Total\ mass\ of\ drug\ in\ formulation}} \times \mathbf{100}$$

Equation 20 Drug loading percent

$$\boldsymbol{Drug\ loading}\% = \frac{(\boldsymbol{Total\ mass\ of\ drug\ in\ formulation\ -\ Free\ drug})}{\boldsymbol{Total\ mass\ of\ nanoparticle}} \times \mathbf{100}$$

4.4.6 Drug release assay

The release of orlistat from the prepared POPC coated NPs was studied under physiological condition to have an insight of the expected behaviour of our prepared NPs under physiological conditions. **Figure 65** represents the release profile in terms of cumulative amount release, of the POPC coated orlistat NPs (2:1) of final concentration of 2 mM over a period of 7 days at 37 ºC and 350 rpm, the data was presented as a mean of 3 measurements with standard deviation.

The release profile of POPC coated orlistat NPs was of controlled manner, with initial burst effect and with sustained release over the 7 days. Drug release assay results shown in **Figure 65** display an initial burst release pattern after 24 hours, with around ~17 % of drug was freed and released in the first 24 hours, the reason behind this is attributed mainly to the presence of free unentrapped drug within the formulation, as agreed before the EE% was around 73-79%.

Afterwards, a slow sustained release pattern was observed over the following 3 days, with no more than 32% of the drug released after the full study. The incomplete release of drug from the coated NPs is attributed to the highly hydrophobic nature of orlistat which will prefer the lipophilicity of its coating structure to the hydrophilicity of the aqueous physiological release medium. This controlled release pattern is expected to ensure that the drug would be delivered within the intact coated nanoparticle structure to the targeted tumour cells, after which the NPs may be indulged and digested to release the drug inside the tumour cells(229).

The release study was carried out in physiological conditions, 37ºC and pH 7.4, however for futher understanding of the formulation behaviour in vivo, release study in serum would be a useful tool in future work.

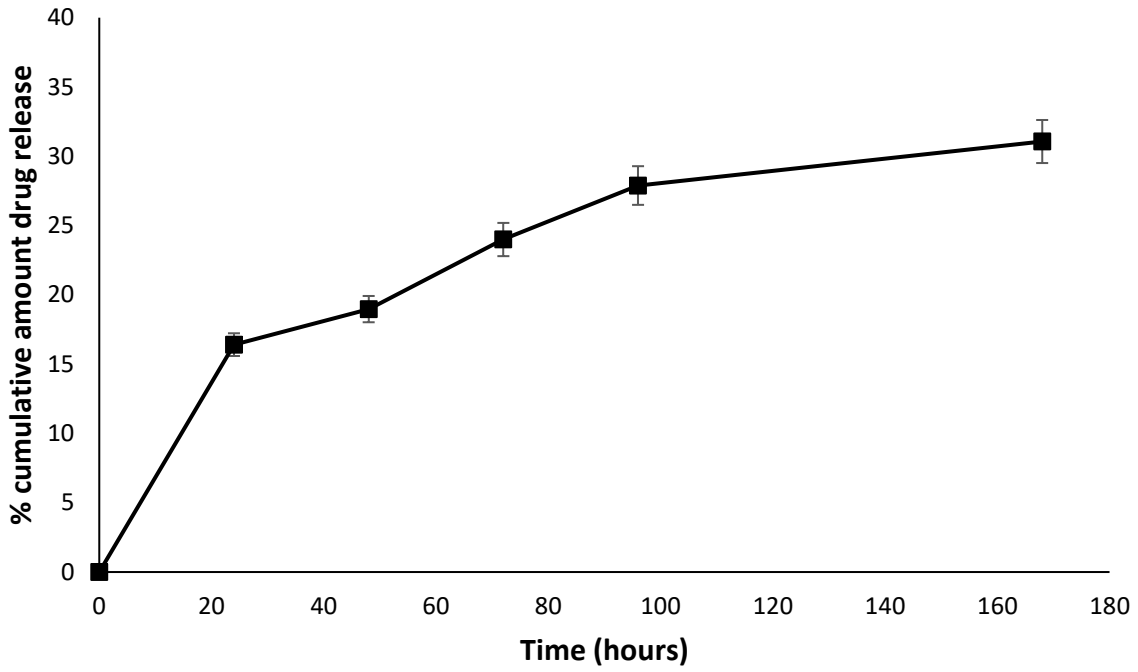

Figure 65 drug release assay for POPC coated orlistat NPs, performed in 400 ml PBS (pH 7.4) at 37ºC and 350 rpm, n=3 ±SD.

4.5 CONCLUSION

- Additional stabilisation of NPs against particle size growth and aggregation could be achieved through the use of various stabilisers, including surfactants and salts, which are added to the anti-solvent phase (SA1).
- Negatively charged surfactant, SDS was the best stabilising agent in prevent further aggregation and in controlling the size even after 2 weeks of storage. This is because of the repulsion forces implied between the particles (SA1).
- Further stabilisation of orlistat NPs could be done through freeze drying, to produce a solid powder for reconstitution, which will not only increase stability over the time, but as well help in better handling and ease of administration of the formulation (SA2).
- Freeze dried orlistat NPs where stable over a period of 6 month with minimal change in particle size and surface properties, this mainly depends on both the type and the amount of the used cryoprotectants (SA3).
- Trehalose in a range between 5-15% helped to conserve the size of the NPs after reconstitution following 6 months storage, while Mannitol failed in this aspect mainly due to the crystallinity of the sugar (SA3).
- Coating of orlistat with POPC was successful in incorporating the drug inside a layer of the lipid in an amorphous mixture, this was shown through the disappearance of the orlistat peak in the DSC thermograms of POPC coated NPs (SA4).
- The coated orlistat NPs with POPC showed similar images with similar light birefringence under the polarised microscope to that of the POPC lipid indicating the presence of the POPC on the surface of the NPs structure (SA4).

- Our NPs formulation prepared through the rapid solvent shift technique showed a high entrapment efficiency of 73-76% with a loading efficiency of 60% which is promising in dose adjustment compared to other NPs formulations (SA5).
- The drug release study showed that the orlistat NPs kept its structure for long period of time in physiological conditions, with no more than 40% of the drug was released from the NPs structure after 1 week. This is required to ensure the delivery of the intact NPs structure in the systemic circulation to the tumour cells, where it could release the drug (SA5).

5 Chapter 5 Surface-functionalised LDL-like orlistat nanoparticles

5.1 INTRODUCTION

5.1.1 LDL-like nanoparticles

In the 1960s, nanotechnology was introduced by Richard P. Feynman, since then it has been an interesting subject for investigation and application in numerous medical, industrial, and environmental fields(230). Various naturally existing organic and inorganic nanoparticles have been present before they were synthesized in labs. Among the naturally occurring nanoparticles is the low-density lipoprotein (LDL), a normal blood constituent, serving as a means of cholesterol delivery to tissues. Cholesterol is one of the main constituents of the cell membranes. Cells get their cholesterol requirement either through making it themselves, taking it up from LDL, or both. Distinctly, being of high proliferation rate, tumour cells need substantial amounts of cholesterol, obtained chiefly from LDL, to establish new membranes. Thus, LDL could be used as a vehicle to carry antitumor drugs, consequently acting as an excellent targeting modality, this concept was introduced in 1981 (231).

5.1.1.1 LDL Structure

The structure of natural LDL is well studied (**Figure 66**). It consists of spherical particles around 22 nm (220 Angstroms) in diameter containing approximately 1500 molecules of cholesterol in the form of nonpolar core, part of them is esterified with long-chain fatty acids such as oleate or linoleate. In the vicinity of the core is a micellar oriented phospholipid layer with the polar heads outward and the hydrophobic fatty acid chains inwards.

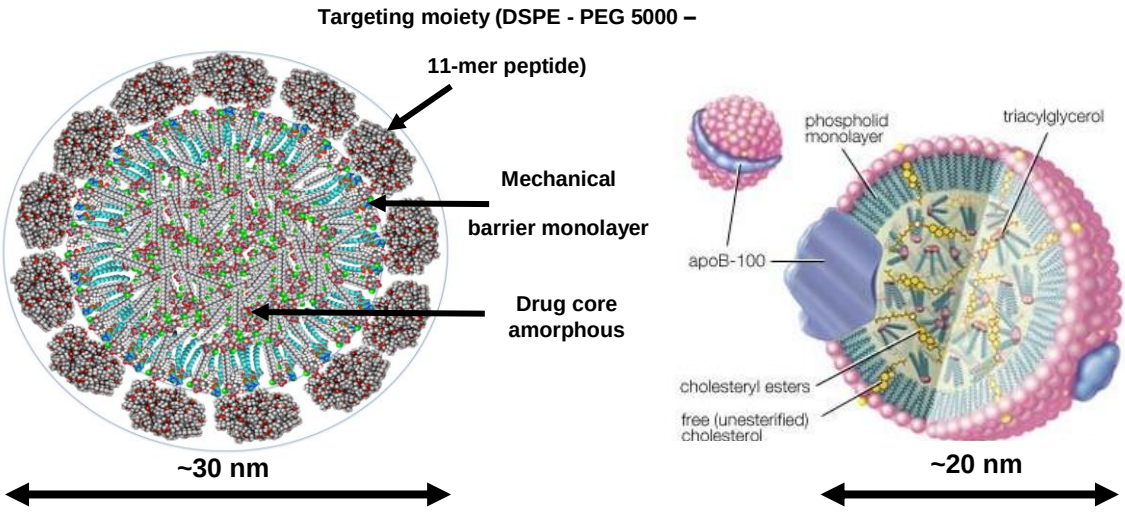

Figure 66 Schematic presentation of the LDL- like nanoparticle compared to a cutaway schematic of the LDL(232)

The phospholipid layer is mixed with unesterified cholesterol, apparently acting as a stabilizer, and also a single molecule of apoprotein B per LDL particle which binds to specific cell surface LDL receptors. Following receptor binding, the complex is internalized by endocytosis and indulged to the lysosomes, where the cholesteryl esters are hydrolysed, releasing free cholesterol to the cell. The LDL receptors are then recycled to the cell surface. The mechanism of the LDL system was illustrated by Brown, Goldstein, and co-workers (233–235).

5.1.1.2 LDL- receptors

Concerning the low-density lipoprotein receptor (LDLR), it consists of a single-chain transmembrane glycoprotein (236). The LDLR structure is formed of five major parts: a ligand binding centre, epidermal growth factor (EGF) domain, O-linked sugar part, membrane-spanning domain, and cytoplasmic tail (237). The role of LDL receptor is to transport chiefly the cholesterol-rich LDL into cells through receptor-mediated endocytosis, mainly through the clathrin-dependent pathway (236). Recently, much evidence was found that the uptake of LDL could occur through both receptor and non-receptor-mediated pathways, yet on average, two thirds of the LDL is internalised by receptor-mediated pathway (238). The LDL particle binds

to the LDLR embedded in clathrin on the cell surface through binding site found on the Apo B protein moiety in the LDL structure(237).

5.1.1.3 LDL Nanoparticles

As mentioned before, malignant cells have high LDL requirements. Indeed, there is a great tendency for rapid growing cells (as in case of cancer) to acquire cholesterol from LDL, while for the differentiated normal cells to synthesize it (239). Early reports describing the relation between cancer and LDL were published in 1978, they showed that human acute myeloid leukaemia (AML) cells uptake up to 100 times more LDL than normal cells(240,241). More studies showed that some human solid tumours are also craving for LDL as in case of endometrial adenocarcinoma and four other gynaecologic cancers which have greater LDL uptake than normal cervical tissues(242). Moreover, Gastric carcinoma and parotid adenoma exceeded normal cell types in LDL uptake(243). Many brain tumours especially medulloblastoma, oligodendroglioma, and malignant meningioma can bind 2-3 times more LDL than normal brain cells (244). As tumour cells uptake abnormally large amounts of LDL, there would be a likelihood of a decrease in plasma cholesterol levels in cancer patients. This has been first reported in 1939 when it was observed that leukaemia patients had remarkably low blood cholesterol level (245).

Besides the potential targeting benefits of LDL, their use as a drug carrier may circumvent many of the issues encountered with other synthetic carriers(246)**,** there has been much work through the past decade concerning the use of LDL nanoparticles as theranostic platform. LDL nanocarrier system has important advantages compared to other nano delivery systems(174). LDL nanoparticles (LDL NPs) resemble naturally occurring carriers; therefore, they are considered biocompatible as they would be able to escape recognition by the reticuloendothelial system (RES). Additionally, LDL NPs are biodegradable, small in particle size (~18–25 nm) which is within the optimum nanoparticles size range. LDL NPs are suitable

for hydrophobic drugs, which can be loaded in the hydrophobic core or even constitute the whole core. Moreover, drugs incorporated can escape hydrolytic and enzymatic degradation in the plasma, as the LDL is a normal constituent of the blood. Furthermore, LDL NPs may prolong the biological half-life of drugs because they are not cleared by the reticuloendothelial system RES. They can be easily targeted to tumour cells because the LDLR is highly expressed in most tumour cells(137).

The LDL nanoparticles is suggested to be prepared by using the rapid solvent shifting technique (151) which provides control over fundamental parameters of the fabrication process and can be easily scaled up for pharmaceutical industrial purposes.

5.2 AIMS AND OBJECTIVES

The main objective of the work is to evaluate the functionalised LDL-like orlistat loaded NPs, in terms of physicochemical properties and efficacy on cancer cell lines.

The prepared LDL-like NPs were compared to other orlistat NPs formulation to evaluate the effect of peptide moiety on the overall behaviour of the formulation.

SA1: Investigating the efficacy of the proposed click chemistry technique on the complete conjugation of the 11-mer peptide to the lipid moiety of the NPs.

SA 2: Investigating the effect of the addition of the 11-mer peptide to the NPs surface on the particle size and surface charge.

SA 3: Evaluation of the behaviour of our prepared formulation in culture media, prior to their use in cell work. This is evaluated in terms of albumin binding assay and particle size stability.

SA 4: Evaluation of the efficacy of our proposed orlistat NPs LDL-like formulations as a targeted anti-cancer medicine. This is done through evaluation of cytotoxicity and cellular uptake on different breast cancer cell line.

5.3 MATERIALS AND METHODS

5.3.1 Materials

Orlistat (Merck life science, >98% purity), 1-palmitoyl-2-oleoyl phosphatidyl choline (POPC) (Merck life science, TLC >99% purity), DSPC (Di stearoyl phosphatidylcholine) (Stratech scientific ltd., Avanti polar lipids > 99% purity, **Figure 67 B**), DSPE PEG 5000 maleimide(Stratech scientific ltd., Avanti polar lipids > 99% purity **Figure 67 A**), Cholesterol (Stratech scientific ltd.,> 99% purity **Figure 67 C**), (ThermoFisher scientific, >97% purity), Sodium dodecyl sulfate (SDS) (Sigma Aldrich, ACS reagent 99% purity), (Sigma Aldrich, ACS reagent 99% purity) , Ellman's reagent powder 5,5'-dithio-*bis*-(2-nitrobenzoic acid) (DTNB) (Fisher scientific ltd, at least 99% pure), pure ethanol (Sigma Aldrich, anhydrous pure >99.5%), 1-mercapto undecanol (Sigma Aldrich, 97% purity), culture medium Dulbecco's Modified Eagle Medium DMEM (VWR scientific ltd. Sterile filtered), phenol red free RPMI medium (ThermoFisher scientific, sterile filtered), Human serum albumin HSA (Merck life science, lyophilized powder, 97% purity agarose gel electrophoresis), 25-NBD cholesterol (Scientific laboratory supplies ltd, Avanti polar lipids, <99% purity), Suramin (Sigma Aldrich >98% purity), breast cancer cell lines MCF-7, BT474 and MDA MB 453 (all supplied by American type culture collection (ATCC) Manassas VA, and stored in liquid nitrogen until used) were grown in DMEM (BT-474, MDA MB 453) or RPMI (MCF-7) with 2% bovine serum albumin (BSA) and 1% penicillin-streptomycin, and MilliQ® water. All other materials were of analytical grade and used as supplied, unless otherwise mentioned.

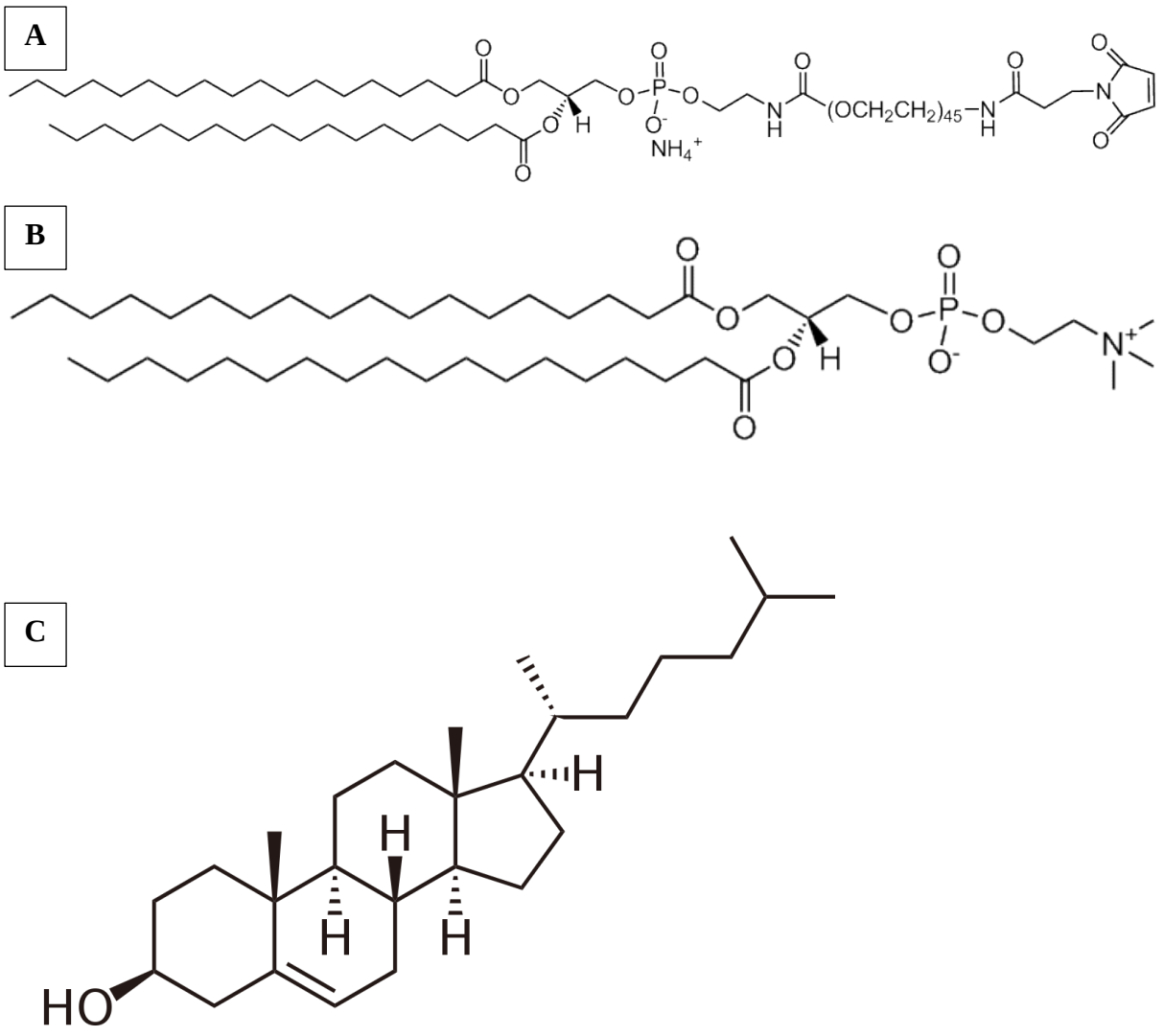

Figure 67 Chemical structure of employed lipids A) DSPE PEG 5000 maleimide, B) DSPC and C) cholesterol.

5.3.2 Methods

5.3.2.1 Preparation of functionalised NPs

Orlistat NPs were functionalised to resemble the structure of the LDL, using a mixture of phospholipids and cholesterol, together with 11-mer peptide that mimics the active site of the apoprotein B in structure. The purchased 11-Mer peptide was prepared with an amino acid sequence [NH_2] CGGSRLTRKRGLKLA [COOH] (Cys-Gly-Gly-Ser-Arg-Leu-Thr-Arg-Lys-Arg-Gly-Leu-Lys-Leu-Ala) (Biosynthesis® Inc USA).

NPs were prepared using the straightforward solvent shift technique. Simply, ethanolic solution of the drug together with a mixture of the phospholipids (A-POPC or B-DSPC), Cholesterol and DSPE PEG 5000 maleimide peptide conjugate in a molar ratio 45:50:5 respectively (with a coat to core molar ratio 1: 1.6) were directly injected into water under stirring as mentioned before.

Concerning DSPE PEG 500 maleimide peptide conjugate, it was prepared by simple click chemistry between the sulfhydryl group of the cysteine amino acid and the maleimide group of the lipid moiety. This is done through incubation of the 11-mer peptide together with DSPE PEG 5000 maleimide in phosphate buffer saline in a molar ratio 1:1 for 24 hours to ensure complete conjugation, followed incorporation of the conjugate into the NPs. Another method was adopted through incorporation of the peptide added into the anti-solvent aqueous PBS and the NPs were prepared as previously mentioned and incubated for 24 hours. The exact composition of the NPs formulations is shown in **Table 6**.

The prepared conjugated NPs were tested for the particle size using DLS and TEM and for the surface charge and zeta potential as well.

5.3.2.1.1 Ellman's test for free sulfhydryl groups

The efficiency of the peptide conjugation to the lipid moiety was confirmed using Ellman's test for the free sulfhydryl groups. To prepare Ellman's reagent, 1 mL of reaction buffer (0.1M sodium phosphate with 1 mM EDTA, pH 8.0) was added to 4 mg Ellman's powder followed by vortexing for 1 minute at RT. Afterwards, 2.5 uL of 4 mg/mL Ellman's reagent was added to 100 uL of sample of interest or buffer only as blank, the absorbance of the samples was measured using UV/Vis spectrophotometer at λ_{max} 412 nm(169). The concentration of the free sulfhydryls was calculated using the extinction coefficient of E = 14150 $M^{-1}cm^{-1}$ (247). The test was carried out for 11-mercapto undecanol as a reference, the 11-mer peptide solution, DSPE PEG 5000 maleimide peptide conjugate, and the peptide functionalized orlistat NPs.

Table 6 Composition of various surface functionalised LDL NPs formulations.

Formula code	Lipid coat constituents	Anti-solvent used
A1	POPC 45% Cholesterol 50% DSPE PEG (5000) maleimide 5%	MilliQ water
A2	POPC 45% Cholesterol 50% DSPE PEG (5000) maleimide 5	3 mM sodium dodecyl sulfate SDS in MilliQ water
A3	POPC 45% Cholesterol 50% DSPE PEG (5000) maleimide 5	2% Tween 80
B1	DSPC 45% Cholesterol 50% DSPE PEG (5000) maleimide 5	MilliQ water
B2	DSPC 45% Cholesterol 50% DSPE PEG (5000) maleimide 5	3 mM sodium dodecyl sulfate SDS in MilliQ water
B3	DSPC 45% Cholesterol 50% DSPE PEG (5000) maleimide 5	2 % Tween 80

5.3.2.1.2 TEM imaging of NPs

TEM images of NPs were captured using negative staining. Samples were prepared, stained using 2% uranyl acetate, fixed over carbon coated copper mesh grids. TEM imaging was done using FEI® Tecnai Biotwin transmission electron microscope (Eindhoven, The Netherlands, located at the NMRC facility University of Nottingham) at 100 KV, equipped with a camera Eagle 4K CCD (Eindhoven, The Netherlands), and TIA software (FEI®) (Eindhoven, The Netherlands).

5.3.2.2 Investigation the effect culture medium on POPC coated orlistat NPs

POPC coated orlistat NPs were prepared either in MilliQ® water and diluted with culture medium (DMEM) or prepared directly in the culture medium (DMEM). The purpose of this study is to have an idea about the stability of the prepared NPs in culture medium in terms of particle size and surface charge (Zeta potential). Preparation of the NPs was done through nanoprecipitation technique using the rapid solvent shift technique as mentioned before. Briefly, POPC together with orlistat was dissolved in ethanol at core to coat molar ratio, of (2:1), and initial concentration of orlistat of 40 mM. Then NPs were prepared through injecting 0.5 ml of each ethanolic solution into 4.5 ml of MilliQ® water containing 3 mM SDS or 4.5 of DMEM, using eVol™ syringe injector. For the POPC coated orlistat NPs prepared in water, they were further diluted into culture medium DMEM to get final concentrations of (1.4, 0.8, 0.4, 0.2, 0.04 mM) respectively.

All the prepared nanoparticle dispersions are subjected immediately to particle size and zeta potential analysis. This was done through pipetting 1 ml of each dispersion of different concentration into either cuvette (for particle size) or zeta cell (for zeta potential), followed by running the analysis at 25ºC, auto-attenuator and wavelength 600 nm.

5.3.2.3 Investigation of orlistat binding to albumin

Binding of orlistat to albumin was studied to investigate the effect of albumin in culture medium on binding to orlistat, which may affect the behaviour of cellular uptake, this would give us further understanding for the behaviour of orlistat when we carry out cell studies(248–250).

Orlistat binding assay was carried out through a fluorescent quenching technique using Fluorescence spectrophotometer, (Agilent® Cary eclipse fluorescence spectrophotometer, USA). First of all, the fluorescence spectrum of human serum albumin (HSA) was studied through scanning a sample of 1.5 μM HSA prepared in PBS (pH 7.4), Fluorescence spectra

were recorded in the range of 300 - 600 nm after excitation at 280 nm and the bandwidth for measuring emission was 5 nm(170). Afterwards 20 uL of stock orlistat ethanolic solution (prepared in stock of 1 mM) were added to the HSA solution, with the final concentration of drug kept in range of 20 to 100 μM (20, 40, 60 100 μM). The fluorescence emission spectra of HSA in the absence and presence of increasing amounts of orlistat were recorded, all data were the average of three scans ±SD. Regarding the quenching effect of ethanol, it is widely studied in literature and the result indicated that there is almost no effect of ethanol on the interaction(251).

The data were analysed by the Stern–Volmer equation(171)

$$\frac{F_0}{F} = 1 + K_q\tau_0[Q] = 1 + K_{SV}[Q]$$ **Equation 21 Stern-Volmer equation**

where F_0 and F are the steady-state fluorescence intensities in the absence and presence of quencher (orlistat), respectively

K_q the bimolecular quenching rate constant,

τ_0 the lifetime of fluorescence in absence of quencher,

K_{SV} the Stern–Volmer quenching constant,

[Q] the concentration of quencher.

Hence the above equation could be applied to determine K_{SV} by linear regression of a plot of F_0/F against [Q].

5.3.2.4 Cytotoxicity assay of NPs Formulations

Three different breast cancer cell lines were used for the cytotoxicity assay, BT-474, MDA MB453 and MCF-7 respectively, this was in order to have a wide range of data across different breast cancer cell lines which will be discussed in the results section.

For the cell growth MCF-7 cell line was grown in phenol red free RPMI medium, while for the other 2 cell lines (BT-474 and MDA MB 453), they were grown in DMEM culture media.

After proliferation, cells of each cell line separately were seeded in a 384 well plate, at 1000 cells per well in their cells regular medium. Afterwards, cells were incubated at 37ºC, and 5% CO_2.

For the cytotoxicity assay, formulations (orlistat in ethanol, POPC coated orlistat NPs in PBS, peptide coated Triolein NPs in PBS and Peptide coated orlistat NPs in PBS all prepared at concentration of 200 µM, and the 2 solvents employed ethanol and PBS) were added separately at required concentrations (6 replicates per concentration), using a 1:2 serial dilution in culture media (100 µM, 50 µM, 25 µM, 12.5 µM, 6.25 µM, 3.125 µM, 1.6 µM, 0.8 µM, 0.4 µM and 0.2 µM). Then cells were incubated at 37 ºC, 5% CO_2 for 48 hours.

After the 48 hours, cells were inspected under the microscope, where none of the wells should be over confluent. Afterwards, 5 µl of Presto Blue was added to each well separately, followed by incubating the plates in the incubator for 1 hour at 37 ºC, and 5% CO_2.

The cytotoxicity was assayed by measuring the fluorescence using Presto Blue settings (Emission wavelength of 535 nm, Excitation wavelength: 615 nm) using Fluostar® Omega plate reader spectrofluorometry (BMG Labtech, Germany). Data was analysed for the IC_{50} and for the cell viability curves using GraphPad Prism® software, and expressed as mean of the 6 replicates ± SD.

5.3.2.5 Cellular uptake study

The cellular uptake was done through fluorescence imaging of the fluorescent labelled NPs formulation in the 3 different breast cancer cell line (MCF-7, BT-474, and MDA MB 453).

5.3.2.5.1 Fluorescence labelling of the NPs formulations

Fluorescent labelling of our NP formulations was done through incorporation of an intrinsic fluorescent cholesterol, 25-NBD cholesterol, into the structure of the NPs during their preparation. Two distinctive formulations (F1 and F2) were prepared for comparison reasons,

the first one (F1) is lipid coated ORL NPs with no peptide incorporated, while the second one (F2) is the LDL-like ORL NPs with the 11-mer peptide moiety. Both formulations contain an amount of 25-NBD cholesterol equals to 10% of the total cholesterol mass in each formulation and prepared by rapid solvent shift technique as described before with final ORL concentration of 400 µM. It is worth mentioning that for the lipid coated ORL NPs with no peptide incorporated, the structure of the lipid coat included POPC and cholesterol in a molar ratio of 1:1, with a core (ORL) to coat molar ratio of 2:1.

5.3.2.5.2 Fluorescent imaging for cellular uptake

The three cell lines were grown in culture media as descried before, and then were seeded separately in 24 well plates, at cell density of $1x10^5$ cells/well, and incubated at 37ºC, and 5% CO_2.

Afterwards cells were washed with PBS three times and were treated separately with both formulations previously mentioned, after being diluted to desired concentrations using the corresponding culture medium. Two different concentrations of both formulations were used for each cell type, the first one is 100 µM and the other one the calculated IC_{50} of the LDL-like ORL NPs from the cytotoxicity assay for each cell line (8 µM, 40 µM, and 65 µM for MCF-7, BT-474 and MDA MB 453 respectively). Each of the 2 formulations were added to the cells in 6 replicates for both concentrations. Afterwards cells were incubated at 37 ºC, and 5% CO_2 for the desired time intervals. Cellular uptake was evaluated at time intervals of 1 hr, 2 hrs, 4 hrs, 8 hrs and 24 hrs using fluorescent microscope (EVOS M5000 Imaging System, ThermoFisher Scientific, USA).

Afterwards images obtained were evaluated using ImageJ® photo editor package to determine the fluorescence peaks and the mean fluorescence intensity of each image as densitogram.

5.3.2.5.3 Cellular uptake mechanism

Investigation of the cellular uptake of our novel LDL-Like NPs through LDLR was done through the use of LDLR blocker Suramin(136,252). The cellular uptake mechanism was investigated through treating the three breast cancer cell lines with the two previously mentioned formulations (F1, F2) at 100 µM ORL concentration in two groups, the treatment group and control group. The treatment group involved the treatment of the three cell lines separately with 10 mM Suramin PBS solution for 1 hours, followed by washing the cells and addition of the formulations (either F1 or F2), while the control group included the use of the formulations (either F1 or F2) without treatment with the blocker Suramin. The cellular uptake was evaluated as previously mentioned and the Intensity of the fluorescence was evaluated using ImageJ®.

5.3.2.6 Statistical analysis

Statistical analysis for the results was done to determine the significance differences between samples. Two-way ANOVA test was utilised using GraphPad Prism® software.

5.4 RESULTS AND DISCUSSION

5.4.1 Functionalised LDL-like Orlistat NPs

Solvent shift technique(112) was adopted to prepare LDL like NPs, the structure of which will resemble the natural LDL. The suggested structure of the LDL-like NPs is shown in **Figure 68**. Simply it consists of a core formed of the drug orlistat, coated with a layer of lipids, at a core to coat ratio of (1.6:1). The coating layer consists of a mixture of Cholesterol and phospholipids (either DSPC or POPC) and PEGylated phospholipid (DSPE PEG 5000 maleimide) to which the peptide moiety is attached to resemble the apoprotein moiety in LDL, the lipid ratio is (50:45:5) respectively. The PEGylation of the NPs using PEG-phospholipids will help the formulation to avoid being recognised by the reticuloendothelial system (RES) in vivo, and hence enhancing its bioavailability by avoiding clearance of NPs in blood stream(253).

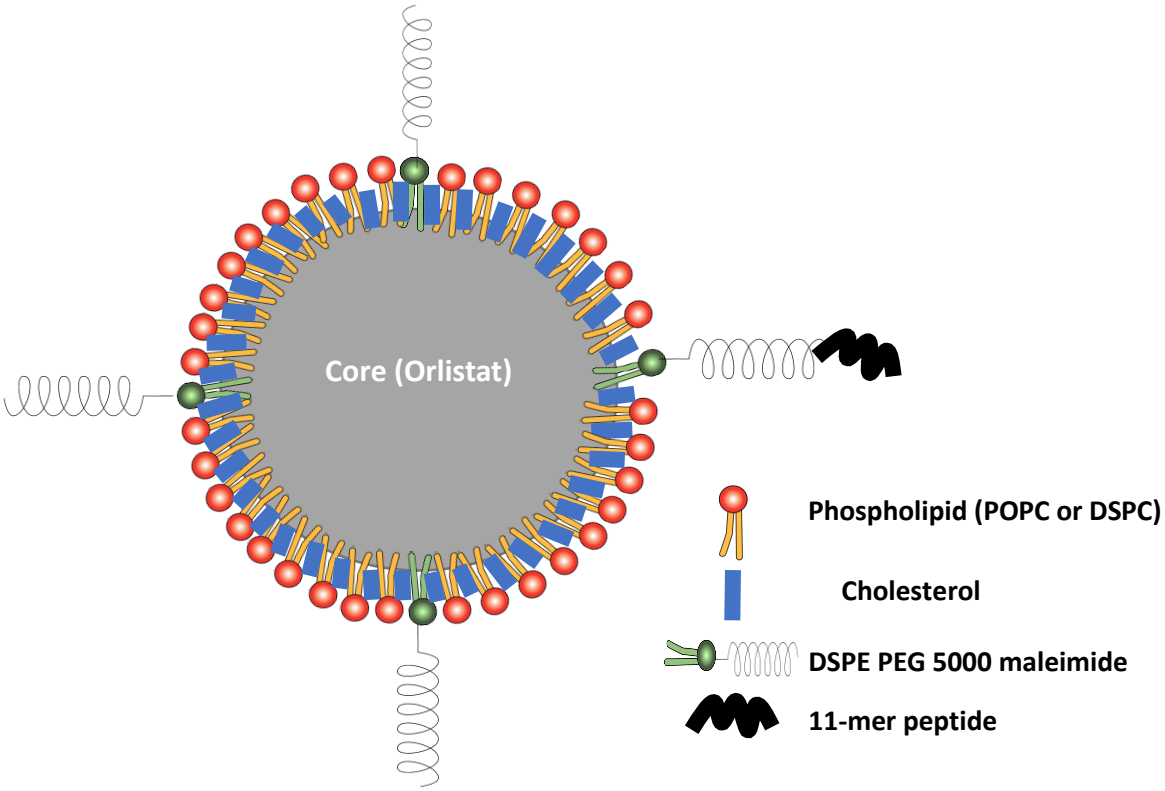

Figure 68 Structure of LDL-like NPs

5.4.1.1 11-Mer peptide evaluation

The peptide moiety that was chosen to be added to the NPs formulation is an 11-mer peptide that resembles the active moiety of Apoprotein B structure, which is responsible for attachment to the LDL receptors(254,255). The 11-mer peptide is significantly small in size compared to the apoprotein structure, and hence is expected to help us control the size of the prepared LDL-like NPs. The 11-mer peptide structure is [NH_2] CGGSRLTRKRGLKLA [COOH] (Cys-Gly-Gly-Ser-Arg-Leu-Thr-Arg-Lys-Arg-Gly-Leu-Lys-Leu-Ala), with a cysteine moiety found on the N terminus of the peptide, which will be attached to the maleimide group in the lipid coat by click chemistry. The supplied 11-mer peptide was of molecular weight = 1615 as confirmed by Mass spectroscopy (**Figure 69A**) and was of high purity > 97% as confirmed by HPLC analysis certificate from the supplier (**Figure 69 B**).

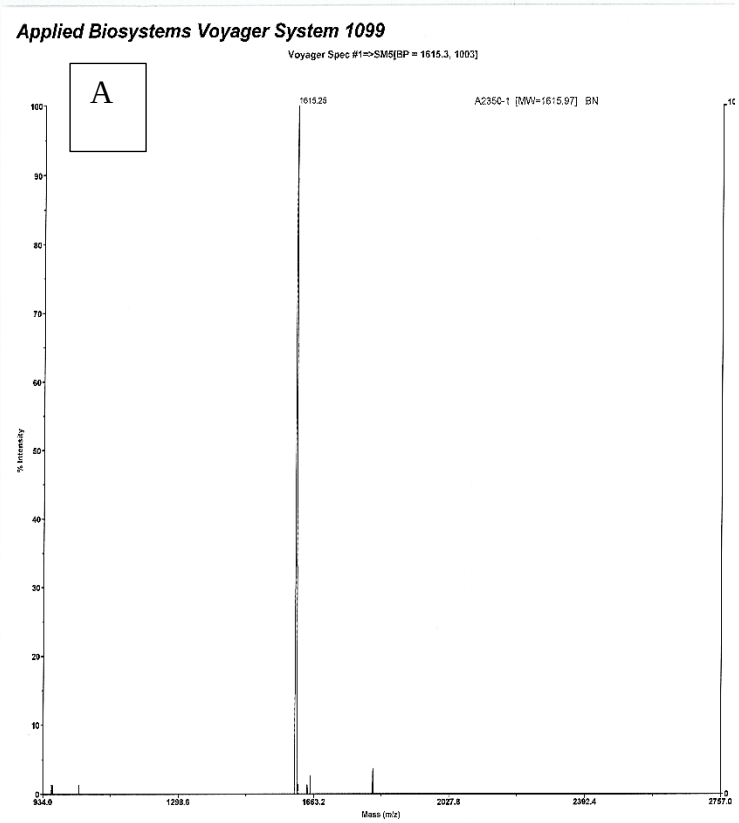

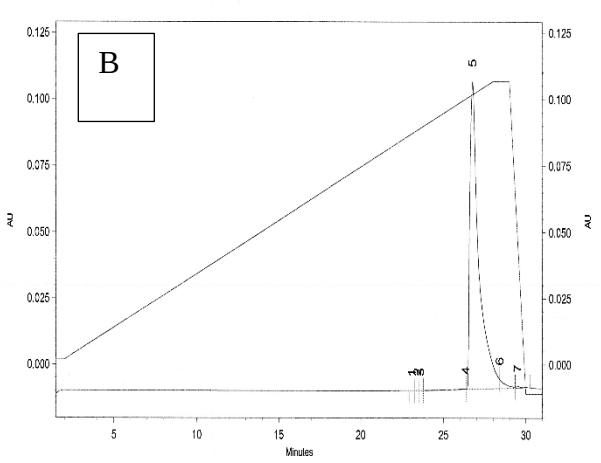

Pk #	Retention Time	Area	Area Percent
1	23.117	418	0.009
2	23.433	606	0.014
3	23.617	359	0.008
4	26.350	629	0.014
5	26.767	4316309	97.840
6	28.400	76173	1.727
7	29.467	17119	0.388
Totals		4411613	100.000

Figure 69 11-mer peptide analysis certificate, A) Mass spectroscopy showing molecular weight, B) HPLC assay showing purity.

5.4.1.2 Evaluation of efficiency of conjugation (Ellman's test)

The efficiency of click chemistry employed for attaching the peptide to the phospholipid moiety was assayed using Ellman's assay(169). The assay was done to show the percentage of free sulfhydryl groups in each formulation. The lower the free sulfhydryl groups content, the higher is the degree of conjugation. As shown in **Table 7**, the percentage of free sulfhydryl groups in our DSPE PEG 5000 peptide conjugate was found to be at minimal level of 0.6%, compared to the free peptide (>60%) and to 11-mercapto undecanol as reference (>80%). This was as well confirmed after incorporation of the conjugate into LDL-like NPs with either POPC or DSPC, where the free sulfhydryl was no more that 0.7%.This results emphasize the success of our click chemistry for the lipid-peptide conjugation, as it resulted in conjugation of most of the sulfhydryl groups of the cysteine moiety of the peptide with the DSPE PEG 5000 lipid moiety, which will reassure coating of our NPs with a peptide moiety on its surface thereafter.

Table 7 percentage free sulfhydryl groups determined by Ellman's assay

Formulation	Concentration (mM)	Concentration of free SH (mM) in 0.1mM sample	% Free sulfhydryl groups
11 mercapto undecanol (reference)	0.072226148	0.0722	80%
Peptide solution	0.057809187	0.0578	60%
DSPE PEG 5000 peptide conjugate	0.001034483	0.00051	0.6%
POPC coated peptide NPs	0.006289753	0.00063	0.7%
DSPC coated peptide NPs	0.006784452	0.00068	0.7%

5.4.2 Effect of peptide coating on the NPs characteristics

Preliminary investigation of particle size and surface charge of the prepared LDL-like NPs was done to explore the effect of peptide coating on the overall size and surface charge of the NPs. **Figure 70** illustrates the particle size distribution of the peptide coated orlistat NPs prepared with two lipids either POPC or DSPC as mentioned before (**Table 6**) and prepared in 3 different media either water, 2% tween 80 or 3 mM SDS, in comparison to the particle size distribution of the uncoated orlistat NPs and the POPC coated orlistat NPs.

Concerning the particle size (**Figure 70**), peptide coating did not show any significant increase of size compared to that without peptide coating at any of the employed media. However, peptide coating of orlistat in presence of POPC resulted in apparent size reduction compared to those formulations without peptide coating and to that with DSPC as the incorporated phospholipid. This could be attributed to the presence of cholesterol as lipid in the structure of the final peptide coating, which may result in proper and intact coating around the precipitated orlistat and prevents it from further growth in size. Additionally, presence of the PEG moiety which confers a steric hindrance against aggregation and the small size of the 11-mer peptide employed will help in further avoidance of condensation or size increase as well. For the POPC, being an unsaturated phospholipid compared to DSPC which is saturated phospholipid, it is suggested that its structure gives a steric resilience(256), which may help in proper coating of the particles and hence preventing the condensation.

Figure 71 shows the TEM of the peptide coated POPC orlistat NPs at final orlistat concentration of 2mM. As shown by TEM images (**Figure 71**) the morphology of the prepared particles was not affected, peptide coated particles were roughly spherical with average particle size of 35 nm as counted by Image J®.

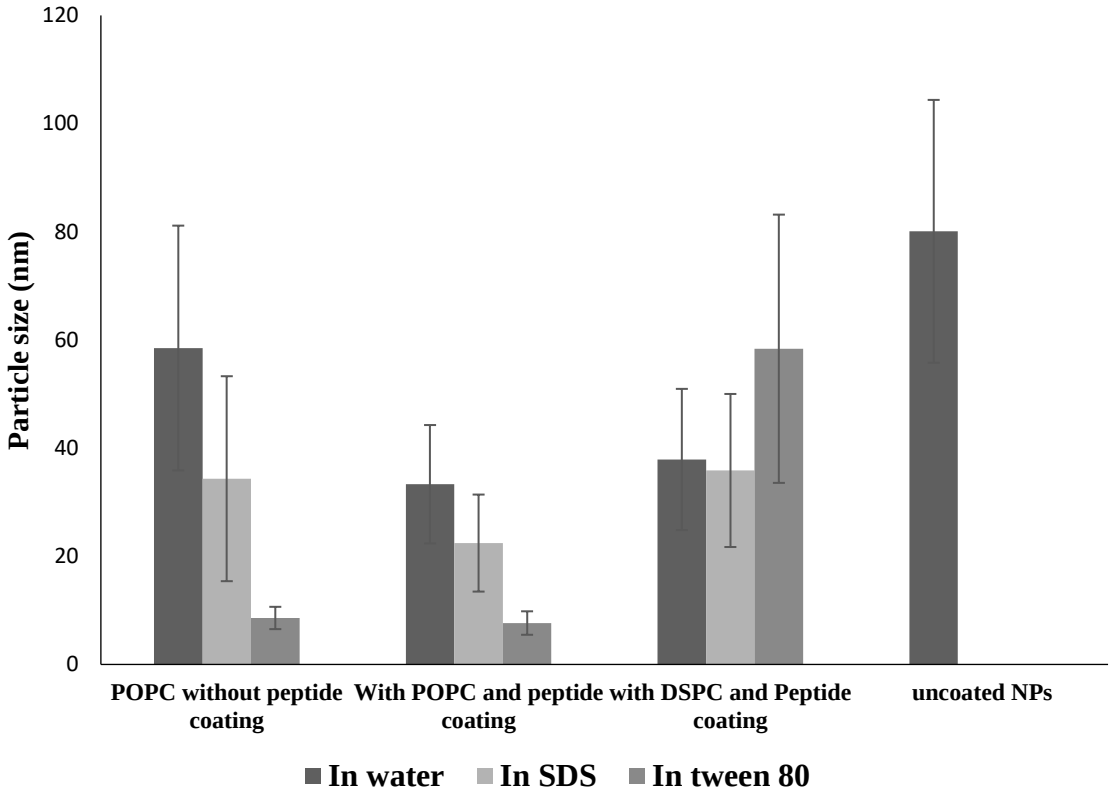

Figure 70 Particle size analysis of LDL like orlistat NPs (containing either POPC or DSPC in the lipid layer) compared to the POPC coated orlistat NPs and the uncoated orlistat NPs in 3 different media (water, 3mM SDS and 2% tween 80), measured directly after preparation, n=3 ± SD.

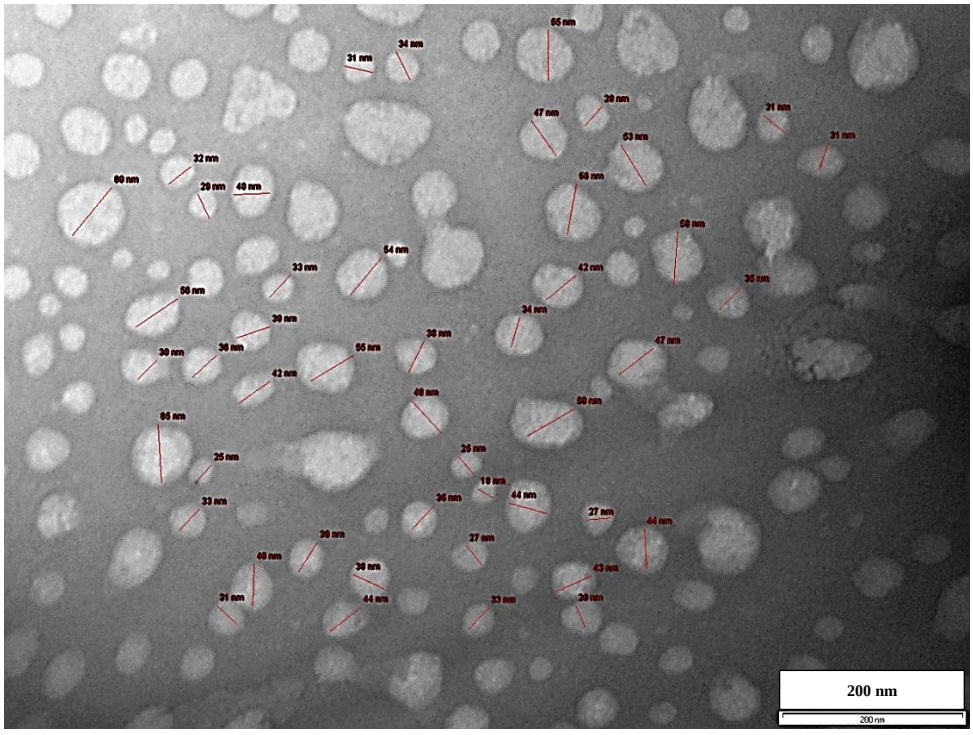

Figure 71 TEM images of LDL-Like orlistat NPs with final orlistat concentration 2 mM.

Figure 72 demonstrates the surface charge expressed as the zeta potential (mV) of the peptide coated orlistat NPs, prepared in 3 different media either water, 2% tween 80 or 3 mM SDS, in comparison to the particle size distribution of the uncoated orlistat NPs and the POPC coated orlistat NPs.

Concerning the surface charge, as shown in **Figure 72**, the addition of the peptide which is rich in arginine (positively charged amino acid) greatly affect the overall surface charge, shifting the zeta potential form the negative to the positive side, especially for NPs prepared in water or in tween 80, this could remarkably affect the surface stability and may result in particles aggregations with time. However, in presence of SDS as stabiliser, being an anionic surfactant, the NPs formulation showed a negative zeta potential which could be beneficial in stabilising the particles against aggregations.

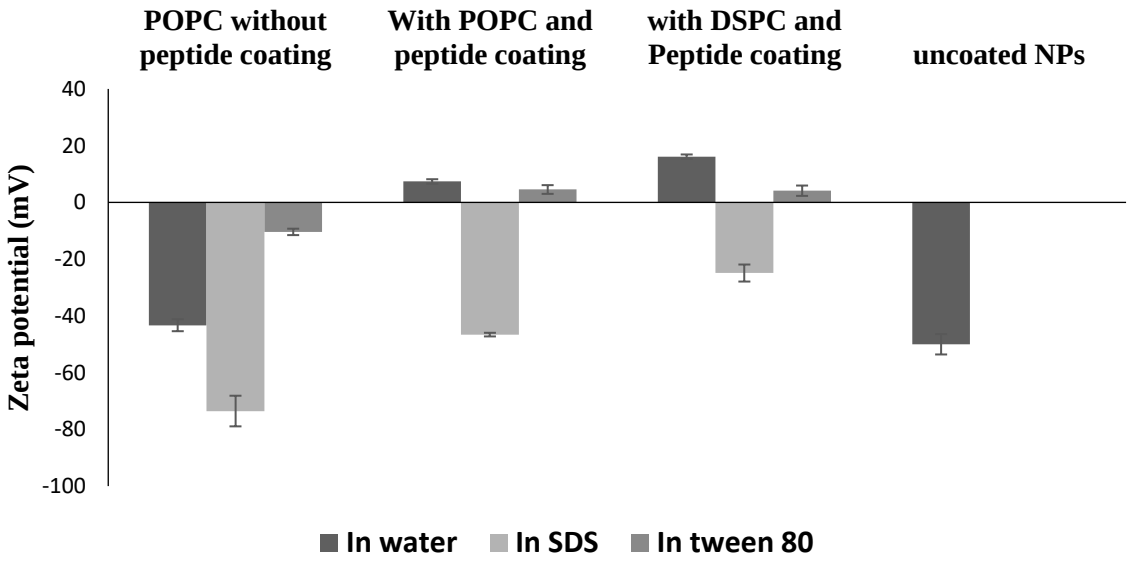

Figure 72 surface charge LDL like orlistat NPs (containing either POPC or DSPC in the lipid layer) compared to the POPC coated orlistat NPs and the uncoated orlistat NPs in 3 different media (water, 3mM SDS and 2% tween 80), n=3 ±SD.

5.4.3 Investigation the effect culture medium on POPC coated orlistat NPs

Preliminary investigation of particle size and surface charge of the prepared POPC coated orlistat NPs in basic culture medium DMEM was done, in order to explore the effect of addition of the particles in culture medium on the overall size and surface charge of the NPs, which will be further included in our cell work.

5.4.3.1 Particle size

Figure 73 and Figure 74 illustrate the particle size distribution (z-average size and volume size respectively) of the POPC coated orlistat NPs (4 mM orlistat and ratio core to coat 2:1) prepared either in fresh medium DMEM, or in MilliQ water followed by dilution in culture medium, in comparison to the POPC coated orlistat NPs prepared in 3 mM SDS.

As shown in **Figure 73 and Figure 74**, preparation of the orlistat NPs in DMEM resulted in an increase in the z-average and volume particle size distribution compared to the formulation prepared in 3 mM SDS. This may be due to the presence of proteins and other constituents in DMEM which enhanced the condensation of the NPs during the preparation process.

Nonetheless, diluting the NPs formulation in DMEM did not significantly affect the particle size of the NPs formulation, where the presence of coating material on the NPs will prevent any further condensation that may occur when the formulation is incorporated into the culture medium DMEM. Additionally at higher dilution volume size of the NPs was reduced significantly, which may be due to the further fractionation and disaggregation of any condensed particles by dilution.

This stability of our NPs formulation upon dilution in culture medium suggests that our method of NPs formulation was successful in keeping its physical size and structure in different media and can be further used for cell culture studies.

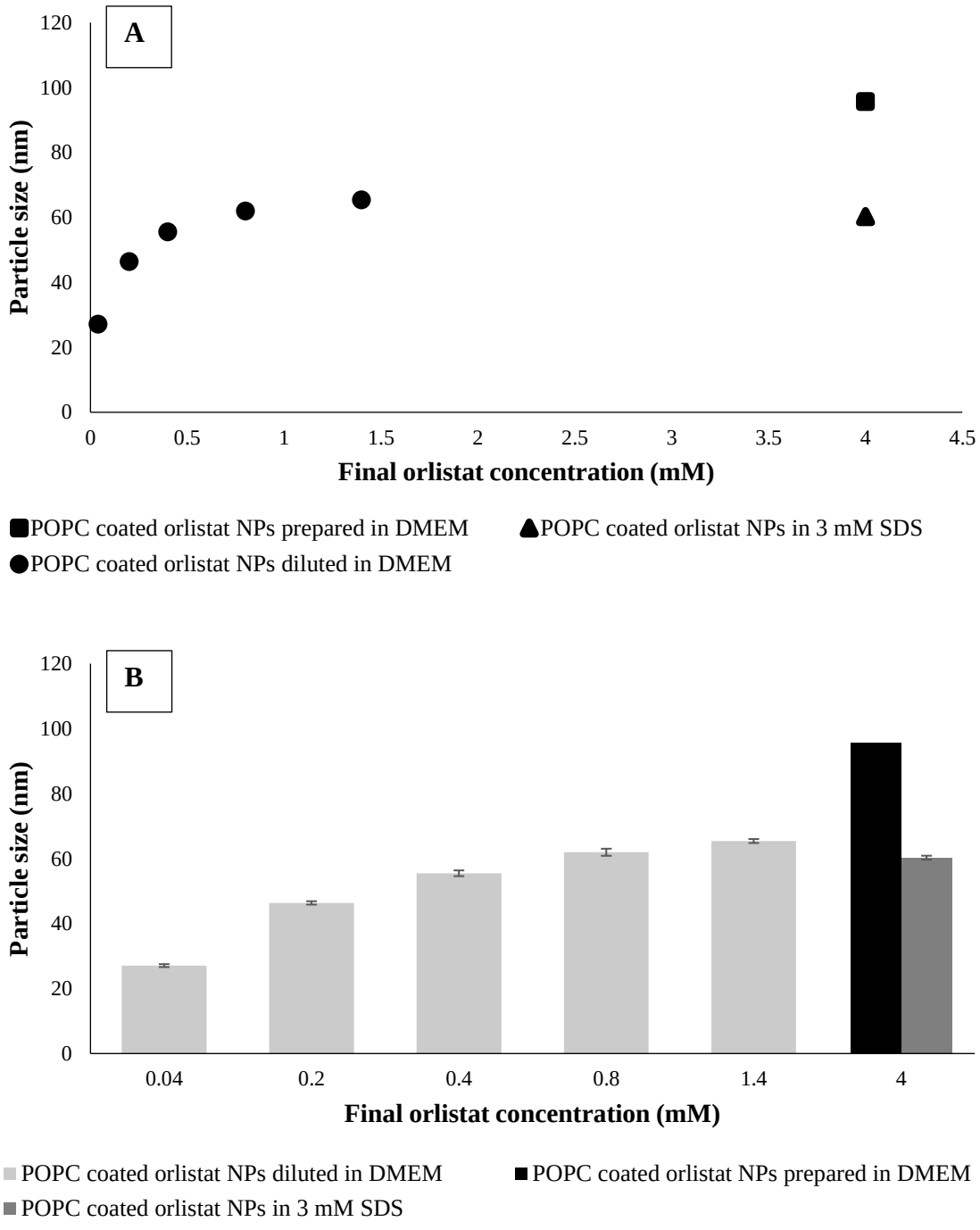

Figure 73 Z-average particle size distribution of POPC coated orlistat NPs (4 mM orlistat and 2:1 core to coat) prepared in water and DMEM, comparted to the particles size of POPC coated orlistat NPs prepared in water and diluted with DMEM at concentrations (1.4, 0.8, 0.4, 0.2, and 0.04 mM). A) XY scatter, B) Bar chart, n=3 ±SD.

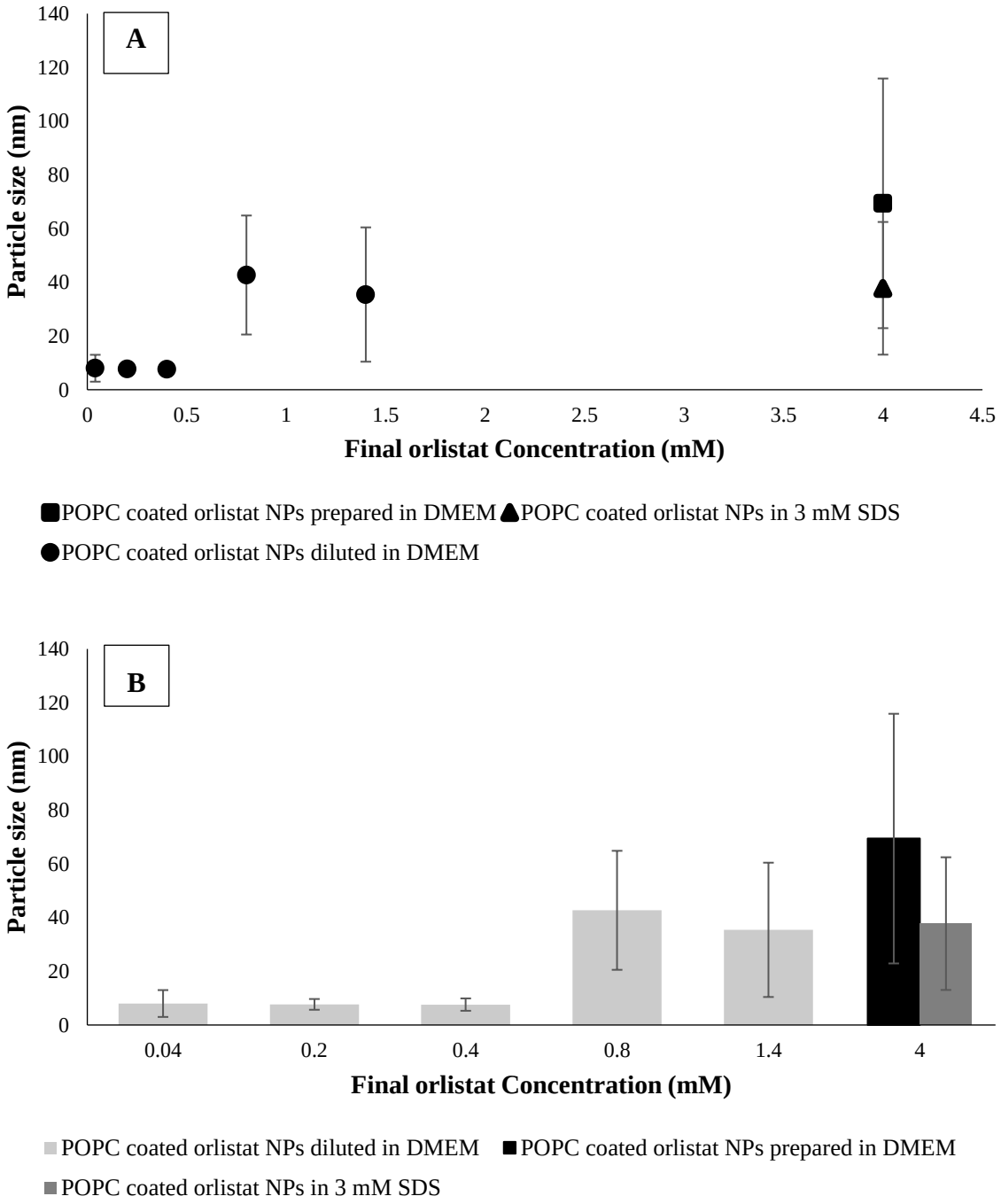

Figure 74 Volume particle size distribution of POPC coated orlistat NPs (4 mM orlistat and 2:1 core to coat) prepared in water and DMEM, comparted to the particles size of POPC coated orlistat NPs prepared in water and diluted with DMEM at concentrations (1.40, 0.8, 0.4, 0.2, and 0.04 mM). A) XY scatter, B) Bar chart, n=3 ±SD.

5.4.3.2 Zeta Potential

Figure 75 demonstrates the surface charge expressed as the zeta potential (mV) of the freshly prepared POPC coated orlistat NPs (4 mM orlistat and ratio core to coat 2:1) prepared either in fresh medium DMEM, or in MilliQ water followed by dilution in culture medium, in comparison to the POPC coated orlistat NPs prepared in 3 mM SDS.

Concerning the surface charge, as shown in **Figure 75**, preparation of the orlistat NPs in DMEM resulted in significant shift of the zeta potential towards the positive side compared to the formulation prepared in 3mM SDS with zeta potential shifting to -5 mV instead of -65 mV. This may be due to the presence of proteins in DMEM which are rich in positively charged amino acids, those proteins could result in this shift in the surface charge, and hence reducing the surface stability.

Yet, diluting the NPs formulation in DMEM did not significantly affect the zeta potential of the NPs formulation (**Figure 75B**) compared to the formulation prepared in 3mM SDS with a decrease in average zeta potential to the range between -6 to -18 mV.

Although Coating of the NPs will prevent any further interactions from the proteins of the medium on the surface of the prepared NPs that may occur during the preparation process, however it could not prevent the interaction of those proteins to the NPs surface when the formulation is incorporated into the culture medium DMEM(257). However, this would have a minimal effect on our cell studies.

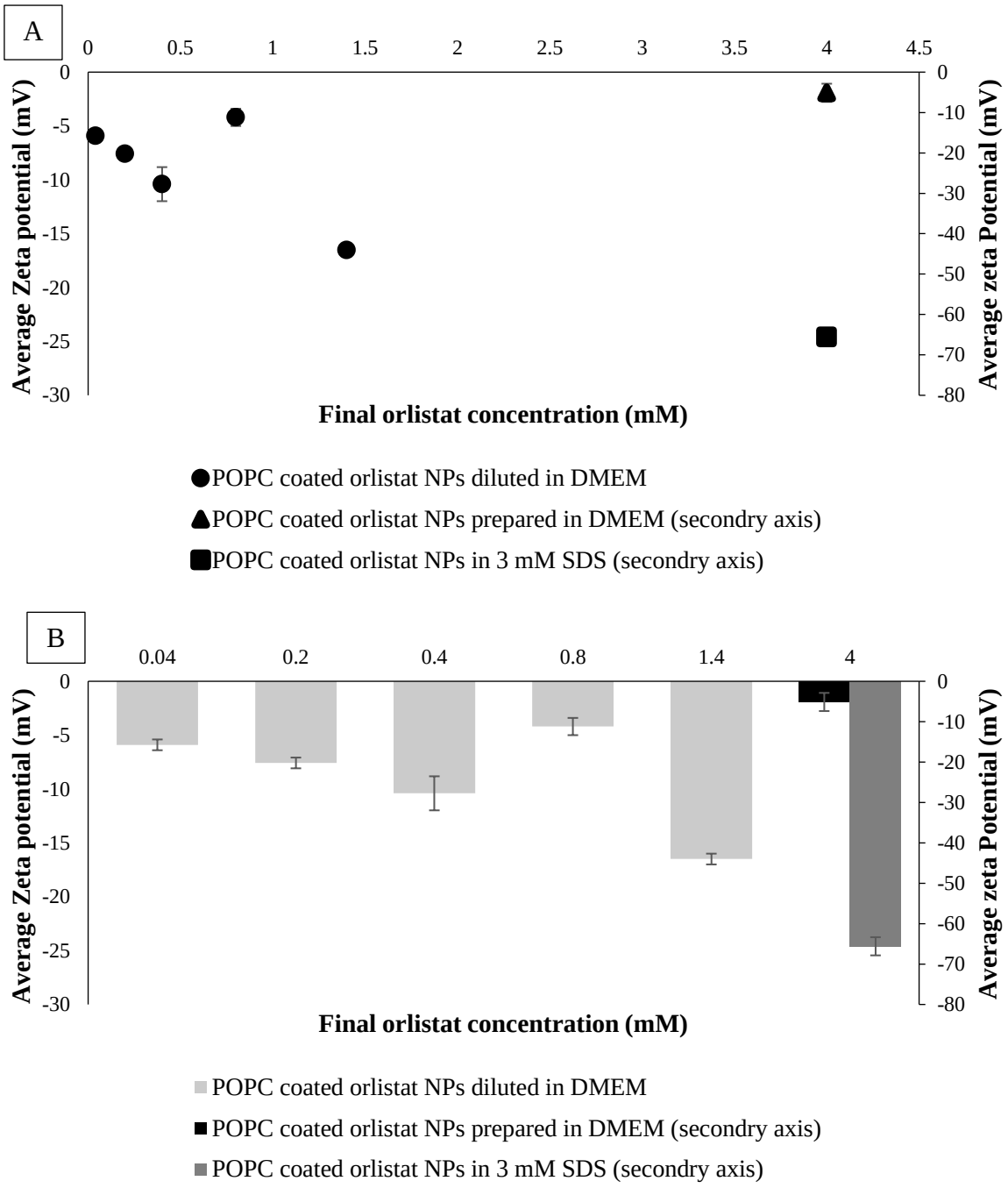

Figure 75 Zeta potential (mV) of POPC coated orlistat NPs (4 mM orlistat and 2:1 core to coat) prepared in water and DMEM shown on secondary axis, comparted to the particles size of POPC coated orlistat NPs prepared in water and diluted with DMEM at concentrations (1.40, 0.8, 0.4, 0.2, and 0.04 mM) showed on primary axis. A) XY scatter, B) Bar chart, n=3 ±SD.

5.4.4 Investigation of orlistat binding to albumin

Fluorescence quenching for a particular substance is defined as the decrease in the fluorescence intensity of the substance in presence of another molecule. This may be caused by several molecular interactions including excited-state reactions, molecular rearrangements energy transfer, ground-state complex formation and collisional quenching. The quenching effect of orlistat on the fluorescence of human serum albumin (HSA) was studied to understand the possible interaction between our drug of investigation and albumin, the latter is a normal constituent of human blood and a common additive in most cell culture media.

Figure 76 shows the fluorescence pattern of HSA at excitation wavelength of 280 nm and an emission wavelength of 330 nm. The quenching of fluorescence intensity of HSA by addition of orlistat is shown as well (**Figure 76**), when the concentration of HSA was stabilized at 1.5×10^{-6} mol L^{-1}, while the content of orlistat (ORL) varied from 0 to 100×10^{-6} mol L^{-1} at an interval of 20×10^{-6} mol L^{-1}.

The figure shows a minimum quenching effect caused by increasing concentration of orlistat on the HSA fluorescence. The emission fluorescence intensity of HSA did not significantly decreases with increasing orlistat concentration, while the emission maximum did not move to shorter or longer wavelength. The results indicates that orlistat (ORL) has minimal interaction with HSA, with no alteration in the local dielectric environment of HSA (**Figure 76**).

The quantitative analysis of the effect of orlistat concentration on the fluorescence intensity of HSA was further studied using Stern Volmer equation and was represented in **Figure 77**, which shows a linear relation with a slope of K_{SV}, the calculated value of K_{SV} and other parameters are shown in **Table 8**.

The value of quenching constant (K_{SV}) from Stern–Volmer plots (**Figure 77, Table 8**) emphasised the absence of fluorescence quenching caused by increasing orlistat ORL concentration. The data demonstrated that the value of the Stern–Volmer quenching constant

K_{SV} was low enough to indicate that the fluorescent quantum yield of HSA did not decrease(258), and that there is minimal binding between HSA and ORL in stable state.

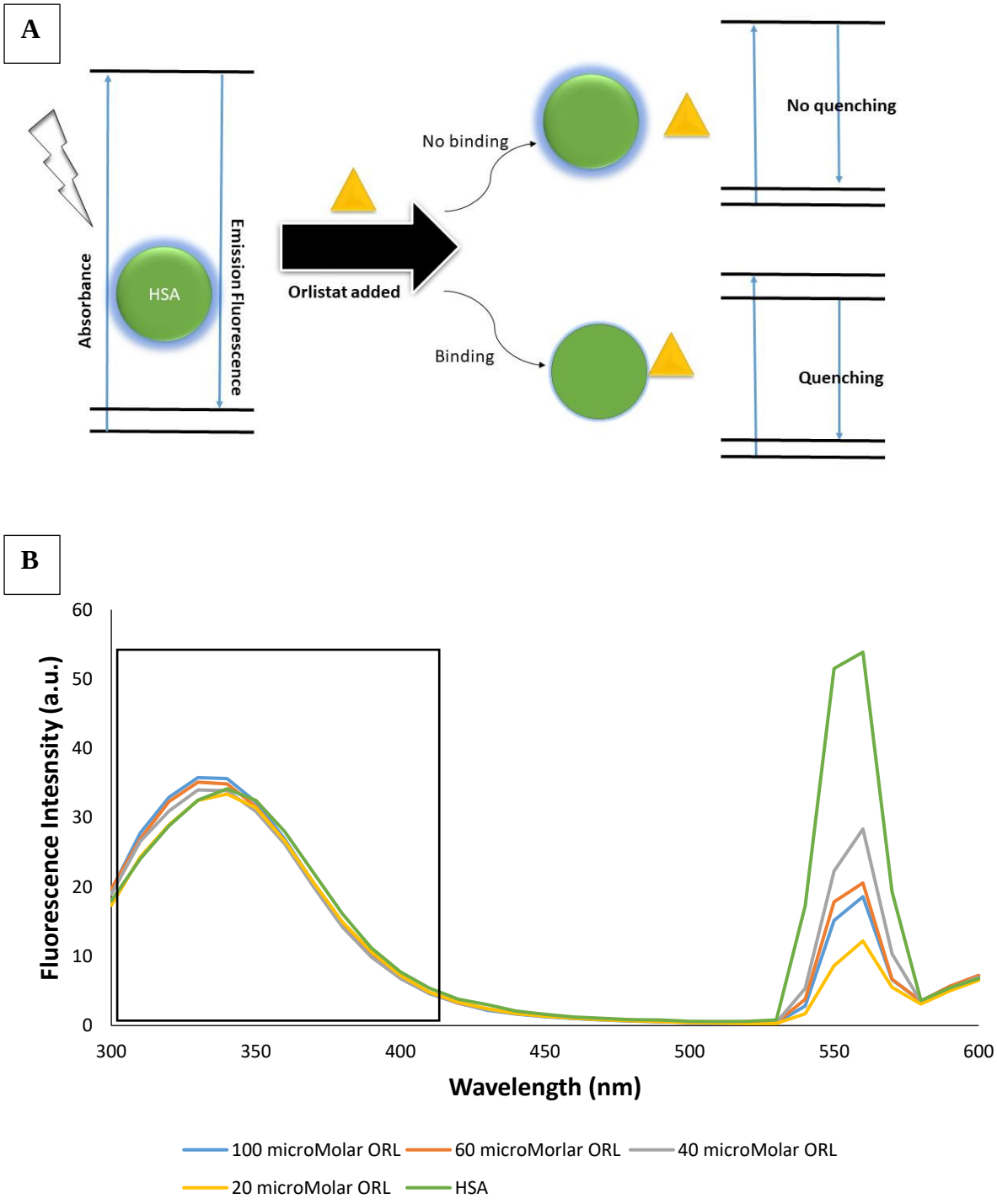

Figure 76 Fluorescence quenching assay of HSA, A) a diagram showing the concept of fluorescence quenching, B) Fluorescence spectra of HSA, measured at zero time, alone and in the presence of various concentrations of orlistat (ORL), at temperature T = 298 K, excitation wavelength = 280 nm, concentration of HSA 1.5×10^{-6} mol L^{-1} (1.5 µM), and at increasing concentration of orlistat (20, 40, 60 and 100 µM).

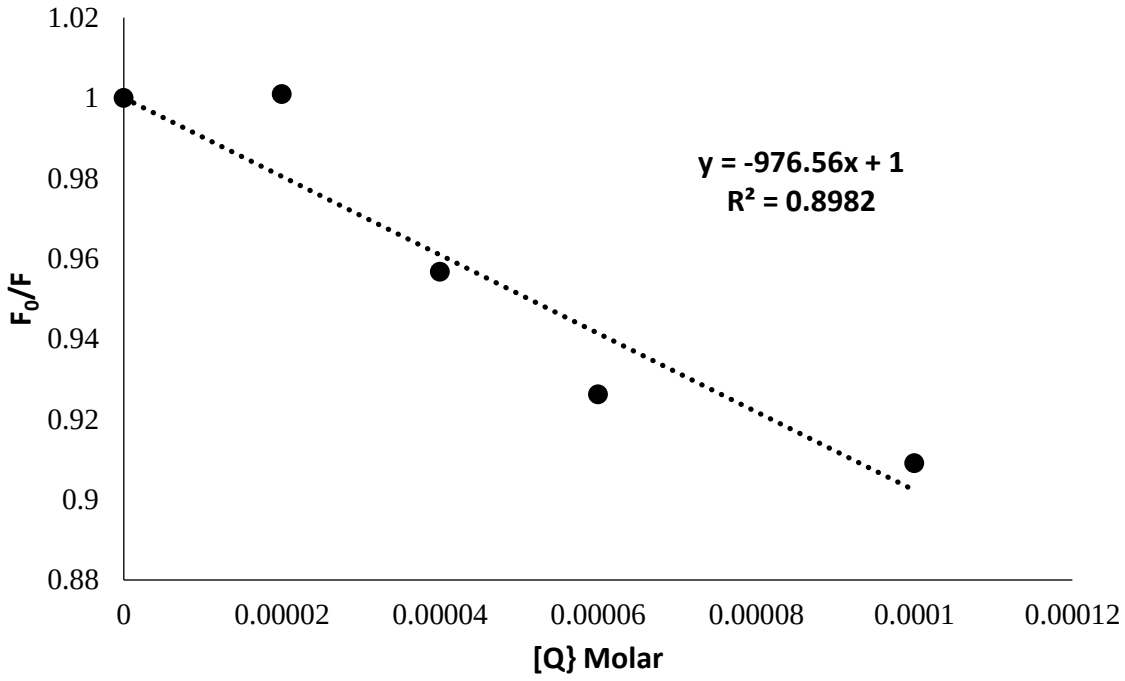

Figure 77 Stern–Volmer plots for the quenching of HSA by ORL at pH 7.4.

Table 8 Stern–Volmer quenching constants for the interaction of ORL with HSA at pH 7.4 and room temperature.

pH	T	K_{SV} (x 10^4 M^{-1})	K_b (x 10^4 M^{-1})	R^2	n
7.4	298	-0.0976	0.0000518	0.8982	-0.063

For more understanding of the binding between orlistat and the sites on HSA, the equilibrium between free and bound molecules is given by the following equation (259)

$$\log\left(\frac{F_0-F}{F}\right) = \log K_b + n\log[Q]$$ **Equation 22 binding constant equation**

where K_b is the observed binding constant to a site, and n is the number of binding sites per HSA. The dependence of log (F_0/F−1) on the value of concentrations of ORL expressed as log [Q] is linear with the slope equal to the value of n and log Kb is fixed on the ordinate.

Figure 78 is the plot of log (F0/F−1) versus log [Q] for the ORL–HSA system. The binding constants K_b and binding sites n were listed in **Table 9**. The results showed that the binding constants K_b indicates minimal binding between the HSA and orlistat, with no binding sites.

Table 9 Stern–Volmer binding constants for the interaction of ORL with HSA at pH 7.4 and room temperature.

Log K_b	-0.285
n	-0.063
K_b (x 10^4 M^{-1})	0.0000518

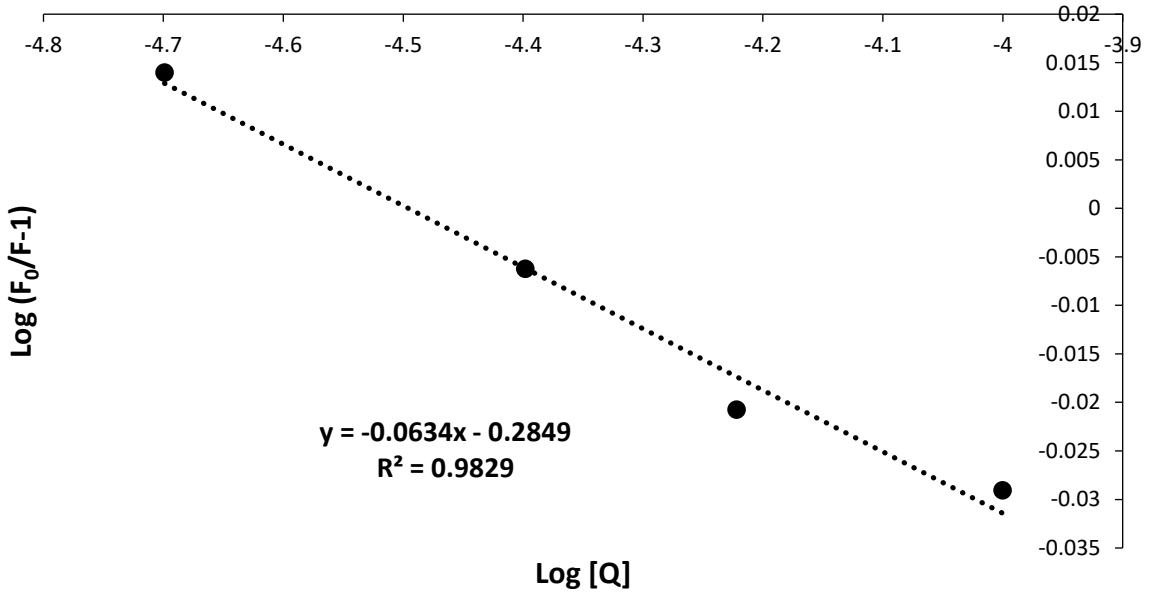

Figure 78 Double-log plots of ORL quenching effect on HSA fluorescence at pH 7.4.

5.4.5 Investigation of the cytotoxicity of orlistat formulations

Different cell lines were used to study the effect of our formulations as a function of variables, including the cell type, the FASN overexpression and LDLR-overexpression.

In our study three cell lines were chosen representing a wide range of breast cancerous tissue, MCF-7 as an example for hormonal Luminal A cell line, BT-474 as an example for Basal Luminal B cell line, and finally MDA MB-453 as an example for HER2 positive cell line (260).

In terms of FASN expression, it is well reported that the FASN is overexpressed in breast cancer tissues compared to the normal human tissues as previously discussed. In the case of breast cancer, the mechanism of FASN overexpression in cell lines remains unclear, but still there is growing evidence on FASN enhanced overexpression in ER+ cell lines(261).

Concerning the LDLR, it was clearly found that tumour tissues mainly consume much cholesterol through indulging LDL(262). In case of breast cancer cell lines, the LDLR are expressed in most of the available cell lines but with a variable extent(263) this depends mainly on the type of the cell line and its proliferation rate.

5.4.5.1 In MCF-7 cell lines

MCF-7, a double positive HER-2 negative cell line which is overly sensitive to orlistat due to the over expression of FASN (264,265). It is as well expected to have LDLR responsible for cholesterol uptake from circulating LDLs(266). Thus, MCF-7 is expected to show high sensitivity toward our LDL-like ORL NPs.

Figure 79 shows the survival curve of MCF-7 cell line after being treated with the peptide coated LDL-like ORL NPs compared to that of POPC coated orlistat NPs. As shown in figure, MCF-7 cell line shows high sensitivity towards ORL, with less than 20% cell survival after 48 hours from treatment with any of the two formulations at concentrations 25 µM and above. The effect of peptide coating on the survival rate of MCF-7 was not prominent, due to the over expression of FASN enzyme and the high sensitivity to ORL. After 48 hours of treatment, it is expected that both used formulation will be concentrated in the cells, resulting in decrease in percentage of cellular survival. Hence, the uptake study will give us a deeper understanding to

the effect of peptide coating on MCF-7 cell lines and the rate of diffusion of both formulations, this will be discussed later.

The toxicity of the utilised peptide coating on MCF-7 was studied to ensure that the toxicity profile discussed was mainly due to the effect of ORL on the cells. This was done using LDL-like peptide coated Triolein NPs as a control. Triolein is a GRAS material with an expected no cytotoxic effect on any cell line. **Figure 80** illustrates the comparison of survival rate curves of MCF-7 between the peptide coated ORL NPs and the vehicle as a negative control, expressed as peptide coated triolein NPs. The results emphasised that the effect on the cells was mainly due to the encapsulated orlistat, with our peptide coating barely affecting the survival profile of MCF-7 cell line following 48 hours treatment, even at the maximum concentrations used.

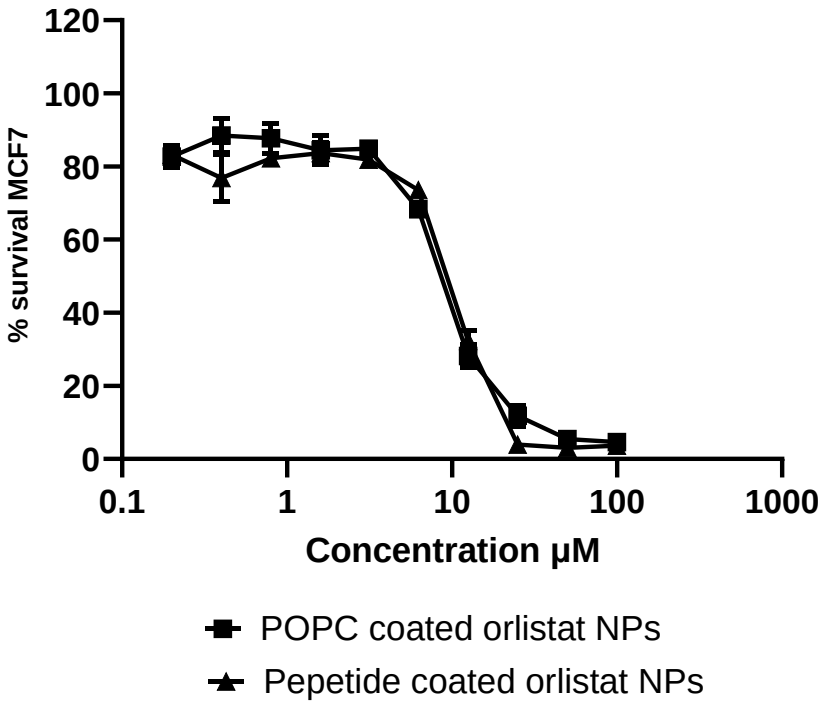

Figure 79 cell survival curve for cytotoxicity assay (48 hrs) of 2 formulations, Peptide coated ORL NPs and POPC coated ORL NPs, in MCF-7 breast cancer cell line, n=6 ±SD.

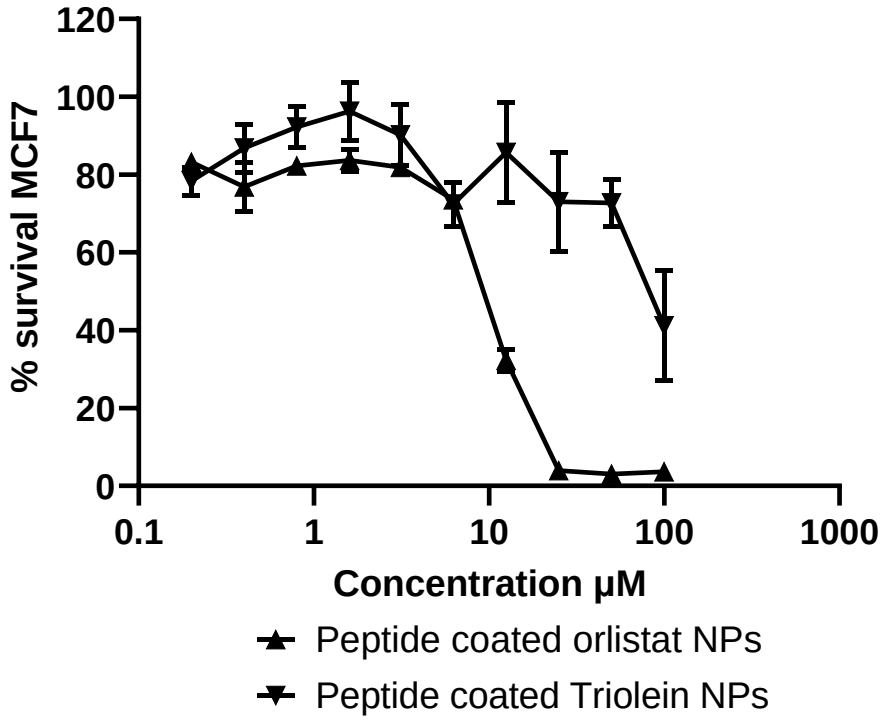

Figure 80 cell survival curve for cytotoxicity assay of 2 formulations, Peptide coated ORL NPs and Peptide coated triolein TO NPs as a negative control, in MCF-7 breast cancer cell line, n=6 ±SD.

Orlistat by itself was studied as a positive control, however, being very hydrophobic, orlistat was prepared in pure ethanol. Orlistat was dissolved in pure ethanol at concentration of 200 µM, followed by serial dilution in culture medium as mentioned before. Similarly, ethanol (the vehicle) was used as negative control and was diluted in culture media with the same dilution factors. **Figure 81** shows the cytotoxicity profile of orlistat ethanolic solution on MCF-7 cell line compared to that of the vehicle ethanol. After 48 hours incubations, orlistat shows similar toxicity profile on MCF-7 comparable to our prepared formulations, regardless of the toxicity of the vehicle ethanol.

In conclusion, due to the over expression of FASN, it is expected that after 48 of incubation of any of the formulations with MCF-7, orlistat will be indulged by passive or active cellular transport, resulting in massive cell death.

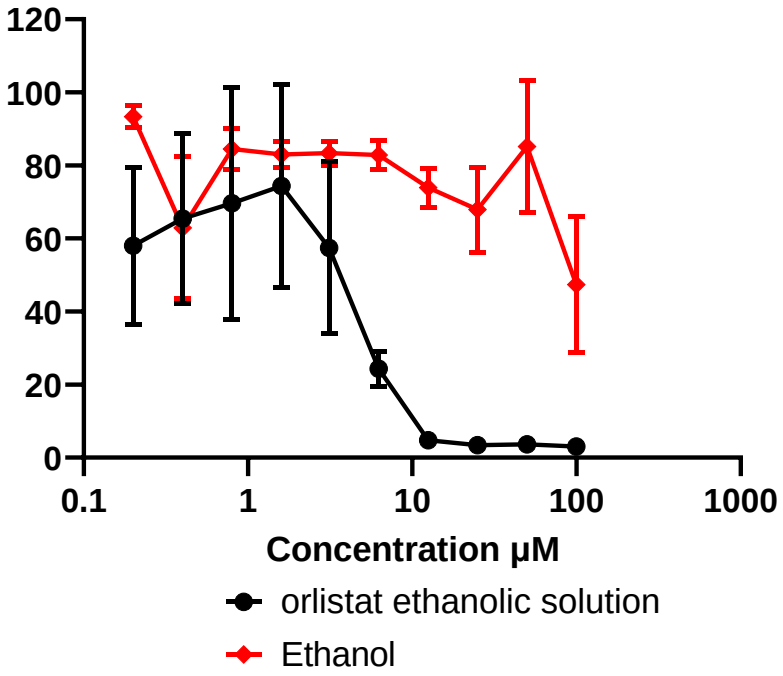

Figure 81 cell survival curve for cytotoxicity assay of ORL ethanolic solution as positive control compared to the vehicle Ethanol, in MCF-7 breast cancer cell line, n=6 ±SD.

5.4.5.2 In BT-474 cell lines

BT-474 is a triple positive cell line, which is as well sensitive to orlistat duet to over expression of FASN(267), as well they are expressing the LDLR (262).

Figure 82 shows the survival curve of BT-474 cell lines after being treated with the peptide coated LDL-like ORL NPs compared to that of POPC coated orlistat NPs. As shown in the figure, BT-474 cell line shows high sensitivity towards ORL, with less than 40% cell survival after 48 hours from treatment with any of the two formulations at concentrations 25 µM and above. There was a significant effect of the peptide coating on the survival rate of BT-474 shown at the higher concentration of 50 and 100µM, where the percentage survival dropped to 20% in case of the peptide coated formulation compared to the 40% in those without peptide coating. This could be due to the higher uptake of the peptide coated formulation by the cells compared to that without the peptide coating.

Moreover, the toxicity of the utilised peptide coating on BT-474 was studied to ensure that the toxicity profile discussed was mainly due to the effect of ORL on the cells. **Figure 83** illustrates the comparison of survival rate curves of BT-474, between the peptide coated ORL NPs and the vehicle as a negative control, expressed as peptide coated triolein NPs. The results emphasised that the effect on the cells was mainly due to the encapsulated orlistat, with our peptide coating sparsely affecting the survival profile of BT-474 cell line following 48 hours treatment, even at the maximum concentrations used.

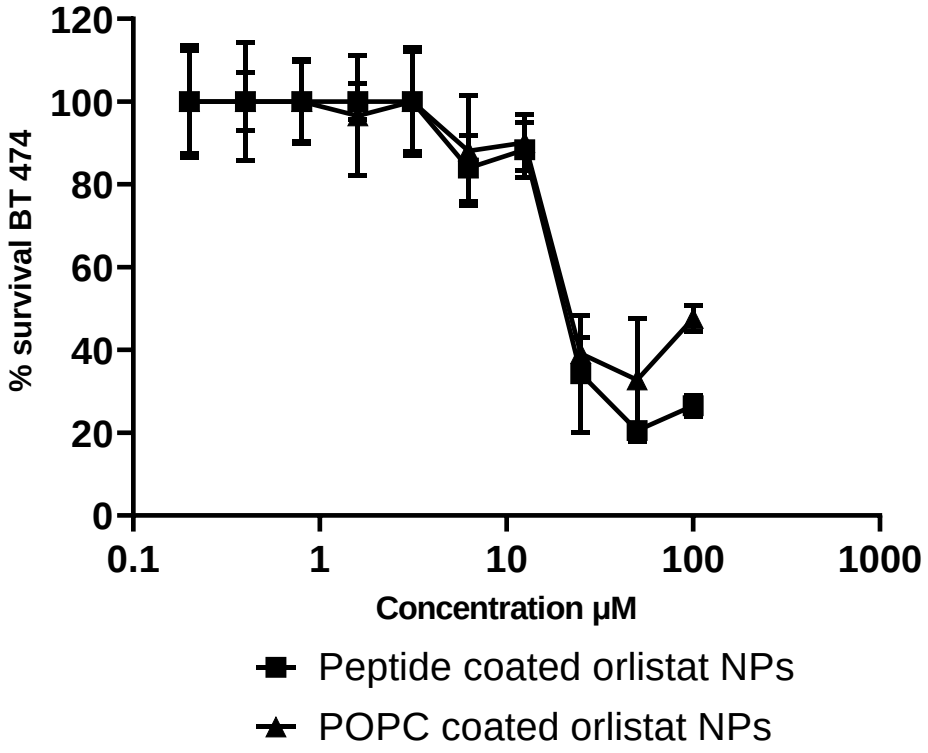

Figure 82 cell survival curve for cytotoxicity assay of 2 formulations, Peptide coated ORL NPs and POPC coated ORL NPs, in BT-474 breast cancer cell line, n=6 ±SD.

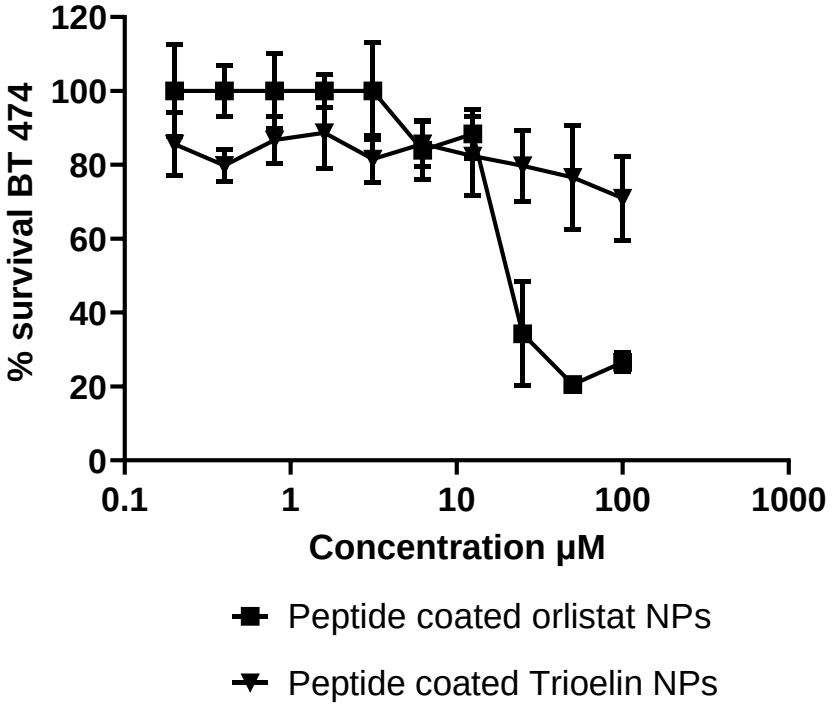

Figure 83 cell survival curve for cytotoxicity assay of 2 formulations, Peptide coated ORL NPs and Peptide coated triolein TO NPs as a negative control, in BT-474 breast cancer cell line, n=6 ±SD.

Additionally, orlistat by itself was studied as a positive control as mentioned before. **Figure 84** shows the cytotoxicity profile of orlistat ethanolic solution on BT-474 cell lines compared to that of the vehicle ethanol. After 48 hours incubations, orlistat shows a toxicity profile on BT-474 comparable to our prepared formulations, however this effect in this case was mainly due to the vehicle ethanol.

In conclusion, due to the over expression of FASN and the upregulation of LDLR, it is expected that after 48 of incubation of any of the formulations with BT-474, orlistat will be indulged mainly by the receptor mediated cellular transport especially at higher concentrations of the formulations, resulting in a difference in the cytotoxicity profile between the LDL-like NPs and the POPC coated NPs.

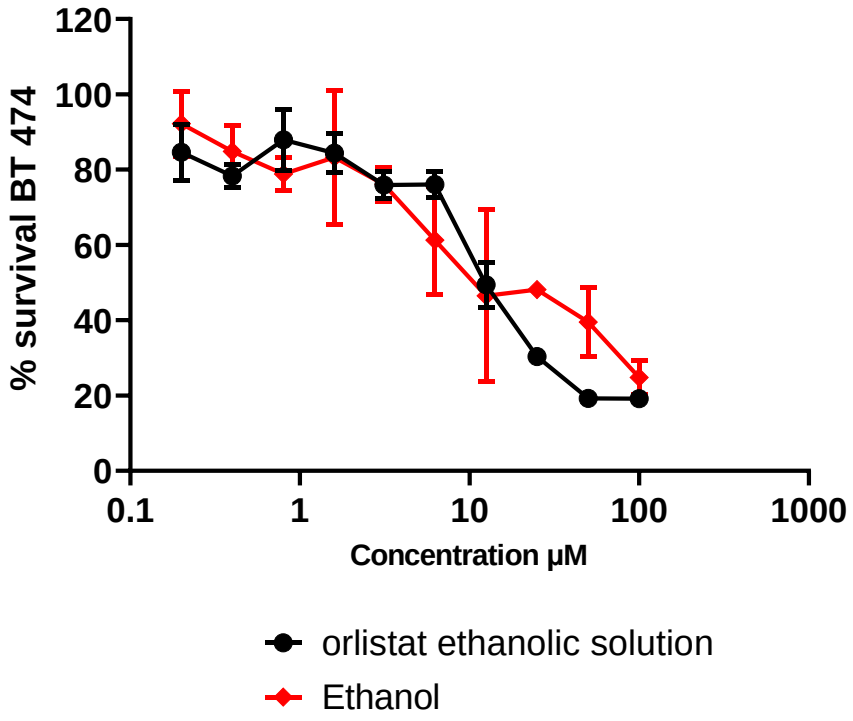

Figure 84 cell survival curve for cytotoxicity assay of ORL ethanolic solution as positive control compared to the vehicle Ethanol, in BT-474 breast cancer cell line, n=6 ±SD.

5.4.5.3 In MDA MB-453 cell lines

MDA MB-453 cell lines are a triple negative cell lines, they are with lower orlistat sensitivity compared to the previous cell lines, mainly due to the low expression of FASN (263). However, they are overexpressing prominent levels of LDLR (268–270), which is interesting to study the effect of LDLR mediated uptake on the cytotoxicity profiles of this cell line.

Figure 85 shows the survival curve of MDA MB 453 cell lines after being treated with the peptide coated LDL-like ORL NPs compared to that of POPC coated orlistat NPs. MDA MB 453 cell lines are considered of low sensitivity towards ORL as mentioned before, hence in **Figure 85**, the POPC coated orlistat NPs showed a low cytotoxic effect on the cell line, with no more than 50% cell death after 48 hours, even at the highest concentration. However, there was significant effect of peptide coating on the survival rate of MDA MB 453 shown at all employed concentrations, where the percentage survival was significantly dropping in case of

the peptide coated formulation compared to that without peptide coating. This could be an indication of the effect of the LDLR mediated uptake of the LDL-like NPs, which resulted in higher uptake of the peptide coated formulation by the cells compared to that without the peptide coating, and thus an increase in the intracellular concentration of the drug that could enhance the rate of cell death.

Furthermore, the toxicity of the utilised peptide coating on MDA MB 453 was studied to ensure that the toxicity profile discussed was mainly due to the effect of ORL on the cells. **Figure 86** illustrates the comparison of survival rate curves of MDA MB 453, between the peptide coated ORL NPs and the vehicle as a negative control, expressed as peptide coated triolein NPs. The results emphasised that the effect on the cells was due to the encapsulated orlistat, with our peptide coating has a minimum effect on the survival profile of MDA MB 453 cell line following 48 hours treatment, especially at the maximum concentrations used.

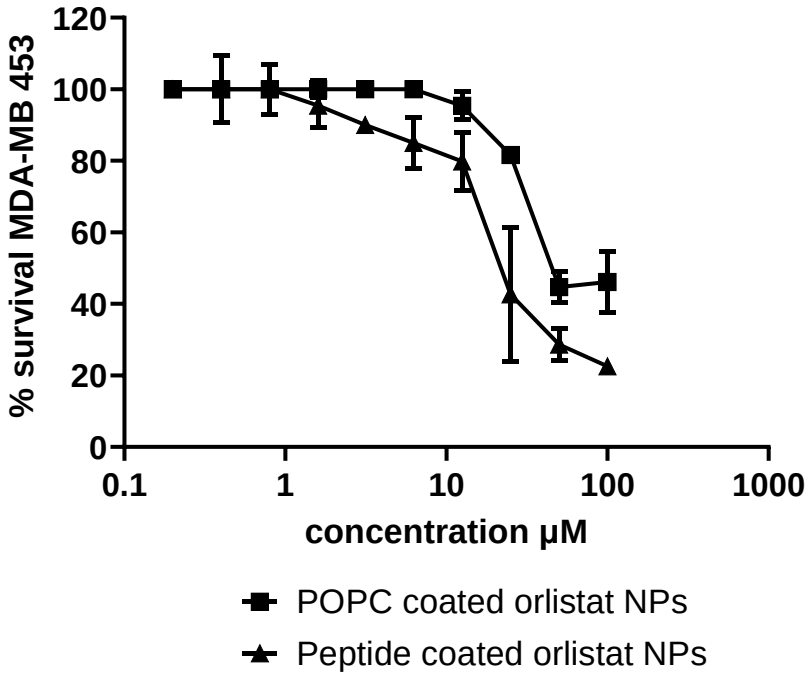

Figure 85 cell survival curve for cytotoxicity assay of 2 formulations, Peptide coated ORL NPs and POPC coated ORL NPs, in MDA MB-453 breast cancer cell line, n=6 ±SD.

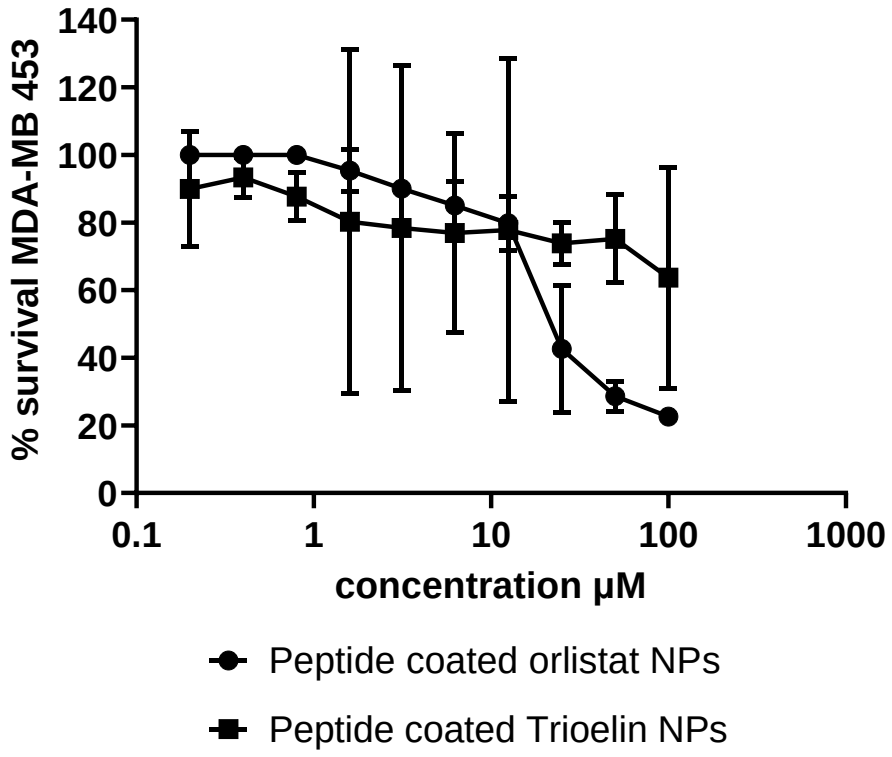

Figure 86 cell survival curve for cytotoxicity assay of 2 formulations, Peptide coated ORL NPs and Peptide coated triolein TO NPs as a negative control, in MDA MB-453 breast cancer cell line, n=6 ±SD.

As mentioned before, orlistat by itself was studied as a positive control. **Figure 87** shows the cytotoxicity profile of orlistat ethanolic solution on MDA MB 453 cell lines compared to that of the vehicle ethanol. After 48 hours incubations, orlistat shows a toxicity profile on MDA MB 453, however this effect in this case was mainly due to the vehicle ethanol.

In conclusion, due to the upregulation of LDLR, it is expected that after 48 of incubation of any of the formulations with MDA MB 453, orlistat will be indulged by the receptor mediated cellular transport, resulting in a difference in an enhanced cytotoxicity profile in case of the peptide coated NPs compared to that without the peptide coating.

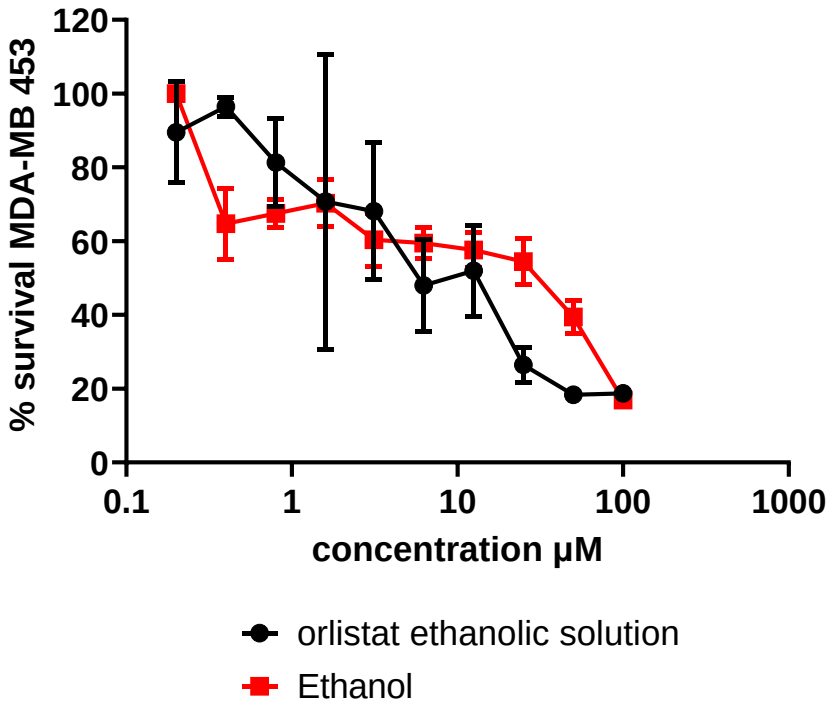

Figure 87 cell survival curve for cytotoxicity assay of ORL ethanolic solution as positive control compared to the vehicle Ethanol, in MDA MB-453 breast cancer cell line, n=6 ±SD.

5.4.5.4 IC_{50} between cell lines

To sum up, in terms of FASN expression it is reported that its overexpression increases between the different cell lines in order MCF7> BT-474> MDA MB453. While the LDLR over expression is increasing from MDA MB 453>BT-474~MCF. This is further emphasized by the comparison of the effect of the peptide coated orlistat NPs on the three cell lines as shown in **Figure 88.** The effect of cell death in ORL sensitive cell line, as in case of MCF-7 and BT-474, was prominent compared to that of lower sensitivity of ORL. However, the higher uptake of LDL-like NPs in MDA MB 453 with higher expression of LDLR, resulted in comparable concentration dependant cytotoxicity profiles as shown in the **Figure 88**.

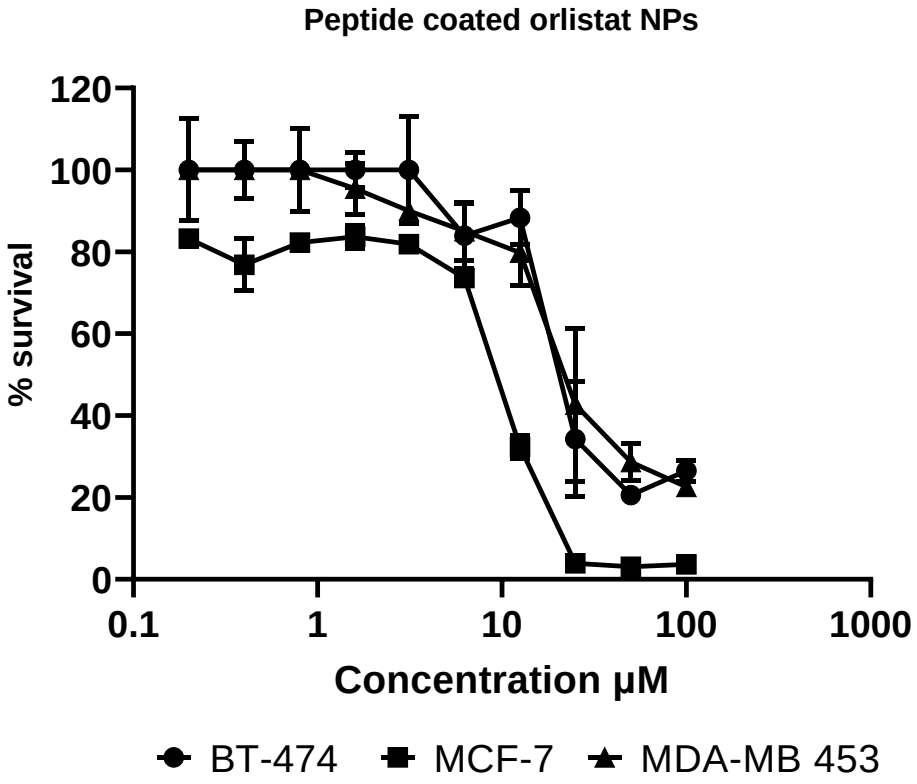

Figure 88 Comparison between the survival rate curves for the cytotoxicity assay of Peptide coated orlistat ORL NPs, in 3 different breast cancer cell lines, n=6 ±SD.

The cytotoxicity of the utilised formulations was studied in terms of the inhibitory concentration (IC_{50}) on the three cell lines. **Figure 89** demonstrates the (IC_{50}) of the peptide coated LDL-like ORL NPs compared to that of the POPC coated ORL NPs in the 3 different cell lines used.

As clearly expressed in the figure, the inhibitory concentration (IC_{50}) for the peptide coated LDL-like ORL NPs was found to be around 24, 8, and 25 µM for the BT-474, MCF-7 and MDA MB 453 cell lines respectively. On the other hand, the IC_{50} for the formulation without peptide coating (POPC coated ORL NPs) was found to be 38, 8, and 66 µM for the BT-474, MCF-7 and MDA MB 453 cell lines respectively. There was a statistically significant difference between the two formulations at P value <0.0001, and on all the employed cell lines, with a significant decrease in (IC_{50}) in case of peptide coating compared to the other

formulation. This indicates the higher efficacy of the proposed LDL-like NPs on inhibiting cancerous cellular growth, which is explained by the enhanced uptake of the prepared NPs, which will be discussed in the following section. The effect of LDL-like NPs was prominent and of great interest in MDA MB 453 higly resistant,triple negative cell lines, this could be prominsing in controlling resistant breast cancer (206,269).

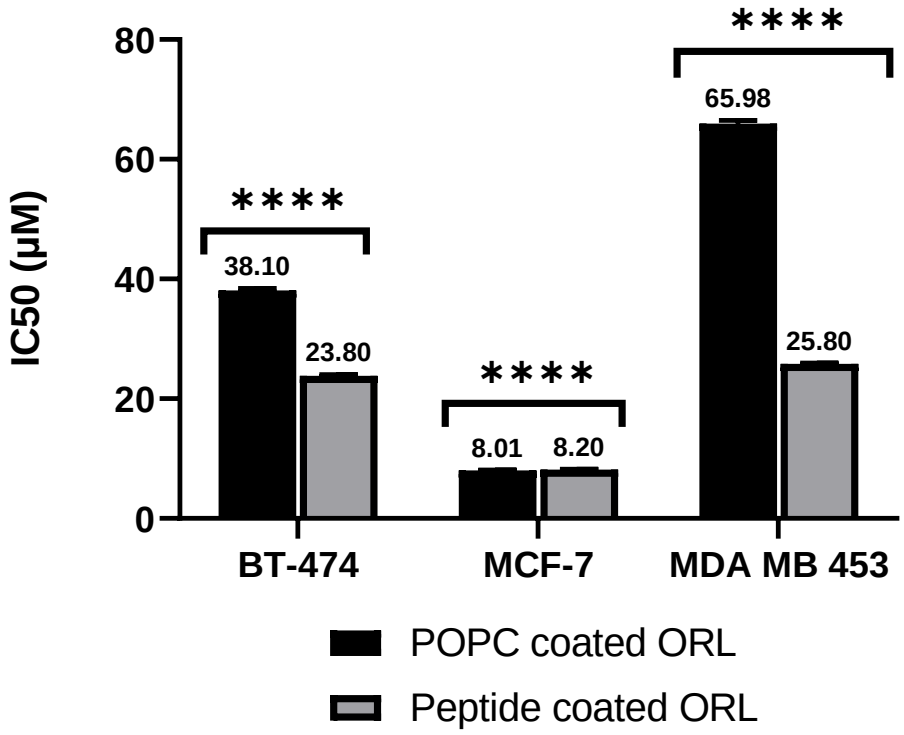

Figure 89 Comparison between the inhibitory concentrations (IC_{50}) of 2 different formulations, POPC coated ORL NPs and Peptide coated ORL NPs respectively, on the 3 utilised breast cancer cell lines, BT-474, MCF-7 and MDA MB-453. ** Statistically significant difference at P value < 0.0001, n=6 ±SD.**

5.4.6 Investigation of cellular uptake

Cellular uptake study was carried out on three breast cancer cell lines, to investigate the difference in the rate of cellular uptake between the POPC coated NPs (F1) and the novel peptide functionalised LDL-like orlistat NPs (F2). **Figure 90 to Figure 92 (A)** illustrate the fluorescent imaging of the three breast cancer cell lines BT-474, MCF-7 and MDA MB 453

respectively, taken after specific time intervals (1, 2, 4, 8 and 24 hours) following the treatment of the cells with either of the 2 formulations F1 or F2 at 2 different concentrations each.

Results in the **Figure 90 to Figure 92 (A)** represent the fluorescent imaging of the marked lipid coated formulations, where the green fluorescence represents our formulations F1 and F2 labelled with the fluorescent 25-NBD cholesterol. The images show an increase in the amount of the indulged formulations F1 and F2 with time in all employed cell lines, represented by increasing the green fluorescence inside the employed cells. While comparing between F1 and F2 at both employed concentrations, F2 LDL-like NPs showed higher cellular uptake, represented by increasing fluorescence compared to F1.

In details, the rate of cellular uptake was markedly increasing in case of F2 LDL-like ORL NPs compared to F1 in all cell lines, and more particularly at the higher employed concentration. It is shown that the LDL-like NPs were indulged in significant amounts after 1 hour following the cell treatment, in all the three employed cell lines.

In case of the BT-474 cell line (**Figure 90**), the results show a higher cellular uptake rate for the LDL-like NPs compared to the other formulation, hence this could give a better explanation for the more cytotoxic effect of the LDL-like formulation compared to the POPC coated orlistat NPs.

It is worth mentioning that in case of MCF-7 cell lines (**Figure 91**), the rate of cellular uptake can give an idea about the effectiveness of our LDL-like formulation, where higher cellular uptake rate could result in better efficacy of the formulation against cancerous cell line. As mentioned before, although the cytotoxic effect of both formulations was similar following the 48 hrs cytotoxicity assay, yet the cellular uptake rate of the LDL-like formulation is much higher than that of the other formulation.

Concerning the MDA MB 453 (**Figure 92**), it showed a higher cellular uptake for the LDL-like NPs compared to the POPC coated NPs. Interestingly,the triple negative MDA MB 453

showed a significant higher rate of cellular uptake for the LDL-like NPs compared to the other two cell lines. This is confirmed in (**Figure 93**), which shows a comparison between the rates of cellular uptake of the LDL-like NPs in the three employed cell lines, BT-474, MCF-7 and MDA MB 453, this can reflect the effect of the 11-mer peptide added to our LDL like NPs on the cellular uptake of the formulation, particularly in the resistant triple negative cell line.

The rate of cellular uptake for the LDL-like NPs was enhanced in MDA MB 453 and BT-474, compared to that of MCF-7 cell lines. This could be due to the over expression of the LDLR in the cell lines in various degrees, resulting in a variation in the rate of cellular uptake of the formulation, yet addition of the 11-mer peptide definitely enhanced the uptake of the LDL-like NPs formulation compared to the other formulation in the three cell line.

However, the receptor mediated uptake of the formulation is still one among many mechanisms of cellular uptake, such as the micropinocytosis, clathrin mediated endocytosis and caveolae mediated uptake. The exact mechanism of cellular uptake requires further investigation.

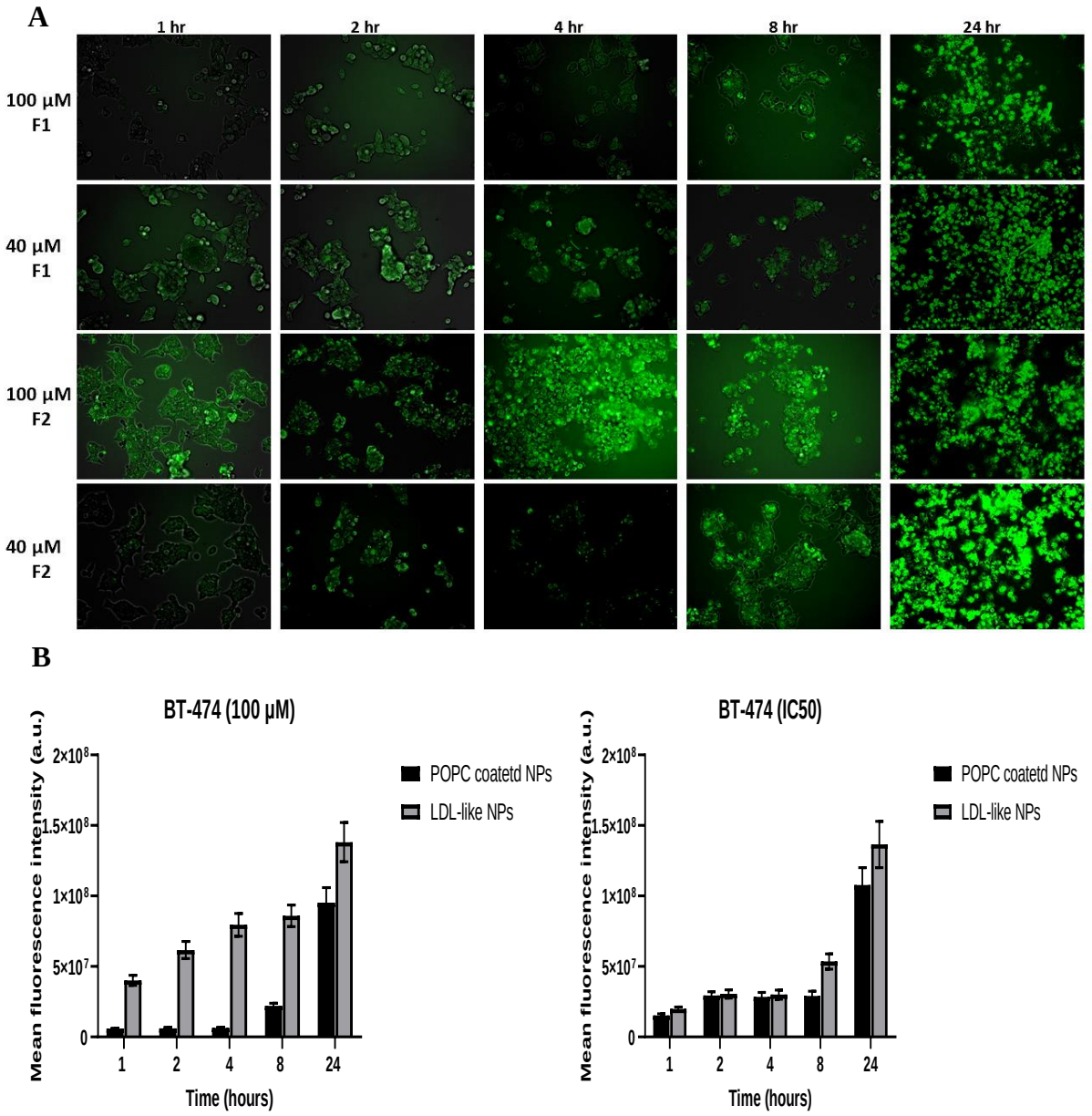

Figure 90 Cellular uptake fluorescent imaging carried out on BT-474 breast cancer cell lines, captured at specific time intervals (1, 2, 4, 8 and 24 hours) following the treatment of the cells with one of the formulations (F1, F2) at two different concentrations each (100µM and 40µM). F1 is fluorescently labelled POPC coated orlistat NPs, F2 fluorescently labelled LDL-like orlistat NPs. A) Fluorescent microscopy images, B) Mean fluorescence intensity plot, n=3 ±SD.

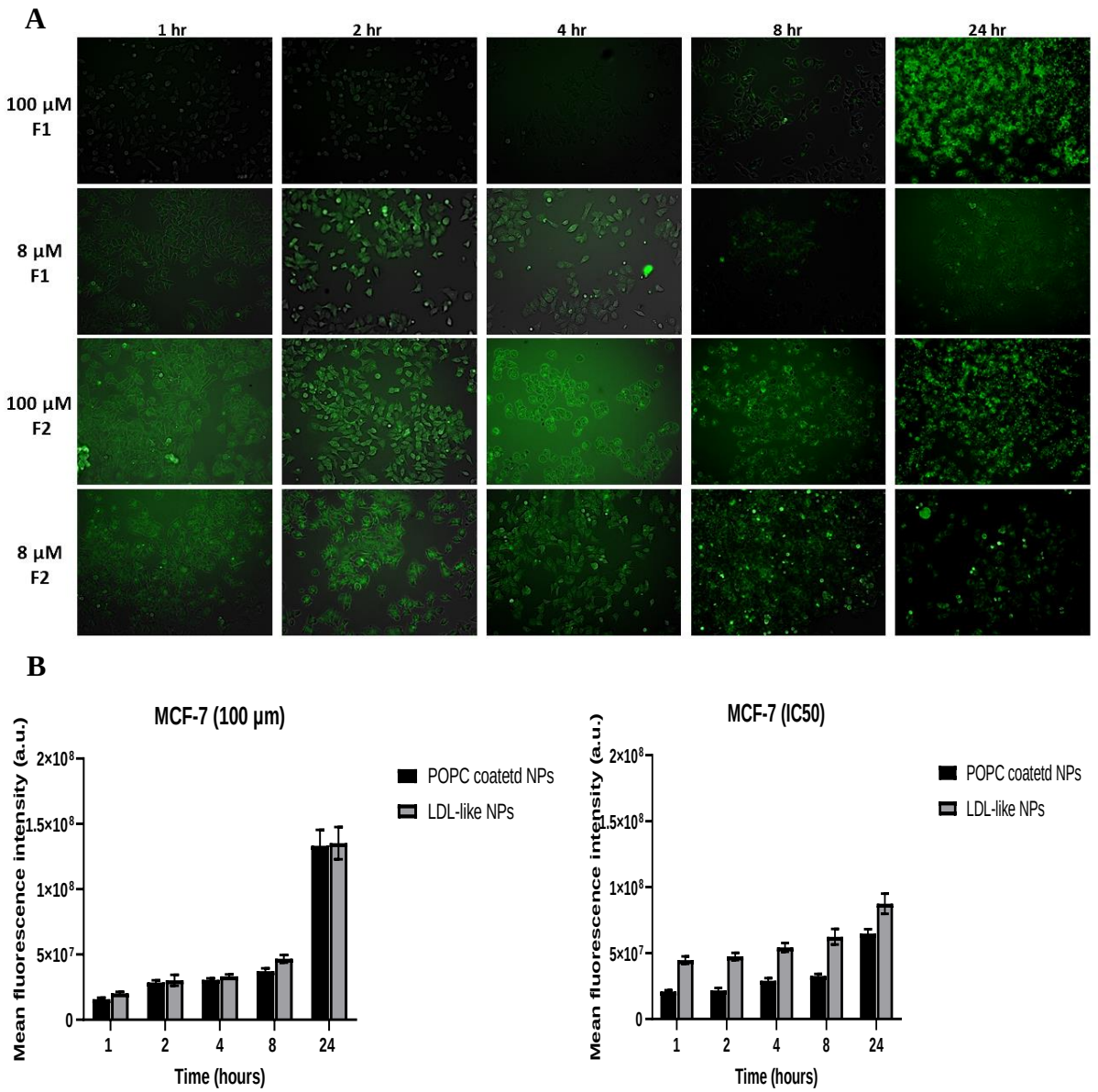

Figure 91 Cellular uptake fluorescent imaging carried out on MCF-7 breast cancer cell lines, captured at specific time intervals (1, 2, 4, 8 and 24 hours) following the treatment of the cells with one of the formulations (F1, F2) at two different concentrations each (100µM and 40µM). F1 is fluorescently labelled POPC coated orlistat NPs, F2 fluorescently labelled LDL-like orlistat NPs. A) Fluorescent microscopy images, B) Mean fluorescence intensity plot, n=3 ±SD.

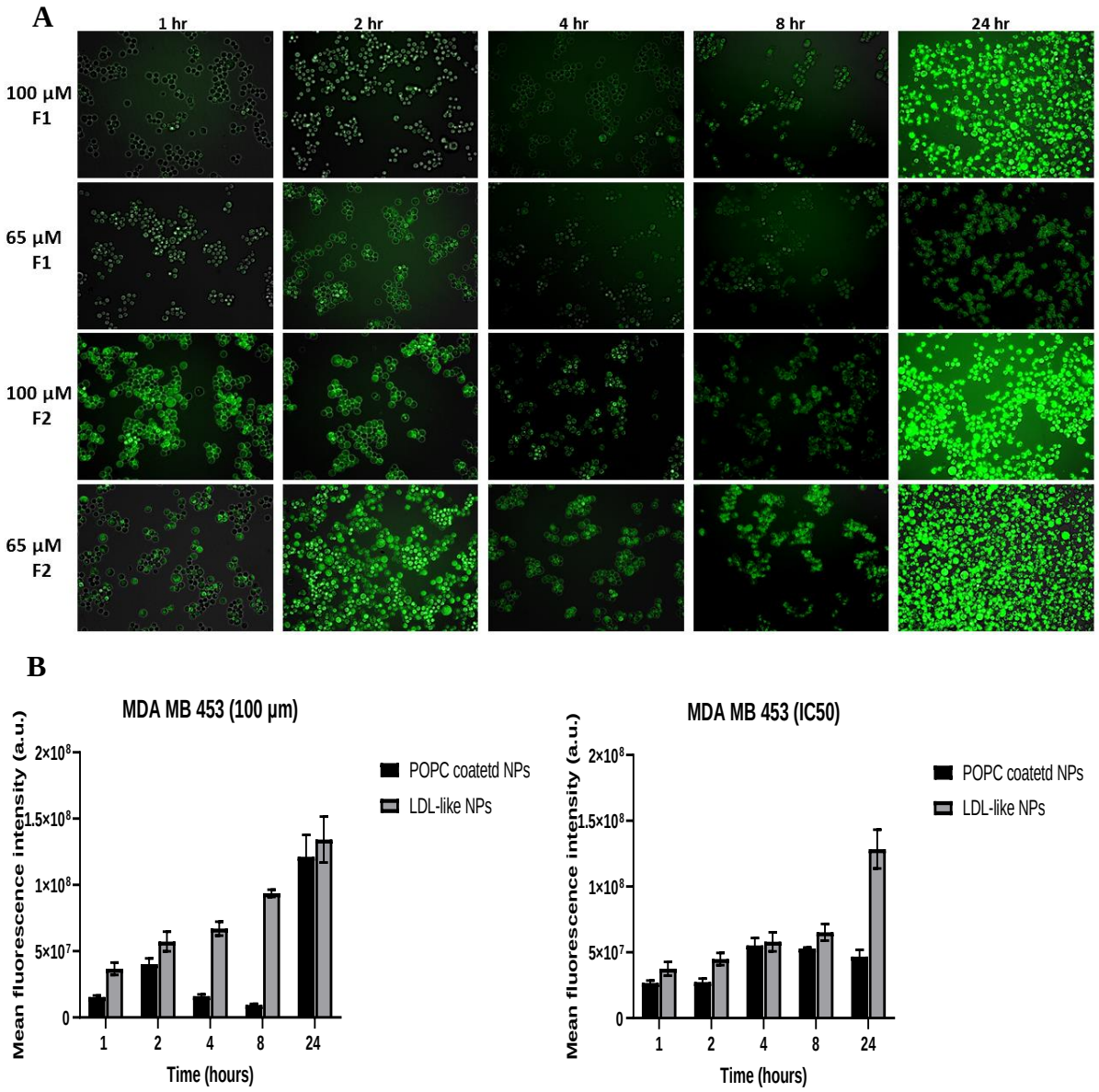

Figure 92 Cellular uptake fluorescent imaging carried out on MDA MB 453 breast cancer cell lines, captured at specific time intervals (1, 2, 4, 8 and 24 hours) following the treatment of the cells with one of the formulations (F1, F2) at two different concentrations each (100µM and 40µM). F1 is fluorescently labelled POPC coated orlistat NPs, F2 fluorescently labelled LDL-like orlistat NPs. A) Fluorescent microscopy images, B) Mean fluorescence intensity plot, n=3 ±SD.

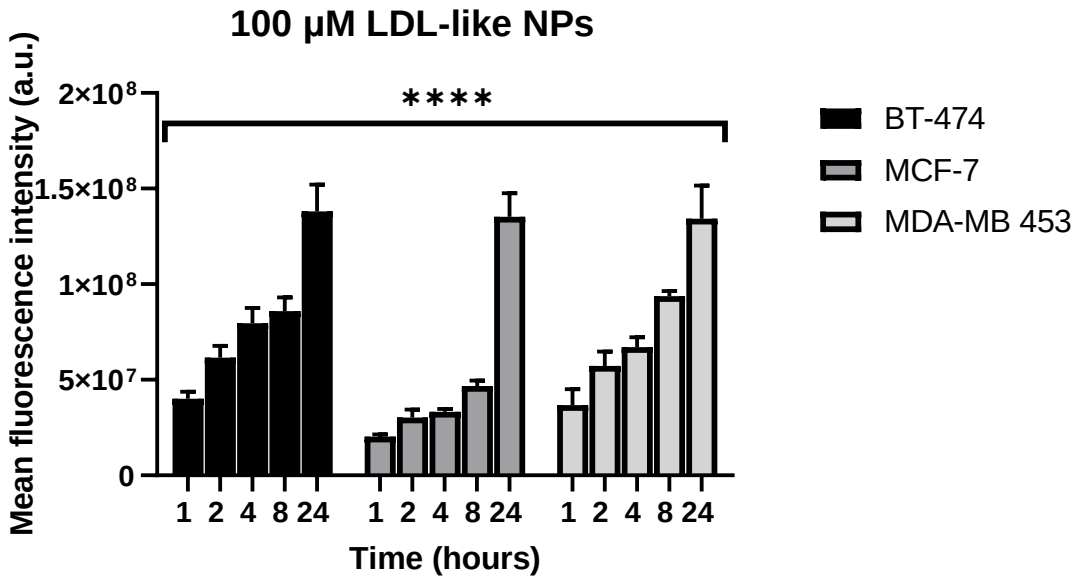

Figure 93 Cellular uptake rate using fluorescence microscopy for LDL-like ORL NPs in 3 different breast cancer cell lines, BT-474, MCF-7 and MDA MB 453 respectively, plotted as mean fluorescence intensity at concentration of 100 µM orlistat. ** Statistically significance between the three cell lines at P<0.0001 for each time point, n=3 ±SD.**

5.4.7 Cellular uptake mechanism

The mechanism of cellular uptake was done to investigate the uptake of the prepared NPs formulation through binding specifically to the LDLR on breast cancer cell lines. This was done through blocking this pathway followed by investigating the rate and amount of cellular uptake to the utilised cell lines using fluorescent imaging. **Figure 94 to Figure 96** (**A)** show the fluorescent images of the two employed formulations F1 and F2 in presence and absence of the LDLR blocker Suramin, followed by quantification of the fluorescence intensity in **Figure 94 to Figure 96 (B)**.

It is clearly illustrated that in presence of the LDLR blocker Suramin, the cellular uptake of the LDL-like ORL NPs F2 is highly reduced compared to its control group, while for the other formulation F1 the uptake was not highly affected compared to the control group. This effect was obvious in the three employed cell lines, indicating that the main mechanism of cellular

uptake for the LDL-like NPs was through binding to the LDLR receptors. Other cellular uptake mechanisms may be involved as well, this will require further investigation, this is illustrated through F1formulation, where the cellular uptake occurs mainly through other uptake mechanisms, rather than the LDLR mediated cellular uptake.

Concerning the BT 474 **Figure 94**, the fluorescent imaging showed blocking of cellular uptake in presence of Suramin at 30 and 60 minutes, compared to the control group without the Suramin. On the other hand, there was a minimum effect on the cellular uptake for F1, compared to the F2 formulation. The fluorescence intensity was significantly decreasing in the presence of Suramin for F2 formulation, indicating that the LDLR mediated transport is the main mechanism of cellular uptake.

For MCF 7 cell line **Figure 95**, the results were similar to that discussed before, however the uptake of F2 formulation in presence of Suramin is more reduced than in case of BT 474. For the MDA MB 453 cell lines **Figure 96**, the results were as well indicative for the LDLR mediated uptake being the main mechanism of uptake for the LDL-Like ORL NPs formulation F2.

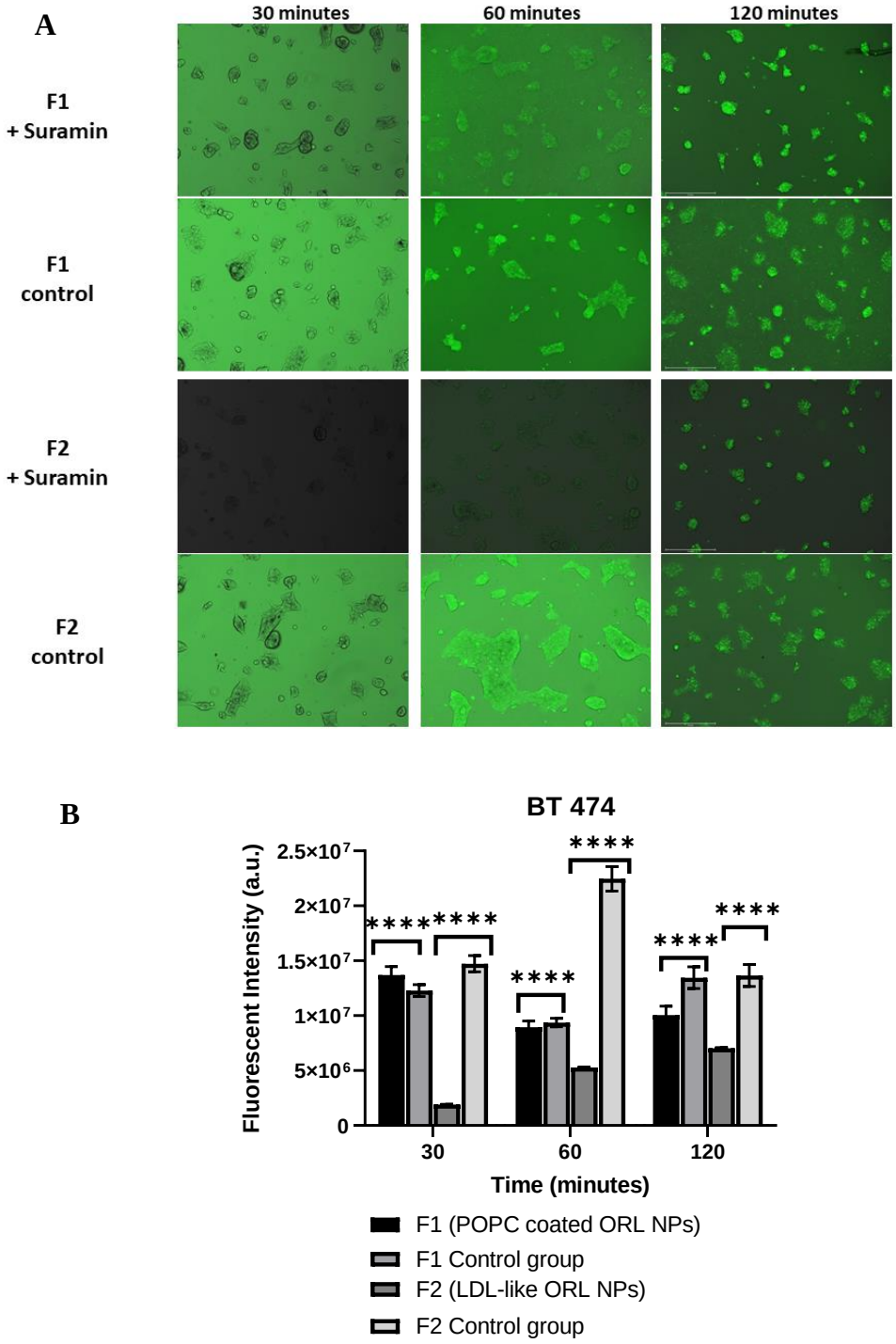

Figure 94 Cellular uptake fluorescent imaging carried out on BT 474 breast cancer cell lines, captured at specific time intervals (30,60 and 120 minutes) following the treatment of the cells with one of the formulations (F1, F2) in presence or absence of Suramin. F1 is fluorescently labelled POPC coated orlistat NPs, F2 fluorescently labelled LDL-like orlistat NPs. A) Fluorescent microscopy images, B) Mean fluorescence intensity plot. ** Statistically significance between the three cell lines at P<0.0001 for each time point, n=3 ±SD.**

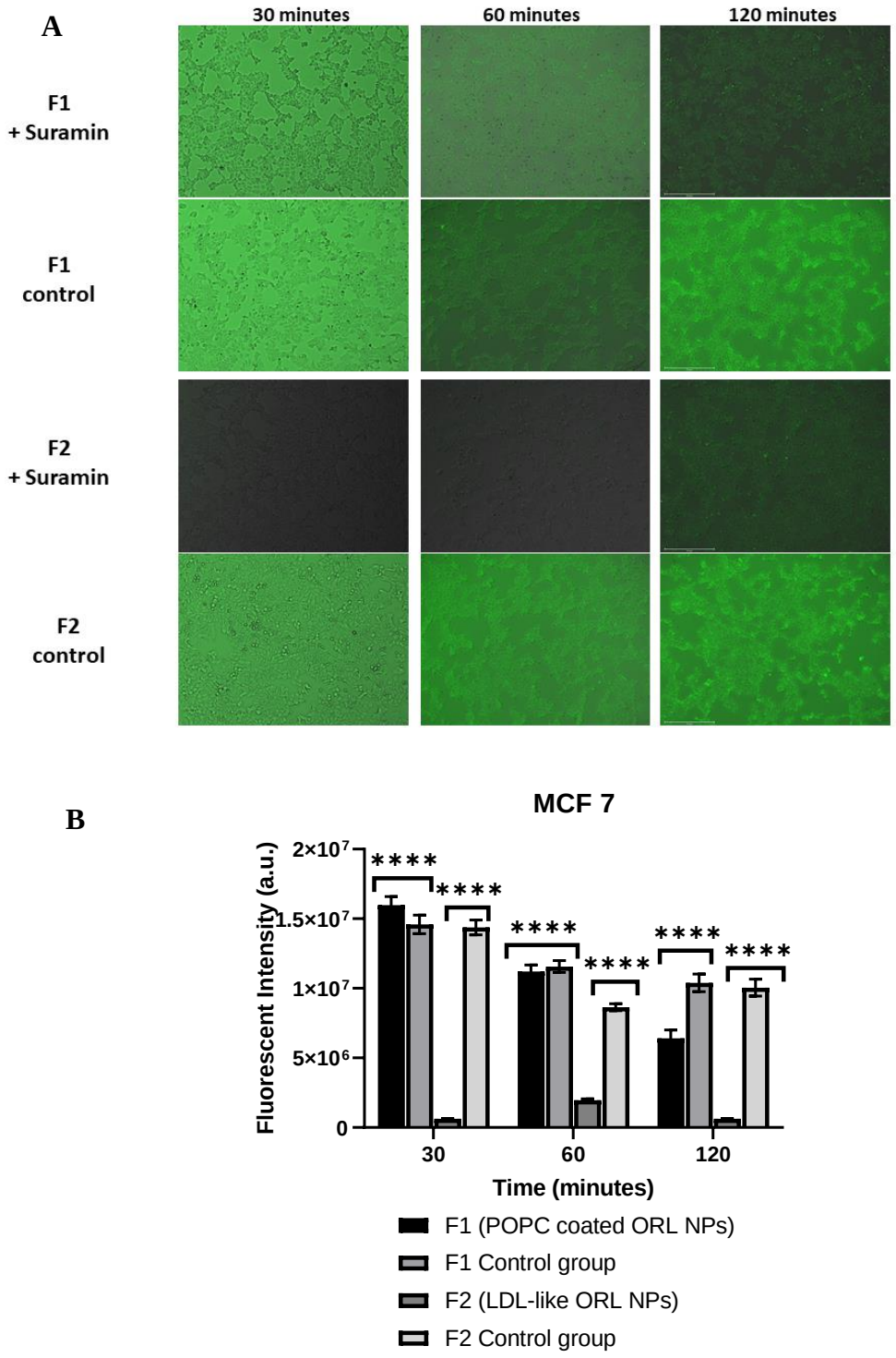

Figure 95 Cellular uptake fluorescent imaging carried out on MCF-7 breast cancer cell lines, captured at specific time intervals (30,60 and 120 minutes) following the treatment of the cells with one of the formulations (F1, F2) in presence or absence of Suramin. F1 is fluorescently labelled POPC coated orlistat NPs, F2 fluorescently labelled LDL-like orlistat NPs. A) Fluorescent microscopy images, B) Mean fluorescence intensity plot. ** Statistically significance between the three cell lines at P<0.0001 for each time point, n=3 ±SD.**

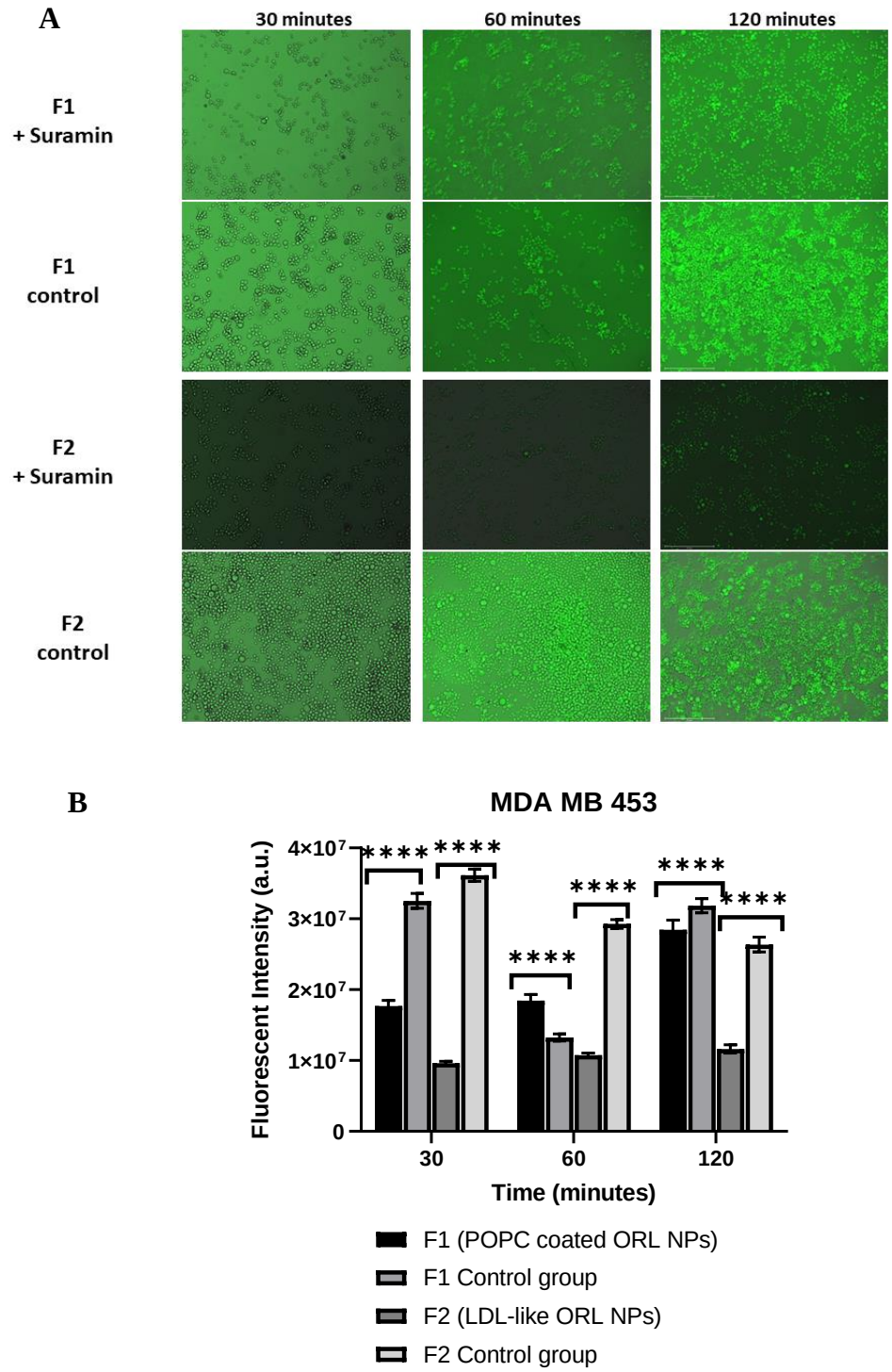

Figure 96 Cellular uptake fluorescent imaging carried out on MDA MB 453 breast cancer cell lines, captured at specific time intervals (30,60 and 120 minutes) following the treatment of the cells with one of the formulations (F1, F2) in presence or absence of Suramin. F1 is fluorescently labelled POPC coated orlistat NPs, F2 fluorescently labelled LDL-like orlistat NPs. A) Fluorescent microscopy images, B) Mean fluorescence intensity plot. ** Statistically significance between the three cell lines at P<0.0001 for each time point, n=3 ±SD.**

5.5 CONCLUSIONS

- Functionalised LDL-like orlistat NPs were prepared through attachment of an 11-mer peptide moiety to the surface of the NPs. This 11-mer peptide resembles the active site of the Apoprotein B found in the natural LDL structure (SA1).
- The proposed click chemistry technique used for attachment of the 11-mer peptide to the DSPE PEG (5000) maleimide moiety on the NPs surface was effective. This is emphasised through complete conjugation of the free sulfhydryl groups in the peptide (SA2).
- The Functionalised LDL-like orlistat NPs had an average zeta potential (~ -25 mV) and a small overall particle size (~40 nm), with no particle size increase compared to that of the orlistat NPs with no peptide incorporated (SA3).
- The Functionalised LDL-like orlistat NPs had an average zeta potential (~ -25 mV), despite the positive nature of the added peptide moiety (SA3).
- The properties of the orlistat NPs prepared by rapid solvent shift technique did not change dramatically after dilution in culture medium DMEM. This was investigated in terms of particle size and surface charge (SA4).
- Orlistat has minimal binding to the human serum album, resulting in minimal quenching of the intrinsic fluorescence of the HSA (SA4).
- Cytotoxicity assay of the LDL-like orlistat NPs showed efficacy of our formulation in reduction of survival rates of the breast cancer cell lines, resulting in an apparent decrease in the IC50 compared to that formulation without peptide coating (SA5).
- Cellular uptake study showed a rapid internalisation of the functionalised orlistat LDL-like NPs compared to the other NPs formulation without peptide coating. This effect was proportion to the over expression of the LDLR receptors in the breast cancer cell lines used (SA5).

6 Chapter 6 Conclusions and future work

6.1 CONCLUSIONS

Through this study we tried to study the rapid solvent shift technique, known also as flash nanoprecipitation, as a method of nanoparticles bottom-up preparation. It is considered one of the straightforward easy methods that could help enhancing industrial production and scale-up. We studied controlling of particle size for NPs prepared of hydrophobic material using this technique, yet other factors for controlling the particle size need to be more extensively studied.

The study started by investigating the flash nanoprecipitation technique, also known rapid solvent shift technique, as an effective method for preparation of nanoparticles NPs of hydrophobic materials and drugs. In Chapter 3 we tried to have a better understanding for the process of nanoprecipitation, and the effect of increasing the concentration of the employed material on the overall physico-chemical properties of the prepared NPs. This was done through using of simple lipid materials including olive oil, trihexanoin and tridecanoate, followed by comparison to some active pharmaceutical ingredients APIs such as orlistat and niclosamide stearate. Through Chapter 3 we concluded that,

- Particle size of the formed nanoparticles by flash nanoprecipitation was found to be dependent on the concentration of the hydrophobic material used.
- Coating of NPs using phospholipids and/or surfactants could help controlling the particles size during nanoprecipitation.
- Flash nanoprecipitation as method of nanoparticle precipitation was studied for a range of hydrophobic materials including olive oil, tricaprin, trihexanoin, niclosamide stearate, and orlistat. Interestingly, they all shared similar trend of particle size growth with increasing employed concentrations. The inflection points **Figure 26** depends on the material used.

- Coating of NPs with POPC, tween 80 and lecithin was useful in controlling particle size growth. The coating material prevents the process of condensation of nuclei and nanoparticle growth.
- The core to coat molar ratio greatly affects the control of particle size. Utilising insufficient coating material may result in incomplete coating of the formed NPs and hence particle size growth. On the other hand, higher amount of coating materials is undesirable leading to formation of unfavourable micelles and decreasing the drug loading.
- Screening various core to coat ratios showed that the optimum ratio should be around 2:1, or to be in the range between 1.5: and 2.3:1.
- Rapid solvent shift technique was better than the slow dripping method for preparing NPs of hydrophobic material and of controlled size.

Orlistat, a recently introduced anticancer candidate was studied for preparation of NPs using the flash nanoprecipitation technique in Chapter 4. The prepared NPs were evaluated in terms of its physico-chemical properties, followed by freeze drying to ensure stability over storage. Orlistat NPs will further be processed into a novel LDL-like surface functionalised NPs formulation for targeted breast cancer delivery. Through Chapter 4 we found that,

- Orlistat NPs were successfully prepared by rapid solvent shift technique. The prepared NPs showed similar behaviour to other hydrophobic materials, showing a particle size growth with increasing concentrations.
- Coating of orlistat with POPC in molar ratio 2:1 (core: coat) was effective in preventing particle size growth.
- Negative surface charge of the prepared orlistat NPs would be a useful tool to protect against any further aggregation.

- Additional stabilisation of NPs against particle size growth and aggregation could be achieved using various stabilisers, including surfactants and salts, which are added to the anti-solvent phase.
- Negatively charged surfactant, SDS was the best stabilising agent in prevent further aggregation and in controlling the size even after 2 weeks of storage. This is because of the repulsion forces implied between the particles.
- Further stabilisation of orlistat NPs could be done through freeze drying, to produce a solid powder for reconstitution, which will not only increase stability over the time, but as well help in better handling and ease of administration of the formulation.
- Freeze dried orlistat NPs where stable over a period of 6 month with minimal change in particle size and surface properties, this mainly depends on both the type and the amount of the used cryoprotectants.
- Coating of orlistat with POPC was successful in incorporating the drug inside a layer of the lipid in an amorphous mixture, this was shown through the disappearance of the orlistat peak in the DSC thermograms of POPC coated NPs.
- The coated orlistat NPs with POPC showed similar images with similar light birefringence under the polarised microscope to that of the POPC lipid indicating the presence of the POPC on the surface of the NPs structure.
- Our NPs formulation prepared through the rapid solvent shift technique showed a high entrapment efficiency of 73-76% with a loading efficiency of 60% which is promising in dose adjustment compared to other NPs formulations.
- The drug release study showed that the orlistat NPs remained intact for long period of time in physiological conditions, with no more than 40% of the drug was released from the NPs structure after 1 week. This is required to ensure the delivery of the intact NPs structure in the systemic circulation to the tumour cells, where it could release the drug.

Novel LDL-like orlistat NPs were prepared and evaluated for their physico-chemical properties, as well as their efficacy in breast cancer cell lines through Chapter 6. The method of preparation of the targeted therapy was relatively straightforward and easy, yet further studies of the formulation efficacy is required. In Chapter 6 we concluded that,

- Functionalised LDL-like orlistat NPs were prepared through attachment of an 11-mer peptide moiety to the surface of the NPs. This 11-mer peptide resemble the active site of the Apoprotein B found in the natural LDL structure.
- The proposed click chemistry technique used for attachment of the 11-mer peptide to the DSPE PEG (5000) maleimide moiety on the NPs surface was effective. This is emphasised through complete conjugation of the free sulfhydryl groups in the peptide.
- The functionalised LDL-like orlistat NPs had an average zeta potential (~ -25 mV) and a small overall particle size (~40 nm), with no particle size increase compared to that of the orlistat NPs with no peptide incorporated.
- The functionalised LDL-like orlistat NPs had an average zeta potential (~ -25 mV), despite the positive nature of the added peptide moiety.
- The properties of the orlistat NPs prepared by rapid solvent shift technique did not change dramatically after dilution in culture medium DMEM. This was investigated in terms of particle size and surface charge.
- Orlistat has minimal binding capacity to the human serum album, resulting in minimal quenching of the intrinsic fluorescence of the HSA.
- Cytotoxicity assay of the LDL-like orlistat NPs showed efficacy of our formulation in reduction of survival rates of the breast cancer cell lines, resulting in an apparent decrease in the IC50 compared to that formulation without peptide coating.
- Cellular uptake study showed a rapid internalisation of the functionalised orlistat LDL-like NPs compared to the other NPs formulation without peptide coating. This effect was

proportion to the over expression of the LDLR receptors in the breast cancer cell lines used.

6.2 FUTURE WORK

Throughout this work, the main aim was to target breast cancer, and to develop a formulation that could be further processed in future for clinical studies. Yet, extensive work in the future is required to transfer our formulation into animal and clinical studies.

- Further understanding of the surface charge of the orlistat NPs prepared by flash nanoprecipitation technique.
- Investigation the preparation of NPs of other hydrophobic APIs of log P <6 to through flash nanoprecipitation.
- Stabilisation of the prepared LDL-like ORL NPs formulation, mainly through studying lyophilisation of the formulation, for preparation of fine re-constitutable powder suitable for IV injection.
- Investigation of the efficacy of the prepared LDL-Like ORL NPs in more breast cancer cell lines, as well as in other cancerous tissues.
- More sstudies regarding the effect of the formulation on cell cycle arrest, cellular respiration, and other cellular metabolic activities
- Further investigation of the mechanism of cellular uptake of the prepared LDL-like NPs.
- Further study of the effect of ORL NPs on FASN inhibition in breast cancer cell lines.
- Stability study of the formulation in serum, to study the expected behaviour of our formulation in physiological conditions.
- Studies regarding steralisation of the formulation and stability after steralisation , for suitability of injection.
- In vivo studies of the efficacy of the formulations on animal models including rats and canines, to investigate the pharmacokinetics and pharmacodynamics of the formulation.

7 Reference

1. Northouse LL, Mood D, Kershaw T, Schafenacker A, Mellon S, Walker J, et al. Quality of Life of Women With Recurrent Breast Cancer and Their Family Members. JCO. 2002 Oct 1;20(19):4050–64.

2. Nounou MI, ElAmrawy F, Ahmed N, Abdelraouf K, Goda S, Syed-Sha-Qhattal H. Breast Cancer: Conventional Diagnosis and Treatment Modalities and Recent Patents and Technologies. Breast Cancer: Basic and Clinical Research. 2015 Jan;9s2:BCBCR.S29420.

3. Cancer Statistics for the UK [Internet]. Cancer Research UK. 2015 [cited 2022 Mar 21]. Available from: https://www.cancerresearchuk.org/health-professional/cancer-statistics-for-the-uk

4. Cancer Control in Egypt - The ASCO Post [Internet]. [cited 2022 Mar 21]. Available from: https://ascopost.com/issues/march-25-2021/cancer-control-in-egypt/

5. Andresen TL, Jensen SS, Jørgensen K. Advanced strategies in liposomal cancer therapy: Problems and prospects of active and tumor specific drug release. Progress in Lipid Research. 2005 Jan 1;44(1):68–97.

6. Markman JL, Rekechenetskiy A, Holler E, Ljubimova JY. Nanomedicine therapeutic approaches to overcome cancer drug resistance. Advanced Drug Delivery Reviews. 2013 Nov 30;65(13):1866–79.

7. Barenholz Y. Doxil®--the first FDA-approved nano-drug: lessons learned. J Control Release. 2012 Jun 10;160(2):117–34.

8. Hare JI, Lammers T, Ashford MB, Puri S, Storm G, Barry ST. Challenges and strategies in anti-cancer nanomedicine development: An industry perspective. Advanced Drug Delivery Reviews. 2017 Jan 1;108:25–38.

9. Global cancer statistics, 2012 - Torre - 2015 - CA: A Cancer Journal for Clinicians - Wiley Online Library [Internet]. [cited 2018 Nov 22]. Available from: https://onlinelibrary.wiley.com/doi/epdf/10.3322/caac.21262

10. Akram M, Siddiqui SA. Breast cancer management: Past, present and evolving. Indian Journal of Cancer. 2012 Jan 7;49(3):277.

11. Halioua B, Ziskind B. Medicine in the Days of the Pharaohs. Harvard University Press; 2005. 300 p.

12. The Edwin Smith Papyrus: Updated Translation of the Trauma Treatise and Modern Medical Commentaries. By Gonzalo M. Sanchez and Edmund S. Meltzer. Atalanta: Lockwood Press, 2012. Pp. xviii+379, illus. $ 250 {Distributed by ISD, Bristol, CT] [Internet]. ResearchGate. [cited 2018 Nov 30]. Available from: https://www.researchgate.net/publication/328791112_Rezension_The_Edwin_Smith_Papyrus_Updated_Translation_of_the_Trauma_Treatise_and_Modern_Medical_Commentaries_By_Gonzalo_M_Sanchez_and_Edmund_S_Meltzer_Atalanta_Lockwood_Press_2012_Pp_xviii379_illus_25

13. The Papyrus Ebers / [Internet]. [S.l. :; 19--?]. Available from: http://hdl.handle.net/2027/coo.31924073200077

14. Papavramidou N, Papavramidis T, Demetriou T. Ancient Greek and Greco–Roman Methods in Modern Surgical Treatment of Cancer. Ann Surg Oncol. 2010 Mar;17(3):665–7.

15. Gómez-Raposo C, Zambrana Tévar F, Sereno Moyano M, López Gómez M, Casado E. Male breast cancer. Cancer Treatment Reviews. 2010 Oct 1;36(6):451–7.

16. Yalaza M, İnan A, Bozer M. Male Breast Cancer. J Breast Health. 2016 Jan 1;12(1):1–8.

17. Giordano SH, Buzdar AU, Hortobagyi GN. Breast cancer in men. Ann Intern Med. 2002 Oct 15;137(8):678–87.

18. Breast Cancer - Statistics [Internet]. Cancer.Net. 2012 [cited 2019 Dec 27]. Available from: https://www.cancer.net/cancer-types/breast-cancer/statistics

19. Latest global cancer data: Cancer burden rises to 18.1 million new cases and 9.6 million cancer deaths in 2018. 2018;3.

20. Liu P, Qin L, Wang Q, Sun Y, Zhu M, Shen M, et al. cRGD-functionalized mPEG-PLGA-PLL nanoparticles for imaging and therapy of breast cancer. Biomaterials. 2012 Oct 1;33(28):6739–47.

21. Theek B, Rizzo LY, Ehling J, Kiessling F, Lammers T. The Theranostic Path to Personalized Nanomedicine. Clin Transl Imaging. 2014 Feb 1;2(1):66–76.

22. Choi KY, Liu G, Lee S, Chen X. Theranostic nanoplatforms for simultaneous cancer imaging and therapy: current approaches and future perspectives. Nanoscale. 2012 Jan 4;4(2):330–42.

23. Subramanian A, Manigandan A, P.R. S, Sethuraman S. Development of nanotheranostics against metastatic breast cancer — A focus on the biology & mechanistic approaches. Biotechnology Advances. 2015 Dec;33(8):1897–911.

24. Breast cancer recurrence and prognosis [Internet]. Breast Cancer Care. 2015 [cited 2018 Mar 26]. Available from: https://www.breastcancercare.org.uk/information-support/facing-breast-cancer/diagnosed-breast-cancer/your-primary-cancer-has-come-back-recurrence/breast-cancer-recurrence-prognosis

25. Hegde GV, de la Cruz C, Eastham-Anderson J, Zheng Y, Sweet-Cordero EA, Jackson EL. Residual Tumor Cells That Drive Disease Relapse after Chemotherapy Do Not Have

Enhanced Tumor Initiating Capacity. Tang DG, editor. PLoS ONE. 2012 Oct 24;7(10):e45647.

26. Khuwaja GA, Abu-Rezq AN. Bimodal breast cancer classification system. Pattern Analysis & Applic. 2004 Sep 1;7(3):235–42.

27. Bennett P, Oza UD, Trout AT, Mintz A, editors. Benign Breast Disease. In: Diagnostic Imaging: Nuclear Medicine (Second Edition) [Internet]. Philadelphia: Elsevier; 2016 [cited 2022 Feb 11]. p. 312–5. (Diagnostic Imaging). Available from: https://www.sciencedirect.com/science/article/pii/B9780323377539500840

28. Sharma GN, Dave R, Sanadya J, Sharma P, Sharma KK. VARIOUS TYPES AND MANAGEMENT OF BREAST CANCER: AN OVERVIEW. J Adv Pharm Technol Res. 2010;1(2):109–26.

29. Akram M, Iqbal M, Daniyal M, Khan AU. Awareness and current knowledge of breast cancer. Biol Res. 2017 Oct 2;50:33.

30. Loibl S, Poortmans P, Morrow M, Denkert C, Curigliano G. Breast cancer. The Lancet. 2021 May;397(10286):1750–69.

31. Feeley LP, Mulligan AM, Pinnaduwage D, Bull SB, Andrulis IL. Distinguishing luminal breast cancer subtypes by Ki67, progesterone receptor or TP53 status provides prognostic information. Mod Pathol. 2014 Apr;27(4):554–61.

32. Hansemann D. Ueber asymmetrische Zelltheilung in Epithelkrebsen und deren biologische Bedeutung. Archiv f pathol Anat. 1890 Feb 1;119(2):299–326.

33. Localization of a breast cancer susceptibility gene, BRCA2, to chromosome 13q12-13 - PubMed [Internet]. [cited 2022 Feb 11]. Available from: https://pubmed.ncbi.nlm.nih.gov/8091231/

34. Vogelstein B, Kinzler KW. Has the breast cancer gene been found? Cell. 1994 Oct 7;79(1):1–3.

35. M Deshpande T, Pandey A, Shyama S. Review: Breast cancer and etiology. Trends Med [Internet]. 2017 [cited 2022 Feb 11];17(1). Available from: http://www.oatext.com/review-breast-cancer-and-etiology.php

36. Breast cancer survival statistics [Internet]. Cancer Research UK. 2015 [cited 2022 Feb 14]. Available from: https://www.cancerresearchuk.org/health-professional/cancer-statistics/statistics-by-cancer-type/breast-cancer/survival

37. Kerlikowske K, Hubbard RA, Miglioretti DL, Geller BM, Yankaskas BC, Lehman CD, et al. Comparative Effectiveness of Digital Versus Film-Screen Mammography in Community Practice in the United States. Ann Intern Med. 2011 Oct 18;155(8):493–502.

38. Van Goethem M, Tjalma W, Schelfout K, Verslegers I, Biltjes I, Parizel P. Magnetic resonance imaging in breast cancer. Eur J Surg Oncol. 2006 Nov;32(9):901–10.

39. O'Connor M, Rhodes D, Hruska C. Molecular breast imaging. Expert Rev Anticancer Ther. 2009 Aug;9(8):1073–80.

40. Palmer ML, Tsangaris TN. Breast biopsy in women 30 years old or less. The American Journal of Surgery. 1993 Jun 1;165(6):708–12.

41. Dhankhar R, Vyas SP, Jain AK, Arora S, Rath G, Goyal AK. Advances in novel drug delivery strategies for breast cancer therapy. Artif Cells Blood Substit Immobil Biotechnol. 2010 Oct;38(5):230–49.

42. Rath GK. RADIATION THERAPY IN THE MANAGEMENT OF CANCER. :9.

43. Houssami N, Cuzick J, Dixon JM. The prevention, detection, and management of breast cancer. Medical Journal of Australia. 2006;184(5):230–4.

44. Callahan R, Hurvitz S. HER2-Positive Breast Cancer: Current Management of Early, Advanced, and Recurrent Disease. Curr Opin Obstet Gynecol. 2011 Feb;23(1):37–43.

45. Swain SM, Im YH, Im SA, Chan V, Miles D, Knott A, et al. Safety Profile of Pertuzumab With Trastuzumab and Docetaxel in Patients From Asia With Human Epidermal Growth Factor Receptor 2-Positive Metastatic Breast Cancer: Results From the Phase III Trial CLEOPATRA. Oncologist. 2014 Jul;19(7):693–701.

46. Findlay M, Minckwitz G von, Wardley A. Effective oral chemotherapy for breast cancer: pillars of strength. Annals of Oncology. 2008 Feb 1;19(2):212–22.

47. Patient compliance with oral chemotherapy as assessed by a novel electronic technique - PubMed [Internet]. [cited 2022 Feb 14]. Available from: https://pubmed.ncbi.nlm.nih.gov/1588365/

48. Toffoli G, Corona G, Sorio R, Robieux I, Basso B, Colussi AM, et al. Population pharmacokinetics and pharmacodynamics of oral etoposide. Br J Clin Pharmacol. 2001 Nov;52(5):511–9.

49. Lush RM, McCune JS, Tetteh L, Thompson JA, Mahany JJ, Garland L, et al. The absolute bioavailability of oral vinorelbine in patients with solid tumors. Cancer Chemother Pharmacol. 2005 Dec;56(6):578–84.

50. Maliepaard M, van Gastelen MA, Tohgo A, Hausheer FH, van Waardenburg RC, de Jong LA, et al. Circumvention of breast cancer resistance protein (BCRP)-mediated resistance to camptothecins in vitro using non-substrate drugs or the BCRP inhibitor GF120918. Clin Cancer Res. 2001 Apr;7(4):935–41.

51. Chemotherapy for Breast Cancer | Breast Cancer Treatment [Internet]. [cited 2022 Feb 14]. Available from: https://www.cancer.org/cancer/breast-cancer/treatment/chemotherapy-for-breast-cancer.html

52. Managing Chemotherapy Side Effects [Internet]. Breastcancer.org. 2020 [cited 2022 Feb 14]. Available from: https://www.breastcancer.org/treatment/chemotherapy/side_effects

53. Davis ME, Chen Z (Georgia), Shin DM. Nanoparticle therapeutics: an emerging treatment modality for cancer. Nature Reviews Drug Discovery. 2008 Sep;7(9):771–82.

54. Torchilin V. Tumor delivery of macromolecular drugs based on the EPR effect. Adv Drug Deliv Rev. 2011 Mar 18;63(3):131–5.

55. Fang J, Nakamura H, Maeda H. The EPR effect: Unique features of tumor blood vessels for drug delivery, factors involved, and limitations and augmentation of the effect. Adv Drug Deliv Rev. 2011 Mar 18;63(3):136–51.

56. Maeda H. The enhanced permeability and retention (EPR) effect in tumor vasculature: the key role of tumor-selective macromolecular drug targeting. Adv Enzyme Regul. 2001;41:189–207.

57. Kobayashi H, Watanabe R, Choyke PL. Improving conventional enhanced permeability and retention (EPR) effects; what is the appropriate target? Theranostics. 2013 Dec 11;4(1):81–9.

58. Tejada-Berges T, Granai CO, Gordinier M, Gajewski W. Caelyx/Doxil for the treatment of metastatic ovarian and breast cancer. Expert Rev Anticancer Ther. 2002 Apr;2(2):143–50.

59. Attia MF, Anton N, Wallyn J, Omran Z, Vandamme TF. An overview of active and passive targeting strategies to improve the nanocarriers efficiency to tumour sites. Journal of Pharmacy and Pharmacology. 2019 Jul 3;71(8):1185–98.

60. Huynh E, Zheng G. Cancer nanomedicine: addressing the dark side of the enhanced permeability and retention effect. Nanomedicine (Lond). 2015;10(13):1993–5.

61. Foged C, Brodin B, Frokjaer S, Sundblad A. Particle size and surface charge affect particle uptake by human dendritic cells in an in vitro model. International Journal of Pharmaceutics. 2005 Jul 25;298(2):315–22.

62. Immordino ML, Dosio F, Cattel L. Stealth liposomes: review of the basic science, rationale, and clinical applications, existing and potential. Int J Nanomedicine. 2006 Sep;1(3):297–315.

63. Leserman LD, Barbet J, Kourilsky F, Weinstein JN. Targeting to cells of fluorescent liposomes covalently coupled with monoclonal antibody or protein A. 1980;288:3.

64. Wang X, Li S, Shi Y, Chuan X, Li J, Zhong T, et al. The development of site-specific drug delivery nanocarriers based on receptor mediation. Journal of Controlled Release. 2014 Nov 10;193:139–53.

65. Alibolandi M, Abnous K, Sadeghi F, Hosseinkhani H, Ramezani M, Hadizadeh F. Folate receptor-targeted multimodal polymersomes for delivery of quantum dots and doxorubicin to breast adenocarcinoma: In vitro and in vivo evaluation. Int J Pharm. 2016 Mar 16;500(1–2):162–78.

66. Chiang CL, Cheng MH, Lin CH. From Nanoparticles to Cancer Nanomedicine: Old Problems with New Solutions. Nanomaterials. 2021 Jul;11(7):1727.

67. Lee ALZ, Wang Y, Cheng HY, Pervaiz S, Yang YY. The co-delivery of paclitaxel and Herceptin using cationic micellar nanoparticles. Biomaterials. 2009 Feb;30(5):919–27.

68. Wong MY, Chiu GNC. Liposome formulation of co-encapsulated vincristine and quercetin enhanced antitumor activity in a trastuzumab-insensitive breast tumor xenograft model. Nanomedicine. 2011 Dec;7(6):834–40.

69. Mohajer G, Lee ES, Bae YH. Enhanced intercellular retention activity of novel pH-sensitive polymeric micelles in wild and multidrug resistant MCF-7 cells. Pharm Res. 2007 Sep;24(9):1618–27.

70. Rouhollah K, Pelin M, Serap Y, Gozde U, Ufuk G. Doxorubicin Loading, Release, and Stability of Polyamidoamine Dendrimer-Coated Magnetic Nanoparticles. Journal of Pharmaceutical Sciences. 2013 Jun;102(6):1825–35.

71. Balakrishnan S, Bhat FA, Raja Singh P, Mukherjee S, Elumalai P, Das S, et al. Gold nanoparticle–conjugated quercetin inhibits epithelial–mesenchymal transition, angiogenesis and invasiveness via EGFR/VEGFR-2-mediated pathway in breast cancer. Cell Prolif. 2016 Sep 18;49(6):678–97.

72. Ahmed M, Douek M. The Role of Magnetic Nanoparticles in the Localization and Treatment of Breast Cancer. Biomed Res Int. 2013;2013:281230.

73. Bae PK, Chung BH. Multiplexed detection of various breast cancer cells by perfluorocarbon/quantum dot nanoemulsions conjugated with antibodies. Nano Convergence. 2014 Dec;1(1):23.

74. Jayakumar R, Prabaharan M, Nair SV, Tamura H. Novel chitin and chitosan nanofibers in biomedical applications. Biotechnol Adv. 2010 Feb;28(1):142–50.

75. Han HD, Mora EM, Roh JW, Nishimura M, Lee SJ, Stone RL, et al. Chitosan hydrogel for localized gene silencing. Cancer Biol Ther. 2011 May 1;11(9):839–45.

76. Dooley WC, Ljung BM, Veronesi U, Cazzaniga M, Elledge RM, O'Shaughnessy JA, et al. Ductal Lavage for Detection of Cellular Atypia in Women at High Risk for Breast Cancer. JNCI: Journal of the National Cancer Institute. 2001 Nov 7;93(21):1624–32.

77. Montemurro F, Aglietta M. Incorporating trastuzumab into the neoadjuvant treatment of HER2-overexpressing breast cancer. Clin Breast Cancer. 2005 Apr;6(1):77–80.

78. Shimizu N, Behzadian MA, Shimizu Y. Genetics of cell surface receptors for bioactive polypeptides: Binding of epidermal growth factor is associated with the presence of human chromosome 7 in human-mouse cell hybrids. Proc Natl Acad Sci U S A. 1980 Jun;77(6):3600–4.

79. Sachdev D, Li SL, Hartell JS, Fujita-Yamaguchi Y, Miller JS, Yee D. A chimeric humanized single-chain antibody against the type I insulin-like growth factor (IGF) receptor renders breast cancer cells refractory to the mitogenic effects of IGF-I. Cancer Res. 2003 Feb 1;63(3):627–35.

80. Pidgeon GP, Barr MP, Harmey JH, Foley DA, Bouchier-Hayes DJ. Vascular endothelial growth factor (VEGF) upregulates BCL-2 and inhibits apoptosis in human and murine mammary adenocarcinoma cells. Br J Cancer. 2001 Jul;85(2):273–8.

81. Zhang Y, Huang Y, Li S. Polymeric Micelles: Nanocarriers for Cancer-Targeted Drug Delivery. AAPS PharmSciTech. 2014 Apr 4;15(4):862–71.

82. Wang AZ, Langer R, Farokhzad OC. Nanoparticle delivery of cancer drugs. Annu Rev Med. 2012;63:185–98.

83. Sharma A. Liposomes in drug delivery: Progress and limitations. International Journal of Pharmaceutics. 1997 Aug 26;154(2):123–40.

84. Sengupta S, Eavarone D, Capila I, Zhao G, Watson N, Kiziltepe T, et al. Temporal targeting of tumour cells and neovasculature with a nanoscale delivery system. Nature. 2005 Jul 28;436(7050):568–72.

85. Singh S, Singh S, Lillard Jr JW, Singh R. Drug delivery approaches for breast cancer. IJN. 2017 Aug;Volume 12:6205–18.

86. Jain S, Hirst DG, O'Sullivan JM. Gold nanoparticles as novel agents for cancer therapy. Br J Radiol. 2012 Feb;85(1010):101–13.

87. Eissa S, Azzazy HME, Matboli M, Shawky SM, Said H, Anous FA. The Prognostic Value of Histidine-Rich Glycoprotein RNA in Breast Tissue Using Unmodified Gold Nanoparticles Assay. Appl Biochem Biotechnol. 2014 Sep 1;174(2):751–61.

88. Gobbo OL, Sjaastad K, Radomski MW, Volkov Y, Prina-Mello A. Magnetic Nanoparticles in Cancer Theranostics. Theranostics. 2015;5(11):1249–63.

89. Chauhan S, Yallapu M, Othman S, Curtis E, Bauer N, Chauhan, et al. Curcumin-loaded magnetic nanoparticles for breast cancer therapeutics and imaging applications. International Journal of Nanomedicine. 2012 Apr;1761.

90. Fernández-Pacheco R, Valdivia JG, Ibarra MR. Magnetic Nanoparticles for Local Drug Delivery Using Magnetic Implants. In: Foote RS, Lee JW, editors. Micro and Nano Technologies in Bioanalysis [Internet]. Totowa, NJ: Humana Press; 2009 [cited 2018 Jun 29]. p. 559–69. Available from: http://link.springer.com/10.1007/978-1-59745-483-4_35

91. Wolinsky JB, Colson YL, Grinstaff MW. Local drug delivery strategies for cancer treatment: Gels, nanoparticles, polymeric films, rods, and wafers. Journal of Controlled Release. 2012 Apr;159(1):14–26.

92. Shah P. Use of Nanotechnologies for Drug Delivery. MRS Bulletin. 2006 Nov 1;31(11):894–9.

93. Van Eerdenbrugh B, Van den Mooter G, Augustijns P. Top-down production of drug nanocrystals: Nanosuspension stabilization, miniaturization and transformation into solid products. International Journal of Pharmaceutics. 2008 Nov 19;364(1):64–75.

94. Keck CM, Müller RH. Drug nanocrystals of poorly soluble drugs produced by high pressure homogenisation. European Journal of Pharmaceutics and Biopharmaceutics. 2006 Jan 1;62(1):3–16.

95. Mu€ller RH, Mo€schwitzer J, Bushrab FN. Manufacturing of Nanoparticles by Milling and Homogenization Techniques. undefined [Internet]. 2006 [cited 2022 Feb 15]; Available from: https://www.semanticscholar.org/paper/Top-down-production-of-drug-nanocrystals%3A-and-into-Eerdenbrugh-Mooter/908e6b0aa29e8d44abadfd77fc77bf954752a416

96. Ding S, Anton N, Vandamme TF, Serra CA. Microfluidic nanoprecipitation systems for preparing pure drug or polymeric drug loaded nanoparticles: an overview. Expert Opinion on Drug Delivery. 2016 Oct 2;13(10):1447–60.

97. Astete CE, Kumar CSSR, Sabliov CM. Size control of poly(d,l-lactide-co-glycolide) and poly(d,l-lactide-co-glycolide)-magnetite nanoparticles synthesized by emulsion evaporation technique. Colloids and Surfaces A: Physicochemical and Engineering Aspects. 2007 May 15;299(1):209–16.

98. Jung J, Perrut M. Particle design using supercritical fluids: Literature and patent survey. The Journal of Supercritical Fluids. 2001 Aug 1;20(3):179–219.

99. Kumar S, Bhushan P, Bhattacharya S. Fabrication of Nanostructures with Bottom-up Approach and Their Utility in Diagnostics, Therapeutics, and Others. In: Bhattacharya S, Agarwal AK, Chanda N, Pandey A, Sen AK, editors. Environmental, Chemical and Medical Sensors [Internet]. Singapore: Springer; 2018 [cited 2022 Feb 15]. p. 167–98. (Energy, Environment, and Sustainability). Available from: https://doi.org/10.1007/978-981-10-7751-7_8

100. Saad WS, Prud'homme RK. Principles of nanoparticle formation by flash nanoprecipitation. Nano Today. 2016 Apr 1;11(2):212–27.

101. Weinberg MC, Poisl WH, Granasy L. Crystal growth and classical nucleation theory. Comptes Rendus Chimie. 2002 Nov 1;5(11):765–71.

102. Martínez Rivas CJ, Tarhini M, Badri W, Miladi K, Greige-Gerges H, Nazari QA, et al. Nanoprecipitation process: From encapsulation to drug delivery. International Journal of Pharmaceutics. 2017 Oct;532(1):66–81.

103. Kalikmanov VI. Classical Nucleation Theory. In: Kalikmanov VI, editor. Nucleation Theory [Internet]. Dordrecht: Springer Netherlands; 2013 [cited 2018 Aug 29]. p. 17–41. (Lecture Notes in Physics). Available from: https://doi.org/10.1007/978-90-481-3643-8_3

104. Dubrovskii V. Fundamentals of Nucleation Theory. In: Nucleation Theory and Growth of Nanostructures [Internet]. Berlin, Heidelberg: Springer Berlin Heidelberg; 2014 [cited 2018 Aug 29]. p. 1–73. Available from: http://link.springer.com/10.1007/978-3-642-39660-1_1

105. Mechanisms of Nucleation and Growth of Nanoparticles in Solution - Chemical Reviews (ACS Publications) [Internet]. [cited 2018 Aug 29]. Available from: https://pubs.acs.org/doi/10.1021/cr400544s

106. Lutsko JF. A dynamical theory of nucleation for colloids and macromolecules. The Journal of Chemical Physics. 2012 Jan 19;136(3):034509.

107. Erdemir D, Lee AY, Myerson AS. Nucleation of Crystals from Solution: Classical and Two-Step Models. Acc Chem Res. 2009 May 19;42(5):621–9.

108. Lifshitz IM, Slyozov VV. The kinetics of precipitation from supersaturated solid solutions. Journal of Physics and Chemistry of Solids. 1961 Apr 1;19(1):35–50.

109. Trefalt G, Palberg T, Borkovec M. Forces between colloidal particles in aqueous solutions containing monovalent and multivalent ions. Current Opinion in Colloid & Interface Science. 2017 Feb;27:9–17.

110. Israelachvili JN. Intermolecular and Surface Forces. Academic Press; 2011. 708 p.

111. Horn D, Rieger J. Organic Nanoparticles in the Aqueous Phase—Theory, Experiment, and Use. Angewandte Chemie International Edition. 2001 Dec 3;40(23):4330.

112. Pustulka KM, Wohl AR, Lee HS, Michel AR, Han J, Hoye TR, et al. Flash Nanoprecipitation: Particle Structure and Stability. Mol Pharmaceutics. 2013 Nov 4;10(11):4367–77.

113. Zhu Z. Flash Nanoprecipitation: Prediction and Enhancement of Particle Stability via Drug Structure. Mol Pharmaceutics. 2014 Mar 3;11(3):776–86.

114. Zhu Z, Margulis-Goshen K, Magdassi S, Talmon Y, Macosko CW. Polyelectrolyte Stabilized Drug Nanoparticles via Flash Nanoprecipitation: A Model Study With β-Carotene. Journal of Pharmaceutical Sciences. 2010 Oct 1;99(10):4295–306.

115. Chow SF, Wan KY, Cheng KK, Wong KW, Sun CC, Baum L, et al. Development of highly stabilized curcumin nanoparticles by flash nanoprecipitation and lyophilization. European Journal of Pharmaceutics and Biopharmaceutics. 2015 Aug 1;94:436–49.

116. Chiou H, Chan HK, Heng D, Prud'homme RK, Raper JA. A novel production method for inhalable cyclosporine A powders by confined liquid impinging jet precipitation. Journal of Aerosol Science. 2008 Jun 1;39(6):500–9.

117. Lince F, Bolognesi S, Stella B, Marchisio DL, Dosio F. Preparation of polymer nanoparticles loaded with doxorubicin for controlled drug delivery. Chemical Engineering Research and Design. 2011 Nov 1;89(11):2410–9.

118. Wan KY, Wong KW, Chow AHL, Chow SF. Impact of molecular rearrangement of amphiphilic stabilizers on physical stability of itraconazole nanoparticles prepared by flash nanoprecipitation. International Journal of Pharmaceutics. 2018 May 5;542(1):221–31.

119. Han J, Zhu Z, Qian H, Wohl AR, Beaman CJ, Hoye TR, et al. A simple confined impingement jets mixer for flash nanoprecipitation. Journal of Pharmaceutical Sciences. 2012 Oct 1;101(10):4018–23.

120. Chow SF, Sun CC, Chow AHL. Assessment of the relative performance of a confined impinging jets mixer and a multi-inlet vortex mixer for curcumin nanoparticle production. European Journal of Pharmaceutics and Biopharmaceutics. 2014 Oct 1;88(2):462–71.

121. Liu Y, Kathan K, Saad W, Prud'homme RK. Ostwald Ripening of $\ensuremath{\beta}$-Carotene Nanoparticles. Phys Rev Lett. 2007 Jan 17;98(3):036102.

122. Van Eerdenbrugh B, Vermant J, Martens JA, Froyen L, Van Humbeeck J, Augustijns P, et al. A screening study of surface stabilization during the production of drug nanocrystals. Journal of Pharmaceutical Sciences. 2009 Jun 1;98(6):2091–103.

123. Duro R, Souto C, Gómez-Amoza JL, Martínez-Pacheco R, Concheiro A. Interfacial adsorption of polymers and surfactants: Implications for the properties of disperse systems of pharmaceutical interest. Drug Development and Industrial Pharmacy. 1999;25(7):817–29.

124. Pattekari P, Zheng Z, Zhang X, Levchenko T, Torchilin V, Lvov Y. Top-down and bottom-up approaches in production of aqueous nanocolloids of low solubility drug paclitaxel. Phys Chem Chem Phys. 2011 Apr 27;13(19):9014–9.

125. Letchford K, Burt H. A review of the formation and classification of amphiphilic block copolymer nanoparticulate structures: micelles, nanospheres, nanocapsules and polymersomes. European Journal of Pharmaceutics and Biopharmaceutics. 2007 Mar 1;65(3):259–69.

126. Guhagarkar SA, Malshe VC, Devarajan PV. Nanoparticles of Polyethylene Sebacate: A New Biodegradable Polymer. AAPS PharmSciTech. 2009 Jul 24;10(3):935.

127. Kim S, Ng WK, Dong Y, Das S, Tan RBH. Preparation and physicochemical characterization of trans-resveratrol nanoparticles by temperature-controlled antisolvent precipitation. Journal of Food Engineering. 2012 Jan;108(1):37–42.

128. Siddiqui SW, Zhao Y, Kukukova A, Kresta SM. Characteristics of a Confined Impinging Jet Reactor: Energy Dissipation, Homogeneous and Heterogeneous Reaction Products, and Effect of Unequal Flow. Ind Eng Chem Res. 2009 Sep 2;48(17):7945–58.

129. Zhang HX, Wang JX, Zhang ZB, Le Y, Shen ZG, Chen JF. Micronization of atorvastatin calcium by antisolvent precipitation process. International Journal of Pharmaceutics. 2009 Jun 5;374(1):106–13.

130. Zhang JY, Shen ZG, Zhong J, Hu TT, Chen JF, Ma ZQ, et al. Preparation of amorphous cefuroxime axetil nanoparticles by controlled nanoprecipitation method without surfactants. International Journal of Pharmaceutics. 2006 Oct 12;323(1):153–60.

131. Sinha B, Müller RH, Möschwitzer JP. Bottom-up approaches for preparing drug nanocrystals: Formulations and factors affecting particle size. International Journal of Pharmaceutics. 2013 Aug 30;453(1):126–41.

132. Zheng G, Chen J, Li H, Glickson JD. Rerouting lipoprotein nanoparticles to selected alternate receptors for the targeted delivery of cancer diagnostic and therapeutic agents. PNAS. 2005 Dec 6;102(49):17757–62.

133. Firestone RA. Low-Density Lipoprotein as a Vehicle for Targeting Antitumor Compounds to Cancer Cells. Bioconjugate Chemistry. 1994 Mar;5(2):105–13.

134. Polo L, Valduga G, Jori G, Reddi E. Low-density lipoprotein receptors in the uptake of tumour photosensitizers by human and rat transformed fibroblasts. The International Journal of Biochemistry & Cell Biology. 2002 Jan 1;34(1):10–23.

135. Radu M, Munteanu MC, Petrache S, Serban AI, Dinu D, Hermenean A, et al. Depletion of intracellular glutathione and increased lipid peroxidation mediate cytotoxicity of hematite nanoparticles in MRC-5 cells. Acta Biochimica Polonica. 2010;57(3):355–60.

136. Nikanjam M, Gibbs AR, Hunt CA, Budinger TF, Forte TM. Synthetic nano-LDL with paclitaxel oleate as a targeted drug delivery vehicle for glioblastoma multiforme. Journal of Controlled Release. 2007 Dec 20;124(3):163–71.

137. Glickson JD, Lund-Katz S, Zhou R, Choi H, Chen IW, Li H, et al. Lipoprotein Nanoplatform for Targeted Delivery of Diagnostic and Therapeutic Agents. In: Liss P, Hansell P, Bruley DF, Harrison DK, editors. Oxygen Transport to Tissue XXX. Springer US; 2009. p. 227–39. (Advances in Experimental Medicine and Biology).

138. Medes G, Thomas A, Weinhouse S. Metabolism of Neoplastic Tissue. IV. A Study of Lipid Synthesis in Neoplastic Tissue Slices in Vitro. Cancer Res. 1953 Jan 1;13(1):27–9.

139. Ookhtens M, Kannan R, Lyon I, Baker N. Liver and adipose tissue contributions to newly formed fatty acids in an ascites tumor. Am J Physiol. 1984 Jul;247(1 Pt 2):R146-153.

140. Kuhajda FP, Jenner K, Wood FD, Hennigar RA, Jacobs LB, Dick JD, et al. Fatty acid synthesis: a potential selective target for antineoplastic therapy. Proc Natl Acad Sci U S A. 1994 Jul 5;91(14):6379–83.

141. Alò PL, Visca P, Botti C, Galati GM, Sebastiani V, Andreano T, et al. Immunohistochemical expression of human erythrocyte glucose transporter and fatty acid synthase in infiltrating breast carcinomas and adjacent typical/atypical hyperplastic or normal breast tissue. Am J Clin Pathol. 2001 Jul;116(1):129–34.

142. Menendez JA, Vellon L, Mehmi I, Oza BP, Ropero S, Colomer R, et al. Inhibition of fatty acid synthase (FAS) suppresses HER2/neu (erbB-2) oncogene overexpression in cancer cells. Proc Natl Acad Sci U S A. 2004 Jul 20;101(29):10715–20.

143. Baron A, Migita T, Tang D, Loda M. Fatty acid synthase: A metabolic oncogene in prostate cancer? Journal of Cellular Biochemistry. 2004;91(1):47–53.

144. Lupu R, Menendez JA. Pharmacological inhibitors of Fatty Acid Synthase (FASN)--catalyzed endogenous fatty acid biogenesis: a new family of anti-cancer agents? Curr Pharm Biotechnol. 2006 Dec;7(6):483–93.

145. Röhrig F, Schulze A. The multifaceted roles of fatty acid synthesis in cancer. Nat Rev Cancer. 2016 Nov;16(11):732–49.

146. Pemble CW, Johnson LC, Kridel SJ, Lowther WT. Crystal structure of the thioesterase domain of human fatty acid synthase inhibited by Orlistat. Nature Structural & Molecular Biology. 2007 Aug;14(8):704–9.

147. Kridel SJ, Axelrod F, Rozenkrantz N, Smith JW. Orlistat Is a Novel Inhibitor of Fatty Acid Synthase with Antitumor Activity. Cancer Research. 2004 Mar 15;64(6):2070–5.

148. Ma G, Zancanella M, Oyola Y, Richardson RD, Smith JW, Romo D. Total synthesis and comparative analysis of orlistat, valilactone, and a transposed orlistat derivative: Inhibitors of fatty acid synthase. Org Lett. 2006 Sep 28;8(20):4497–500.

149. Hill TK, Davis AL, Wheeler FB, Kelkar SS, Freund EC, Lowther WT, et al. Development of a Self-Assembled Nanoparticle Formulation of Orlistat, Nano-ORL, with Increased Cytotoxicity against Human Tumor Cell Lines. Mol Pharmaceutics. 2016 Mar 7;13(3):720–8.

150. Bhargava-Shah A, Foygel K, Devulapally R, Paulmurugan R. Orlistat and antisense-miRNA-loaded PLGA-PEG nanoparticles for enhanced triple negative breast cancer therapy. Nanomedicine (Lond). 2016 Feb;11(3):235–47.

151. Zhigaltsev IV, Belliveau N, Hafez I, Leung AKK, Huft J, Hansen C, et al. Bottom-Up Design and Synthesis of Limit Size Lipid Nanoparticle Systems with Aqueous and

Triglyceride Cores Using Millisecond Microfluidic Mixing. Langmuir. 2012 Feb 21;28(7):3633–40.

152. Fuentes de Mendoza M, De Miguel Gordillo C, Marín Expóxito J, Sánchez Casas J, Martínez Cano M, Martín Vertedor D, et al. Chemical composition of virgin olive oils according to the ripening in olives. Food Chemistry. 2013 Dec;141(3):2575–81.

153. Glyceryl Trioleate [Internet]. [cited 2022 Feb 7]. Available from: https://go.drugbank.com/drugs/DB13038

154. Walke P. Physico-Chemical Parameters of Nanoparticles that Govern Prodrug Design and Application in Anticancer Nanomedicine. [Center for Single Particle Science and Engineering (SPSE), Department of Physics, Chemistry and Pharmacy]: University of Southern Denmark; 2018.

155. Stolnik S, Illum L, Davis SS. Long circulating microparticulate drug carriers. Advanced Drug Delivery Reviews. 2012 Dec;64:290–301.

156. Jiang W, Kim BYS, Rutka JT, Chan WCW. Nanoparticle-mediated cellular response is size-dependent. Nature Nanotechnology. 2008 Mar;3(3):145–50.

157. Casettari L, Vllasaliu D, Castagnino E, Stolnik S, Howdle S, Illum L. PEGylated chitosan derivatives: Synthesis, characterizations and pharmaceutical applications. Progress in Polymer Science. 2012 May;37(5):659–85.

158. Cabral H, Matsumoto Y, Mizuno K, Chen Q, Murakami M, Kimura M, et al. Accumulation of sub-100 nm polymeric micelles in poorly permeable tumours depends on size. Nature Nanotechnology. 2011 Dec;6(12):815–23.

159. Orlistat [Internet]. [cited 2019 Dec 6]. Available from: https://www.drugbank.ca/drugs/DB01083

160. Intensity - Volume - Number | Malvern Panalytical [Internet]. [cited 2021 May 17]. Available from: https://www.malvernpanalytical.com/en/learn/knowledge-center/technical-notes/TN101104IntensityVolumeNumber

161. Barhoum A, García-Betancourt ML, Rahier H, Van Assche G. Chapter 9 - Physicochemical characterization of nanomaterials: polymorph, composition, wettability, and thermal stability. In: Barhoum A, Makhlouf ASH, editors. Emerging Applications of Nanoparticles and Architecture Nanostructures [Internet]. Elsevier; 2018 [cited 2022 Jan 10]. p. 255–78. (Micro and Nano Technologies). Available from: https://www.sciencedirect.com/science/article/pii/B9780323512541000099

162. Doane TL, Chuang CH, Hill RJ, Burda C. Nanoparticle ζ -Potentials. Acc Chem Res. 2012 Mar 20;45(3):317–26.

163. Clogston JD, Patri AK. Zeta Potential Measurement. In: McNeil SE, editor. Characterization of Nanoparticles Intended for Drug Delivery [Internet]. Totowa, NJ: Humana Press; 2011 [cited 2022 Jan 10]. p. 63–70. (Methods in Molecular Biology). Available from: https://doi.org/10.1007/978-1-60327-198-1_6

164. de Jonge N, Ross FM. Electron microscopy of specimens in liquid. Nature Nanotech. 2011 Nov;6(11):695–704.

165. Kumar PS, Pavithra KG, Naushad Mu. Characterization techniques for nanomaterials. In: Nanomaterials for Solar Cell Applications [Internet]. Elsevier; 2019 [cited 2022 Jan 14]. p. 97–124. Available from: https://linkinghub.elsevier.com/retrieve/pii/B9780128133378000047

166. Kumar TH, Reddy KM, Rishika D, Kumar RP. ESTIMATION OF ORLISTAT BY UV SPECTROPHOTOMETRIC METHOD. 2:3.

167. Yue PF, Lu XY, Zhang ZZ, Yuan HL, Zhu WF, Zheng Q, et al. The Study on the Entrapment Efficiency and In Vitro Release of Puerarin Submicron Emulsion. AAPS PharmSciTech. 2009 Jun 1;10(2):376–83.

168. Gonzalez Gomez A, Syed S, Marshall K, Hosseinidoust Z. Liposomal Nanovesicles for Efficient Encapsulation of Staphylococcal Antibiotics. ACS Omega. 2019 Jun 30;4(6):10866–76.

169. Ellman GL. Tissue sulfhydryl groups. Archives of biochemistry and biophysics : ABB. 1959;82(1):70–7.

170. Yasseen ZJ, El Ghossain MO. Studies on Binding of Widely used Drugs with Human Serum Albumin at Different Temperatures and PHs. J Biomed Sci [Internet]. 2016 [cited 2022 Jan 18];5(3). Available from: http://www.jbiomeds.com/biomedical-sciences/studies-on-binding-of-widely-used-drugs-with-human-serum-albumin-at-different-temperatures-and-phs.php?aid=9467

171. Lakowicz JR, editor. Principles of Fluorescence Spectroscopy [Internet]. Boston, MA: Springer US; 2006 [cited 2022 Jan 18]. Available from: http://link.springer.com/10.1007/978-0-387-46312-4

172. Bertrand N, Wu J, Xu X, Kamaly N, Farokhzad OC. Cancer nanotechnology: The impact of passive and active targeting in the era of modern cancer biology. Advanced Drug Delivery Reviews. 2014 Feb 1;66:2–25.

173. Chauhan VP, Popović Z, Chen O, Cui J, Fukumura D, Bawendi MG, et al. Fluorescent Nanorods and Nanospheres for Real-Time In Vivo Probing of Nanoparticle Shape-Dependent Tumor Penetration. Angewandte Chemie International Edition. 2011;50(48):11417–20.

174. Huntosova V, Buzova D, Petrovajova D, Kasak P, Nadova Z, Jancura D, et al. Development of a new LDL-based transport system for hydrophobic/amphiphilic drug delivery to cancer cells. International Journal of Pharmaceutics. 2012 Oct 15;436(1):463–71.

175. Brick MC, Palmer HJ, Whitesides TH. Formation of Colloidal Dispersions of Organic Materials in Aqueous Media by Solvent Shifting. Langmuir. 2003 Aug 1;19(16):6367–80.

176. Stone HA, Kim S. Microfluidics: Basic issues, applications, and challenges. American Institute of Chemical Engineers AIChE Journal. 2001 Jun;47(6):1250.

177. Reinhard PG, Suraud E. Introduction to Cluster Dynamics. John Wiley & Sons; 2008. 342 p.

178. Styliari ID, Conte C, Pearce AK, Hüsler A, Cavanagh RJ, Limo MJ, et al. High-Throughput Miniaturized Screening of Nanoparticle Formation via Inkjet Printing. Macromol Mater Eng. 2018 Aug;303(8):1800146.

179. Danaei M, Dehghankhold M, Ataei S, Hasanzadeh Davarani F, Javanmard R, Dokhani A, et al. Impact of Particle Size and Polydispersity Index on the Clinical Applications of Lipidic Nanocarrier Systems. Pharmaceutics [Internet]. 2018 May 18 [cited 2021 May 18];10(2). Available from: https://www.ncbi.nlm.nih.gov/pmc/articles/PMC6027495/

180. Heiligtag FJ, Niederberger M. The fascinating world of nanoparticle research. Materials Today. 2013 Jul 1;16(7):262–71.

181. Tao J, Chow SF, Zheng Y. Application of flash nanoprecipitation to fabricate poorly water-soluble drug nanoparticles. Acta Pharmaceutica Sinica B. 2019 Jan;9(1):4–18.

182. TRICAPRIN - CAS - 621-71-6 (02105297) - MP Biomedicals [Internet]. [cited 2018 Nov 30]. Available from: https://www.mpbio.com/product.php?pid=02105297&country=222

183. Lepeltier E, Bourgaux C, Couvreur P. Nanoprecipitation and the “Ouzo effect”: Application to drug delivery devices. Advanced Drug Delivery Reviews. 2014 May;71:86–97.

184. D’Addio SM, Prud’homme RK. Controlling drug nanoparticle formation by rapid precipitation. Advanced Drug Delivery Reviews. 2011 May;63(6):417–26.

185. Clarke Z. Lecithin. In: Enna SJ, Bylund DB, editors. xPharm: The Comprehensive Pharmacology Reference [Internet]. New York: Elsevier; 2007 [cited 2021 Oct 25]. p. 1–3. Available from: https://www.sciencedirect.com/science/article/pii/B9780080552323620161

186. Liu D, Ma F. Soybean Phospholipids. In InTech; 2011. p. 20. Available from: http://www.intechopen.com/books/recent-trends-for-enhancing-the-diversity-and-quality-of-soybeanproducts/ soybean-phospholipids

187. Verheijen M, Lienhard M, Schrooders Y, Clayton O, Nudischer R, Boerno S, et al. DMSO induces drastic changes in human cellular processes and epigenetic landscape in vitro. Sci Rep. 2019 Mar 15;9(1):4641.

188. Chogale MM, Ghodake VN, Patravale VB. Performance Parameters and Characterizations of Nanocrystals: A Brief Review. Pharmaceutics. 2016 Sep;8(3):26.

189. Lonare AA, Patel SR. Antisolvent Crystallization of Poorly Water Soluble Drugs. International Journal of Chemical Engineering and Applications. 2013;337–41.

190. Kakran M, Sahoo NG, Li L, Judeh Z. Particle size reduction of poorly water soluble artemisinin via antisolvent precipitation with a syringe pump. Powder Technology. 2013 Mar 1;237:468–76.

191. Naqvi Saba, Mohiyuddin Shanid, Gopinath P. Niclosamide loaded biodegradable chitosan nanocargoes: an in vitro study for potential application in cancer therapy. Royal Society Open Science. 4(11):170611.

192. Reddy GB, Kerr DL, Spasojevic I, Tovmasyan A, Hsu DS, Brigman BE, et al. Preclinical Testing of a Novel Niclosamide Stearate Prodrug Therapeutic (NSPT) Shows Efficacy Against Osteosarcoma. Mol Cancer Ther. 2020 Jul;19(7):1448–61.

193. On-line Lipophilicity/Aqueous Solubility Calculation Software [Internet]. [cited 2021 Oct 6]. Available from: http://www.vcclab.org/lab/alogps/

194. Milgraum LZ, Witters LA, Pasternack GR, Kuhajda FP. Enzymes of the fatty acid synthesis pathway are highly expressed in in situ breast carcinoma. Clin Cancer Res. 1997 Nov 1;3(11):2115–20.

195. Esslimani-Sahla M, Thezenas S, Simony-Lafontaine J, Kramar A, Lavaill R, Chalbos D, et al. Increased expression of fatty acid synthase and progesterone receptor in early steps of human mammary carcinogenesis. Int J Cancer. 2007 Jan 15;120(2):224–9.

196. Menendez JA, Lupu R, Colomer R. Targeting fatty acid synthase: potential for therapeutic intervention in her-2/neu-overexpressing breast cancer. Drug News Perspect. 2005 Aug;18(6):375–85.

197. Menendez JA, Lupu R. Fatty acid synthase-catalyzed de novo fatty acid biosynthesis: from anabolic-energy-storage pathway in normal tissues to jack-of-all-trades in cancer cells. Arch Immunol Ther Exp (Warsz). 2004 Dec;52(6):414–26.

198. Menéndez J. Fine-tuning the lipogenic/lipolytic balance to optimize the metabolic requirements of cancer cell growth: molecular mechanisms and therapeutic perspectives. Biochimica et biophysica acta. 2010;

199. Flavin R, Peluso S, Nguyen PL, Loda M. Fatty acid synthase as a potential therapeutic target in cancer. Future Oncology. 2010 Apr;6(4):551–62.

200. Pandey PR, Liu W, Xing F, Fukuda K, Watabe K. Anti-cancer drugs targeting fatty acid synthase (FAS). Recent Pat Anticancer Drug Discov. 2012 May 1;7(2):185–97.

201. The multifaceted roles of fatty acid synthesis in cancer. Nature Reviews Cancer. 2016 Nov;16(11):732–49.

202. Browne CD, Hindmarsh EJ, Smith JW. Inhibition of endothelial cell proliferation and angiogenesis by orlistat, a fatty acid synthase inhibitor. The FASEB Journal. 2006 Oct 1;20(12):2027–35.

203. Crystal Structure and Substrate Specificity of Human Thioesterase 2: INSIGHTS INTO THE MOLECULAR BASIS FOR THE MODULATION OF FATTY ACID SYNTHASE - PubMed [Internet]. [cited 2021 Nov 23]. Available from: https://pubmed.ncbi.nlm.nih.gov/26663084/

204. Menendez JA, Vellon L, Lupu R. Antitumoral actions of the anti-obesity drug orlistat (XenicalTM) in breast cancer cells: blockade of cell cycle progression, promotion of apoptotic cell death and PEA3-mediated transcriptional repression of Her2/neu (erbB-2) oncogene. Ann Oncol. 2005 Aug;16(8):1253–67.

205. Paulmurugan R, Bhethanabotla R, Mishra K, Devulapally R, Foygel K, Sekar TV, et al. Folate Receptor-Targeted Polymeric Micellar Nanocarriers for Delivery of Orlistat as a Repurposed Drug against Triple-Negative Breast Cancer. Mol Cancer Ther. 2016 Feb;15(2):221–31.

206. Bianchini G, Balko JM, Mayer IA, Sanders ME, Gianni L. Triple-negative breast cancer: challenges and opportunities of a heterogeneous disease. Nat Rev Clin Oncol. 2016 Nov;13(11):674–90.

207. Fako VE, Zhang JT, Liu JY. Mechanism of Orlistat Hydrolysis by the Thioesterase of Human Fatty Acid Synthase. ACS Catal. 2014 Oct 3;4(10):3444–53.

208. Menendez JA, Lupu R. Fatty acid synthase (FASN) as a therapeutic target in breast cancer. Expert Opinion on Therapeutic Targets. 2017 Nov 2;21(11):1001–16.

209. Menendez JA, Lupu R. Fatty acid synthase and the lipogenic phenotype in cancer pathogenesis. Nature Reviews Cancer. 2007 Oct;7(10):763–77.

210. Alli PM, Pinn ML, Jaffee EM, McFadden JM, Kuhajda FP. Fatty acid synthase inhibitors are chemopreventive for mammary cancer in neu- N transgenic mice. Oncogene. 2005 Jan;24(1):39–46.

211. Dowling S, Cox J, Cenedella RJ. Inhibition of Fatty Acid Synthase by Orlistat Accelerates Gastric Tumor Cell Apoptosis in Culture and Increases Survival Rates in Gastric Tumor Bearing Mice In Vivo. Lipids. 2009 Jun 1;44(6):489–98.

212. Abdelwahed W, Degobert G, Stainmesse S, Fessi H. Freeze-drying of nanoparticles: Formulation, process and storage considerations☆. Advanced Drug Delivery Reviews. 2006 Dec 30;58(15):1688–713.

213. Abdelwahed W, Degobert G, Fessi H. A pilot study of freeze drying of poly(epsilon-caprolactone) nanocapsules stabilized by poly(vinyl alcohol): Formulation and process optimization. International Journal of Pharmaceutics. 2006 Feb 17;309(1):178–88.

214. Roy D, Guillon X, Lescure F, Couvreur P, Bru N, Breton P. On shelf stability of freeze-dried poly(methylidene malonate 2.1.2) nanoparticles. International Journal of Pharmaceutics. 1997 Mar 28;148(2):165–75.

215. Fouarge M, Dewulft M, Couvreur P, Roland M, Vranckx H. Development of dehydroemetine nanoparticles for the treatment of visceral leishmaniasis. Journal of Microencapsulation. 1989 Jan 1;6(1):29–34.

216. Heiati H, Tawashi R, Phillips NC. Drug retention and stability of solid lipid nanoparticles containing azidothymidine palmitate after autoclaving, storage and lyophilization. Journal of Microencapsulation. 1998 Jan 1;15(2):173–84.

217. Abdelwahed W, Degobert G, Fessi H. Investigation of nanocapsules stabilization by amorphous excipients during freeze-drying and storage. European Journal of Pharmaceutics and Biopharmaceutics. 2006 Jun 1;63(2):87–94.

218. Pikal MJ. Mechanisms of Protein Stabilization During Freeze-Drying Storage: The Relative Importance of Thermodynamic Stabilization and Glassy State Relaxation Dynamics. In: Freeze-Drying/Lyophilization of Pharmaceutical and Biological Products. 3rd ed. CRC Press; 2010.

219. Tang X (Charlie), Pikal MJ. Design of Freeze-Drying Processes for Pharmaceuticals: Practical Advice. Pharm Res. 2004 Feb 1;21(2):191–200.

220. Allison SD, Molina M d.C, Anchordoquy TJ. Stabilization of lipid/DNA complexes during the freezing step of the lyophilization process: the particle isolation hypothesis. Biochimica et Biophysica Acta (BBA) - Biomembranes. 2000 Sep;1468(1–2):127–38.

221. Is trehalose special for preserving dry biomaterials? [Internet]. [cited 2021 Nov 23]. Available from: https://www.ncbi.nlm.nih.gov/pmc/articles/PMC1233675/

222. Schwarz null, Mehnert null. Freeze-drying of drug-free and drug-loaded solid lipid nanoparticles (SLN). Int J Pharm. 1997 Nov 28;157(2):171–9.

223. Gualbert J, Shahgaldian P, Lazar A, Coleman AW. Solid Lipid Nanoparticles (SLNs): Preparation and Properties of Calix[4]resorcinarene Derived Systems. Journal of Inclusion Phenomena. 2004 Feb 1;48(1):37–44.

224. Almalik A, Alradwan I, Kalam MA, Alshamsan A. Effect of cryoprotection on particle size stability and preservation of chitosan nanoparticles with and without hyaluronate or alginate coating. Saudi Pharmaceutical Journal. 2017 Sep 1;25(6):861–7.

225. Freeze-drying of itraconazole-loaded nanosphere suspensions: a feasibility study - de Chasteigner - 1996 - Drug Development Research - Wiley Online Library [Internet]. [cited

2021 Nov 17]. Available from: https://onlinelibrary.wiley.com/doi/abs/10.1002/(SICI)1098-2299(199606)38:2%3C116::AID-DDR6%3E3.0.CO;2-M

226. Kim DH, Kim JY, Kim RM, Maharjan P, Ji YG, Jang DJ, et al. Orlistat-loaded solid SNEDDS for the enhanced solubility, dissolution, and in vivo performance. Int J Nanomedicine. 2018 Nov 5;13:7095–106.

227. Singh A. Evaluation of orlistat solid dispersion using poloxomer 188 as hydrophilic carrier. Scholar's Research Journal. 2012 Aug 11;1.

228. Qu Z, Ren Y, Shen H, Wang H, Shi L, Tong D. Combination Therapy of Metastatic Castration-Recurrent Prostate Cancer: Hyaluronic Acid Decorated, Cabazitaxel-Prodrug and Orlistat Co-Loaded Nano-System. Drug Des Devel Ther. 2021 Aug 20;15:3605–16.

229. Malkawi A, Jalil A, Nazir I, Matuszczak B, Kennedy R, Bernkop-Schnürch A. Self-Emulsifying Drug Delivery Systems: Hydrophobic Drug Polymer Complexes Provide a Sustained Release in Vitro. Molecular Pharmaceutics. 2020 Oct 5;17(10):3709–19.

230. Gal D, Ohashi M, MacDonald PC, Buchsbaum HJ, Simpson ER. Low-density lipoprotein as a potential vehicle for chemotherapeutic agents and radionucleotides in the management of gynecologic neoplasms. Am J Obstet Gynecol. 1981 Apr 15;139(8):877–85.

231. Counsell RE, Pohland RC. Lipoproteins as potential site-specific delivery systems for diagnostic and therapeutic agents. J Med Chem. 1982 Oct;25(10):1115–20.

232. Needham D. Development of clinically effective formulations: Why it is so difficult? In 2019.

233. Goldstein JL, Anderson RG, Brown MS. Coated pits, coated vesicles, and receptor-mediated endocytosis. Nature. 1979 Jun 21;279(5715):679–85.

234. Brown MS, Kovanen PT, Goldstein JL. Evolution of the LDL receptor concept-from cultured cells to intact animals. Ann N Y Acad Sci. 1980;348:48–68.

235. Brown MS, Kovanen PT, Goldstein JL. Regulation of plasma cholesterol by lipoprotein receptors. Science. 1981 May 8;212(4495):628–35.

236. Xu S, Olenyuk BZ, Okamoto CT, Hamm-Alvarez SF. Targeting receptor-mediated endocytotic pathways with nanoparticles: Rationale and advances. Advanced Drug Delivery Reviews. 2013 Jan 1;65(1):121–38.

237. Brown MS, Goldstein JL. A receptor-mediated pathway for cholesterol homeostasis. Science. 1986;232(4746):34–47.

238. Wasan KM, Cassidy SM. Role of Plasma Lipoproteins in Modifying the Biological Activity of Hydrophobic Drugs. Journal of Pharmaceutical Sciences. 1998 Apr 1;87(4):411–24.

239. Ponec M, Havekes L, Kempenaar J, Lavrijsen S, Wijsman M, Boonstra J, et al. Calcium-mediated regulation of the low density lipoprotein receptor and intracellular cholesterol synthesis in human epidermal keratinocytes. J Cell Physiol. 1985 Oct;125(1):98–106.

240. Vitols S, Gahrton G, Peterson C. Significance of the low-density lipoprotein (LDL) receptor pathway for the in vitro accumulation of AD-32 incorporated into LDL in normal and leukemic white blood cells. Cancer Treat Rep. 1984 Mar;68(3):515–20.

241. Ho YK, Smith RG, Brown MS, Goldstein JL. Low-density lipoprotein (LDL) receptor activity in human acute myelogenous leukemia cells. Blood. 1978 Dec;52(6):1099–114.

242. Gal D, MacDonald PC, Porter JC, Simpson ER. Cholesterol metabolism in cancer cells in monolayer culture. III. Low-density lipoprotein metabolism. Int J Cancer. 1981 Sep 15;28(3):315–9.

243. Rudling MJ, Reihner E, Einarsson K, Ewerth S, Angelin B. Low density lipoprotein receptor-binding activity in human tissues: quantitative importance of hepatic receptors and

evidence for regulation of their expression in vivo. Proceedings of the National Academy of Sciences. 1990 May 1;87(9):3469–73.

244. Rudling MJ, Angelin B, Peterson CO, Collins VP. Low Density Lipoprotein Receptor Activity in Human Intracranial Tumors and Its Relation to the Cholesterol Requirement. :6.

245. Muller GL. THE CHOLESTEROL METABOLISM IN HEALTH AND IN ANEMIA. Medicine. 1930 May;9(2):119.

246. Corbin IR, Zheng G. Mimicking nature's nanocarrier: synthetic low-density lipoprotein-like nanoparticles for cancer-drug delivery. Nanomedicine. 2007 Jun;2(3):375–80.

247. Riddles PW, Blakeley RL, Zerner B. [8] Reassessment of Ellman's reagent. In: Methods in Enzymology [Internet]. Academic Press; 1983 [cited 2022 Mar 11]. p. 49–60. (Enzyme Structure Part I; vol. 91). Available from: https://www.sciencedirect.com/science/article/pii/S0076687983910108

248. Liu C, Liu Z, Wang J. Uncovering the molecular and physiological processes of anticancer leads binding human serum albumin: A physical insight into drug efficacy. Chamani J, editor. PLoS ONE. 2017 Apr 20;12(4):e0176208.

249. Maltas E. Binding interactions of niclosamide with serum proteins. Journal of Food and Drug Analysis. 2014 Dec;22(4):549–55.

250. Takehara K, Yuki K, Shirasawa M, Yamasaki S, Yamada S. Binding Properties of Hydrophobic Molecules to Human Serum Albumin Studied by Fluorescence Titration. Anal Sci. 2009;25(1):115–20.

251. Han XL, Mei P, Liu Y, Xiao Q, Jiang FL, Li R. Binding interaction of quinclorac with bovine serum albumin: A biophysical study. Spectrochimica Acta Part A: Molecular and Biomolecular Spectroscopy. 2009 Oct;74(3):781–7.

252. Schneider WJ, Beisiegel U, Goldstein JL, Brown MS. Purification of the low density lipoprotein receptor, an acidic glycoprotein of 164,000 molecular weight. J Biol Chem. 1982 Mar 10;257(5):2664–73.

253. Suk JS, Xu Q, Kim N, Hanes J, Ensign LM. PEGylation as a strategy for improving nanoparticle-based drug and gene delivery. Adv Drug Deliv Rev. 2016 Apr 1;99(Pt A):28–51.

254. Elmore B, Triplett K, Hall P. Apolipoprotein B48, the Structural Component of Chylomicrons, Is Sufficient to Antagonize Staphylococcus aureus Quorum-Sensing. PLOS ONE. 2015 May 5;10:e0125027.

255. Cladaras C, Hadzopoulou-Cladaras M, Nolte RT, Atkinson D, Zannis VI. The complete sequence and structural analysis of human apolipoprotein B-100: relationship between apoB-100 and apoB-48 forms. The EMBO Journal. 1986 Dec;5(13):3495–507.

256. Drabik D, Chodaczek G, Kraszewski S, Langner M. Mechanical Properties Determination of DMPC, DPPC, DSPC, and HSPC Solid-Ordered Bilayers. Langmuir. 2020 Apr 14;36(14):3826–35.

257. L. Moore T, Rodriguez-Lorenzo L, Hirsch V, Balog S, Urban D, Jud C, et al. Nanoparticle colloidal stability in cell culture media and impact on cellular interactions. Chemical Society Reviews. 2015;44(17):6287–305.

258. Zhang J, Xiong D, Chen L, Kang Q, Zeng B. Interaction of pyrrolizine derivatives with bovine serum albumin by fluorescence and UV–Vis spectroscopy. Spectrochimica Acta Part A: Molecular and Biomolecular Spectroscopy. 2012 Oct;96:132–8.

259. Xie MX, Long M, Liu Y, Qin C, Wang YD. Characterization of the interaction between human serum albumin and morin. Biochim Biophys Acta. 2006 Aug;1760(8):1184–91.

260. Holliday DL, Speirs V. Choosing the right cell line for breast cancer research. Breast Cancer Research. 2011 Aug 12;13(4):215.

261. Menendez JA, Lupu R. Fatty acid synthase regulates estrogen receptor-α signaling in breast cancer cells. Oncogenesis. 2017 Feb;6(2):e299–e299.

262. Cedó L, Reddy ST, Mato E, Blanco-Vaca F, Escolà-Gil JC. HDL and LDL: Potential New Players in Breast Cancer Development. Journal of Clinical Medicine. 2019 Jun;8(6):853.

263. Kim S, Lee Y, Koo JS. Differential Expression of Lipid Metabolism-Related Proteins in Different Breast Cancer Subtypes. PLoS One. 2015 Mar 9;10(3):e0119473.

264. Yeh CW, Chen WJ, Chiang CT, Lin-Shiau SY, Lin JK. Suppression of fatty acid synthase in MCF-7 breast cancer cells by tea and tea polyphenols: a possible mechanism for their hypolipidemic effects. Pharmacogenomics J. 2003 Oct;3(5):267–76.

265. Keane M, Ettenberg SA, Lowrey A, Russell K, Lipkowitz' S. Fas Expression and Function in Normal and Malignant Breast Cell Lines. :9.

266. Ye J, Xia X, Dong W, Hao H, Meng L, Yang Y, et al. Cellular uptake mechanism and comparative evaluation of antineoplastic effects of paclitaxel–cholesterol lipid emulsion on triple-negative and non-triple-negative breast cancer cell lines. Int J Nanomedicine. 2016 Aug 24;11:4125–40.

267. Schroeder B, Vander Steen T, Espinoza I, Venkatapoorna CMK, Hu Z, Silva FM, et al. Fatty acid synthase (FASN) regulates the mitochondrial priming of cancer cells. Cell Death Dis. 2021 Oct 21;12(11):1–10.

268. Campion O, Al Khalifa T, Langlois B, Thevenard-Devy J, Salesse S, Savary K, et al. Contribution of the Low-Density Lipoprotein Receptor Family to Breast Cancer Progression.

Frontiers in Oncology [Internet]. 2020 [cited 2022 Feb 2];10. Available from: https://www.frontiersin.org/article/10.3389/fonc.2020.00882

269. Scully T, Kase N, Gallagher EJ, LeRoith D. Regulation of low-density lipoprotein receptor expression in triple negative breast cancer by EGFR-MAPK signaling. Sci Rep. 2021 Sep 9;11(1):17927.

270. Guan X, Liu Z, Zhao Z, Zhang X, Tao S, Yuan B, et al. Emerging roles of low-density lipoprotein in the development and treatment of breast cancer. Lipids in Health and Disease. 2019 Jun 10;18(1):137.

8 Appendix

8.1 Calculations of number of particles, distance and amount of POPC for coating particles

Concentration (mM)	concentration (g/L)	Concentration g/ml	Particle size diameter(nm)	Radius (nm)	Radius in cm	Volume (cm3)	mass (g)	number (particle/ml)	distance (cm)	Distance (nm)	Surface area of 1 particle (nm2)	number of Vesivax / particle	number of Vesivaxto coat all particles/ml	Concentration of POPC required (mol/ml)	Concentration (mol/L)	concentration mmol/L	Ratio (olive oil : POPC)	Ratio POPC : Olive oil)
0.001	0.000885	8.85E-07	13.3	6.65	6.65E-07	1.23E-18	1.12E-18	7.9E+11	0.000108	1081.8	555.7163	1292.364	1.02E+15	1.7E-09	1.7E-06	0.001695694	0.589729	1.695694

0.01	0.008854	8.85E-06	15.49	7.745	7.75E-07	1.95E-18	1.77E-18	5E+12	5.85E-05	584.8081	753.7941	1753.009	8.76E+15	1.46E-08	1.46E-05	0.014559542	0.686835	1.455954
0.1	0.088543	8.85E-05	42.49	21.245	2.12E-06	4.02E-17	3.66E-17	2.42E+12	7.45E-05	744.5868	5671.832	13190.31	3.2E+16	5.31E-08	5.31E-05	0.053077739	1.884029	0.530777
0.2	0.177086	0.000177	71.49	35.745	3.57E-06	1.91E-16	1.74E-16	1.02E+12	9.94E-05	994.33	16056.11	37339.8	3.8E+16	6.31E-08	6.31E-05	0.063093387	3.169904	0.315467
0.4	0.354172	0.000354	72.3	36.15	3.62E-06	1.98E-16	1.8E-16	1.97E+12	7.98E-05	798.1421	16422.02	38190.73	7.51E+16	1.25E-07	0.000125	0.124773063	3.20582	0.311933

0.8	0.708344	0.000708	97.44	48.72	4.87E-06	4.84E-16	4.41E-16	1.61E+12	8.54E-05	853.7601	29828.02	69367.49	1.11E+17	1.85E-07	0.000185	0.185161997	4.320541	0.2314522
1	0.88543	0.000885	100.2	50.1	5.01E-06	5.27E-16	4.79E-16	1.85E+12	8.15E-05	815.0101	31541.72	73352.83	1.35E+17	2.25E-07	0.000225	0.225077158	4.442921	0.2250777
0.006	0.005313	5.31E-06	12.05	6.025	6.03E-07	9.16E-19	8.34E-19	6.37E+12	5.39E-05	539.3846	456.1671	1060.854	6.76E+15	1.12E-08	1.12E-05	0.011229576	0.530433	1.871596
0.008	0.007083	7.08E-06	14.44	7.22	7.22E-07	1.58E-18	1.43E-18	4.94E+12	5.87E-05	587.2628	655.0648	1523.406	7.52E+15	1.25E-08	1.25E-05	0.012494588	0.640277	1.561823

0.04	0.035417	3.54E-05	20.77	10.385	1.04E-06	4.69E-18	4.27E-18	8.3E+12	4.94E-05	493.9827	1355.261	3151.769	2.61E+16	4.34E-08	4.34E-05	0.043433281	0.920953	1.0858322
0.06	0.053126	5.31E-05	29.37	14.685	1.47E-06	1.33E-17	1.21E-17	4.4E+12	6.1E-05	610.2139	2709.928	6302.158	2.77E+16	4.61E-08	4.61E-05	0.046072995	1.302281	0.767883

8.2 Olive oil NPs

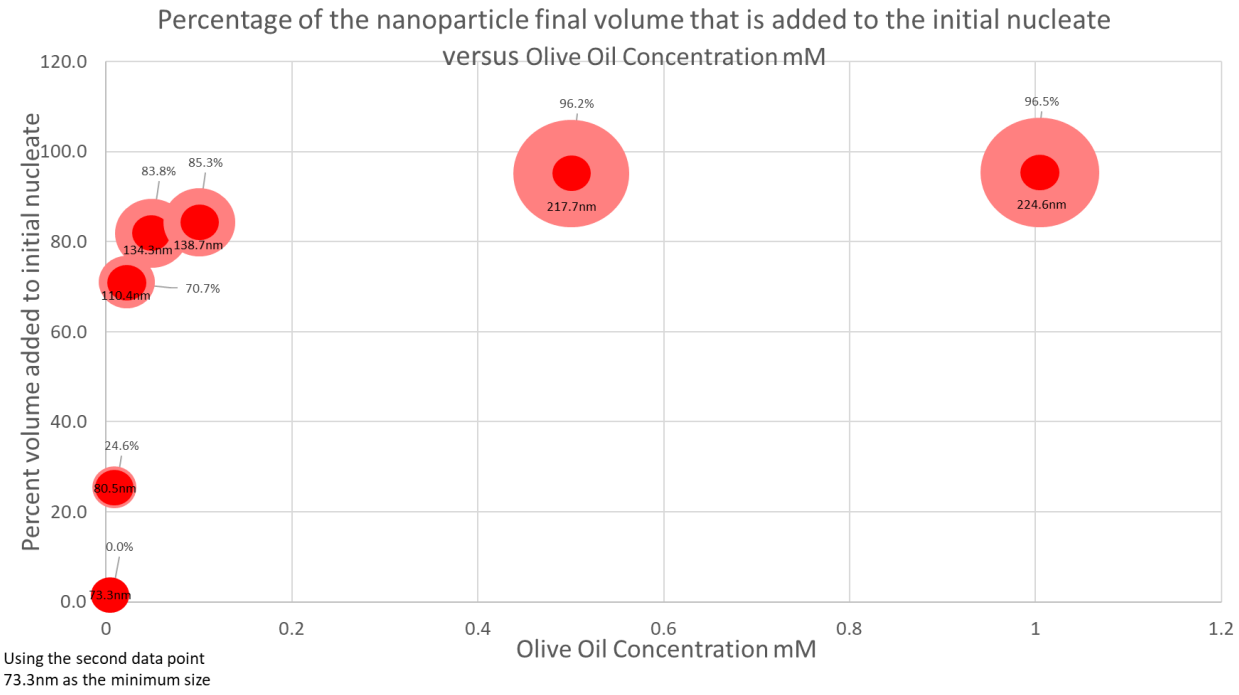

Using the second data point 73.3nm as the minimum size

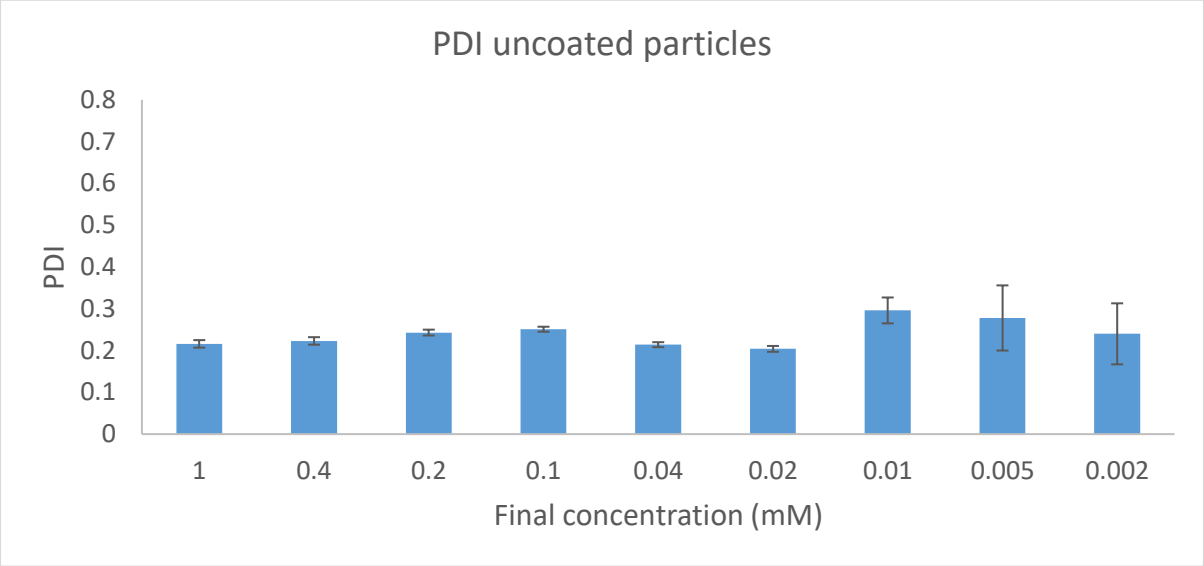

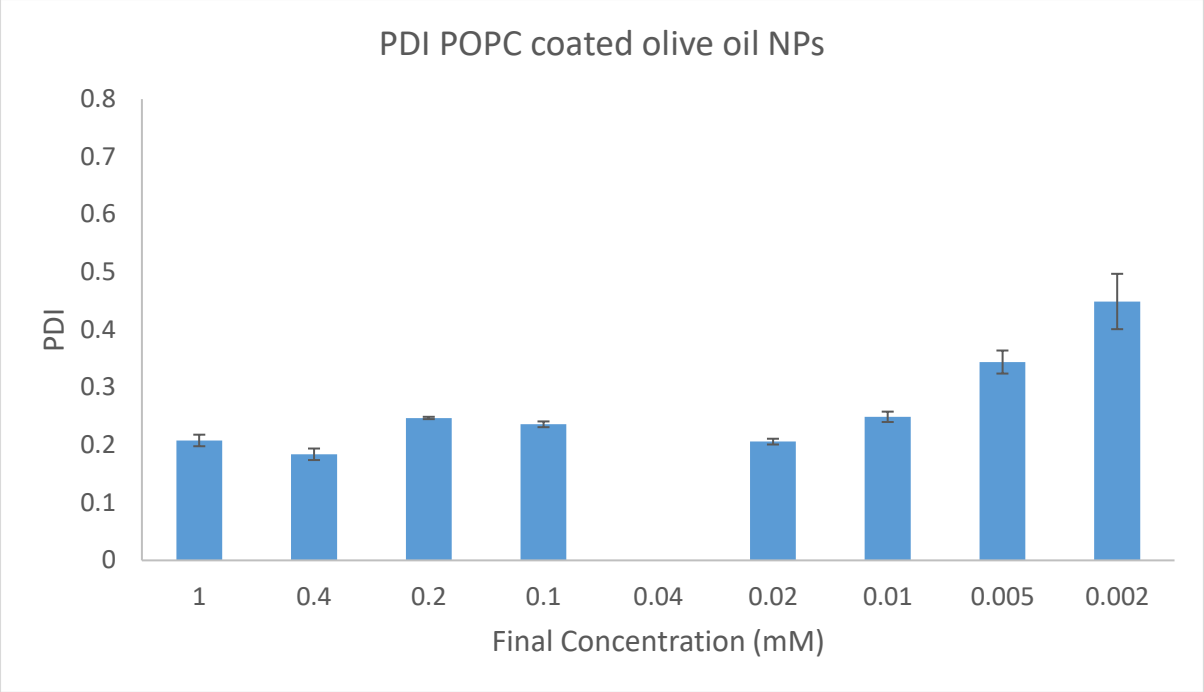
PDI POPC coated olive oil NPs
PDI
0.8
0.7
0.6
0.5
0.4
0.3
0.2
0.1
0
1
0.4
0.2
0.1
0.04
0.02
0.01
0.005
0.002
Final Concentration (mM)

8.3 2D printer of tween 80 coated olive oil NPs particle size

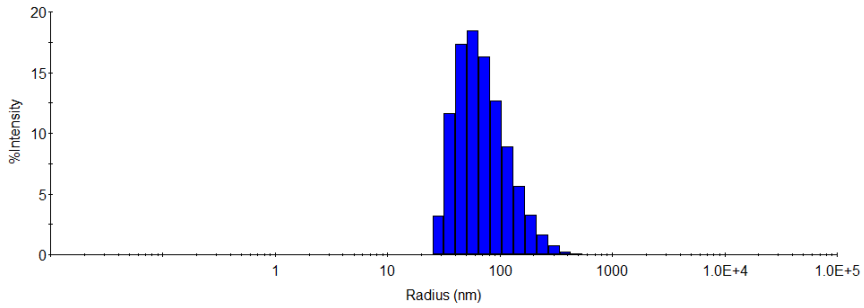

10 mM olive oil

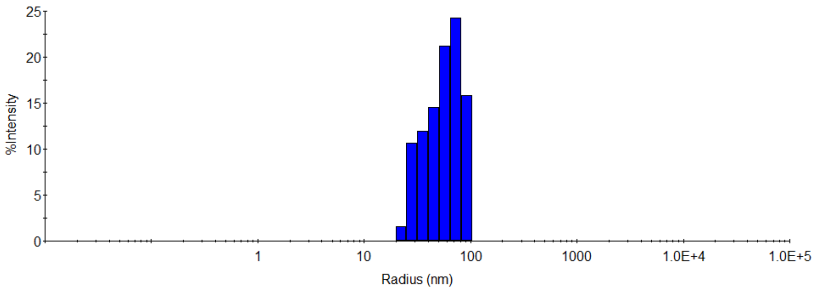

1 mM olive oil

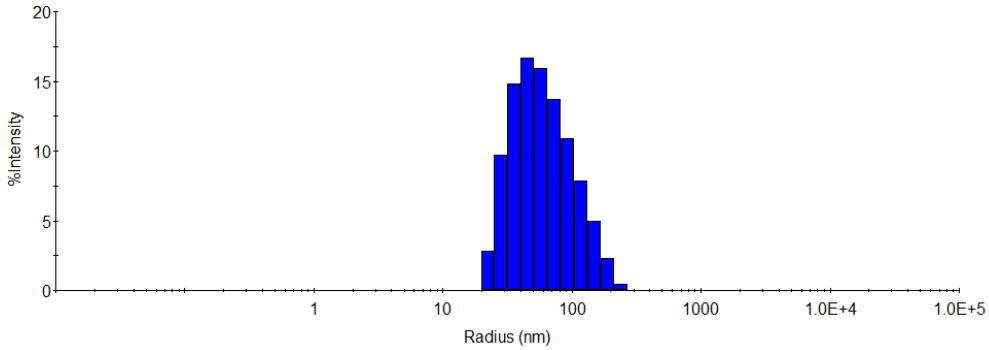

0.1 mM olive oil

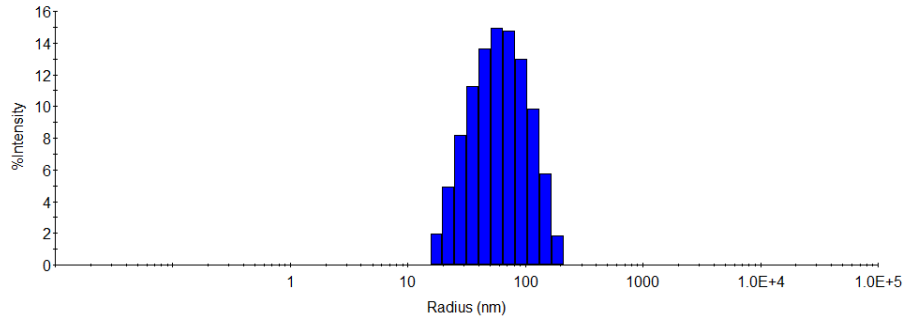

0.01 mM olive oil

8.4 Uncoated orlistat NPs

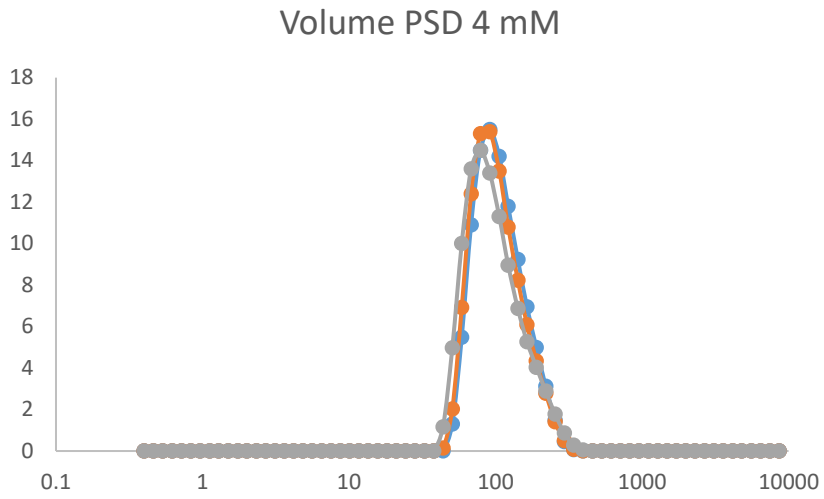

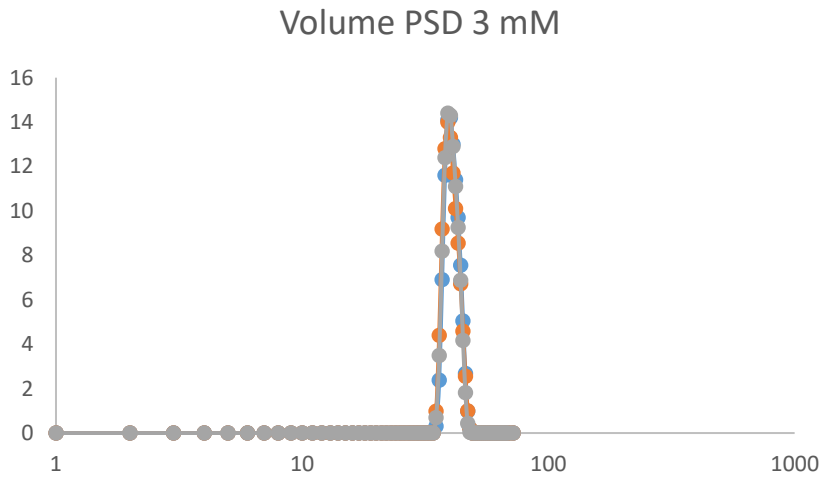

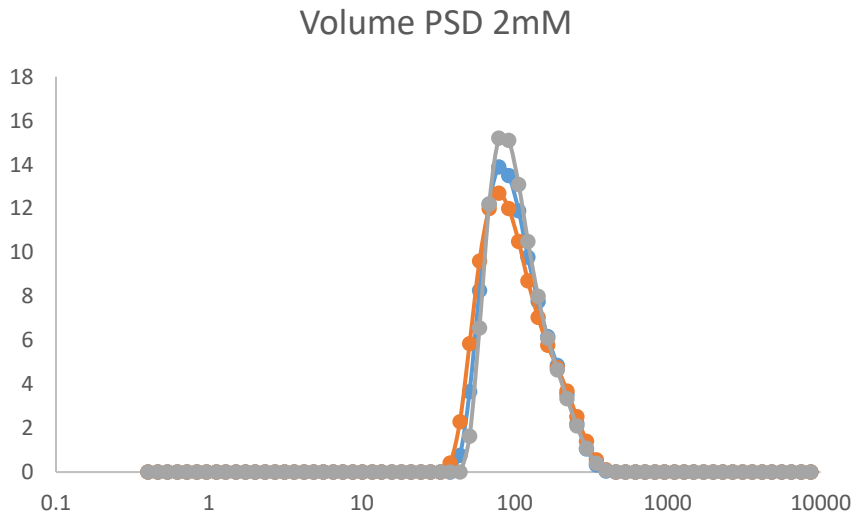

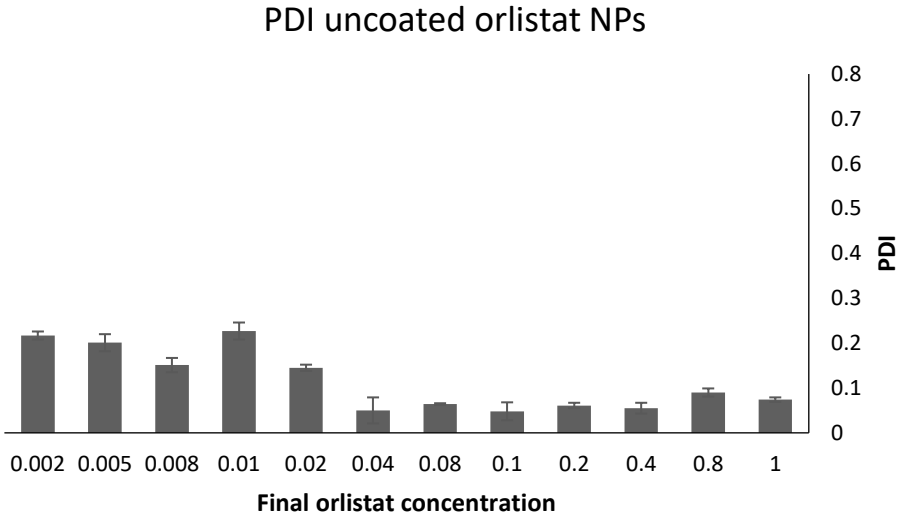
PDI uncoated orlistat NPs
0.8
0.7
0.6
0.5
0.4
0.3
0.2
0.1
0
PDI
0.002 0.005 0.008 0.01 0.02 0.04 0.08 0.1 0.2 0.4 0.8 1
Final orlistat concentration

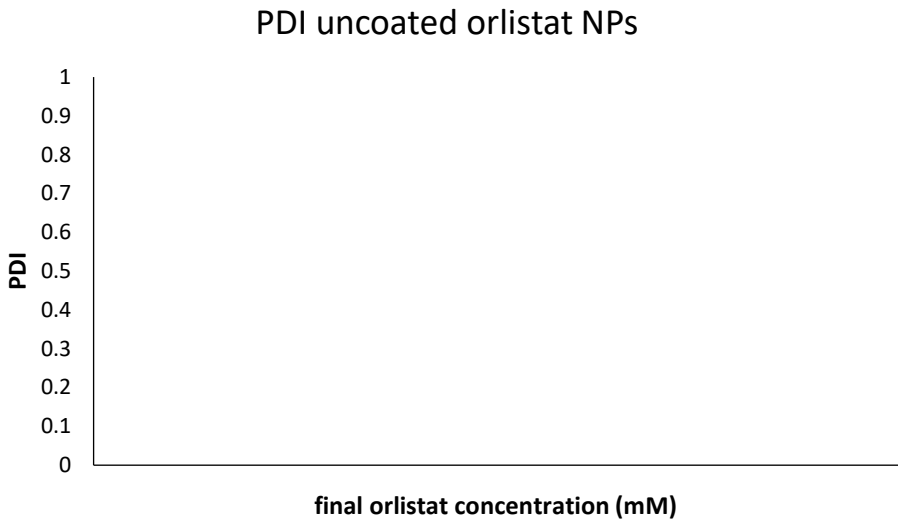
PDI uncoated orlistat NPs
1
0.9
0.8
0.7
0.6
0.5
0.4
0.3
0.2
0.1
0
PDI
final orlistat concentration (mM)

8.5 Slow Vs Fast injection

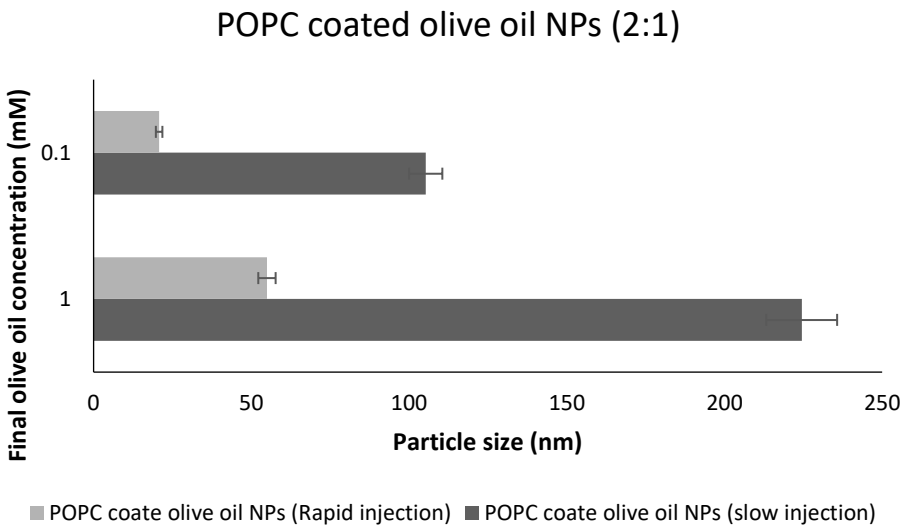

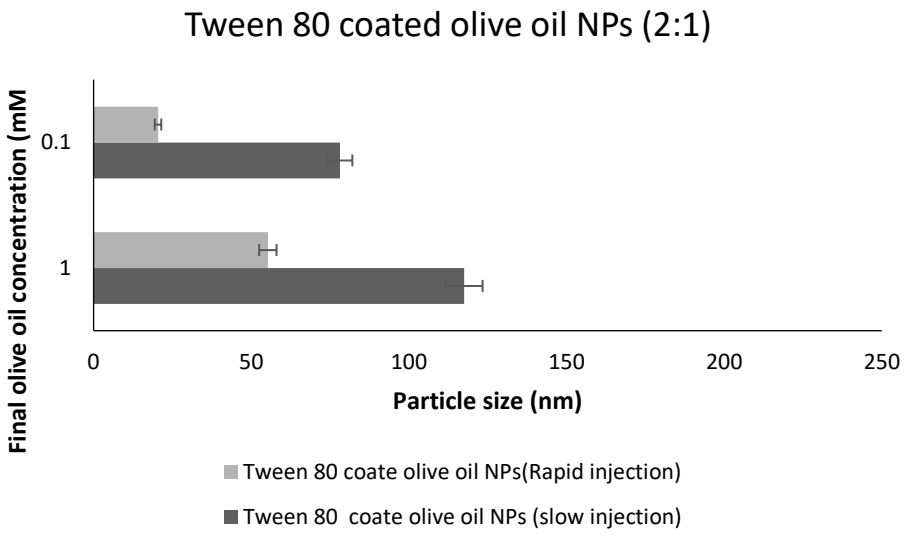

8.6 POPC coated orlistat NPs

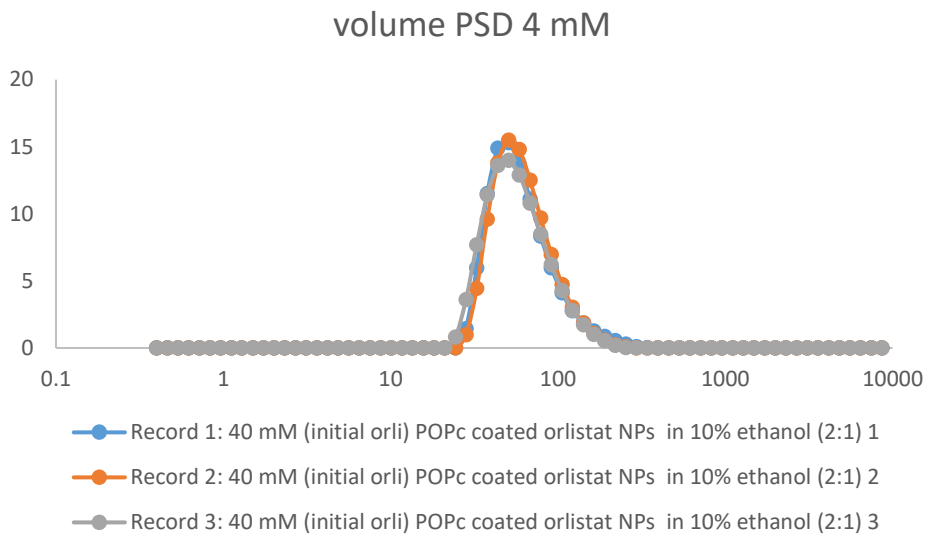

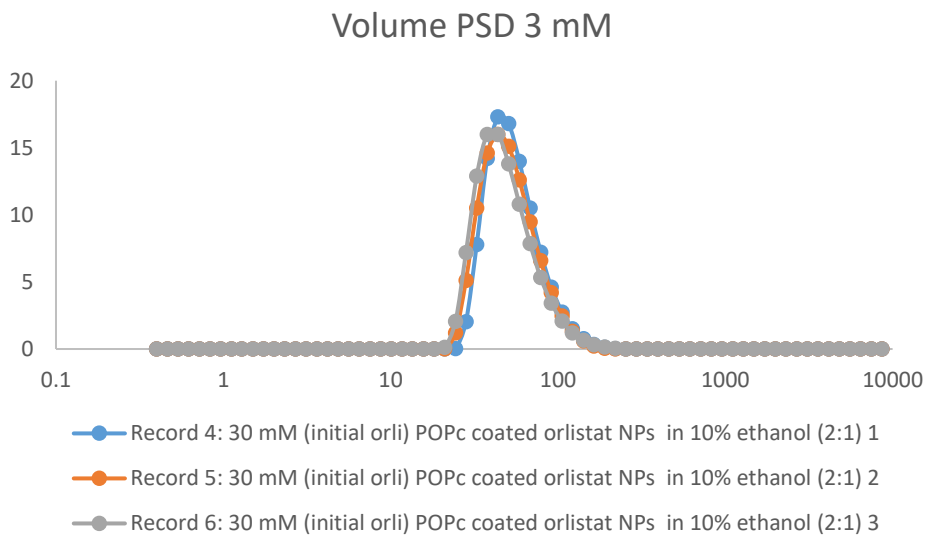

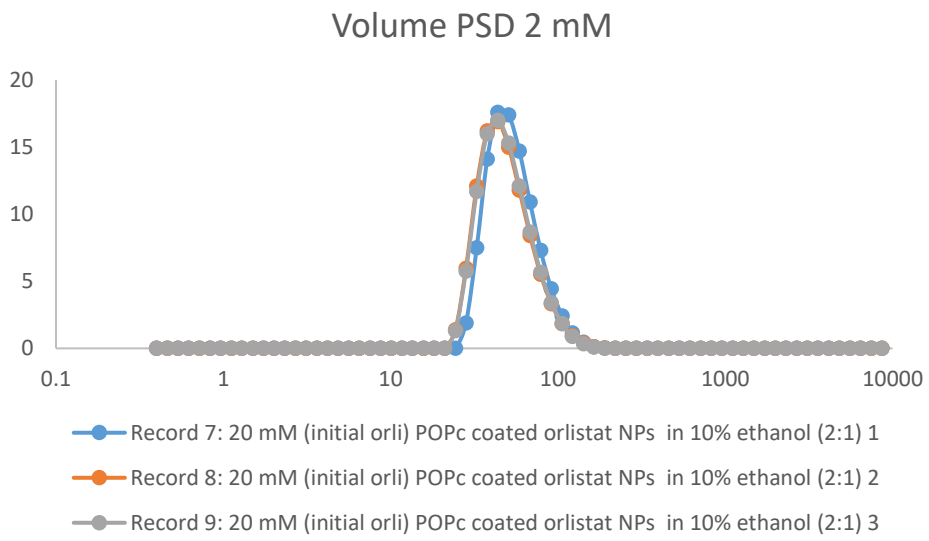
Volume PSD 2 mM
20
15
10
5
0
0.1
1
10
100
1000
10000
Record 7: 20 mM (initial orli) POPc coated orlistat NPs in 10% ethanol (2:1) 1
Record 8: 20 mM (initial orli) POPc coated orlistat NPs in 10% ethanol (2:1) 2
Record 9: 20 mM (initial orli) POPc coated orlistat NPs in 10% ethanol (2:1) 3

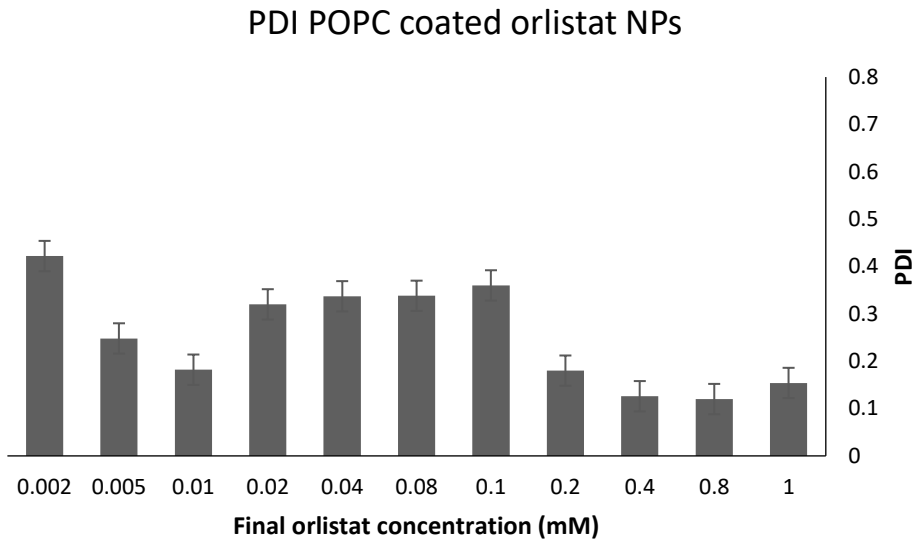
PDI POPC coated orlistat NPs
0.8
0.7
0.6
0.5
0.4
0.3
0.2
0.1
0
PDI
0.002
0.005
0.01
0.02
0.04
0.08
0.1
0.2
0.4
0.8
1
Final orlistat concentration (mM)

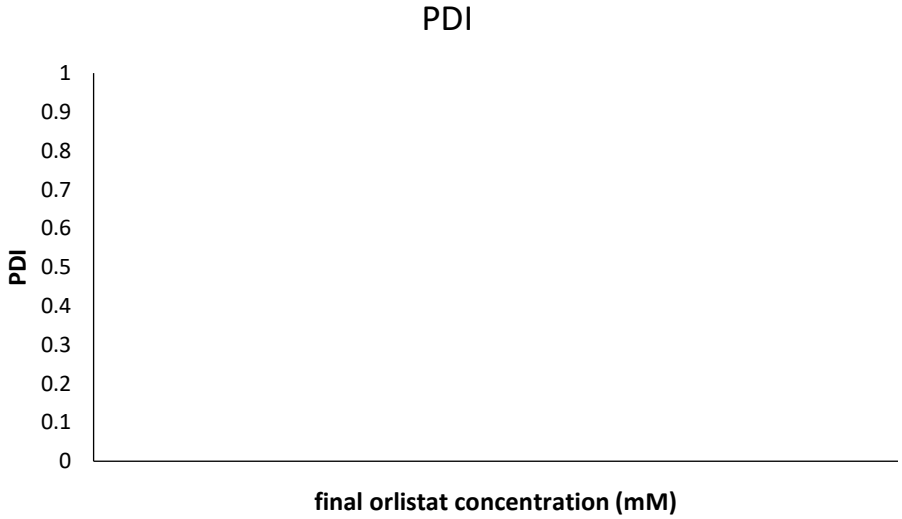
PDI
1
0.9
0.8
0.7
0.6
0.5
0.4
0.3
0.2
0.1
0
PDI
final orlistat concentration (mM)

8.7 Size analysis of POPC coated orlistat NPs in different stabilisers

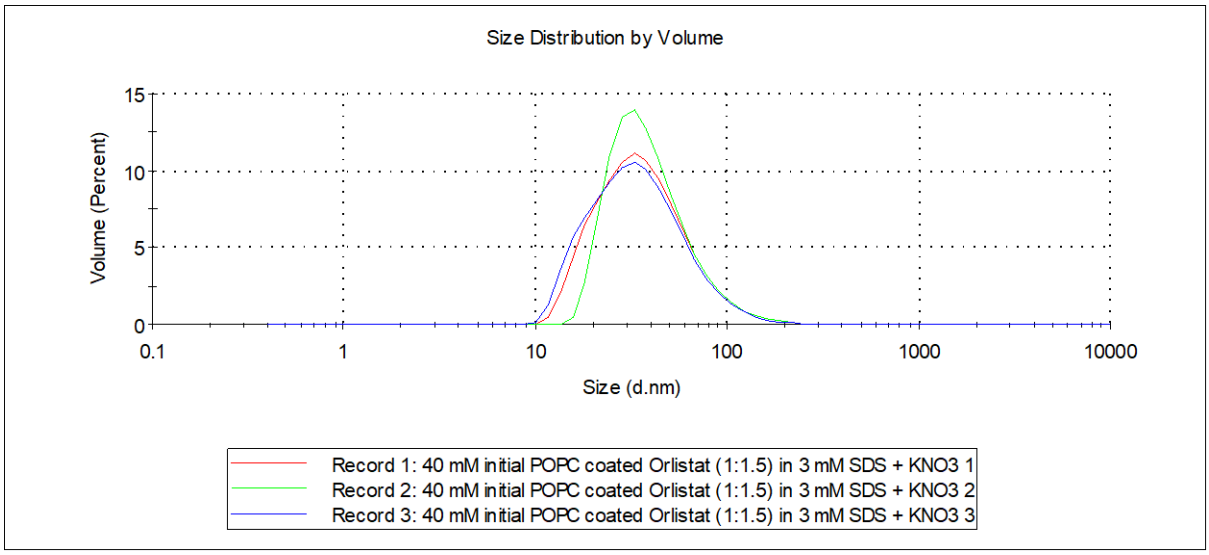

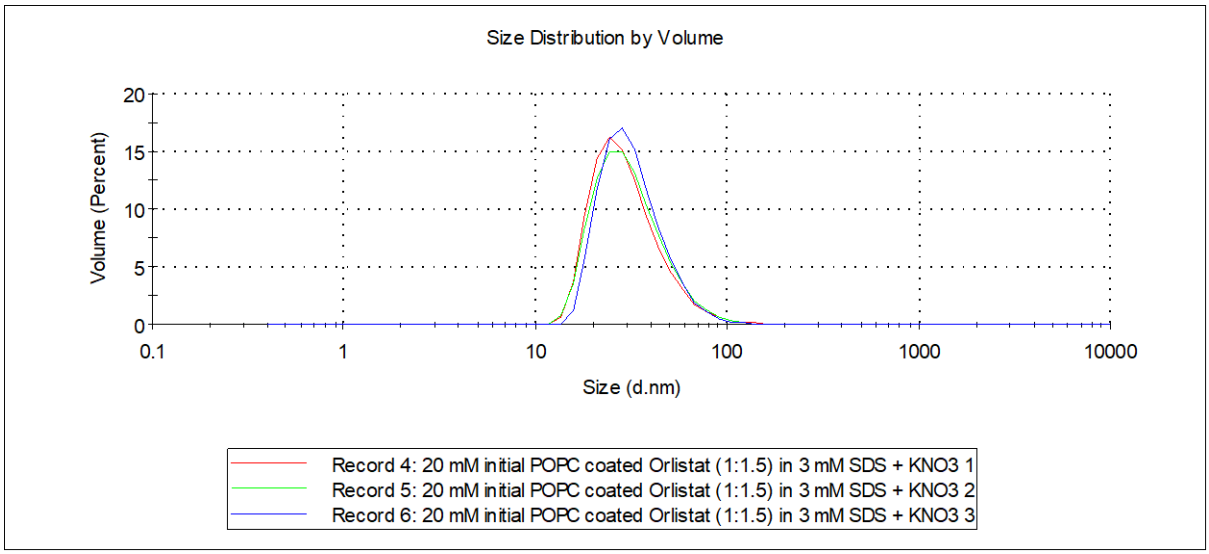

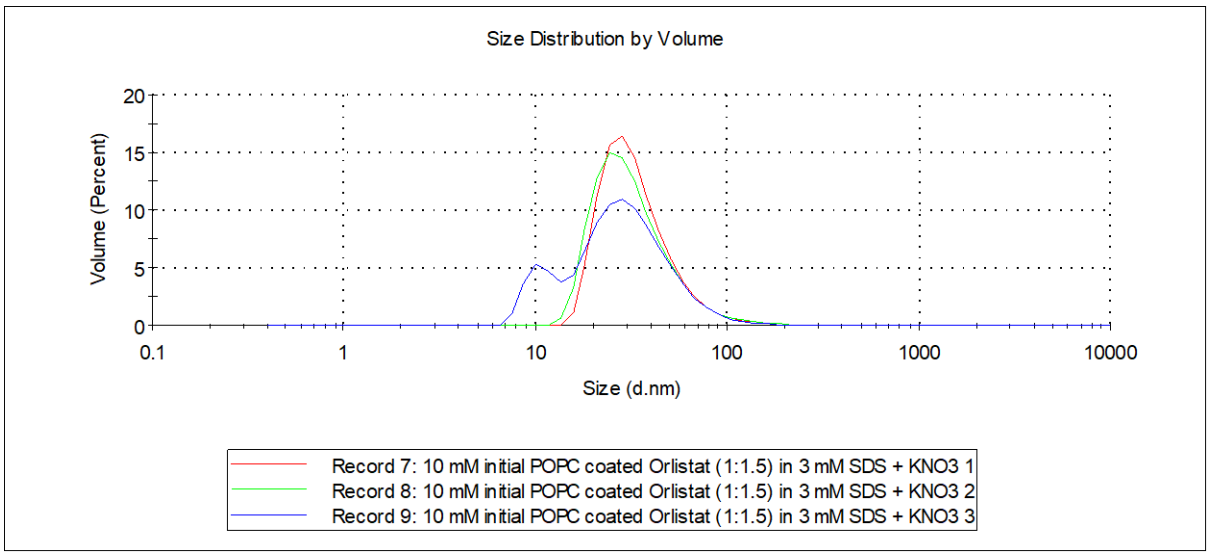

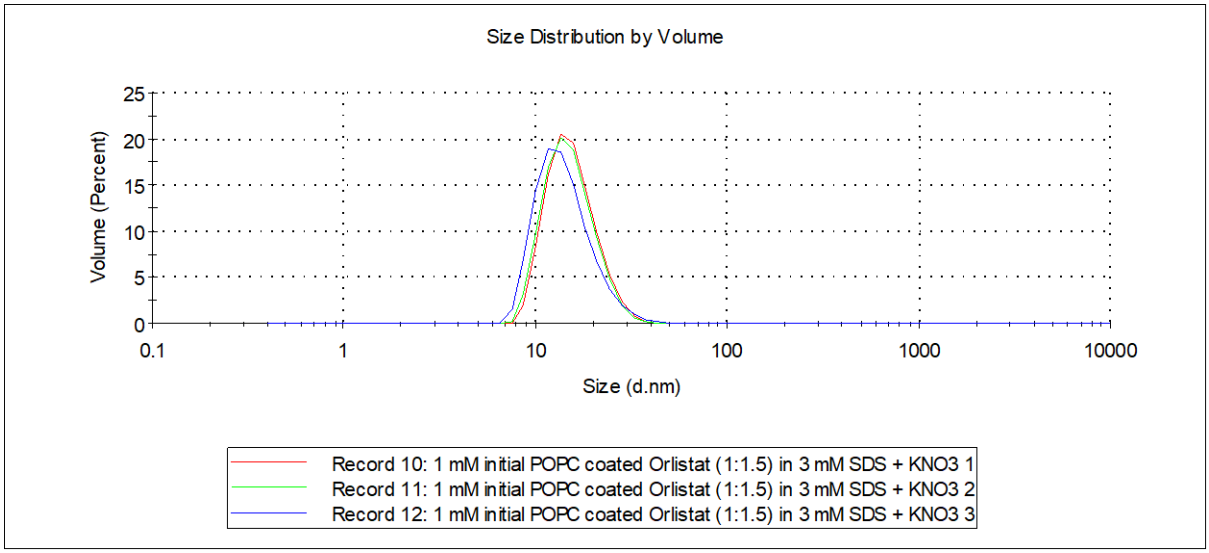
Size Distribution by Volume
Volume (Percent)
25
20
15
10
5
0
0.1
1
10
100
1000
10000
Size (d.nm)
Record 10: 1 mM initial POPC coated Orlistat (1:1.5) in 3 mM SDS + KNO3 1
Record 11: 1 mM initial POPC coated Orlistat (1:1.5) in 3 mM SDS + KNO3 2
Record 12: 1 mM initial POPC coated Orlistat (1:1.5) in 3 mM SDS + KNO3 3

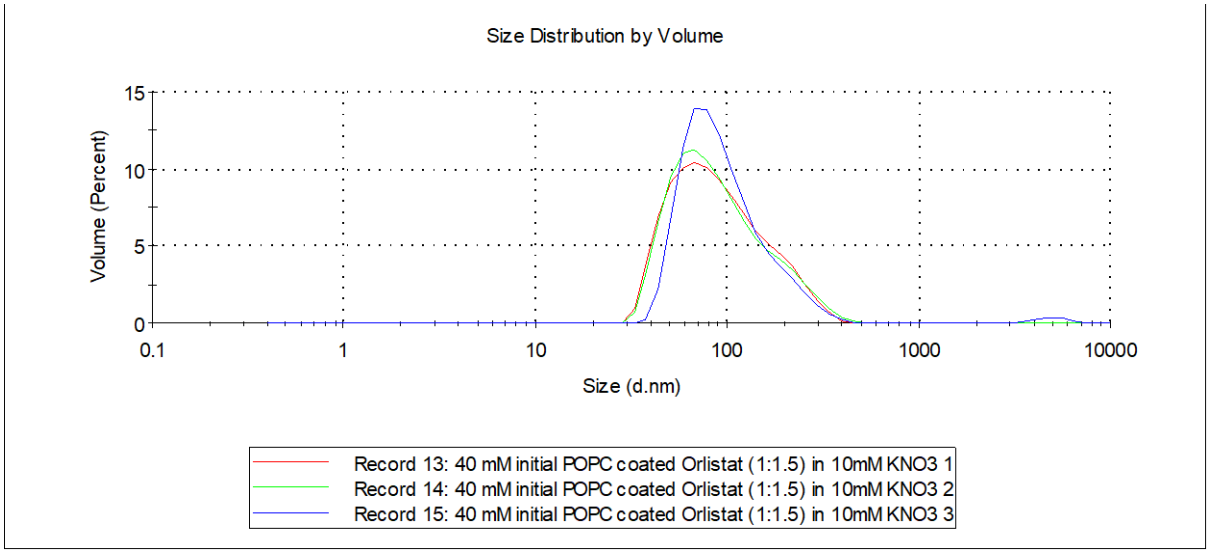
Size Distribution by Volume
Volume (Percent)
15
10
5
0
0.1
1
10
100
1000
10000
Size (d.nm)
Record 13: 40 mM initial POPC coated Orlistat (1:1.5) in 10mM KNO3 1
Record 14: 40 mM initial POPC coated Orlistat (1:1.5) in 10mM KNO3 2
Record 15: 40 mM initial POPC coated Orlistat (1:1.5) in 10mM KNO3 3

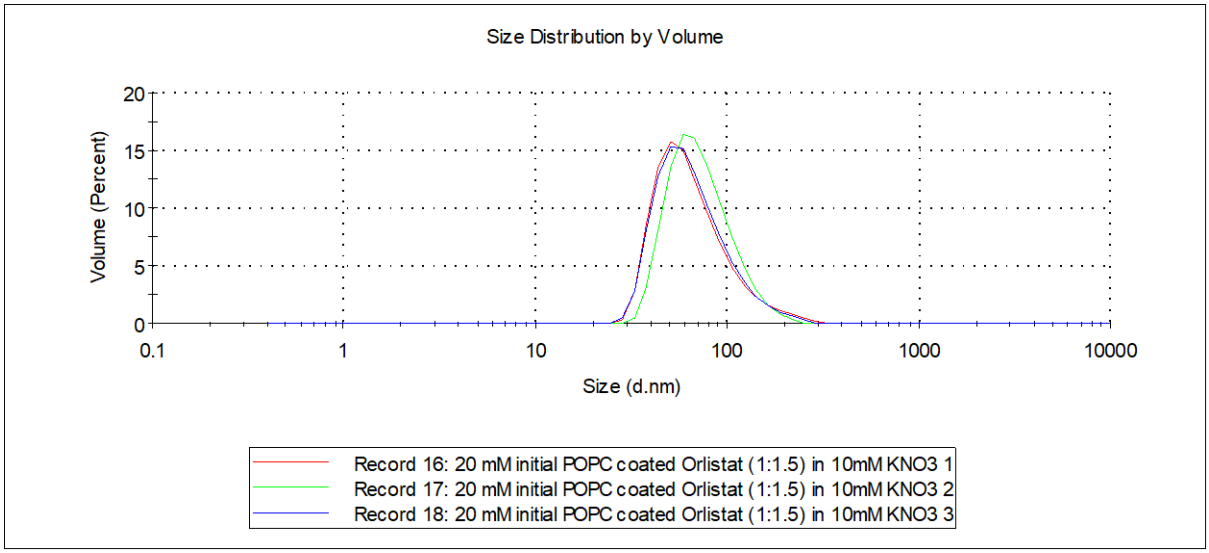
Size Distribution by Volume
Volume (Percent)
20
15
10
5
0
0.1
1
10
100
1000
10000
Size (d.nm)
Record 16: 20 mM initial POPC coated Orlistat (1:1.5) in 10mM KNO3 1
Record 17: 20 mM initial POPC coated Orlistat (1:1.5) in 10mM KNO3 2
Record 18: 20 mM initial POPC coated Orlistat (1:1.5) in 10mM KNO3 3

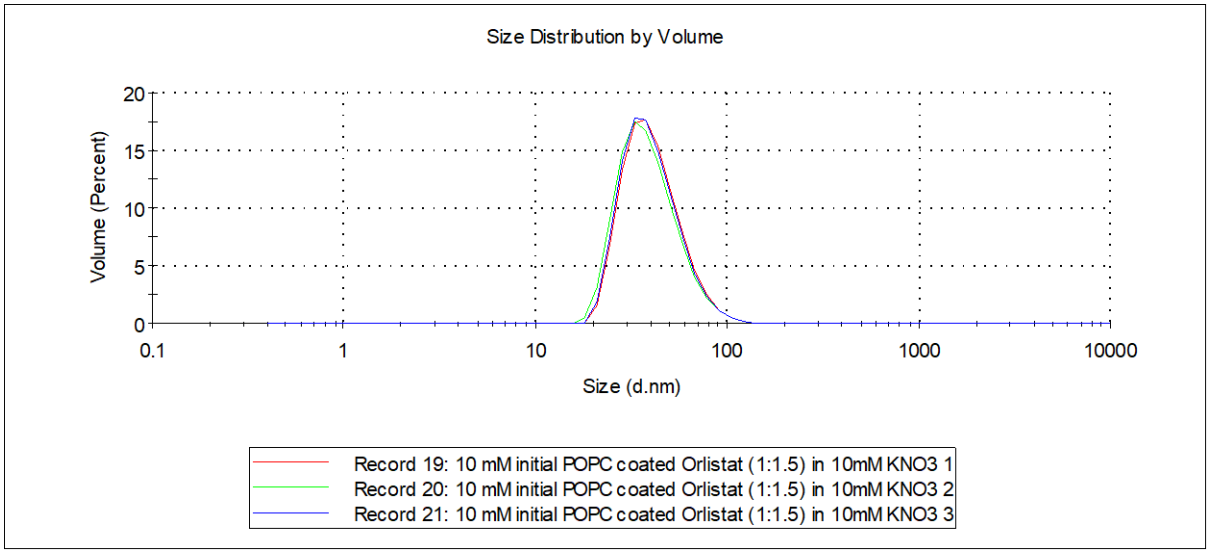
Size Distribution by Volume
Volume (Percent)
20
15
10
5
0
0.1
1
10
100
1000
10000
Size (d.nm)
Record 19: 10 mM initial POPC coated Orlistat (1:1.5) in 10mM KNO3 1
Record 20: 10 mM initial POPC coated Orlistat (1:1.5) in 10mM KNO3 2
Record 21: 10 mM initial POPC coated Orlistat (1:1.5) in 10mM KNO3 3

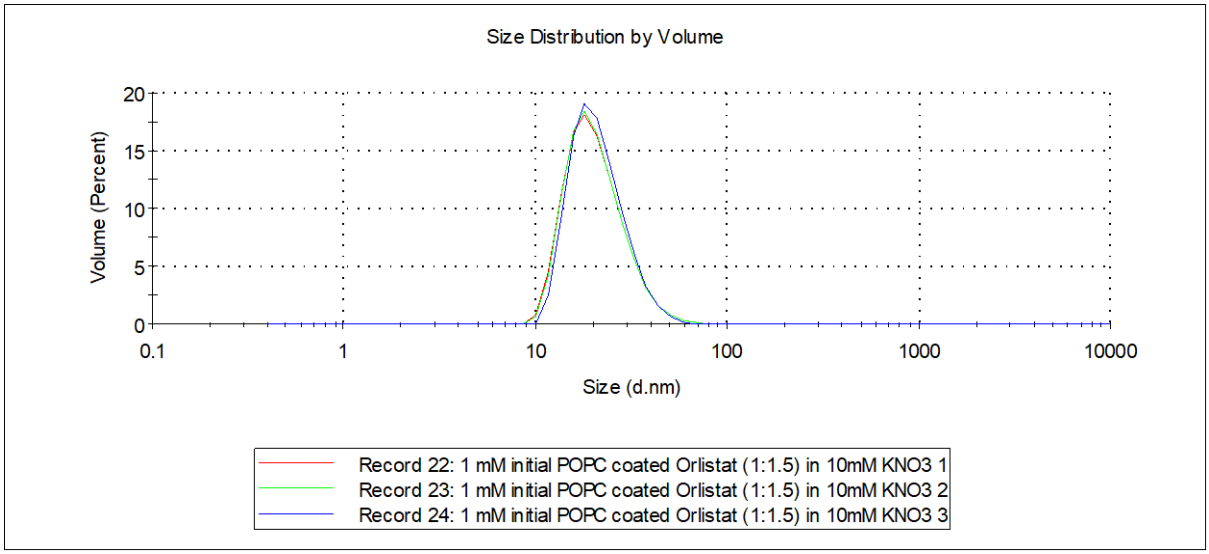
Size Distribution by Volume
Volume (Percent)
20
15
10
5
0
0.1
1
10
100
1000
10000
Size (d.nm)
Record 22: 1 mM initial POPC coated Orlistat (1:1.5) in 10mM KNO3 1
Record 23: 1 mM initial POPC coated Orlistat (1:1.5) in 10mM KNO3 2
Record 24: 1 mM initial POPC coated Orlistat (1:1.5) in 10mM KNO3 3

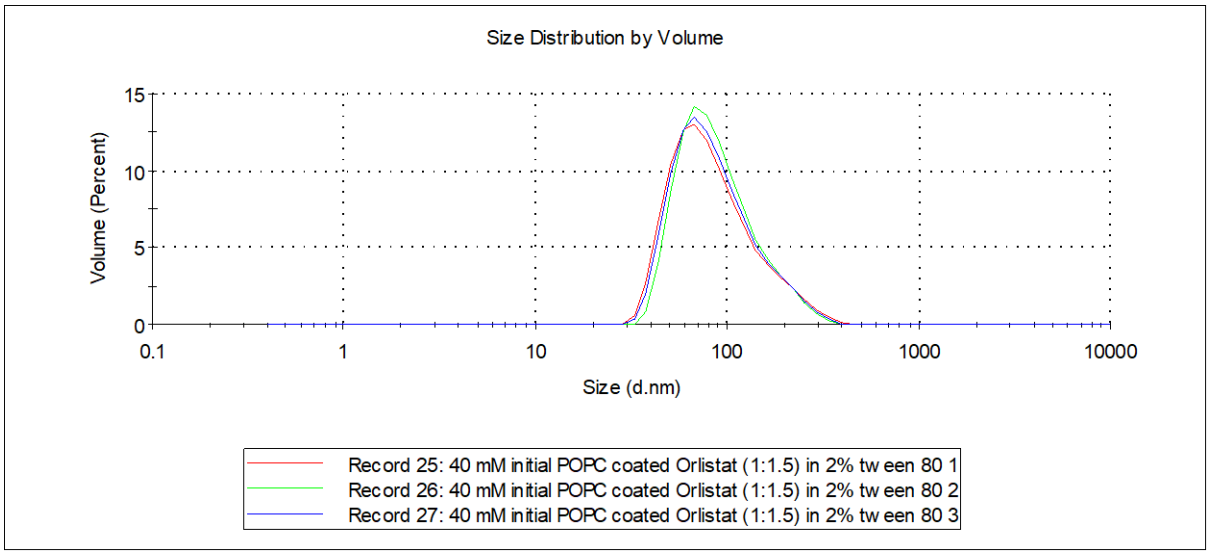
Size Distribution by Volume
Volume (Percent)
15
10
5
0
0.1
1
10
100
1000
10000
Size (d.nm)
Record 25: 40 mM initial POPC coated Orlistat (1:1.5) in 2% tw een 80 1
Record 26: 40 mM initial POPC coated Orlistat (1:1.5) in 2% tw een 80 2
Record 27: 40 mM initial POPC coated Orlistat (1:1.5) in 2% tw een 80 3

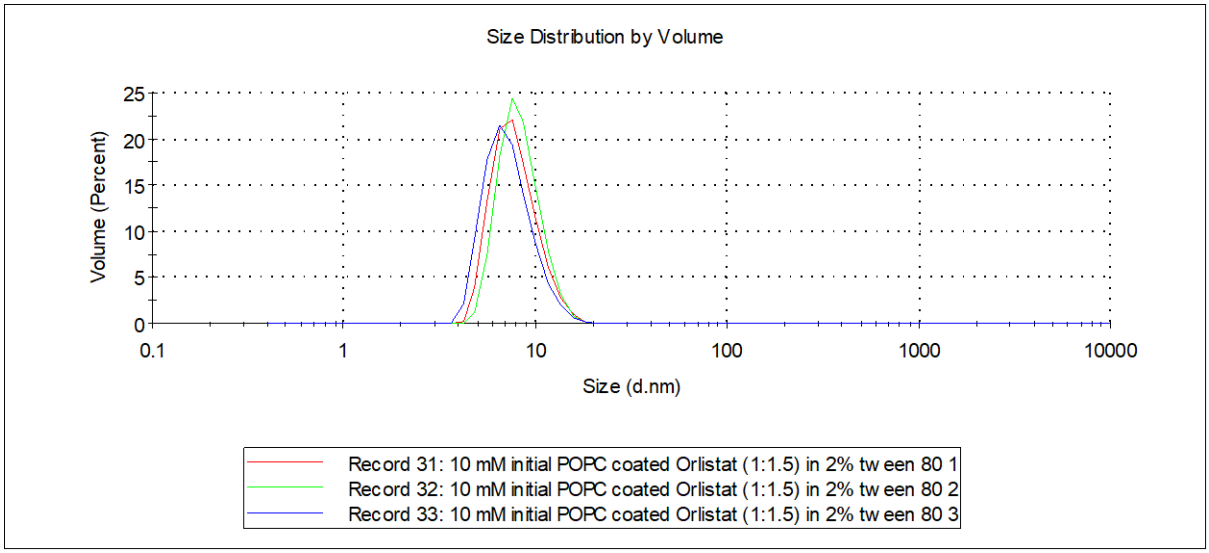
Size Distribution by Volume
Volume (Percent)
25
20
15
10
5
0
0.1
1
10
100
1000
10000
Size (d.nm)
Record 31: 10 mM initial POPC coated Orlistat (1:1.5) in 2% tw een 80 1
Record 32: 10 mM initial POPC coated Orlistat (1:1.5) in 2% tw een 80 2
Record 33: 10 mM initial POPC coated Orlistat (1:1.5) in 2% tw een 80 3

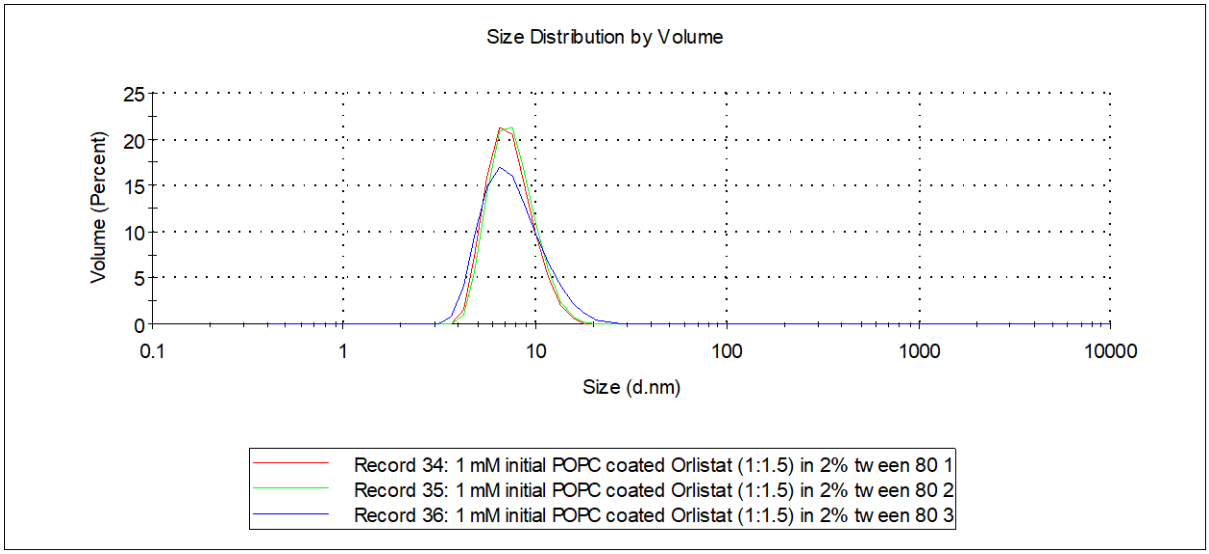
Size Distribution by Volume
Volume (Percent)
25
20
15
10
5
0
0.1
1
10
100
1000
10000
Size (d.nm)
Record 34: 1 mM initial POPC coated Orlistat (1:1.5) in 2% tw een 80 1
Record 35: 1 mM initial POPC coated Orlistat (1:1.5) in 2% tw een 80 2
Record 36: 1 mM initial POPC coated Orlistat (1:1.5) in 2% tw een 80 3

8.8 TEM Orlistat NPs (coated vs uncoated)

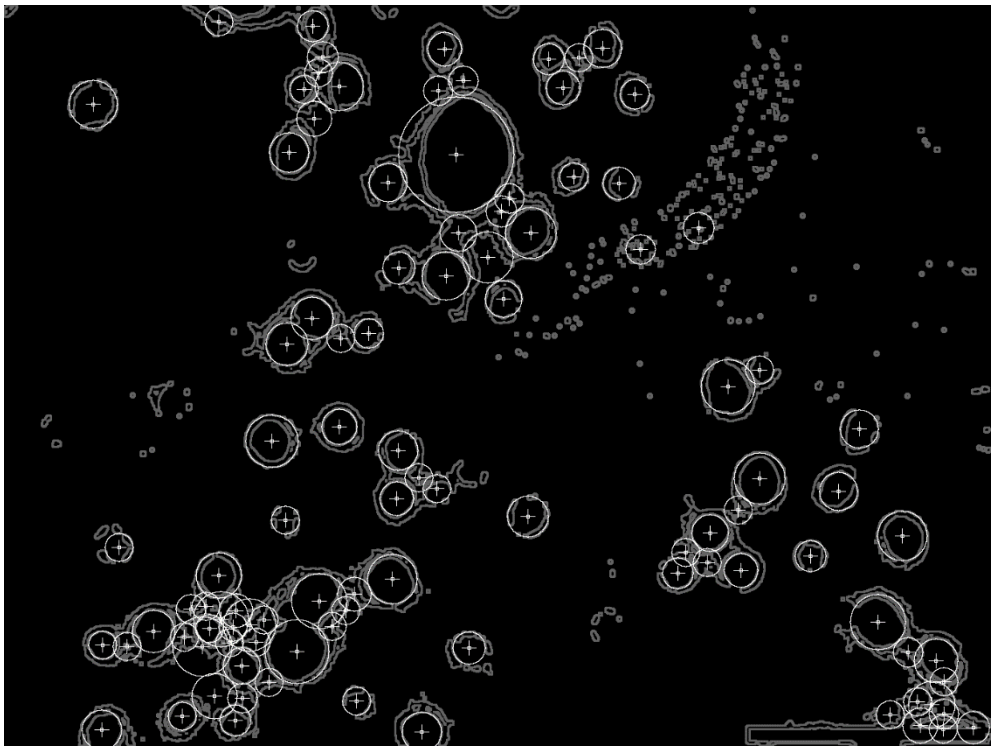

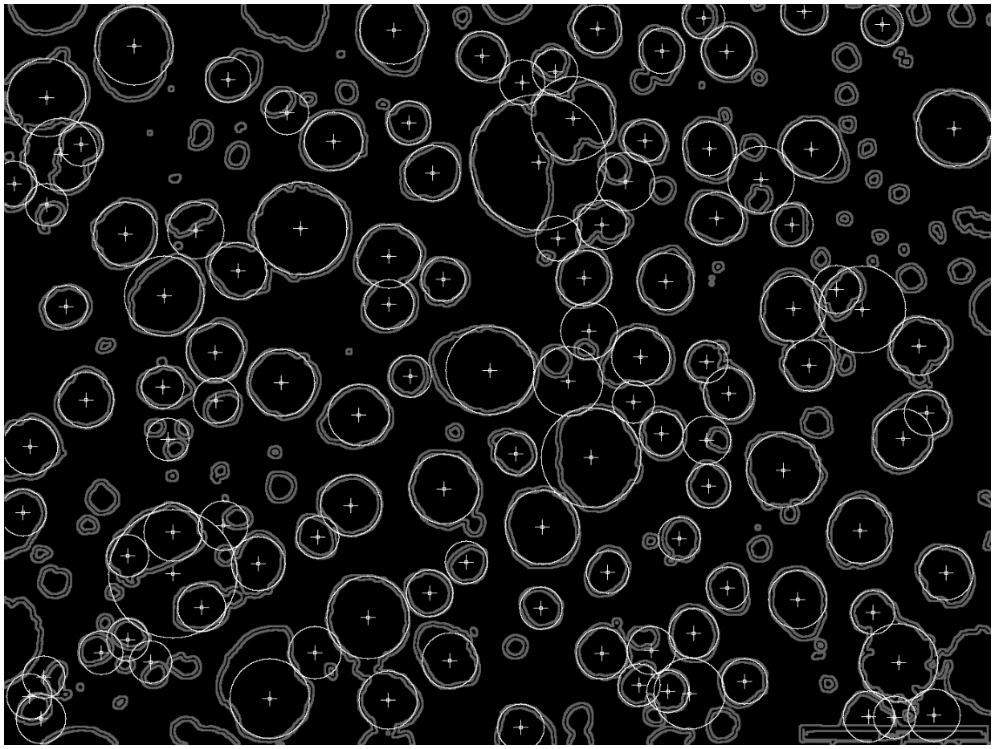

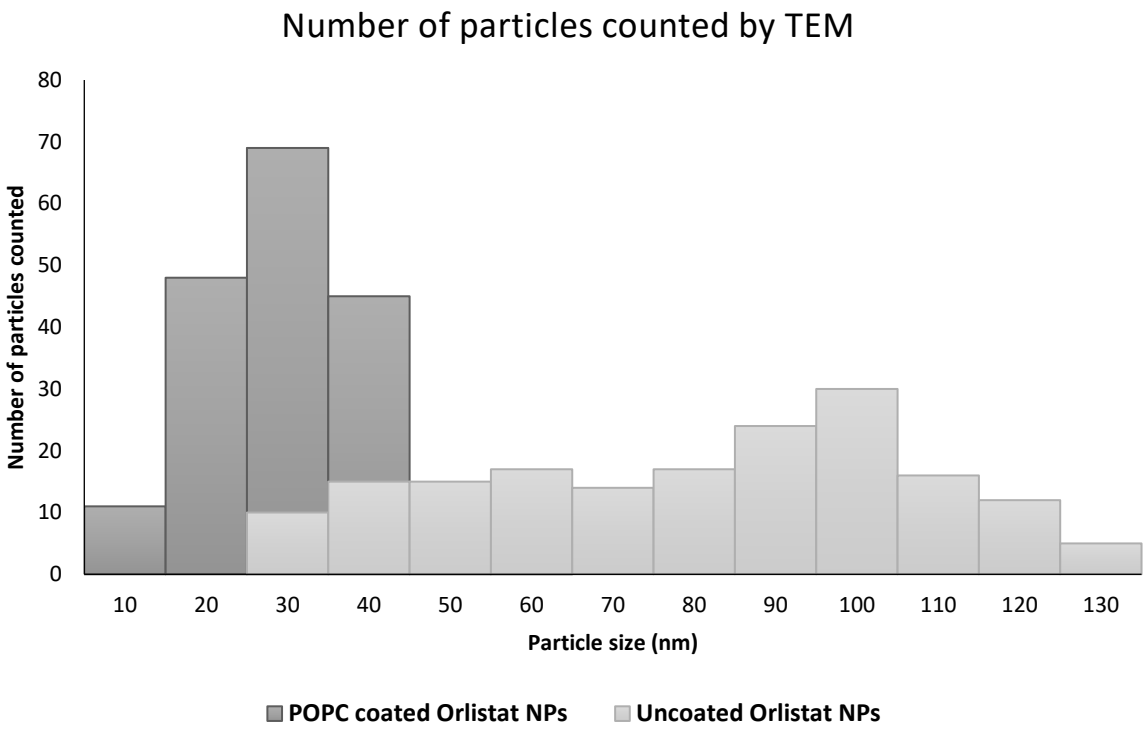

8.9 Orlistat in Dimethyl acetamide DMA

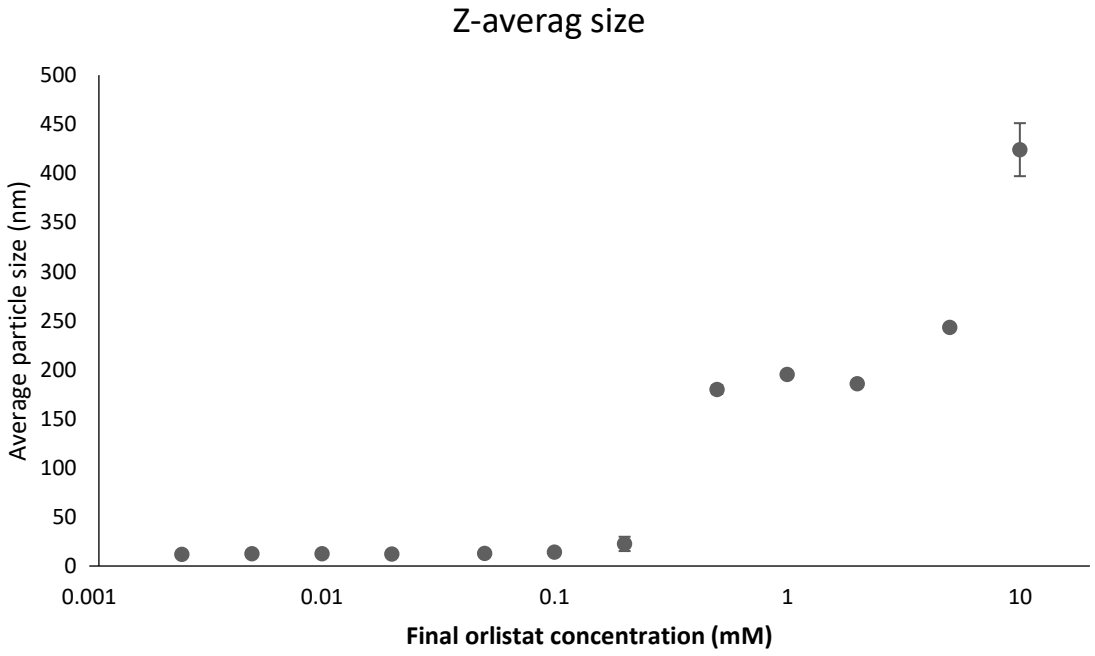

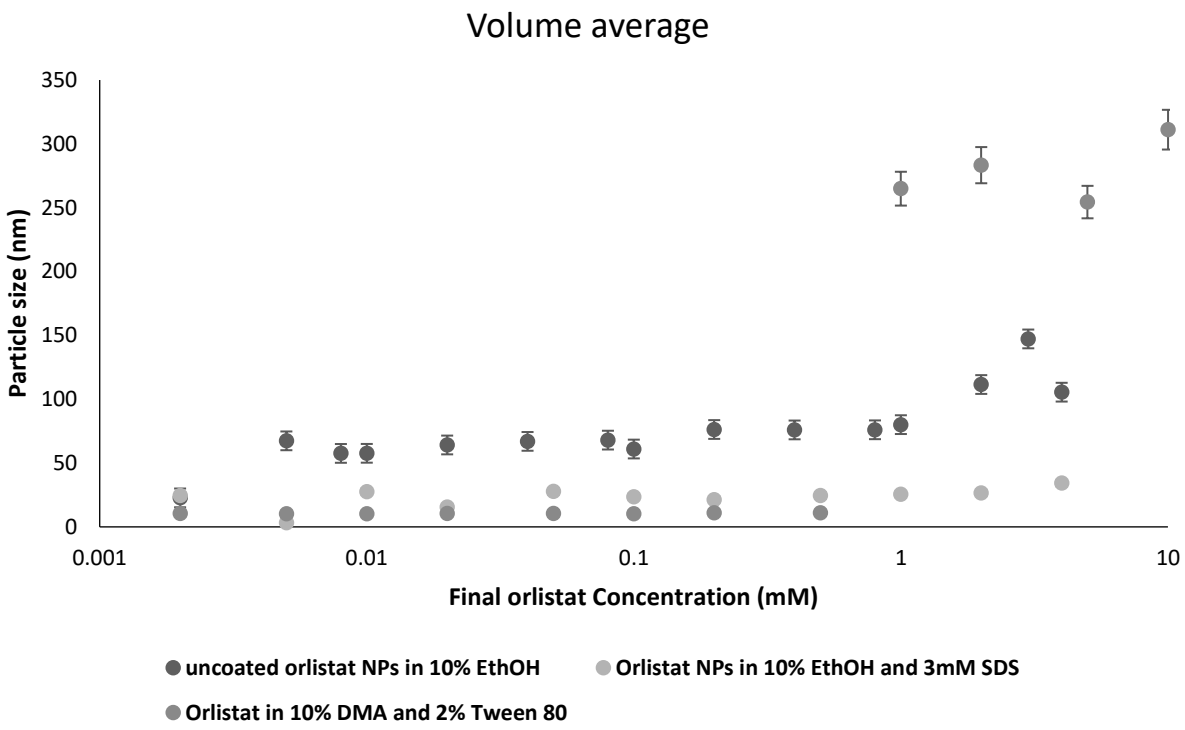

8.10 Peptide coated NPs DLS

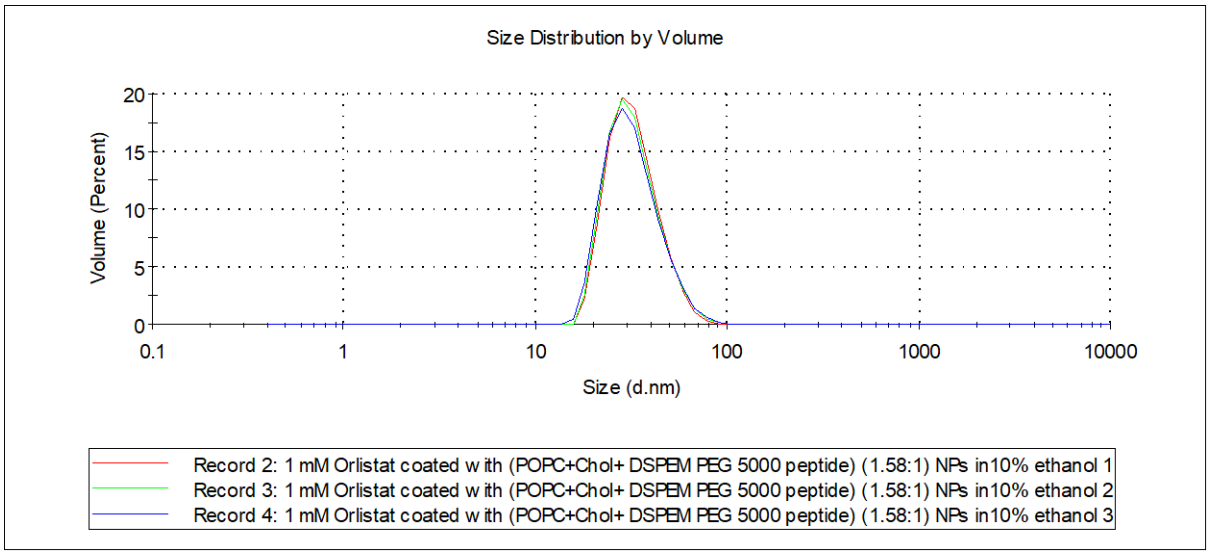

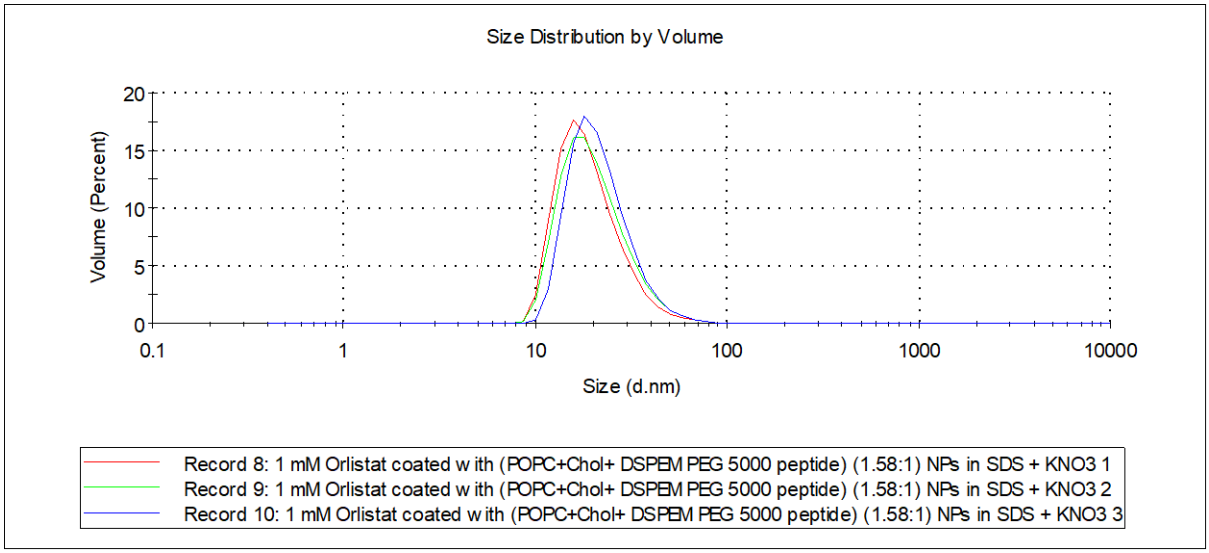
Size Distribution by Volume
Volume (Percent)
Size (d.nm)
0.1
1
10
100
1000
10000
Record 8: 1 mM Orlistat coated w ith (POPC+Chol+ DSPEM PEG 5000 peptide) (1.58:1) NPs in SDS + KNO3 1
Record 9: 1 mM Orlistat coated w ith (POPC+Chol+ DSPEM PEG 5000 peptide) (1.58:1) NPs in SDS + KNO3 2
Record 10: 1 mM Orlistat coated w ith (POPC+Chol+ DSPEM PEG 5000 peptide) (1.58:1) NPs in SDS + KNO3 3

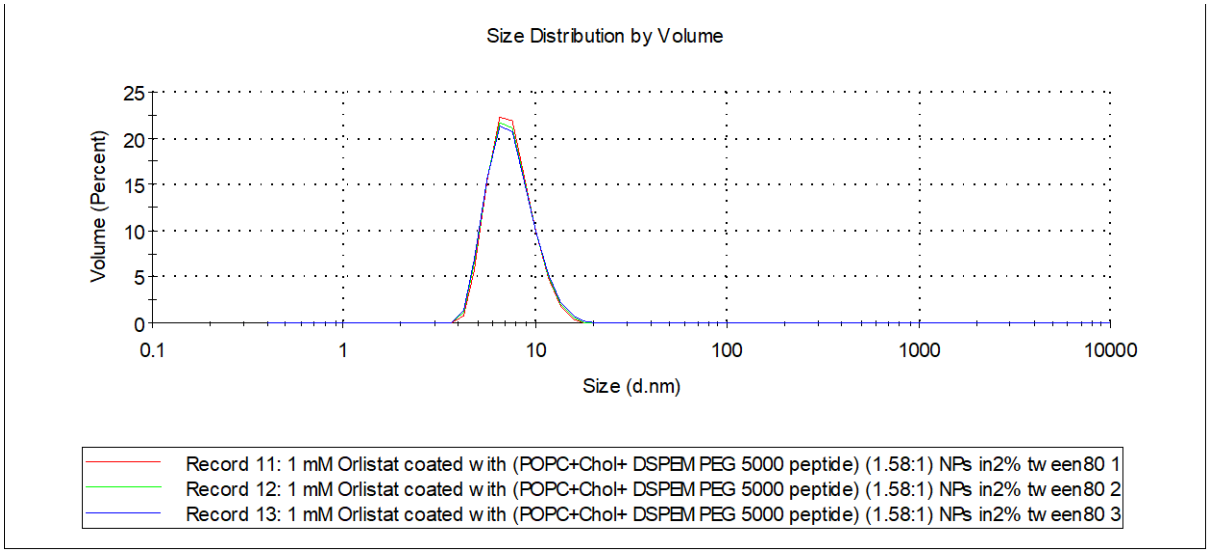
Size Distribution by Volume
Volume (Percent)
Size (d.nm)
0.1
1
10
100
1000
10000
Record 11: 1 mM Orlistat coated w ith (POPC+Chol+ DSPEM PEG 5000 peptide) (1.58:1) NPs in2% tw een80 1
Record 12: 1 mM Orlistat coated w ith (POPC+Chol+ DSPEM PEG 5000 peptide) (1.58:1) NPs in2% tw een80 2
Record 13: 1 mM Orlistat coated w ith (POPC+Chol+ DSPEM PEG 5000 peptide) (1.58:1) NPs in2% tw een80 3

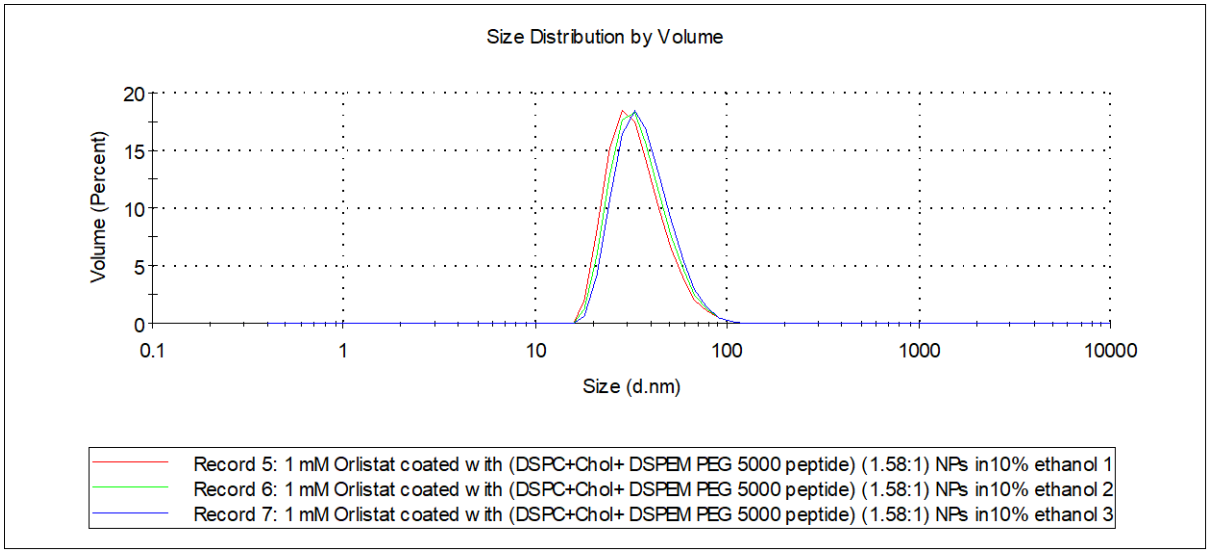
Size Distribution by Volume
Volume (Percent)
Size (d.nm)
0.1
1
10
100
1000
10000
Record 5: 1 mM Orlistat coated w ith (DSPC+Chol+ DSPEM PEG 5000 peptide) (1.58:1) NPs in10% ethanol 1
Record 6: 1 mM Orlistat coated w ith (DSPC+Chol+ DSPEM PEG 5000 peptide) (1.58:1) NPs in10% ethanol 2
Record 7: 1 mM Orlistat coated w ith (DSPC+Chol+ DSPEM PEG 5000 peptide) (1.58:1) NPs in10% ethanol 3

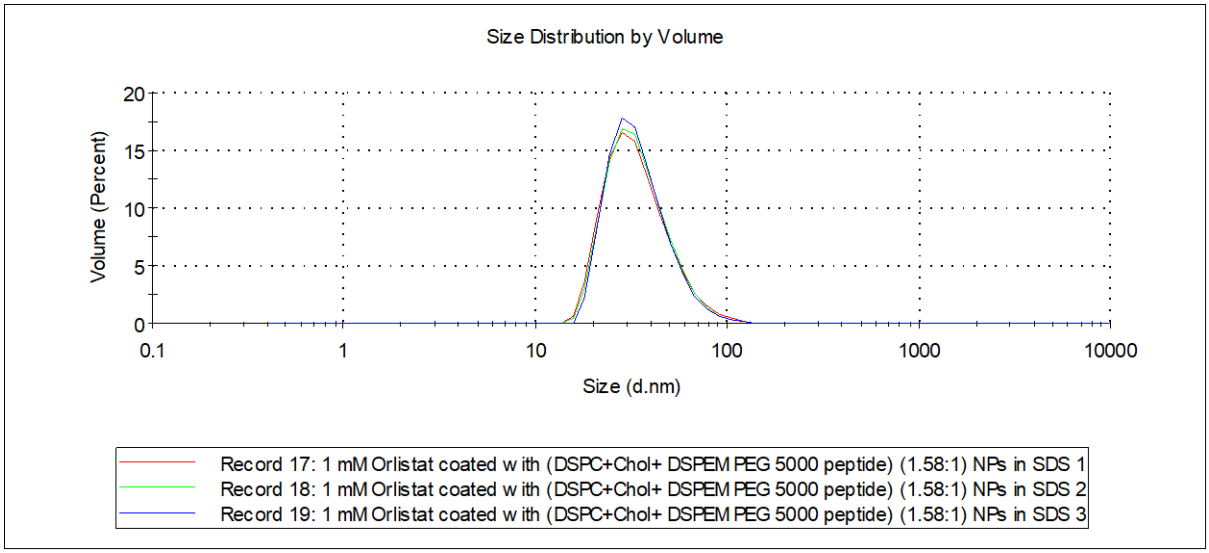
Size Distribution by Volume
Volume (Percent)
20
15
10
5
0
0.1
1
10
100
1000
10000
Size (d.nm)
Record 17: 1 mM Orlistat coated w ith (DSPC+Chol+ DSPEM PEG 5000 peptide) (1.58:1) NPs in SDS 1
Record 18: 1 mM Orlistat coated w ith (DSPC+Chol+ DSPEM PEG 5000 peptide) (1.58:1) NPs in SDS 2
Record 19: 1 mM Orlistat coated w ith (DSPC+Chol+ DSPEM PEG 5000 peptide) (1.58:1) NPs in SDS 3

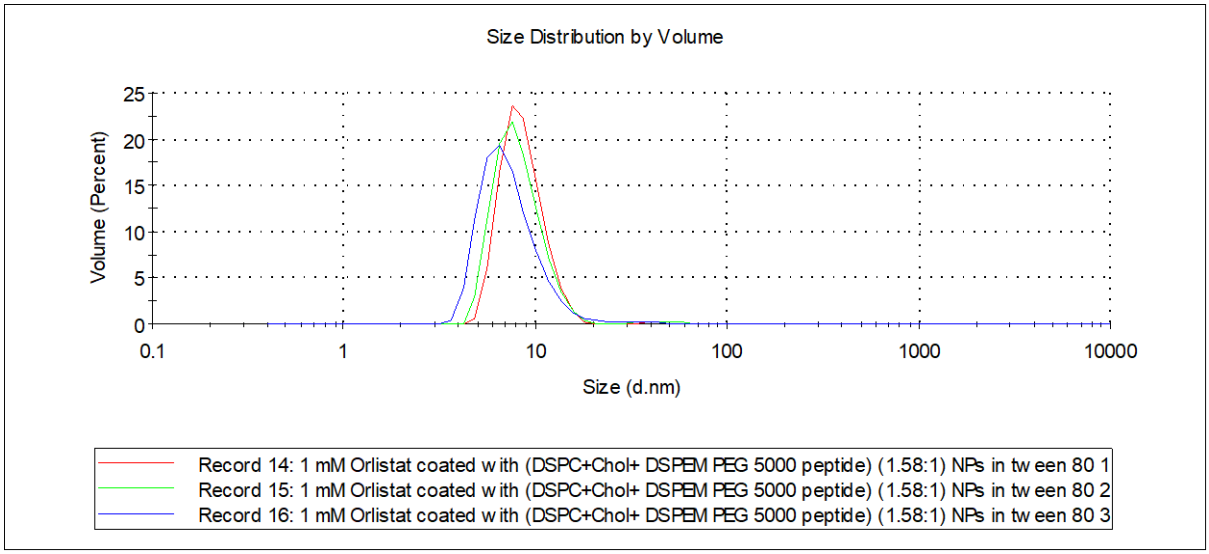
Size Distribution by Volume
Volume (Percent)
25
20
15
10
5
0
0.1
1
10
100
1000
10000
Size (d.nm)
Record 14: 1 mM Orlistat coated w ith (DSPC+Chol+ DSPEM PEG 5000 peptide) (1.58:1) NPs in tw een 80 1
Record 15: 1 mM Orlistat coated w ith (DSPC+Chol+ DSPEM PEG 5000 peptide) (1.58:1) NPs in tw een 80 2
Record 16: 1 mM Orlistat coated w ith (DSPC+Chol+ DSPEM PEG 5000 peptide) (1.58:1) NPs in tw een 80 3